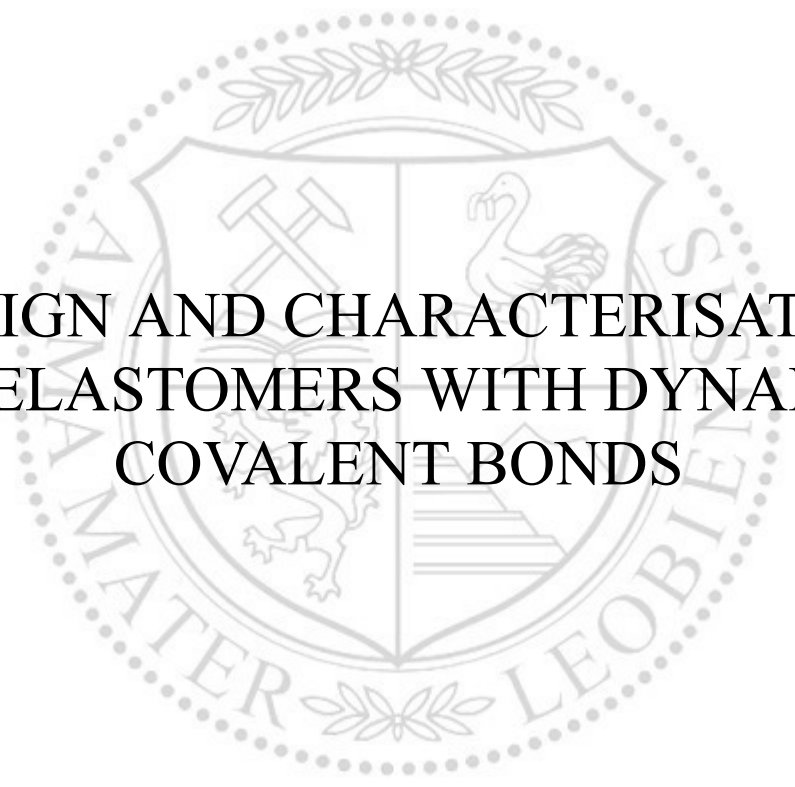




Chair of Chemistry of Polymeric Materials

Doctoral Thesis



DESIGN AND CHARACTERISATION  
OF ELASTOMERS WITH DYNAMIC  
COVALENT BONDS

Simon Johannes Kaiser, M.Sc.

October 2020

## **AFFIDAVIT**

I declare on oath that I wrote this thesis independently, did not use other than the specified sources and aids, and did not otherwise use any unauthorised aids.

I declare that I have read, understood, and complied with the guidelines of the senate of the Montanuniversitaet Leoben for "Good Scientific Practice".

Furthermore, I declare that the electronic and printed version of the submitted thesis are identical, both, formally and with regard to content.

Leoben, .....

Date

.....

Signature

The research work was performed within the COMET-project “New strategies towards thin elastomer films with advanced functionality“ (project-no.: VI-1.02) at the Polymer Competence Center Leoben GmbH (PCCL, Austria) within the framework of the COMET-program of the Federal Ministry for Transport, Innovation and Technology and Federal Ministry of Economy, Family and Youth with contributions by the Montanuniversitaet Leoben (Institute of Chemistry of Polymeric Materials and Institute of Material Science and Testing of Polymers, Austria) and Semperit Technische Produkte GmbH (Austria). The PCCL is funded by the Austrian Government and the State Governments of Styria, Lower Austria and Upper Austria.

## ACKNOWLEDGEMENT

Firstly, I would like to thank *Sandra Schlögl*. Your great support as a supervisor exceeds everything that can be expected. I am extremely grateful for all the helpful discussions, the scientific advice, for directing my topic in this very exciting direction, and your special ability to remind someone that there is always a solution to every problem.

I would also like to thank *Prof. Wolfgang Kern* for giving me the opportunity to carry out this research and the academic support.

Furthermore, I would like to express my thanks to all my colleagues from the PCCL and the Montanuniversitaet Leoben who have accompanied me over the past couple of years. Particular appreciation goes to *Evelyn Sattler*, my bachelor students *Julius Jandl* and *Patrick Novak*, and my co-authors that have contributed to the successful preparation of the papers presented in this thesis. I also want to thank *Gerald Pilz* and his colleagues for the excellent cooperation with the Institute of Materials Science and Testing of Polymers.

In addition, I would like to thank my project partner Semperit Technische Produkte GmbH, in particular *Dr. Armin Holzner* and *Dr. Raimund Schaller* for the pleasant and interesting meetings as well as the opportunity for two highly rewarding research visits in Malaysia.

My greatest gratitude goes to my family. *Mama & Papa*, your unconditional love accompanies me every day of my life. Without your support and advice, I would have lost my way many times. *Verena & Michi*, just knowing that you are there gives me so much strength and stability. *Sophia & Raphael & Emily*, you make me the happiest Onkel Simon in the world. I always think of you, and I just cannot wait to spend more time with you.

In the end, I thank the Love of My Life for everything you give to me. *Nastia*, it is an incredible journey with you and I cannot wait for what is about to come.

Simon Kaiser

October 2020

## COOPERATIONS

**The results of this thesis were published in four peer-reviewed scientific papers.**

- (1) Kaiser, Simon; Radl, Simone Viola; Manhart, Jakob; Ayalur-Karunakaran, Santhosh; Griesser, Thomas; Moser, Andreas; Ganser, Christian; Teichert, Christian; Kern, Wolfgang; Schlögl, Sandra (2018): Switching "on" and "off" the adhesion in stimuli-responsive elastomers. In: *Soft Matter* 14 (13), 2547–2559. DOI: 10.1039/c8sm00284c.
- (2) Kaiser, Simon; Wurzer, Stefan; Pilz, Gerald; Kern, Wolfgang; Schlögl, Sandra (2019): Stress relaxation and thermally adaptable properties in vitrimer-like elastomers from HXNBR rubber with covalent bonds. In: *Soft Matter* 15 (30), 6062–6072. DOI: 10.1039/c9sm00856j.
- (3) Kaiser, Simon; Jandl, Julius; Novak, Patrick; Schlögl, Sandra (2020): Design and characterisation of vitrimer-like elastomeric composites from HXNBR rubber. In: *Soft Matter* 16 (37), 8577–8590. DOI: 10.1039/d0sm00362j.
- (4) Kaiser, Simon; Novak, Patrick; Giebler, Michael; Gschwandl, Mario; Novak, Philipp; Pilz, Gerald; Morak, Matthias; Schlögl, Sandra (2020): The crucial role of external force in the estimation of the topology freezing transition temperature of vitrimers by elongational creep measurements. In: *Polymer* (204): 122804. DOI: 10.1016/j.polymer.2020.122804.

**Two bachelor theses were completed in the course of this research work.**

### **Julius Jandl**

New strategies towards the preparation of elastomers from high molecular weight HXNBR rubber with vitrimer-like properties, bachelor thesis, 2020, MU Leoben.

Some of the results of this work are presented in Chapter 5.

### **Patrick Novak**

Analysis of the topology freezing transition temperature of vitrimers by elongational creep measurements, bachelor thesis, 2020, MU Leoben.

Some of the results of this work are presented in Chapter 6.

# DESIGN AND CHARACTERISATION OF ELASTOMERS WITH DYNAMIC COVALENT BONDS

## ABSTRACT

Conventional elastomers comprise covalent cross-links, which endows them with outstanding chemical and physical properties such as their exceptionally high elasticity. However, similar to thermosets, the permanent nature of the linkages brings along certain problems, preventing any further adaptability or (re)processing of the materials after curing. The aim of this thesis was the preparation of stimuli-responsive elastomers from an industrially relevant hydrogenated carboxylated nitrile butadiene rubber (HXNBR). The incorporation of reversible cross-links was envisaged to enable a temporally controllable adaptability of the prepared networks. A detailed characterisation of the material's structure-property relationship was conducted, revealing a macroscopic responsiveness towards external stimuli.

In the first part of the thesis, the incorporation of reversible covalent bonds into HXNBR based on a dissociative bond exchange mechanism was explored. Covalently attached anthracene moieties were exploited for a light-induced cross-linking of the rubber *via* the [4+4] photocycloaddition. The photodimers were shown being susceptible to controlled cleavage by exposure to UV-light or heat, and a repeatable switching over multiple cross-linking and cleavage cycles was demonstrated. The associated modulation of the viscoelastic properties was employed for switchable, spatially controllable bonding properties, which paves the way for the application of the materials as reversible dry adhesive.

The second part of the thesis focused on the introduction of dynamic covalent bonds into HXNBR relying on an associative bond exchange mechanism following vitrimer chemistry. Exchangeable  $\beta$ -hydroxyl-ester cross-links were incorporated into HXNBR for the first time, and in the presence of catalyst, thermo-activated transesterifications allowed for a distinctive stress relaxation of the networks. Thermal adaptability of the elastomers was demonstrated by lap shear tests, shape change experiments and stress-rupture tests. The data confirmed the susceptibility of the prepared rubbery materials for weldability, reprocessability, and repairability. The study constitutes a straightforward and scalable methodology towards vitrimer-like elastomers, with the synthesis relying on facile chemical strategies and readily available materials.

In the third part of the thesis, the step towards filled vitrimer-like HXNBR composites was taken, since the reinforcement of rubbers is essential to ensure high mechanical properties. Combining cross-linker and reinforcing filler in a single compound, a significant improvement in mechanical properties was achieved. Yet, the exchangeable nature of the linkages at the rubber-filler interface enabled thermo-activated and catalytically controlled topology rearrangements, rendering the cured composites thermally adaptable. Interestingly, compared to the unfilled analogue, the network dynamics could almost be preserved, which was remarkable considering the high filler content of up to 30 phr.

Finally, a new analysis strategy for the determination of the topology freezing transition temperature ( $T_v$ ) of vitrimers was presented. The direct and precise analysis of the  $T_v$  of vitrimers is challenging because measurement methods such as dynamic mechanical analysis (DMA) and dynamic scanning calorimetry (DSC) are not suitable. On the example of different literature-known epoxy-vitrimers, it was shown that the estimation of  $T_v$  from elongational creep measurements is feasible. However, a screening of various stresses at increasing temperature revealed the significance of external force in order to obtain precise  $T_v$  values. The method constitutes a facile measurement routine and allows a direct acquisition of the  $T_v$ .

# ENTWICKLUNG UND CHARAKTERISIERUNG VON ELASTOMEREN MIT DYNAMISCHEN KOVALENTEN BINDUNGEN

## ZUSAMMENFASSUNG

Konventionelle Elastomere enthalten kovalente Vernetzungsstellen, welche diesen hervorragende chemische und physikalische Eigenschaften verleihen wie beispielsweise eine außergewöhnliche Elastizität. Ähnlich wie für Duromere erschweren die permanenten Bindungen jedoch eine nachhaltigere Herstellung solcher Polymere, indem sie eine Anpassungsfähigkeit und Weiterverarbeitung nach deren Aushärtung verhindern. Das Ziel der vorliegenden Arbeit war die Herstellung stimuli-responsiver Elastomere aus einem hydrierten und carboxylierten Nitrilbutadienkautschuk (HXNBR). Durch die Inkorporation reversibler Vernetzungsstellen wurde eine zeitaufgelöste Anpassungsfähigkeit der hergestellten Netzwerke bei Anwendung des entsprechenden Stimulus erwartet. Die detaillierte Charakterisierung der Struktur-Eigenschafts-Beziehungen der Materialien hat ergeben, dass die Anwendung des Stimulus eine makroskopische Reaktion induziert.

Im ersten Teil dieser Arbeit wurde die Inkorporierung reversibler kovalenter Vernetzungsstellen in HXNBR verfolgt, welche Bindungsaustauschreaktionen eingehen können die auf einem dissoziativen Mechanismus beruhen. Die kovalente Anbindung eines Anthracen-Derivates an HXNBR ermöglichte eine lichtinduzierte Vernetzung der Polymerketten über die [4+4]-Cycloaddition. Danach wurde die Möglichkeit zur kontrollierten Spaltung der Photodimere mittels Wärme oder UV-Licht bestätigt sowie die Wiederholbarkeit einer mehrmaligen Vernetzung mit anschließender Spaltung. Die einhergehende Einstellbarkeit der Viskoelastizität der Netzwerke wurde für schaltbare Klebeeigenschaften genutzt, wobei die Adaptierungen aufgrund der Lichtsensitivität der Materialien orts aufgelöst möglich waren. So wurde die potenzielle Anwendbarkeit der Elastomere als reversibler Trockenklebstoff aufgezeigt.

Im zweiten Teil dieser Arbeit wurde die Inkorporierung von dynamischen kovalenten Vernetzungsstellen in HXNBR erforscht, welche auf einem assoziativen Bindungsaustauschmechanismus in Anlehnung an Vitriemer-Chemie beruhen. So wurde HXNBR erstmals mit  $\beta$ -Hydroxyester-Bindungen ausgestattet, die in Anwesenheit eines Katalysators thermisch induzierte Umesterungen eingehen konnten, was Spannungsrelaxationen der Netzwerke ermöglichte. Die Anpassungsfähigkeit der Materialien wurde mittels Zugscher-, Verformungs- und Zeitstandsversuchen veranschaulicht, die eine gewisse Schweißbarkeit, Reprozessierbarkeit und Heilbarkeit aufzeigen. Die vorliegende Studie präsentiert eine praktikable und hochskalierbare Vorgehensweise hin zu vitriemerähnlichen Elastomeren und beruht auf einfachen chemischen Konzepten sowie großtechnisch verfügbaren Materialien.

Der dritte Teil der Arbeit behandelte die Synthese von gefüllten, vitriemerähnlichen Kompositen aus HXNBR. Die Kombination von Füllstoff und Vernetzungskemikalie in Form oberflächenmodifizierter Füllstoffpartikel erzielte eine bedeutende Verbesserung



der mechanischen Eigenschaften der Materialien. Gleichzeitig zeigten die Komposite eine thermische Anpassungsfähigkeit in Anwesenheit eines Katalysators, ermöglicht durch die Austauschbarkeit der kovalenten Bindungen an der Kautschuk-Füllstoff-Grenzfläche. Die Netzwerkdynamik der Komposite konnte dabei im Vergleich zu den ungefüllten Materialien nahezu erhalten werden, sogar für Füllstoffanteile von bis zu 30 phr.

Weiterhin wurde im Rahmen dieser Arbeit eine neue Analyseverfahren zur Bestimmung der Vitrifizierungstemperatur ( $T_v$ ) von Vitrimeren erarbeitet. Die direkte und präzise Erfassung des  $T_v$  mittels Messmethoden wie der dynamisch-mechanische Analyse (DMA) oder dynamischen Differenzkalorimetrie (DSC) ist nicht möglich. So wurde am Beispiel diverser Epoxy-Vitrimere aufgezeigt, dass die genaue Messung des  $T_v$  mittels Kriechversuchen unter Zugbeanspruchung dann möglich ist, wenn eine geeignete äußere Kraft angewendet wird. Diese neue Methode stellt eine einfache Messprozedur dar, die eine direkte Messung des  $T_v$  von Vitrimeren ermöglicht.

# TABLE OF CONTENTS

CHAPTER 1	INTRODUCTION AND STRUCTURE OF THE THESIS.....	- 1 -
1.1	Introduction.....	- 1 -
1.2	Structure of the thesis.....	- 4 -
1.3	References.....	- 6 -
CHAPTER 2	THEORETICAL BACKGROUND.....	- 7 -
2.1	Nitrile butadiene rubber (NBR).....	- 7 -
2.1.1	Synthesis, properties, and types of NBR rubber.....	- 7 -
2.1.2	Cross-linking of NBR rubber and its derivatives.....	- 8 -
2.2	Dynamic covalent chemistry.....	- 21 -
2.2.1	The strive for a new polymer class.....	- 21 -
2.2.2	Covalent adaptable networks.....	- 23 -
2.2.3	Dynamic covalent networks from anthracene.....	- 27 -
2.2.4	Chemistry of vitrimers.....	- 29 -
2.2.5	Vitrimer(-like) chemistry in rubbers.....	- 37 -
2.2.6	Fillers in associative dynamic covalent networks.....	- 41 -
2.2.7	Characterisation of dynamic covalent networks.....	- 43 -
2.3	References.....	- 50 -
CHAPTER 3	SWITCHABLE ADHESION IN ELASTOMERS FROM HXNBR.....	- 59 -
3.1	Bibliographic information.....	- 60 -
3.2	Abstract.....	- 61 -
3.3	Introduction.....	- 62 -
3.4	Results and discussion.....	- 64 -
3.5	Conclusions.....	- 76 -
3.6	Experimental.....	- 77 -
3.7	Acknowledgements.....	- 80 -
3.8	References.....	- 81 -
3.9	Supporting information.....	- 83 -
CHAPTER 4	VITRIMER-LIKE ELASTOMERS FROM HXNBR RUBBER.....	- 85 -
4.1	Bibliographic information.....	- 86 -
4.2	Abstract.....	- 87 -
4.3	Introduction.....	- 88 -
4.4	Results and discussion.....	- 90 -

4.5	Experimental.....	- 100 -
4.6	Conclusions.....	- 102 -
4.7	Acknowledgements.....	- 103 -
4.8	References.....	- 104 -
4.9	Supporting information.....	- 106 -
CHAPTER 5	VITRIMER-LIKE ELASTOMERIC COMPOSITES FROM HXNBR RUBBER.....	- 111 -
5.1	Bibliographic information .....	- 112 -
5.2	Abstract .....	- 113 -
5.3	Introduction.....	- 114 -
5.4	Results and discussion .....	- 116 -
5.5	Conclusions.....	- 131 -
5.6	Experimental.....	- 132 -
5.7	Acknowledgements.....	- 134 -
5.8	References.....	- 135 -
5.9	Supporting information.....	- 137 -
CHAPTER 6	ANALYSIS OF THE T <sub>v</sub> OF VITRIMERS BY CREEP MEASUREMENTS .....	- 142 -
6.1	Bibliographic information .....	- 143 -
6.2	Abstract .....	- 144 -
6.3	Introduction.....	- 145 -
6.4	Results and discussion .....	- 148 -
6.5	Experimental.....	- 156 -
6.6	Conclusions.....	- 158 -
6.7	Acknowledgements.....	- 160 -
6.8	References.....	- 160 -
6.9	Supporting information.....	- 162 -
CHAPTER 7	FINAL CONCLUSIONS AND PERSPECTIVES.....	- 164 -
7.1	Objectives of the work .....	- 164 -
7.2	Overview of the results .....	- 165 -
7.3	Perspectives.....	- 168 -

# Chapter 1

## INTRODUCTION AND STRUCTURE OF THE THESIS

### 1.1 Introduction

The discovery of the vulcanisation in 1839 by Charles Goodyear constitutes not only a milestone in polymer chemistry, and particularly in the field of rubbers, but the invention contributed decisively to the industrial revolution of the 19<sup>th</sup> century.<sup>1</sup> Whereas the term vulcanisation initially described the covalent cross-linking of natural rubber (NR) with sulphur resulting in a three-dimensional network, today it refers generally to the process of transforming thermoplastic natural or synthetic rubbers into elastomeric polymer networks. The invention enabled the commercial use of rubbers, and thereby had a crucial influence on an entire branch of polymer industry whose products have become an integral part of our everyday life. Due to the exceptional elasticity and resilience of cross-linked rubbers these materials exhibit a unique versatility regarding numerous applications. Elastomers from rubbers are ubiquitous in industry and daily life, for instance as tires, seals, rubber bands, damping materials, and in a multitude of consumer goods. Rubber products can be found in all major industries, such as construction, automotive and aviation, health care, and transportation.<sup>2</sup>

Vulcanised rubbers belong to the polymer class of elastomers, which in turn can be assigned to thermosets, owing to the covalent nature of the formed cross-links. The other major class of polymers constitute thermoplastics that display a fundamentally different material response upon heating due to exclusively weak intermolecular forces of noncovalent nature. Comprising long linear (but entangled) polymer chains with intrinsically reversible physical interactions between them, thermoplastics can flow upon heating and the chain's movements are controlled by reptation.<sup>3</sup> In contrast, the strong chemical and irreversible bonds in thermosets severely restrict the polymer chain diffusion and thus, ensure a high structural integrity. However, the molecular architecture is permanent once cured, thereby preventing any thermal adaptability thereafter, which in contrast is given for thermoplastics making them recyclable and reprocessable.

For many decades, the classification of thermosets and thermoplastics has been the most widely used for polymeric materials, with each type displaying specific advantages and disadvantages. In the last two decades, increased efforts have been made to combine the merits of both and the classical division has been become somewhat blurred. In particular, researchers are interested in the introduction of plasticity into thermosets, creating highly sought-after permanent yet malleable materials that combine the strength and durability of thermosets with the adaptability of thermoplastics. For this purpose, thermosets would need to be equipped with reversible covalent bonds.

Stimuli-responsive polymers generally describe polymer-based materials that are capable of undergoing chemical and/or physical changes in their properties on demand, subsequent

to the application of a stimulus (e.g. heat, light, force, pH).<sup>4</sup> While supramolecular chemistry specialises on noncovalent interactions, a specific and exciting group of stimuli-responsive polymer networks are so-called covalent adaptable networks (CANs).<sup>5</sup> Although these smart materials constitute covalently cross-linked polymers, the linkages are designed in a manner that renders them dynamically reversible, enabling a temporary switching of the phase (i.e. solid to fluid). The transient network dynamics of CANs relies either on a breaking and reforming of covalent bonds or on a rearrangement of the network connectivity *via* a higher cross-linked intermediate (i.e. addition/elimination).<sup>6</sup> These two strategies are referred to as dissociative and associative bond exchange mechanisms, leading to a fundamentally different viscoelasticity of the respective materials at increasing temperature.<sup>7</sup> Independent of the particular exchange mechanism, the unique network dynamics and specific macroscopic responses of these materials arise from the chemistry occurring on the molecular level (i.e. bond rearrangements), which explains the emerging interest and fascination of this scientific field.

Regarding dissociative CANs, the Diels-Alder reaction constitutes the most exciting chemistry to implement reversible covalent cross-links into polymers, with the first attempts dating back to the 1970s. However, it was not until 2002 that the thermo-reversible Diels-Alder cycloaddition has been employed for the efficient incorporation of repeatable healing capabilities into thermosets, as reported in the pioneering work of Wudl et al.<sup>8</sup> In terms of imparting photosensitivity into reversibly cross-linked networks, the versatile [4+4] photocycloaddition of anthracene has received much attention. While the potential of this photodimerisation reaction has been demonstrated for photo-cross-linking some time ago<sup>9</sup>, more sophisticated applications exploiting the light-induced dissociation of the dimer towards dynamic covalent networks have been developed recently.<sup>10</sup>

In 2011, the previously limited (i.e. involving radical species) class of associative CANs has been revolutionised with the introduction of vitrimers by Leibler and co-workers.<sup>11</sup> Through an ingenious network design, covalently cross-linked but at the same time malleable epoxy-based networks were obtained, showing an Arrhenius dependency in viscosity upon heating. This glass-like plasticity has never been observed before in organic polymer networks. While various strategies towards photo-responsive dissociative CANs exist, all current existent vitrimers rely on thermal activation. Vitrimers represent a significant contribution towards (re)processable and recyclable covalently cross-linked polymers, which is a substantial challenge for classical thermosets.<sup>12</sup> Since their introduction, the scientific community investigated various methodologies for the preparation of vitrimeric polymeric materials<sup>13</sup>, and the chemistry has recently been extended to elastomers from high molecular weight rubbers, such as natural rubber<sup>14</sup> (NR) and styrene-butadiene rubber (SBR)<sup>15</sup>.

Uncrosslinked rubbers usually exhibit insufficient mechanical properties and chemical resistance. For the use in structural applications, the covalent cross-linking of rubbers is essential to achieve high strength and elasticity. The classical yet still most important cross-linking techniques are sulphur and peroxide curing.<sup>16</sup> The vulcanised rubbers then meet the high requirements of the many possible applications. On the downside, the permanent and irreversible nature of the covalent bonds causes serious issues for a sustainable production and a (re)processing and/or recycling of the materials, a similar

situation as for typical thermosets. In 2019, the total global production of rubber (natural and synthetic) amounted to 29 million tons.<sup>17</sup> Consequently, new opportunities and innovative approaches have to be explored to extend the lifetime and circularity of cross-linked elastomers, as well as new technologies for managing the products at the end-of-life.<sup>18</sup>

As a pioneer in the research of the viscoelasticity of polymers, Tobolsky and co-workers reported for the first time on the observation of dynamic behaviour in covalently cross-linked polymeric materials in 1946.<sup>19</sup> The stress relaxation obtained at elevated temperatures in rubbers comprising polysulphide linkages was attributed to the rearrangement of disulphide moieties, catalysed by ionic impurities introduced through curing additives.

In order to expand the horizon of dynamic covalent polymer networks from rubbers, the present thesis aims to explore reversible covalent elastomers from a high molecular weight polymer consisting of long linear macromolecular chains. The studies are carried out using a hydrogenated carboxylated nitrile butadiene rubber (HXNBR), which constitutes a commercially available and technically relevant high-performance polymer. To achieve topology rearrangements in elastomeric networks from HXNBR, both a dissociative and an associative approach for the incorporation of covalent cross-links of dynamic character are followed. Moreover, these strategies take advantage of light and/or heat as the stimuli to trigger the material response. Motivated by the need for more sustainable rubbery materials, an important aspect of this project is the employment of basic materials, straightforward synthesis methodologies, and facile chemical strategies. Thereby, the work operates at the interface between basic research and technical feasibility. Consequently, a major objective of the thesis is to demonstrate the potential of the materials prepared for high-tech applications, for instance highlighted by their (re)processability, recyclability, repairability, and adaptability. Such properties are the key to sustainable product design of polymers with advanced properties.

## 1.2 Structure of the thesis

**Chapter 2** provides a theoretical introduction to nitrile butadiene rubber (NBR) and its hydrogenated and/or carboxylated derivatives (XNBR and HXNBR) describing their molecular composition and the associated chemical and physical properties. Next, a selection of available cross-linking techniques for these rubbers are presented. Besides the industrially most important ones, namely sulphur and peroxide curing, cross-linking by epoxides, ionic interactions, and (photochemical) cycloadditions is discussed in detail. Afterwards, an introduction is provided to the field of covalent adaptable networks (CANs). The two classes of CANs, relying on either a dissociative or an associative bond exchange mechanism, are reviewed. In the context of dissociative CANs, a special focus is placed on networks taking advantage of the reversible photo-cycloaddition of anthracenes. Due to the further relevance in this thesis, a particular class of CANs that undergoes thermally triggered associative bond exchanges, vitrimers, is then discussed in detail. The section includes their synthesis, available bond exchange chemistries, and most importantly the unique rheological properties. Finally, vitrimer(-like) networks from classical rubbers are presented, the preparation of filled vitrimers, and the characterisation of vitrimers with specific emphasis on the analysis of the topology freezing transition with its characteristic temperature  $T_v$ .

**Chapter 3** explores the design of (photo-)reversible elastomeric networks from HXNBR rubber that rely on a dissociative bond exchange mechanism. In particular, the rubber was endowed with anthracene moieties that were covalently attached to its carboxylic acid groups. Afterwards, photodimerisation of the pending anthracenes was exploited for covalent cross-linking of the linear rubber chains. Controlled cleavage of the linkages was achieved by either UV-light or heat, highlighting a dual-responsiveness of the networks. Besides a detailed characterisation of the reversible switching between the cross-linked and decrosslinked state by UV-Vis spectroscopy and low-field NMR spectroscopy, the resulting impact on the mechanical properties was studied by means of dynamic mechanical analysis. Importantly, a repeatable switching over multiple cross-linking and cleavage cycles has been demonstrated. Finally, the materials were shown to exhibit switchable bonding capabilities, which makes these rubbery networks promising candidates as dry adhesives with reversible adhesion properties.

**Chapter 4** presents research about the successful incorporation of vitrimer chemistry into HXNBR rubber, a matrix used for the first time in this context. Curing of the rubber with a di-epoxide cross-linker yielded chemically cross-linked materials that showed typical characteristics of an elastomer at moderate temperatures. However, due to the special chemical structure of the covalent linkages, these bonds could be effectively exchanged *via* thermo-activated transesterifications when a suitable catalyst was added. The exchangeable nature of the cross-links enabled fast and substantial stress relaxation of the networks at elevated temperature, and shape change experiments further confirmed a thermal adaptability. Moreover, thermal repair capabilities were demonstrated by stress-rupture tests of fractured and subsequently healed samples, and the improvement of adhesion properties by lap shear tests. This approach widened the scope of skeletons in the preparation of vitrimer(-like) elastomers from high molecular weight polymers. The study further paved the way towards the preparation of mendable elastomers from

technically relevant carboxylated rubbers, relying on readily available materials and common compounding techniques employed in rubber industry.

**Chapter 5** describes an approach from unfilled to filled vitrimer-like networks from HXNBR rubber. Choosing a network design that combines filler and cross-linker, curing with epoxy group-functionalised calcium silicate particles (Esilicate) resulted in the formation of exchangeable covalent bonds at the rubber-filler interface. In the presence of a transesterification catalyst, the composites were susceptible to thermo-activated topology rearrangements, enabling a distinctive stress relaxation. The filled networks were characterised in detail regarding their physical properties by tensile testing, dynamic mechanical analysis, and cyclic stress-strain experiments. The results demonstrate that the Esilicate is highly compatible with the present HXNBR and provides a pronounced reinforcement effect due to the strong physical and chemical interactions with the matrix. Nevertheless, the interfacial molecular bond exchanges significantly alter the viscoelastic properties of the composites, which was shown by creep and cyclic creep-recovery experiments. Importantly, chemically cross-linked yet dynamic composites were obtained even at high filler loadings (30 phr), which is of great importance for structural applications of rubbers where reinforcement is essential to satisfy the high demands on the mechanical properties. In general, the strategy pursued constitutes a straightforward, scalable, and solvent-free procedure towards vitrimer-like composites from a commercial rubber.

**Chapter 6** presents a newly established procedure for the analysis of the vitrification transition temperature ( $T_v$ ) of vitrimers. Regarding possible structural applications of vitrimers, precise knowledge about the vitrification transition is crucial, especially considering the upper service temperature of these novel polymers. Commonly, the network dynamics of vitrimers is characterised by stress relaxation measurements. However, this procedure relies on measurement data acquired at temperatures (far) above  $T_v$ , wherefore the mathematically obtained values for  $T_v$  are hypothetical. Alternatively, so-called dilatometry is a regularly conducted analysis method for the characterisation of the vitrification transition and the  $T_v$  of vitrimers. Interestingly, this analysis method shows significant discrepancies in values of  $T_v$  when comparing to the data from stress relaxation experiments. Consequently, a comprehensive investigation of the creep behaviour as a function of temperature has been conducted on different epoxy-vitrimers by elongational creep measurements. Varying the external force applied on the samples, a clear stress dependency of the onset temperature of plastic flow was derived from the creep data. It was concluded that only the application of the proper measurement parameters, which is a suitable external force, allows receiving precise values for the  $T_v$  of vitrimers. The study gave highly interesting insights into the analysis of vitrimers applying dilatometry, highlighting that this novel and facile measurement routine enables the direct analysis of the  $T_v$ , and further indicating possible inaccuracies of  $T_v$  values reported in literature.

**Chapter 7** provides general conclusions and discusses some perspectives.



### 1.3 References

- 1 a) C. A.I. Guise-Richardson, *Technology and Culture*, 2010, 51, 357–387; b) C. Goodyear, *Gum-elastic and Its Varieties: With a Detailed Account of Its Applications and Uses, and of the Discovery of Vulcanization*, Published for the author, 1853.
- 2 a) S. Kohjiya, ed., *Chemistry, manufacture and applications of natural rubber*, Elsevier/Woodhead Publ, Amsterdam, 2014; b) D. C. Blackley, *Synthetic Rubbers: Their Chemistry and Technology*, Springer Netherlands, Dordrecht, 1983.
- 3 P. G. de Gennes, *Scaling Concepts in Polymer Physics*, Cornell University Press, 1979.
- 4 F. Liu and M. W. Urban, *Progress in Polymer Science*, 2010, 35, 3–23.
- 5 a) C. J. Kloxin, T. F. Scott, B. J. Adzima and C. N. Bowman, *Macromolecules*, 2010, 43, 2643–2653; b) C. N. Bowman and C. J. Kloxin, *Angewandte Chemie*, 2012, 51, 4272–4274.
- 6 W. Denissen, J. M. Winne and F. E. Du Prez, *Chemical science*, 2016, 7, 30–38.
- 7 J. M. Winne, L. Leibler and F. E. Du Prez, *Polym. Chem.*, 2019, 10, 6091–6108.
- 8 X. Chen, M. A. Dam, K. Ono, A. Mal, H. Shen, S. R. Nutt, K. Sheran and F. Wudl, *Science*, 2002, 295, 1698–1702.
- 9 a) J. R. Jones, C. L. Liotta, D. M. Collard and D. A. Schiraldi, *Macromolecules*, 2000, 33, 1640–1645; b) Y. Chujo, K. Sada, R. Nomura, A. Naka and T. Saegusa, *Macromolecules*, 1993, 26, 5611–5614.
- 10 a) L. A. Connal, R. Vestberg, C. J. Hawker and G. G. Qiao, *Adv. Funct. Mater.*, 2008, 18, 3315–3322; b) Y. Zheng, M. Micic, S. V. Mello, M. Mabrouki, F. M. Andreopoulos, V. Konka, S. M. Pham and R. M. Leblanc, *Macromolecules*, 2002, 35, 5228–5234; c) J.-F. Xu, Y.-Z. Chen, L.-Z. Wu, C.-H. Tung and Q.-Z. Yang, *Organic letters*, 2013, 15, 6148–6151; d) J. van Damme, O. van den Berg, J. Brancart, L. Vlamincx, C. Huyck, G. van Assche, B. van Mele and F. Du Prez, *Macromolecules*, 2017, 50, 1930–1938.
- 11 D. Montarnal, M. Capelot, F. Tournilhac and L. Leibler, *Science*, 2011, 334, 965–968.
- 12 a) J. C. Capricho, B. Fox and N. Hameed, *Polymer Reviews*, 2020, 60, 1–41; b) W. Alabiso and S. Schlögl, *Polymers*, 2020, 12; c) T. Liu, B. Zhao and J. Zhang, *Polymer*, 2020, 194, 122392.
- 13 a) M. Hayashi, *Polymers*, 2020, 12, 1322; b) Z. P. Zhang, M. Z. Rong and M. Q. Zhang, *Progress in Polymer Science*, 2018, 80, 39–93.
- 14 L. Imbernon, S. Norvez and L. Leibler, *Macromolecules*, 2016, 49, 2172–2178.
- 15 Y. Liu, Z. Tang, Y. Chen, C. Zhang and B. Guo, *ACS applied materials & interfaces*, 2018, 10, 2992–3001.
- 16 B. L. Chan, D. J. Elliott, M. Holley and J. F. Smith, *J. polym. sci., C Polym. symp.*, 1974, 48, 61–86.
- 17 a) *Natural rubber global production 2019*, Statista, available at: <https://www.statista.com/statistics/275387/global-natural-rubber-production/>, accessed 11 August 2020; b) *Global synthetic rubber production 2019*, Statista, available at: <https://www.statista.com/statistics/280536/global-natural-rubber-production/>, accessed 11 August 2020.
- 18 W. Post, A. Susa, R. Blaauw, K. Molenveld and R. J. I. Knoop, *Polymer Reviews*, 2020, 60, 359–388.
- 19 M. D. Stern and A. V. Tobolsky, *The Journal of chemical physics*, 1946, 14, 93–100.

# Chapter 2

## THEORETICAL BACKGROUND

### 2.1 Nitrile butadiene rubber (NBR)

#### 2.1.1 Synthesis, properties, and types of NBR rubber

Nitrile butadiene rubber (NBR) was invented in 1934 and constitutes an unsaturated copolymer of acrylonitrile and 1,3-butadiene. An alteration of NBR is carboxylated NBR rubber (XNBR), which is a terpolymer composed of acrylonitrile, butadiene, and monomers containing carboxylic acid groups, such as acrylic or methacrylic acid. Both of these polymer types are produced by emulsion polymerisation.<sup>1</sup> Through selective catalytic hydrogenation, chemical modifications of NBR and XNBR are obtained, namely HNBR and HXNBR.<sup>2</sup> Carboxylation and/or hydrogenation enhance the properties of NBR and the rubber can meet a more specified range of physical and chemical requirements, thereby extending its fields of application.<sup>3</sup>

NBR and its chemical modifications (Figure 1) exhibit an excellent chemical resistance to aliphatic hydrocarbon oils and fuels. The physical and chemical properties of NBR can be adjusted by the polymer's monomer composition. An important parameter is the acrylonitrile (ACN) content, which is classified into three categories, high nitrile (>45% ACN), medium nitrile (30-45% ACN), and low nitrile (<30% ACN). The chemical resistance increases with the ACN content due to the polar nature of the nitrile groups. Moreover, tensile strength, hardness, abrasion and heat resistance improve with the ACN content, while low temperature flexibility and compression set get poorer. The mechanical properties of XNBR are usually superior in comparison to NBR, and a higher continuous service temperature can be achieved. By hydrogenation of unsaturated and rigid C-C double bonds in NBR and XNBR, the mobility of the polymer chains increases which leads to lower  $T_g$  for HNBR and HXNBR rubbers. Various mechanical properties are positively affected through hydrogenation, such as tensile strength and ultimate elongation. The same applies to chemical and heat resistance. Due to the saturation of the C-C double bonds the polymer is less susceptible to ozone and oxidative degradation, and to ageing processes in general.<sup>4,5</sup>

NBR rubber is widely employed in the automotive and aeronautical industry, which is also because of its applicability in a wide temperature range (-50 to 150 °C). Common applications include hoses and seals, particularly in contact with chemicals. Others are rubber belts, O-rings, and gloves. For hydrogenated and carboxylated NBR types the scope of applications does not change radically. These modifications are simply more suitable for extreme operating conditions where a higher resistance to ozone, temperature, UV-light, and oxidative processes is required, as well as enhanced elastic resilience, abrasion and wear resistance.<sup>3,5</sup>

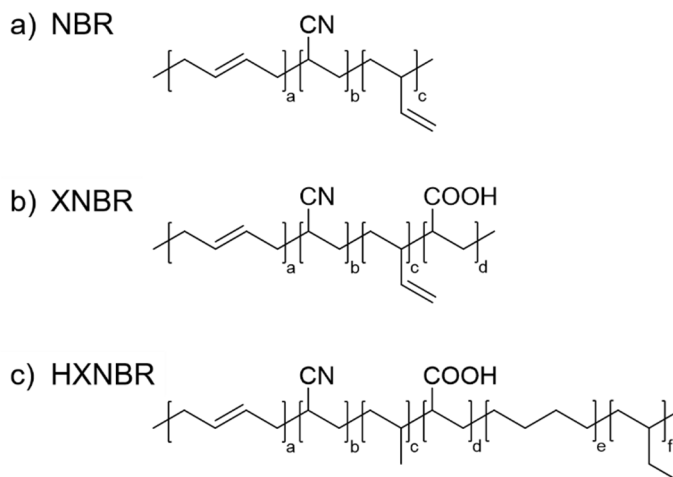


**Figure 1.** Chemical structures of (a) nitrile butadiene rubber (NBR), (b) carboxylated NBR (XNBR), and (c) hydrogenated and carboxylated NBR (HXNBR).

### 2.1.2 Cross-linking of NBR rubber and its derivatives

NBR rubber and its derivatives, HNBR, XNBR, and HXNBR contain different reactive functional groups in the polymer backbone or as pending side chain that can participate in cross-linking reactions to obtain the respective elastomeric networks. In NBR, these are nitrile groups ( $-\text{CN}$ ) and carbon-carbon ( $\text{C}-\text{C}$ ) double bonds, and for (H)XNBR additionally carboxylic acid groups ( $-\text{COOH}$ ). Regarding covalent cross-linking, the  $\text{C}-\text{C}$  double bonds and  $-\text{COOH}$  groups are of relevance. Alternatively, the  $-\text{COOH}$  moieties may be exploited for the formation of ionic cross-links. By the selection of a particular curing system or the combination of various, the polymer can be endowed with different types of cross-links that vary in structure and quality. The type, number and composition of the linkages in turn largely determine the final material properties of the elastomers and their alteration under service conditions.

The most widely used cross-linking method for rubbers is sulphur curing, since the largest class of rubbers are diene rubbers with high unsaturation (e.g. SBR, NR, IR, BR, NBR)<sup>a</sup>. Regarding NBR and its derivatives, sulphur curing is limited to (partially) unsaturated rubbers (NBR and XNBR) because of the necessity of  $\text{C}-\text{C}$  double bonds, more specifically allylic hydrogen atoms. In contrast, organic peroxide curing is also applicable to hydrogenated and thus (fully) saturated types of NBR rubber (HNBR and HXNBR). Commercially, rubbers with low (e.g. EPDM<sup>b</sup>) and without alkenic unsaturation (e.g. EPM<sup>c</sup>, silicone, epoxy, acrylate, polyurethane rubbers) may be cross-linked relying on organic peroxides. Considering the industrial relevance, the chemistry of both sulphur and peroxide curing is discussed in more detail below.

<sup>a</sup> SBR: styrene-butadiene rubber; NR: natural rubber; IR: polyisoprene rubber; BR: polybutadiene rubber; NBR: acrylonitrile-butadiene rubber.

<sup>b</sup> EPDM: ethylene-propylene-diene copolymer rubber.

<sup>c</sup> EPM: ethylene-propylene rubber.

Of the various covalent curing techniques exploiting the carboxylic acid moieties in carboxylated NBR derivatives, here only the usage of epoxides will be discussed due to the further major importance in the course of this thesis. Other curing strategies involving the formation of covalent bonds across the –COOH groups include amines forming amide cross-links<sup>6</sup>, alcohols forming ester linkages<sup>7</sup>, isocyanates yielding amide (and acyl urea) bonds *via* mixed anhydrides and CO<sub>2</sub> release<sup>8,9</sup>, and carbodiimides generating acyl urea cross-links<sup>8</sup>.

Besides the formation of covalent linkages using epoxides, carboxylated NBR derivatives are susceptible to chemical cross-linking through ionic bonding across the pending carboxylic acid moieties. The interaction with metal cations results in ionic associations acting as cross-links. This type of network formation is also discussed in this section.

### *Sulphur cross-linking*

In general, sulphur-based curing procedures rely on the availability of C–C double bonds in rubbers, which exist in NBR and XNBR. More specifically, sulphur cross-linking usually refers to the application of accelerated sulphur curing systems, as opposed to sulphur-only curing. Accelerated implies the usage of both accelerators and activators and thus, it is more efficient in terms of curing temperature and time as well as the amount of sulphur required.<sup>10</sup> Typical organic accelerators are derived from sulfonamides and thiazoles, and are classified into primary and secondary accelerators, whereby mostly a combination of those is used.<sup>11</sup> For further enhancement of sulphur curing, activators are added, with zinc oxide and stearic acid as the most common ones.<sup>11,12</sup> The composition of the applied sulphur curing system (sulphur + accelerator + activator) significantly determines the resulting network structure, and consequently the physical and chemical properties of the respective elastomer.<sup>13</sup>

The cross-linking process for diene rubbers applying accelerated sulphur curing is complex and involves multiple reaction steps (Figure 2a). The following generally accepted mechanism is proposed in literature, although the mechanistic aspects are not yet fully understood. In a first step, the formation of an active accelerator complex takes place upon the interaction between accelerators and activators. Second, an active sulphurating agent is generated by the reaction between the active accelerator complex and elemental sulphur (or a sulphur donor). Next, the active sulphurating agent substitutes an allylic hydrogen atom at the polymer chain (Figure 2c) and by this, sulphur is transferred to the rubber backbone forming a cross-link site, the so-called rubber-bound intermediate. The subsequent reaction with a second polymer chain creates the cross-link, which initially consists of a polysulphide structure. In a final step, the shortening and alteration of the polysulphide cross-links occurs through several competing reactions, which are desulphuration, thermal decomposition, and S-S exchanges.<sup>14</sup> An important parameter that largely determines the final cross-link composition of networks is the ratio between accelerator and sulphur. A high ratio promotes desulphuration and suppresses thermal decomposition, yielding stable monosulphides and thus, a highly-cross-linked as well as heat-resistant network with excellent physical properties (so-called efficient vulcanisation system, as opposed to conventional vulcanisation).

It should be mentioned that di- and poly-sulphidic linkages and other species formed (Figure 2b) are still reactive towards secondary reactions, wherefore the physical properties of sulphur cured networks cannot be considered set after their preparation. Moreover, di- and poly-sulphidic cross-links are known to undergo exchange reactions *via* bond-breakage and bond-forming reactions, thereby enhancing the stress relaxation behaviour of the materials.<sup>15</sup>

Noteworthy, the described reaction scheme was originally proposed for NR, and certain differences exist in sulphur curing of BR rubbers. In presence of radical species originating from the sulphur curing system and at high temperatures, BR rubber is susceptible to thermal cross-linking *via* carbon-carbon bonds. Moreover, the extent of cis-trans isomerisation is higher than for NR. In general, for rubbers other than NR the particular reaction scheme may deviate distinctively from Figure 2a, especially in the later stages of the curing process.<sup>14</sup>

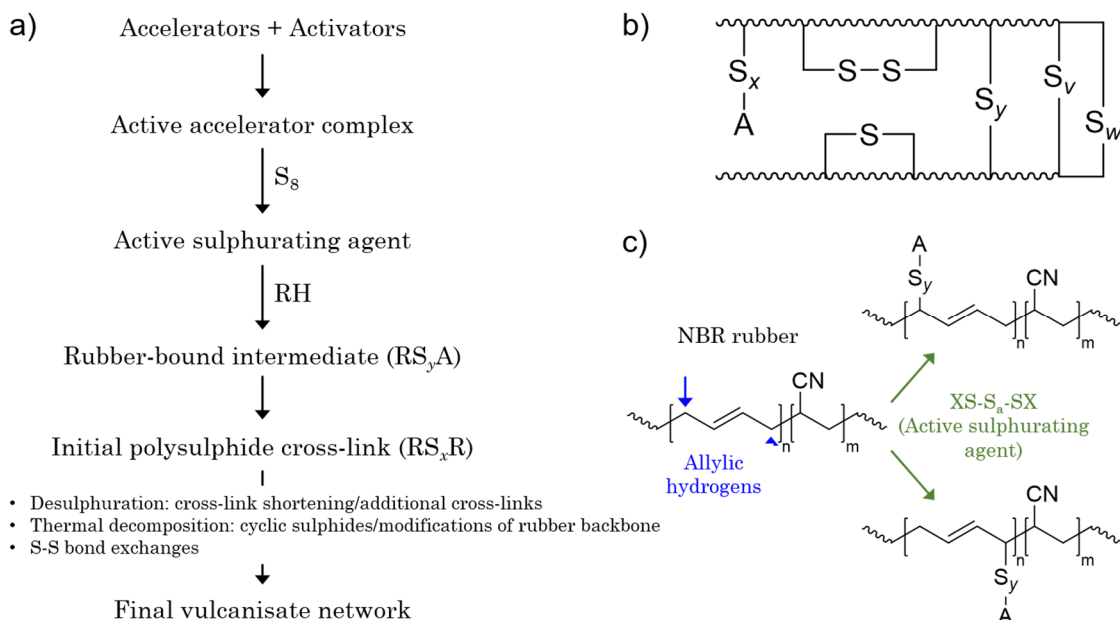


**Figure 2.** Schematic representation (a) of the reactions in accelerated sulphur curing of diene rubbers, and (b) of the different sulphur-containing species formed in the course of curing (from left to right: accelerator-terminated pendant sulphidic group; cyclic sulphides; mono-, di- and poly-sulphidic cross-links; vicinal sulphur cross-links.  $v, w, x, y = 1-6$ ;  $R$ =rubber chain;  $H$ =usually an allylic hydrogen atom;  $A$ =accelerator fragment), and (c) of the methylene groups on NBR rubber backbone for potential attack by the active sulphurating agent. Schemes adapted from literature.<sup>14</sup>

### Peroxide cross-linking

As opposed to sulphur curing, peroxide curing systems do not rely on C–C double bonds, more precisely on allylic hydrogen abstraction. Thus, peroxides are applicable to rubbers comprising saturated as well as unsaturated polymer backbones.<sup>16</sup> Peroxides are further the cross-linking agents of choice to vulcanise blends consisting of both saturated and unsaturated rubbers.<sup>17</sup>

Peroxide cross-linking exhibits some advantages over sulphur curing, such as the possibility to use higher processing temperatures, vulcanisation without reversion, and

most importantly superior heat resistance and better thermo-oxidative ageing properties of the final networks. This is in particular true for saturated rubbers, with the effect relying on the higher dissociation energy of C–C bonds (i.e. cross-links) compared to S–S and C–S bonds in sulphur cross-links. On the other hand, sulphur-cured networks usually display superior tensile and tear strength, elasticity, and dynamic behaviour.<sup>17</sup> Moreover, peroxide curing is sensitive to oxygen due to the presence of reactive carbon-centered polymer radicals. The reaction with oxygen (oxygenation) leads to chain scission reactions and consequently to polymer degradation.<sup>18</sup> Peroxides may further be sensitive to fillers or other additives (e.g. antidegradants) present in the rubber compound, since peroxide derived radicals can also abstract hydrogen atoms from these sources instead of the rubber backbone (so-called cure interference). These processes are referred to as radical transfer and are determined by the particular C–H bond strengths.<sup>17</sup>

Various classes of organic peroxides are available for peroxide curing of rubbers, with dialkyl and diaryl peroxides as the most frequently used.<sup>19</sup> The key criterion for the selection of a suitable peroxide for a specific application is the half-life<sup>d</sup>, which serves as a measure of the optimum cure temperature and reflects the reactivity of a peroxide.

Unlike for accelerated sulphur vulcanisation, the chemistry of peroxide curing is well established. The curing process<sup>17,19</sup> (Figure 3) starts with the thermally induced homolytic cleavage of the peroxide molecules, yielding peroxide free radical species. Next, two potential reactions with the rubber backbone can occur. The radicals either abstract hydrogen atoms from the polymer chains (abstraction mechanism) or add to C–C double bonds in case of unsaturated rubbers (addition mechanism). Noteworthy, peroxide radicals may undergo more hydrogen abstraction or add to C–C double bonds depending on their chemical nature (e.g. steric hindrance, bond dissociation energy with hydrogen), and thereby strongly influence the final network properties.<sup>20</sup> Moreover, allylic hydrogens are more easily abstractable as for example secondary and primary hydrogen atoms.<sup>14</sup> Either way, both mechanisms yield reactive carbon-centered radicals at the polymer chain (polymer-radical). Regarding the desired formation of covalent carbon-carbon cross-links, two polymer radicals must finally recombine. For saturated rubbers, this is the only mechanism towards cross-link formation and thus usually yields low cross-link efficiencies (or peroxide efficiency<sup>e</sup>) that amount to a maximum of 1. Normally, in such systems the number of cross-links formed is directly proportional to the quantity of decomposed peroxide. However, in unsaturated rubbers a polymer radical may cause more than one covalent cross-link by adding to a C–C double bond (addition mechanism), and consequently generates another polymer radical capable of forming a cross-link. Thus, the peroxide efficiency in unsaturated rubbers usually exceeds the value 1 by far<sup>21</sup>, leading to high cross-link densities. However, for instance, the peroxide efficiency for cross-linking of BR was reported to be higher than 1 ( $> 10$ )<sup>22</sup>, whereas it was found to be about 1 in NBR<sup>23</sup>. While in the former the addition mechanism is prevailing, for the latter hydrogen abstraction is predominant.<sup>23</sup> This is due to the high number of available alkenyl moieties and the decrease in double bond reactivity by electron withdrawing nitrile groups,

---

<sup>d</sup> Time required for half of the initial peroxide quantity to decompose at a given temperature. Usually presented as the temperature at which the half-life amounts to a certain time (e.g. 1 h).<sup>17</sup>

<sup>e</sup> Number of moles of chemical cross-links formed from a mole of reacted peroxide.<sup>17</sup>

respectively. In this context, it should also be mentioned that pendant vinyl moieties are more susceptible to addition reactions than in-chain C–C double bonds.<sup>24</sup> Besides the cross-linking reaction, several competing side reactions occur in peroxide curing systems, such as main chain scission, disproportionation, and as stated above oxygenation and radical transfer. In order to overcome the kinetically favored side reactions and obtain effectively cross-linked networks, very high concentrations of reactive radical species are required. Similar to the role of activators and accelerators for sulphur curing, the employment of co-agents<sup>f</sup> in peroxide curing is common. Their application is of particular interest in saturated rubbers and in systems prone to side reactions. In general, co-agents enhance productive radical reactions (i.e. peroxide efficiency) and by this lead to increased cross-link densities in the final vulcanisate. Furthermore, significant beneficial effects on the physical properties of rubber networks have been demonstrated, and today the knowledge about co-agent performance is recognised as fundamentally important to understand and tailor structure-property relationships in peroxide cured rubber networks.<sup>18,25</sup>

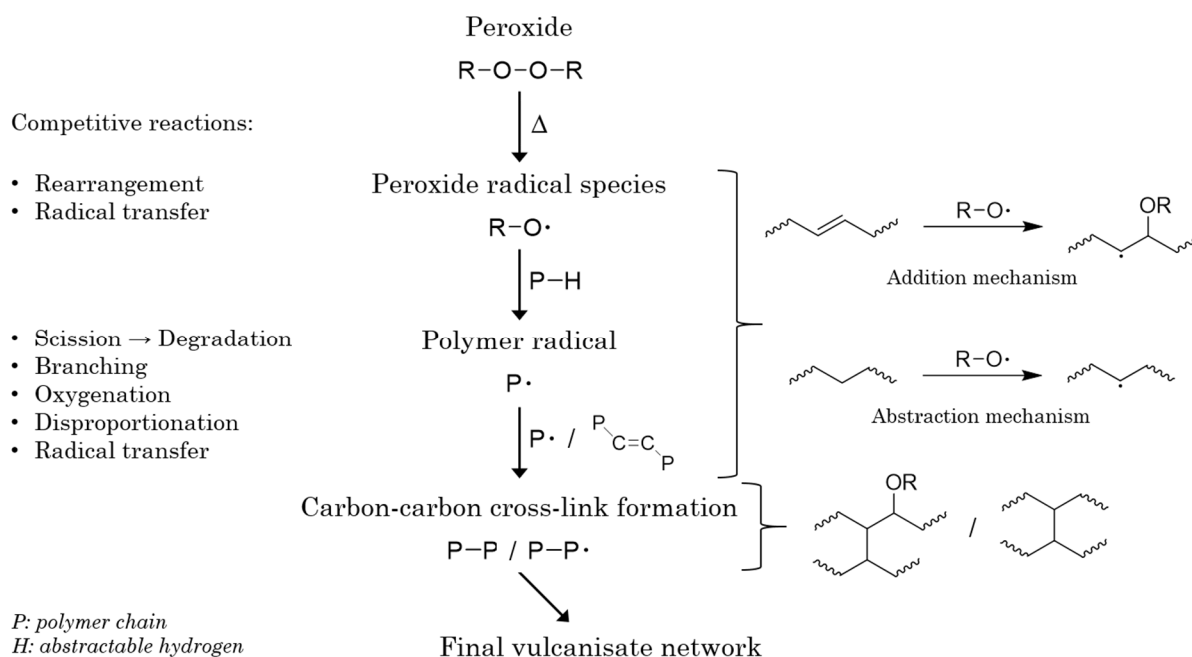


**Figure 3.** Overview of reactions involved in the curing of rubbers with saturated and unsaturated backbones using organic peroxides in absence of co-agents. Scheme adapted from literature.<sup>17,18</sup>

### Cross-linking with epoxides

The introduction of carboxylic acid groups into NBR rubber (XNBR and HXNBR) provides the polymer with additional cross-link sites. The –COOH moieties are particularly interesting because they can be exploited for both covalent and ionic cross-link formation. In terms of covalent curing, the application of epoxides is an attractive strategy.

<sup>f</sup> Co-agents are multifunctional organic molecules that are highly reactive towards free radicals.<sup>17</sup>

1,2-epoxides are powerful building blocks in organic chemistry. The three-membered ring is highly reactive and the reaction with various nucleophiles is well studied.<sup>26</sup> The reaction with carboxylic acid groups as the nucleophile plays an important role in polymer industry and yields hydroxyalkyl esters.<sup>27</sup> Usually, catalysis is applied to obtain reasonable reaction rates, to avoid high curing temperatures, and to decrease the proportion of side reactions. Thereby, both acid and base catalysis is applicable.<sup>28</sup> For base catalysis, an anionic mechanism is anticipated, and common base catalysts include tertiary amines and imidazoles.<sup>28,29</sup> Furthermore, metal salts<sup>30</sup> were also demonstrated to be efficient catalysts, in particular zinc salts, which show a tunable behaviour by the choice of the counterion<sup>28</sup>. The epoxy-carboxyl reaction follows a nucleophilic ring opening reaction, and the different functional groups evolving in the course of the reaction lead to various competing side reactions.<sup>27,31</sup> Relying on catalysis, these side reactions can be controlled and largely eliminated.<sup>32</sup> Without catalyst, four main reactions can occur (Figure 4). Ideally, in the case of stoichiometric amounts of epoxide and carboxylic acid functions, only hydroxyalkyl esters are formed *via* addition esterification (Figure 4-i). The resulting hydroxyl groups are preferentially of either primary (S<sub>N</sub>1 product) or secondary (S<sub>N</sub>2 product) nature, depending on the reaction conditions (acidic catalysis: S<sub>N</sub>1; basic catalysis: S<sub>N</sub>2).<sup>32</sup> As a consecutive reaction, etherification (i.e. epoxy homopolymerisation) may take place by the reaction between an initially formed β-hydroxyl group and another oxirane ring (Figure 4-ii). This reaction pathway is of greater significance in the case of an excess of epoxide as well as under acidic conditions.<sup>28</sup> A further (side) reaction that normally requires high temperatures is condensation esterification, yielding diesters (Figure 4-iii). This is a result of the reaction of hydroxyl groups of initially formed monoesters with a free carboxylic acid. However, in presence of base catalysis the reaction rate of the desired nucleophilic addition of carboxylic acids to epoxides is very fast and thereby suppresses esterification (the same applies in principle to etherification). Finally, in the presence of (formed) water, epoxides can undergo hydrolysis that generates diols, albeit this reaction is of minor relevance (especially in open systems) (Figure 4-iv).

Considering the reaction of stoichiometric quantities of telechelic diepoxides and dicarboxylic acids applying appropriate catalysis, essentially linear polyhydroxyalkyl esters would be formed. In the interest of three-dimensionally covalently cross-linked networks, esterification and etherification are not disadvantageous, but instead necessary.<sup>27,33</sup> Otherwise, polyfunctional monomers have to be employed.

Another potential reaction in carboxylic acid-epoxy networks is transesterification<sup>g,34</sup> (Figure 4 v), which can significantly alter the network structure by increasing the number of cross-links and the systems heterogeneity.<sup>33,35</sup> Importantly, this reaction can take place at both times during network synthesis and afterwards in the cured material when already all epoxide or carboxyl groups have been consumed. To ensure that the reaction proceeds significantly fast, the usage of catalysts is essential.<sup>36</sup> For instance, in networks from telechelic diepoxides and di- or tricarboxylic acids with the carboxylic acid groups and epoxide groups in stoichiometry, two linear (β-hydroxyl) monoesters are converted into a terminal glycol fragment and a branching diester unit (disproportionation reaction).

---

<sup>g</sup> Transesterification is an exchange reaction where an ester is transformed into another through interchange of the alkoxy moiety.<sup>34</sup>



While transesterifications increase the cross-link density, however, the quantity of pendant chains increases as well, generating a sol fraction.<sup>33,37</sup>

Regarding rubbers, the reactivity of the oxirane ring towards carboxylic acid groups can be exploited for the cross-linking of carboxylated polymers by multifunctional epoxides.<sup>8,38</sup> Suitable epoxides include low molecular weight compounds<sup>8</sup>, epoxy resins<sup>38</sup>, and epoxidised oils<sup>28,39</sup>. Alternatively, the usage of modified filler particles may be attractive.<sup>40</sup> Such particles comprise reactive organic surface moieties, for instance epoxy or amino groups. This approach not only allows the covalent attachment of the filler to the polymer backbone, but furthermore the combination of cross-linker and filler in a single chemical compound.

Besides catalysis, an important influence factor in the reaction kinetics is the epoxide's molecular structure, more specifically the chemical neighbourhood of the oxirane ring.<sup>41,42</sup> For instance, ether functions in proximity to the oxirane ring were reported to have a tremendous activating effect on the nucleophilic attack by acids and amines. Moreover, the proportion of side reactions and thus the selectivity of the reaction is affected by the oxirane's neighbourhood as well.<sup>41</sup>

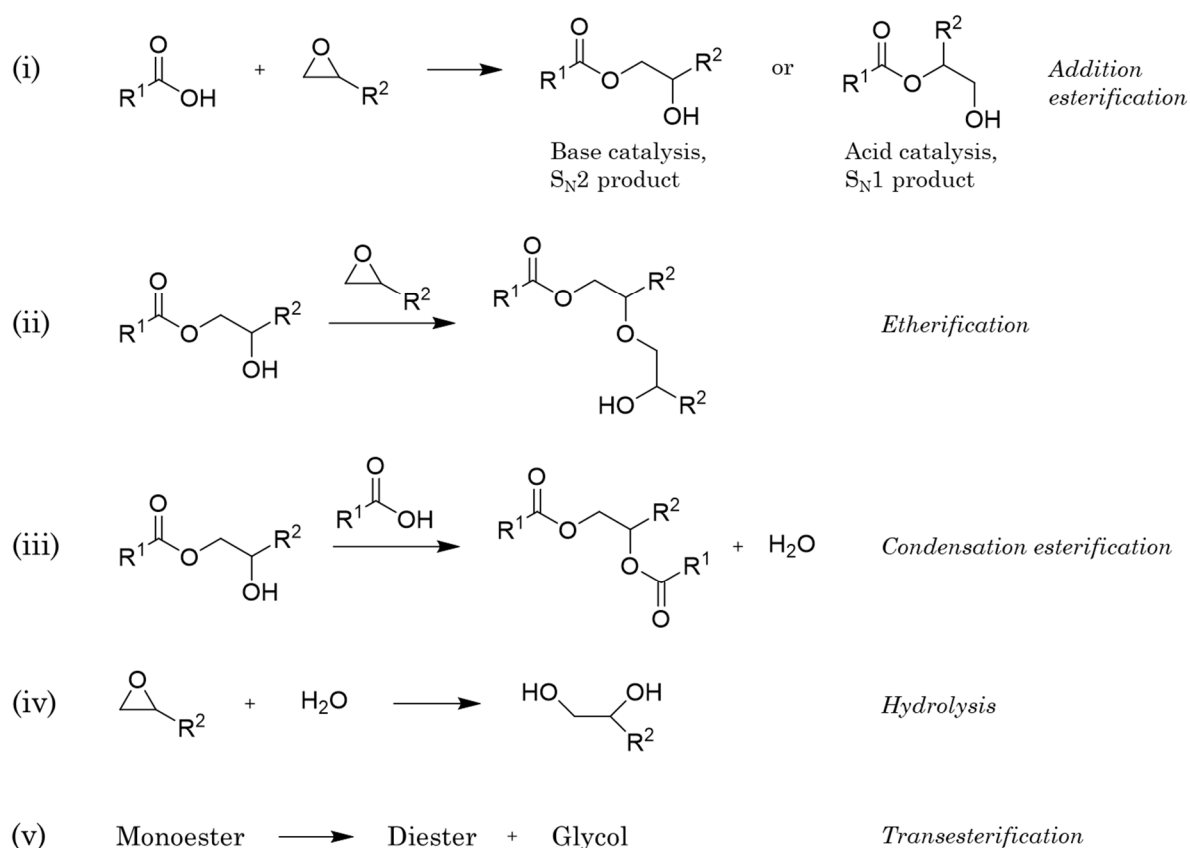


**Figure 4.** Possible reactions in the network formation from carboxylic acids and epoxides: (i) addition esterification between epoxide and carboxylic acid under base or acid catalysis; subsequent (ii) etherification with epoxide or (iii) esterification with carboxylic acid; (iv) hydrolysis of epoxide in presence of water; (v) transesterification reaction causing disproportionation of monoester. Scheme adapted from literature.<sup>27,33</sup>

*Ionic interactions/cross-linking in carboxylated NBR rubber*

Confined to carboxylated types of NBR rubber (XNBR and HXNBR), the pendant carboxylic acid groups constitute an ionisable functionality. As an alternative to covalent curing, these moieties can be exploited for the formation of ionic cross-links, which are a type of non-covalent chemical bonds. Solely ionically cross-linked carboxylated rubbers are referred to as ionomers<sup>h</sup> or ionic elastomers and belong to the group of thermoplastic elastomers.<sup>44</sup>

The carboxylic acid groups that are randomly distributed along the polymer backbone allow for ionic interactions with metal cations, and the respective carboxylic salt formed then acts as ionic cross-link site. Upon the introduction of metal cations into the carboxylated polymer so-called neutralisation occurs, resulting in ion pairs.<sup>45</sup> The association of two ion pairs (dimer) represents the simplest form of polymer chain interaction in ionic elastomers. Depending on the cation concentration (and a number of other factors)<sup>46</sup> different assemblies of structures may be formed.<sup>47,48</sup> Through association/aggregation of ion pairs, first ionic multiplets are generated and eventually larger ionic clusters, acting like multifunctional cross-links (Figure 5a). Clusters are an association of multiplets and manifest as an ionic microphase (eventually with its own  $T_g$ ), typically leading to phase separation and thus, polymer chain mobility gradients across the material.<sup>45</sup> All variants of ionic aggregates act as physical cross-links, however, only clusters additionally as reinforcing fillers, and thereby largely determine the ionomer's physical properties.<sup>49</sup>

Various mono- (e.g. lithium and sodium)<sup>8,50</sup> or multivalent metal cations are capable of ionic cross-link formation, whereas most are divalent in nature and originate for example from metal oxides or metal salts. While ionomers from zinc<sup>51,52</sup> are the most commonly encountered, other metal cations that have been reported actively in the cross-linking of carboxylated rubbers include calcium, magnesium, and aluminium.<sup>44,53</sup> The type and concentration of cation affects the bond strength, the cure rate, matrix compatibility, and further influences size and morphology of the ionic aggregates by determining the volume and surface area of the ion pair.<sup>8,45,54,55</sup> Regarding ionomer formation from carboxylated NBR rubbers, mostly zinc oxide is applied for polymer neutralisation.<sup>56,57</sup> Figure 5b displays the formation of metal carboxylate salt in XNBR rubbers on the example of divalent zinc cations. Depending on the ZnO concentration, different local structures of zinc carboxylate interaction may be generated.<sup>57,58</sup> Usually, the carboxylic acid moieties are partially to fully neutralised<sup>58,59</sup>, and the physical properties of ionomers were reported to undergo an optimum with increasing metal ion content and decrease thereafter. This may be attributed to a weakened ionic microphase by agglomeration of the ionic curing agent arising above a certain metal ion loading.<sup>60</sup>

In contrast to chemical bonds, the ionic domains in ionomers are not permanent in nature but thermolabile, wherefore ionomers are considered as viscoelastic liquids when heated.

---

<sup>h</sup> A polymer composed of ionomer molecules with the latter being macromolecules in which a small but significant proportion (<15%) of the constitutional units have ionisable or ionic groups, or both.<sup>43</sup>

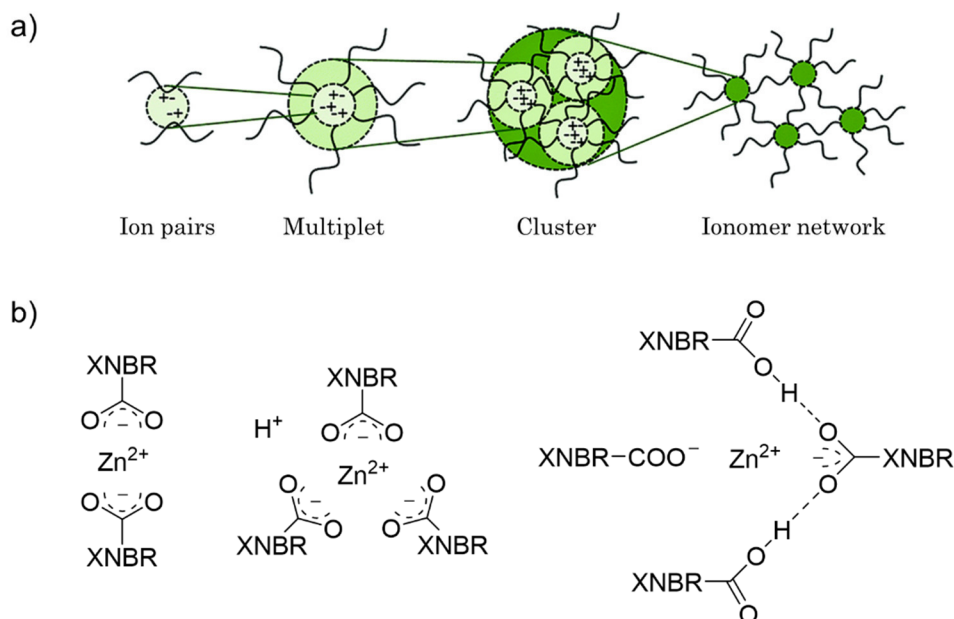


**Figure 5.** Schematic illustration (a) of the hierarchy of structures acting as physical cross-link points in ionic elastomers resulting from ionic aggregation, and (b) of possible ionic structures formed in the neutralisation of pending carboxylic acid groups in carboxylated NBR rubbers with divalent zinc ions (from left to right: tetracoordinated zinc carboxylate; hexacoordinated zinc carboxylate; zinc acid salt). Schemes adopted from literature.<sup>57,61</sup>

Rigid at low temperature, ionic aggregates (i.e. multiplets and clusters) constitute reversible associations at elevated temperatures, inducing thermoplastic behaviour that permits melt processing. Besides heat, solvents or stress are potential triggers of the ionic dissociation-association equilibrium. This process is referred to as ion hopping, which is more precisely the exchange of ion pairs among ionic domains.<sup>62</sup> Experimentally, the transient nature can be displayed by analysis methods relying on oscillatory (e.g. DMA) or steady deformations (e.g. stress relaxation). For instance, in DMA measurements the loss factor ( $\tan\delta$ ) undergoes two transitions, which are the glass transition temperature ( $T_g$ ) at low temperatures and an ionic transition<sup>45</sup> ( $T_i$ ) occurring at higher temperatures. The network rearrangements result in an improved stress relaxation compared to covalently cross-linked elastomers<sup>47,63</sup>, whereas both the ionic content<sup>50</sup> and the ion's valency<sup>51,54</sup> affect the transient behaviour by controlling the association life-time<sup>i</sup>. The migration of ionic bonds (i.e. ion hopping) further enhances the tensile properties distinctively.<sup>60</sup> Besides exceptional mechanical properties, reprocessability<sup>64</sup>, recyclability<sup>65</sup>, and self-healing<sup>66</sup> abilities were demonstrated for ionomers. It should be noted that the overall cross-link density of ionomers remains unaffected by application of the particular stimulus, since after its removal the ionic structures are reformed.<sup>50</sup> Back to either the original multiplet/cluster or involving ion pair migration between nearby ionic aggregates. However, heat-induced transformations of local ionic structures into others (e.g. from tetra- to hexacoordinated metal carboxylate) may also occur.<sup>58</sup>

<sup>i</sup> Average time for an ion pair to reside in an ionic cluster before its dissociation.<sup>50</sup>

However, the thermolability of the physical cross-links in ionomers strongly limits their high-temperature performance. Consequently, the incorporation of covalent bonds is often necessary to ensure good mechanical properties under heat influence, to reduce creep and to increase resistance to solvolysis.

### *Cross-linking relying on (photochemical) cycloadditions*

Photochemistry generally deals with the chemical effects that occur because of the absorption of light by molecules. In terms of organic chemistry, it is commonly associated with the initiation of chemical reactions, resulting from electronic excitation of molecules by the absorption of a photon following the irradiation with light of a particular wavelength. Besides the formation of chemical bonds, also the rearrangement and cleavage of covalent bonds can be accomplished by light. Photochemical reactions offer several attractive features, such as temporal and spatial control, low energy requirement, high reaction rates, solventless processing, and the conduction of reactions otherwise inaccessible by thermal processes.<sup>67</sup> Specifically with regard to a more sustainable material production, the remarkable characteristics of photo-induced reactions are very promising and of increasing scientific interest.

Today, a wide range of photochemical reactions in polymer chemistry is implemented. For instance, photochemistry is a well-known tool for the initiation of polymerisations. The presence of a suitable photoinitiating system allows for a light-induced generation of reactive intermediates or catalysts for further reaction. For this purpose, a vast number of photoinitiators has been developed, yielding radical (Norrish type I and II systems), base (photobase generators, PBGs) or acid (photoacid generators, PAGs) species upon their photo-induced activation/decomposition. These species in turn, enable radical, anionic and cationic photopolymerisations to take place, respectively. Today, even (photoinitiator-free) light-induced step-growth polymerisations are feasible.<sup>68</sup>

Another important application field of photochemistry is the usage of photoresists in photolithographic processes. These light-sensitive materials are of crucial importance in the (micro)electronic industry in the context of positive and negative photoresists for the manufacture of printed circuit boards (PCB) and integrated circuits (ICs).<sup>69</sup>

There exist a few general restrictions of photochemistry in polymer science. For instance, the limited penetration depth of light, in particular of short wavelength (UV) light, which is normally in the range of 10-100  $\mu\text{m}$ .<sup>70</sup> In general, gradients in light intensity (i.e. reaction rate) in illuminated polymeric materials are inevitable. Thus, thick-layered, highly absorptive, opaque or coloured/pigmented polymers are subject to significant constraints in photoinduced processes. Moreover, effects such as photo-darkening<sup>71</sup> and photo-bleaching<sup>72</sup> strongly govern the efficiency of photoreactions. A common tool for the tuning of photo-sensitive reaction mixtures are photosensitisers<sup>73</sup>, which primarily circumvent the problem of absorption at short wavelengths of some molecules by shifting the absorption window towards longer wavelengths. Thereby, the penetration depth may be altered as well. Photosensitisers can also be applied for molecules with low absorption coefficients at their designated excitation wavelengths, or in case of interference with competitive processes, such as fluorescence and trans-cis isomerisation.<sup>74</sup>

It should also be considered that photo-induced reactions involving the generation of reactive intermediates (e.g. radicals, ionic species) proceed much faster compared to reactions where a single photon is directly absorbed by the molecule undergoing the particular photoreaction (e.g. photo-cycloadditions).<sup>75</sup> This so-called secondary amplification is due to the reactive intermediates obtained through the initial (primary) photochemical reaction, which then promote several chemical reactions (e.g. radical-induced chain-growth polymerisation using a photoinitiator).

In the framework of this thesis, the interest in photochemistry arises from photochemical reactions inducing polymer network formation by covalent cross-linking. For instance, this can be realised by attaching photo-active groups to polymer chains. In a next step, the pending moieties can undergo light-induced (dimerisation) reactions forming a covalent bond. In general, there are non-reversible and reversible photocuring chemistries available, whereas here the reversible approaches are of particular interest. Non-reversible strategies include photocuring of acrylates and vinyl groups, thiol-ene/yne reactions, and nitrogen radical cross-linking based on azides or diazirines.<sup>76</sup> Reversible reactions, in particular photocycloadditions, provide a unique concept for the design of covalently cross-linked networks that can revert to the decrosslinked state in a controlled way. In the following, a selection of the most frequently applied (photo)cycloaddition reactions applicable for the reversible cross-linking of polymers are discussed.

Cycloaddition reactions often follow a concerted and thus pericyclic mechanism, meaning that no ionic or radical intermediates are formed in the course of the reaction. Cycloadditions are a powerful tool in the formation of carbon-carbon sigma bonds, and some cycloadditions are reversible (retro-cycloaddition). According to the Woodward-Hoffmann rules and with regard to photochemistry, the  $[2\pi+2\pi]$  and  $[4\pi+4\pi]$  suprafacial-suprafacial (index s) cycloaddition reactions are photochemically allowed. Well-studied reversible  $[2\pi_s+2\pi_s]$  cycloadditions employed in reversibly cross-linked polymers rely on coumarin<sup>77</sup>, cinnamic acid<sup>78</sup>, thymine<sup>79</sup>, and stilbene<sup>80</sup> moieties. Upon exposure to UV-light, dimerisation proceeds *via* the formation of a cyclobutane structure, and the reverse reaction occurs by UV irradiation with shorter wavelengths. The selection of the suitable chemistry for a particular application may be guided by the wavelengths necessary for photocuring and photoscission, the extent of photoreversibility, and the possibility of modifying the chemical neighbourhood of the reactive double bonds by substituents. Moreover, it should be considered that  $[2\pi+2\pi]$  cycloadditions normally are accompanied by trans-cis isomerisation (e.g. cinnamic acid) that adversely affect the efficiency of the photoreaction, with the exception of rigid molecular structures (e.g. coumarin). Another disadvantage of the  $[2\pi_s+2\pi_s]$  photocycloaddition is the requirement of an accurate alignment of the reactive double bonds in order to undergo dimerisation, which decreases the rate and efficiency of the reaction compared to light-induced radical strategies. Figure 6 shows the reversible  $[2\pi_s+2\pi_s]$  photocycloaddition on the example of coumarin dimerisation, and the (reversible) trans-cis isomerisation occurring for cinnamic acid.

On the other hand, suprafacial-suprafacial  $[4\pi+2\pi]$  cycloadditions are thermally allowed. Considered as click reaction<sup>81</sup>, the most prevalent  $[4\pi_s+2\pi_s]$  cycloaddition is the Diels-Alder (DA) reaction that occurs through a concerted mechanism between a conjugated diene and a dienophile. The latter typically bears an alkenyl moiety, and usually comprises an electron-withdrawing substitute. In the course of the reaction, the initial three  $\pi$  bonds

are converted into two  $\sigma$  and one  $\pi$  bond and a cyclohexene derivative is formed. The DA cycloaddition is of great synthetic importance in organic chemistry, and of particular interest in the preparation of (thermoreversible) dynamic covalent networks due to the reversibility of the DA adduct (retro-Diels-Alder reaction).<sup>82</sup> The retro-DA reaction occurs at higher temperatures than the forward DA cycloaddition. The most attractive combination of reactants involves furans and maleimides (Figure 6c), exhibiting relatively low dissociation temperatures ( $\approx 100$  °C) for the retro-DA reaction.<sup>83</sup>

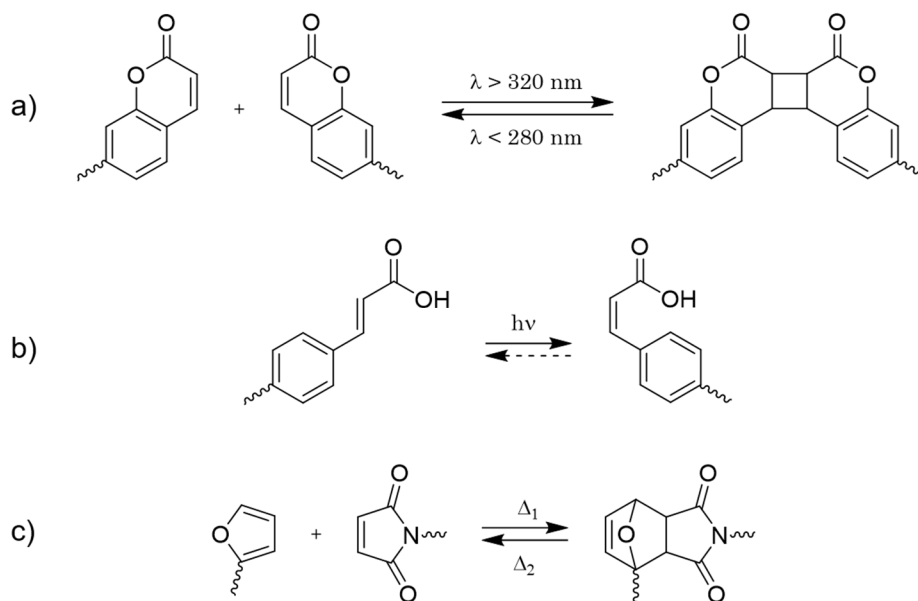


**Figure 6.** Schemes illustrating (a) the reversible  $[2\pi_s + 2\pi_s]$  photocycloaddition of coumarin, (b) the photo-induced trans-cis isomerisation of cinnamic acid, and (c) the reversible thermo-activated  $[4\pi_s + 2\pi_s]$  Diels-Alder cycloaddition reaction between furan and maleimide moieties.

Besides the  $[2+2]$  cycloaddition, another well-studied and versatile photochemical reaction of synthetic interest is the  $[4+4]$  cycloaddition, with anthracene being the most prominent example. In particular, anthracene undergoes photo-cycloaddition forming an anthracene dimer that is photochemically and thermally reversible (Figure 7). Anthracene is very reactive in the 9- and 10-position (meso-positions) and the dimerisation occurs upon exposure to UV-light with a wavelength higher than 300 nm. Upon photochemical excitation and the subsequent formation of an excimer intermediate, anthracenes undergo a  $[4\pi + 4\pi]$  cycloaddition in a suprafacial-suprafacial (s+s) manner ( $[4\pi_s + 4\pi_s]$ ).<sup>84</sup> The reaction involves two dienes forming two new sigma bonds at the expense of two pi bonds. The reverse reaction of the photoadduct is feasible *via* two reaction pathways.<sup>85</sup> On the one hand, photo-induced dissociation of the anthracene dimer takes place by exposure to UV-light with a wavelength lower than 300 nm. On the other hand, thermo-activated dissociation is achievable at elevated temperatures. It is worth noting that photolysis causes an equilibrium between free anthracene and dianthracene, since deep UV-light also triggers the photodimerisation. In contrast, thermolysis does not lead to an equilibrium but proceeds entirely. In each case, the conjugated double bond system is regenerated. The  $[4\pi_s + 4\pi_s]$  cycloaddition is thermally forbidden, but anthracene is susceptible to thermo-activated  $[4\pi_s + 2\pi_s]$  cycloadditions.

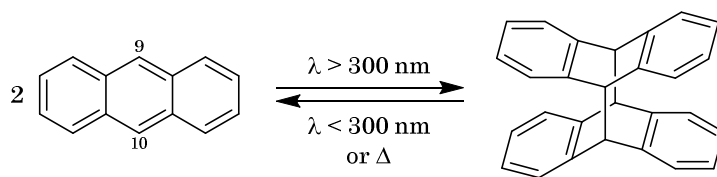


**Figure 7.** General Scheme of the photo-induced dimerisation of anthracene by a  $[4\pi_s+4\pi_s]$  cycloaddition reaction upon irradiation with wavelengths  $>300$  nm, and the dissociation of anthracene dimer by either irradiation with wavelengths  $<300$  nm or exposure to heat.

The dimerisation of anthracene is a very fast process, occurring within nanoseconds.<sup>86</sup> However, steric effects significantly influence the formation of the photodimer.<sup>86,87</sup> In general, substituents on the 9- and 10-position of anthracene decrease the dimerisation rate, and may even inhibit the reaction.<sup>88</sup> This is due to steric hindrance, preventing the close enough approach of the anthracenes. In presence of substituents, the formation of head-to-tail dimers over head-to-head dimers is preferred.<sup>86</sup> In contrast, substituents not attached at the meso-positions are unlikely to impede the dimerisation reaction, at least not in the case of comparatively small groups.

Another fundamental factor in the design of photo-responsive polymeric materials from anthracene is the network mobility. The polymer chain flexibility strongly affects both dimerisation and dissociation rate.<sup>89,90</sup> Only a sufficient chain mobility enables high conversions. Moreover, a simultaneous enhancement of the chain interdiffusion is provided, which is of particular interest regarding self-healing materials. It has even been reported that the mobility of anthracene moieties is of greater relevance than their concentration to obtain an efficient photodimerisation.<sup>89,91</sup>

Anthracene chemistry provides certain advantage over  $[2+2]$  cycloadditions. For instance, the  $[4+4]$  cycloaddition is not subject to competing isomerisation reactions and it is less prone to hydrolysis.<sup>92</sup> Moreover, anthracene dimerisation does not result in a cyclobutane ring, wherefore a highly stable dimer is obtained due to the smaller ring strain. Besides, in the dissociated state, free anthracene moieties were shown to align within a polymer matrix because of strong  $\pi$ - $\pi$  interactions.<sup>93</sup> This phenomenon further contributes to the high efficiency of the dimerisation reaction.

Noteworthy, anthracene cycloaddition also exhibits some drawbacks. In the excited state, the (photoreversible) reaction with oxygen leads to the formation of anthracene peroxide.<sup>94</sup> This photooxidation reaction usually occurs *via* the 9- and 10-position and thus, the presence of oxygen must be excluded when conducting photochemistry involving anthracenes. Furthermore, usually rather high temperatures<sup>87</sup> ( $\gg 90$  °C) are required to induce thermolysis of the photoadduct, which may limit compatibility with certain applications. On the other hand, the cleavage temperature determines the upper service temperature of polymeric materials taking advantage of anthracene dimerisation.

Anthracene chemistry offers a unique versatility in the design of smart polymers due to its multiple stimuli responsiveness. The reversible cycloaddition can be employed to alter the physical and chemical properties of polymers in a defined manner. For instance, the light-sensitivity allows for an energy efficient cross-linking of polymers<sup>95</sup> and a spatially

controlled material response used for surface patterning<sup>89</sup>. Furthermore, it is ideally suited for low temperature applications because both dimerisation and cycloreversion are photochemically allowed. In terms of covalent cross-linking, the functionalisation of polymer chains with anthracenes allows to exploit the photo-induced dimerisation for network formation. Thereby, anthracene may be introduced as a side group, end-group, or within the main polymer chain. These strategies are referred to as pendant group, cross-linker, and main chain modified approach, respectively.<sup>76</sup> Going a step further and considering the reversibility of the photodimer, compounds comprising anthracene moieties are interesting candidates for the synthesis of photosensitive polymeric materials with dynamic covalent bonds, which are covered in more detail in section 2.2.3.

## 2.2 Dynamic covalent chemistry

### 2.2.1 The strive for a new polymer class

There are different ways to classify organic polymers, and one of them is the distinction regarding the nature of the intermolecular interactions. While in thermoplastics solely relatively weak physical forces are present (and entanglements of long polymer chains), thermosets and elastomers exhibit chemical bonds. More specifically, chemical bond refers to a covalent cross-link. The different types of intermolecular interactions largely determine the physical and chemical properties of the particular polymer network. For instance, the thermomechanical behaviour of the different polymer classes is very different (Figure 8).

Upon heating, thermoplastics undergo a transition from a hard and glassy state to a rubbery material, accompanied by a substantial drop in modulus. This transition is referred to as the glass transition with its associated temperature  $T_g$ . It occurs due to the strongly increasing molecular mobility of the high molecular weight polymer chains with temperature, overcoming the weak intermolecular forces. Beyond  $T_g$ , the presence of a rubbery plateau reflects the (visco)elastic behaviour of the materials, which is governed by the number of entanglements of the long polymer chains as well as by their molecular weight. With further heating, reptation<sup>j</sup> predominates<sup>96</sup>, and thermoplastics eventually exhibit a liquid character, which usually allows for a straightforward (re)processing, (re)shaping, and often a recycling of these materials. In the state of plastic flow, thermoplastics are processable by common industrially relevant polymer processing techniques, such as injection and compression molding or extrusion. In principle, the process of softening by heat and solidification by cooling is arbitrarily repeatable without the loss of the material's initial properties. This attribute explains the wide range of applications of thermoplastics.

In contrast to thermoplastics, thermosetting networks exhibit chemical bonds. During curing, covalent cross-links are formed resulting in hard and rigid, but durable three-dimensional polymer networks. Commonly, thermosets are prepared from rather low

---

<sup>j</sup> Reptation describes the dynamics of very long linear, entangled macromolecules in polymer melts.<sup>96</sup>



molecular weight molecules, wherefore the networks naturally comprise very high cross-link densities. Consequently, thermosets exhibit extremely high moduli and the drop in modulus during the glass transition is less pronounced compared to thermoplastics. The irreversible nature of the covalent bonds formed provides thermosets with a permanent shape, but prevents melting of these polymer networks upon heating. Thus, a distinctive rubbery plateau is observed at temperatures above  $T_g$ , and the materials are subject to decomposition at a certain (high) temperature without undergoing a transition to a polymer melt.

Similar to thermosets, elastomers comprise chemical bonds. However, the properties of these two classes of polymers differ considerably.<sup>97</sup> This is mainly due to the different degree of cross-links, which is relatively low in elastomers compared to typical thermosets. Elastomers are amorphous polymers and consist of long macromolecular chains of high molecular weight, which are loosely cross-linked by covalent bonds forming wide meshed networks. The molecular weight may be a few thousand but is mostly much higher, usually amounting to  $1 \cdot 10^5$  to  $5 \cdot 10^5$  daltons.<sup>98</sup> Typically, the cross-linking occurs after polymerisation, but may also take place during polymerisation.<sup>99</sup> The chemical bonds prevent irreversible flow by unrestricted slippage of the polymer chains past each other, and thereby ensure a permanent shape of the networks. Moreover, apart from the low number of covalent linkages, the intermolecular forces between the polymer chains are rather weak. Thus, the mobility of the polymer chains is still high. As a result, elastomers exhibit an exceptionally high flexibility and elasticity. They can undergo very large deformations already at comparatively low stresses, but return to their original dimensions upon the release of the external force. The elastomer's unique elastic behaviour is only given above its glass transition temperature, which is typically found well below room temperature. In contrast, thermoplastics and thermosets are normally employed below their respective  $T_g$ . Elastomers have a low Young's modulus and during glass transition they undergo a distinct drop in modulus. Beyond  $T_g$ , a rubbery plateau is reached and the material exhibits rubber elasticity. Similar to thermosets, elastomers do not reach a state of plastic flow upon further heating, but retain their network integrity until thermal degradation.

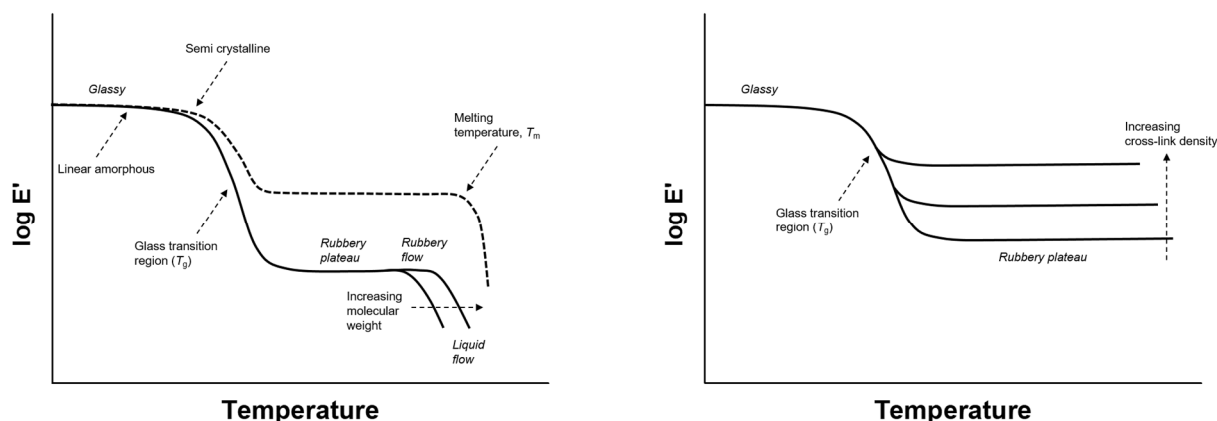


**Figure 8.** Schematic illustration of the effect of temperature on the elastic modulus (left) for thermoplastics without covalent cross-links, and (right) for amorphous thermosets and elastomers both comprising chemical bonds.

Apart from the differences in the thermomechanical behaviour, the nature of the intermolecular interactions in the different classes of polymers also influences the chemical and mechanical properties of the networks. Regarding the interaction with solvents, thermoplastics are soluble in good solvents, while thermosets and elastomers swell but do not dissolve. Normally, the degree of solvent absorption decreases with increasing molecular weight of the polymer chains and the cross-link density.<sup>100</sup> Thus, the chemical resistance is usually higher for covalently cross-linked polymers, in particular thermosets. The permanent cross-links further endow thermosets (and elastomers) with dimensional stability, creep resistance, and outstanding mechanical properties. However, chemically cross-linked polymeric materials lack the easy processability and often recyclability that is typical for thermoplastics.

It should be noted that the above-mentioned differences between thermoplastics, thermosets, and elastomers are considerably overlapping, and the discussion did not consider intermediate types of polymers such as thermoplastic elastomers (TPEs). However, the differences in physical and chemical properties of the different types of polymer networks are distinct, each of them coming along with their particular advantages and disadvantages. In the field of polymer science, it has been of great interest to combine the merits of both physically cross-linked thermoplastics and covalently cross-linked thermosets (or elastomers). It is of particular interest to introduce plasticity into polymer networks consisting of covalent bonds. In the last two decades, various strategies have been developed to serve this purpose, which are discussed in the following section.

### 2.2.2 Covalent adaptable networks

To endow covalently bonded organic polymer networks with plasticity, covalent cross-links of dynamic nature have to be incorporated. This type of polymeric materials are referred to as covalent adaptable networks (CANs), which are considered a new class of polymers.<sup>101–103</sup> Polymer networks comprising dynamic covalent linkages are capable of undergoing bond exchange reactions upon the application of a stimulus. The exchange of covalent bonds that occurs on the molecular level then causes a macroscopic response, which is the plastic flow of the material under external force. Ideally, the bond exchange reactions take place without any secondary reactions<sup>104</sup>, and the network properties are preserved after the topology rearrangements once the stimulus is removed. This enables a controllable and reversible switching between a more fluidlike or solidlike material behaviour, manifested in the mechanical and rheological properties of the polymer network. In other words, CANs resemble thermosets once cured, comprising covalent cross-links which endow the materials with the typical characteristics expected from permanent networks. Yet, while the dynamic chemistry is triggered, a rather thermoplastic behaviour evolves (thermoset-to-thermoplastic transition). Following a broad subdivision, CANs are commonly separated into two groups. Based on the underlying bond exchange mechanism, polymeric materials comprising dynamic covalent chemistry are either of dissociative or associative nature (Figure 9). These two fundamentally different reversible bond rearrangement mechanisms are described in the following.

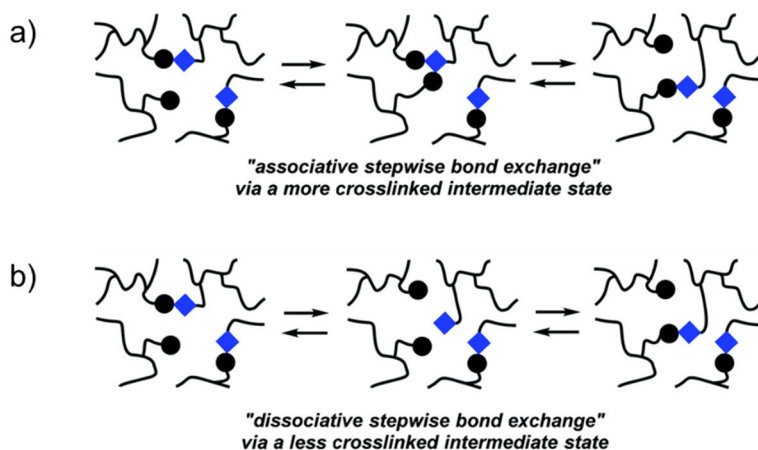


**Figure 9.** Schematic illustration of the (a) bond-breaking, bond-forming reaction sequence in dissociative CANs, and (b) bond-forming, bond-breaking reaction mechanism in associative CANs. Scheme adopted from literature.<sup>104</sup>

### *Dissociative CANs*

CANs relying on a dissociative bond exchange mechanism follow a bond-breakage, bond-forming reaction sequence (Figure 9a).<sup>103</sup> Once a covalent bond is broken, the new bond may be formed at another or the same cross-link site. This kind of bond exchange situation determines the key features of dissociative networks.

Upon the application of the particular stimulus, the bond-breaking, bond-forming process is activated and the conversion equilibrium shifts to the endothermic side of the reaction, yielding the respective initial chemical functional groups (i.e. reactants). In other words, a stimuli-triggered bond dissociation occurs, leading to a decrease in cross-link density of the networks. In fact, the networks may be easily pushed below the gel point by depolymerisation to the respective monomers. Depending on the extent of the equilibrium displacement, a wide range in viscosity can be achieved, ranging from plastic flow behaviour to a low-viscosity liquid. Thereby, the decrease in viscosity typically occurs rather abruptly (i.e. in a narrow temperature range), which is similar to thermoplastics. The cleavage and reformation process of covalent bonds in dissociative CANs accompanied by the changes in viscosity enables a (re)processing of such polymer networks in a manner resembling thermoplastics.

In this context, it should also be mentioned that the composition of the polymer networks plays a crucial role regarding their response in mechanical properties and viscosity to the stimulus. Briefly, dissociative networks can be synthesised from low molecular weight monomers or high molecular weight (linear) polymer chains, which are referred to as the reversible monomer and reversible macromer approach, respectively.<sup>103</sup> While for the former a high conversion is necessary to reach the gel point, the latter reaches the gel point already at low conversions (i.e. low number of covalent cross-links). As a result, these two types of polymer networks comprise significantly different densities of (reversible) cross-links once fully cured. Consequently, the highly cross-linked network undergoes a sharp and pronounced drop in viscosity upon the application of the stimulus, since the network can be easily driven below the gel point. Already at relatively low dissociation

degrees, an oligomeric melt with fluidlike character is obtained. In contrast, networks consisting of macromolecules cross-linked with dynamic covalent bonds do not undergo a gel-to-sol transition that easily. Upon the application of the stimulus, a more gradual decrease in viscosity takes place, and the extent is less distinctive as for the former case. In general, in these networks the viscosity is not only controlled by the rate of the bond exchange reactions, but also by the mobility of the high molecular weight polymer chains. High dissociation degrees are required to obtain a macromer-based polymer melt.

It is essential to note that all types of dissociative networks become soluble in presence of a good solvent while the stimulus is applied, which is an inherent feature of the underlying bond exchange mechanism.

Another limitation of (thermally triggered) dissociative CANs is the preparation of high  $T_g$  networks.<sup>105,106</sup> Briefly, the target  $T_g$  of a particular network should be lower than the temperature necessary to activate bond dissociation reactions. Only in this case, the cross-linking reaction may reach completion (at a temperature above  $T_g$ ) without stimulating the equilibrium of the reversible covalent cross-links at the same time.

In 2002, Chen et al. presented the first covalent adaptable network in their pioneering work.<sup>107</sup> The bond dynamics was based on the thermoreversible Diels-Alder [4+2] cycloaddition (Figure 6c) in networks from multifunctional maleimide and furan monomers. Today, the reversible Diels-Alder reaction is the most known and studied chemistry exploited in dissociative CANs, and its potential is still unmatched by other reversible strategies. Other synthetic methodologies towards dissociative CANs rely on the thermoreversibility of the reaction between isocyanates and imidazoles (Figure 10a)<sup>108</sup>, or the thermoreversible homolytic cleavage of the alkoxyamine bond, for instance exploited for cross-linking in networks with TEMPO<sup>k</sup> and styryl radicals attached to linear polymer chains (Figure 10b)<sup>109</sup>. Apart from heat as the trigger, CANs utilising light to photochemically revert covalent cross-links to the reactants were developed. In terms of photoinduced cyclisation reactions, the [2+2] and [4+4] cycloadditions were employed (Figures 6a and 7, respectively). While for the former several functionalities have been explored (see section 2.1.2), the latter is limited to anthracenes (see section 2.2.3). Another strategy to photosensitive dissociative CANs proceeds *via* photochemical cleavage of disulphides (Figure 10c).<sup>110,111</sup> Upon long wavelength UV irradiation, homolytic cleavage of disulphide bonds occurs, yielding thiyl radicals that readily recombine in the absence of light. The network dynamics is attributed to disulphide exchange reactions, the so-called disulphide metathesis.

---

<sup>k</sup> TEMPO: 2,2,6,6-tetramethylpiperidiny-1-oxy.

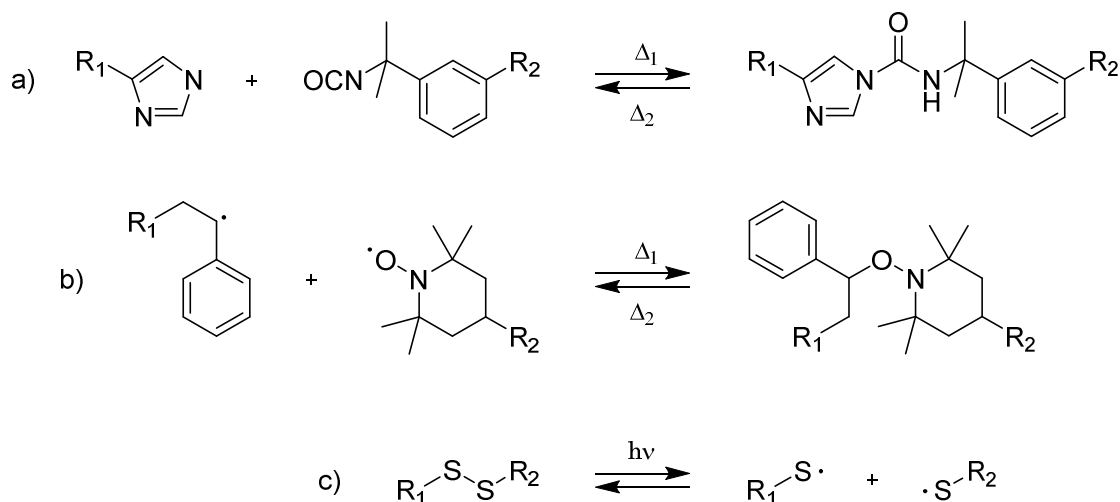


**Figure 10.** Illustration of a selection of cross-linking reactions employed in the formation of dissociative covalent adaptable polymer networks, showing the thermoreversible reaction between (a) isocyanate and imidazole, (b) between TEMPO and a styryl radical, and (c) the reversible photodissociation of disulphide bonds. Schemes adopted from literature.<sup>101</sup>

### Associative CANs

CANs relying on an associative bond exchange mechanism follow a bond-forming, bond-breaking reaction sequence (Figure 9b).<sup>103</sup> First, a new bond is formed to an existing cross-link, before the original bond is broken. More precisely, a free reactive moiety within the polymer network attaches to an existing covalent bond forming an intermediate species. Subsequently, this species spontaneously fragments, releasing a reactive functional group from the initial cross-link, which can then initiate another bond exchange reaction and so forth. This type of exchange reaction mechanism leads to a stimuli-triggered material response that is fundamentally different from dissociative CANs.

Upon application of the particular stimulus, bond exchange reactions are activated, but due to their associative manner, the overall number of covalent cross-links within the polymer network is maintained. Thus, associative CANs stay above the gel point at all times, also during the application of the stimulus. As a result, the observed changes in viscosity of these networks occur less abruptly compared to dissociative CANs (and thermoplastics), but rather in a gradual manner. Nevertheless, the stimuli-triggered network rearrangements cause a temporary and time-dependent change in viscosity, enabling a (re)processing of these networks. Though it is more difficult to obtain a fluidlike behaviour (polymer melt) than for dissociative CANs. Noteworthy, any shape changes of associative polymer networks rely on the application of an external force, and the deformations occur plastically (i.e. irreversible). Associative CANs exhibit both, on the one hand a permanent character in terms of the network functionality (number of covalent cross-links and number of functional chemical groups) and, on the other hand a dynamic character with respect to the network connectivity, which changes over time during application of the stimulus. In general, the rheological behaviour of associative CANs depends on the exchange reaction kinetics. In dissociative CANs, the rheological properties primarily depend on the thermodynamics of the particular reversible reaction.

A very important characteristic of associative CANs, which is directly related to the specific molecular exchange chemistry, is their insolubility at all times, even in good solvents and while the bond exchange reactions are triggered.

In contrast to dissociative CANs, networks relying on an associative exchange mechanism may exhibit a  $T_g$  higher than the respective temperature stimulating the covalent bond exchanges. Ongoing associative bond exchange reactions are usually not detrimental to a full curing of such networks. In fact, topology rearrangements can even contribute to three-dimensional cross-linking in networks from linear monomers.<sup>112</sup>

The first dynamic covalent networks following an associative exchange mechanism relied on photo-induced free radical addition-fragmentation chain transfer (AFCT) reactions. In 2005, Bowman and co-workers synthesised covalent cross-linked elastomeric networks containing allyl sulphide groups in the polymer backbone, capable of undergoing associative bond exchange reactions upon irradiation with light (Figure 11).<sup>113,114</sup> The materials showed stress relaxation and shape change capabilities. However, due to the involvement of (highly) reactive radical species, these materials were prone to side reactions, which limit the lifetime of the network dynamics. Similar approaches then followed, whereby all of them involved radical chemistry.<sup>110,115</sup>

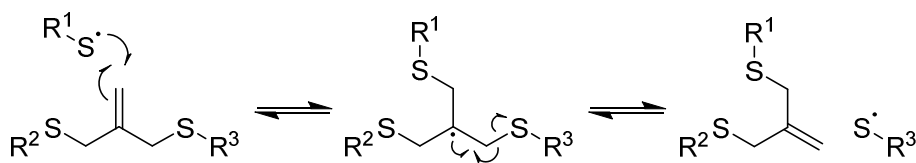


**Figure 11.** Schematic illustration of associative bond exchange reactions involving radical species in CANs exhibiting allyl sulphides in the polymer backbone.<sup>113</sup>

In 2011, Leibler and co-workers accomplished a remarkable step forward in the field of adaptable associative covalent networks with the introduction of vitrimers<sup>116</sup>, which are covered in section 2.2.4.

### 2.2.3 Dynamic covalent networks from anthracene

Dynamic polymeric materials relying on the reversible photo-cycloaddition of anthracenes are an exciting example for (photo-responsive) dissociative CANs. In the following, some approaches taking advantage of this chemistry in the design of polymer networks with reversible covalent bonds are discussed. In particular, strategies relying on the pendant group approach, which is the most used. The mechanistic details of the  $[4\pi_s + 4\pi_s]$  photo-cycloaddition of anthracenes and key parameters influencing the efficiency of the reaction within a polymer matrix have been covered in section 2.1.2.

Our group reported the preparation of a covalently cross-linked and photo-responsive epoxy-based prepolymer bearing anthracene groups (Figure 12).<sup>117</sup> In the first step, epoxy-functionalised anthracene (photoreactive epoxy monomer) was synthesised and blended with another monofunctional epoxy monomer, yielding a dual-curable epoxy resin. Next, the mixture was thermally cured at low temperature with an anhydride hardener to obtain

the prepolymer. The covalently incorporated photoreactive anthracene moieties were then exploited for a covalent cross-linking of the prepolymer *via* the  $[4\pi_s+4\pi_s]$  cycloaddition by exposure to UV-light with a wavelength higher than 300 nm. Dissociation of the anthracene dimers was feasible at 130 °C, and a repeated switching between the two cross-linking states was demonstrated. Accordingly, a repeated healing effect for mechanically introduced macroscopic cracks even in bulk was shown. The healing was carried out by UV exposure ( $\lambda > 300$  nm) and simultaneous heating to 60 °C. The healing process was followed taking advantage of the fluorescence of free anthracene moieties and further quantified by three-point bending tests, revealing healing efficiencies from 84 to 100% in the first repair step. The healing efficiency depended on both the number of available anthracene groups (by tuning the network composition) at the damage site and their mobility that was ensured by heating above  $T_g$ . Notably, the networks were not susceptible to a significant photo-induced de-crosslinking upon UV exposure with 254 nm, which was attributed to the high rigidity of the network. Thus, the healing mostly relied on the phenomenon of anthracene dimers being preferentially cleaved upon damage. In general, emphasis was placed on the importance of finding a balance between the degree of anthracene functionalisation and the  $T_g$  of the networks regarding an optimum compromise of cross-link density and sufficient polymer chain mobility. This is due to the effect of bulky (anthracene) side groups generally increasing the  $T_g$  of polymer networks<sup>118</sup>, and the key role of anthracene mobility in enhancing the reversible photodimerisation. The latter parameter has already been investigated previously by Grießer et al. on the basis of the photodimer formation in anthracene-functionalised polynorbornenes.<sup>89</sup>

Going from epoxy-based thermosets to elastomers, our group followed a similar approach as above for the preparation of photo-reversible rubber networks (Figure 12).<sup>119</sup> Pending anthracene groups were covalently attached to HXNBR rubber *via* the carboxylic acid functions of the linear polymer using 2-(anthracene-9-yl)oxirane. Covalent cross-linking of the rubber by photodimerisation was achieved with light with a wavelength higher than 300 nm, and subsequent de-crosslinking by exposure with deep UV-light ( $\lambda = 254$  nm). Again, a repeated switching between the two cross-linking states was demonstrated. Interestingly, the distinctive photo-induced material response was obtained for modification yields of only 1.3 mol%. The dynamic of the rubbery networks also benefited from a high mobility of the polymer chains due to a low  $T_g$  ( $< -5$  °C). A disadvantage of this approach is the solvent-based synthesis of the networks.

Besides the stimuli-controlled changes of the thermo-mechanical properties, both networks presented enabled the preparation of photoresists, highlighting the versatility of these chemistries.

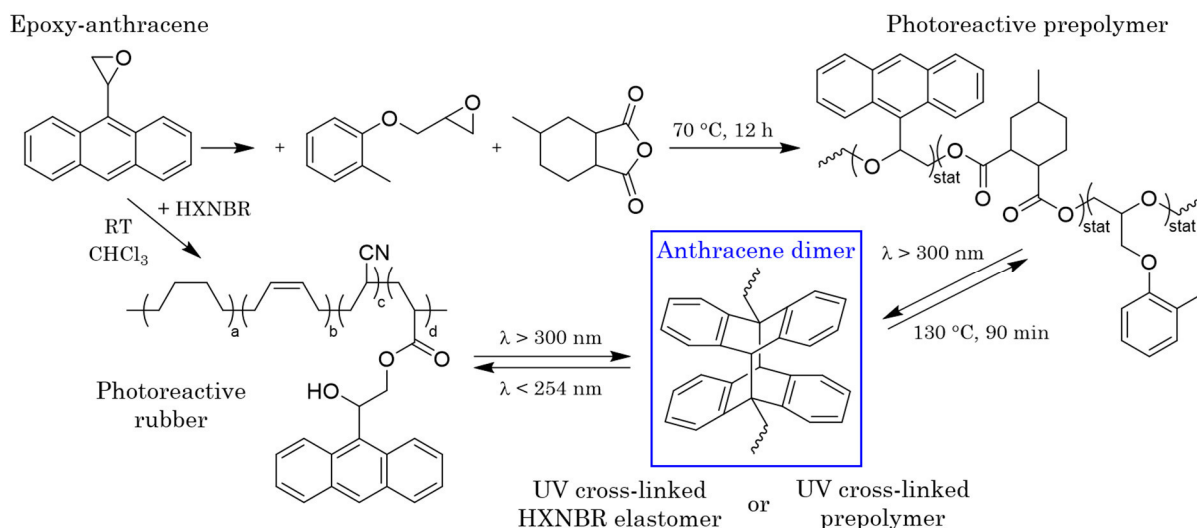


**Figure 12.** Strategies towards the preparation of photoreactive HXNBR rubber and photoreactive epoxy prepolymer starting from 2-(anthracene-9-yl)oxiran (epoxy-anthracene) as reported by our group.<sup>117,119</sup> Both networks are susceptible to reversible photo-induced cross-linking *via* the anthracene dimer.

Fróimowicz et al. reported anthracene dimer cross-linked hyper-branched polyglycerol networks.<sup>120</sup> This pendant group approach resulted in a rapid and highly efficient photo-healable network even at room temperature. However, an extremely low  $T_g$  ( $-46^\circ\text{C}$ ) of the uncrosslinked polymer is primarily accountable for the system's remarkable healing capabilities, providing a high flowability of the material from low temperatures. While the photoreversibility of the dimers was high, only 35% of the anthracene groups participated in the initial cross-linking step due to high steric hindrance.

Xu et al. exploited the reversible photo-dimerisation of anthracene in double-dynamic covalent networks, where the different reversible bonds were triggered at different temperatures and time-scales.<sup>121</sup> Another field of application was covered with mechanoluminescent networks from polyurethanes cross-linked *via* anthracene dimers.<sup>122</sup>

## 2.2.4 Chemistry of vitrimers

In 2011 the pioneering concept of vitrimers was presented by Leibler and co-workers<sup>116</sup>, and considered a new class of organic polymeric materials. Vitrimers belong to the group of covalent adaptable networks (CANs) relying on an associative bond exchange mechanism. The details of this type of exchange chemistry were explained in section 2.2.2.

Despite being covalently cross-linked, vitrimers can alter their network connectivity by covalent bond exchange reactions without changing the overall number of covalent linkages and chemical functions. Consequently, in vitrimers that are susceptible to heat as stimulus the cross-link density is preserved at all temperatures and times, even in good (but inert) solvents.<sup>116</sup> This also ensures the conservation of material properties once the stimulus is removed. At low temperatures, the networks essentially behave like classical thermosets/elastomers, since the bond exchange reactions are very slow. By heating, bond exchange reactions are triggered and lead to a decrease in viscosity, creating a viscoelastic



melt. The resulting macroscopic flow of the materials under external force allows adaptations in their topology, whereby the deformation is of irreversible nature. Importantly, the change in viscosity occurs gradually and follows the Arrhenius law. For the first time, this unique phenomenon was observed in cross-linked organic polymers, and it is in striking contrast to the abrupt drop in viscosity occurring for thermoplastics and certain dissociative CANs that follow the Williams-Landel-Ferry (WLF) model. However, it is similar to the temperature-dependent rheological behaviour of materials from inorganic silica, from which the term vitrimer is derived.<sup>116</sup> In analogy to vitreous silica, which is a so-called strong glass former, vitrimers are considered strong organic liquids. Figure 13 displays typical viscosity profiles over temperature for thermoplastics, vitreous silica, and the first vitrimer compositions introduced by Leibler et al. The smaller the rate of change in viscosity from temperatures above  $T_g$ , the lower the so-called fragility of a material, which reflects the broadness of the transition. Accordingly, thermoplastic melts are fragile, whereas vitrimers do not require a precise temperature control when taking advantage of their malleability.

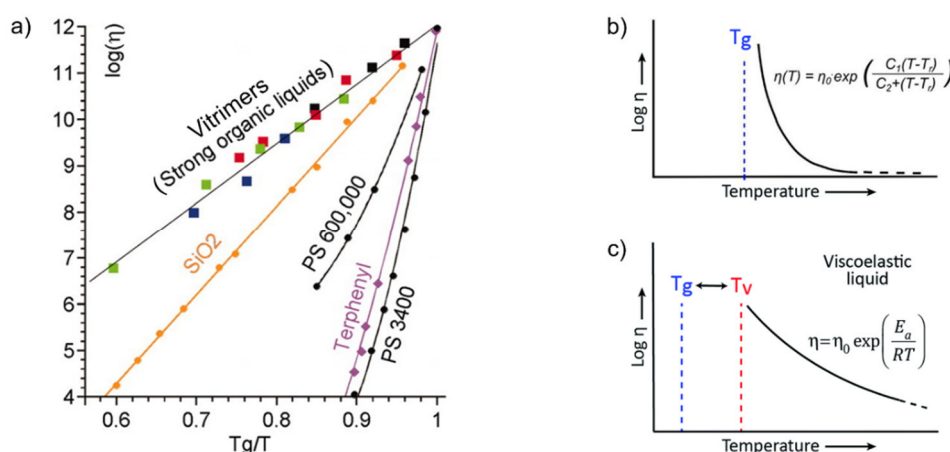


**Figure 13.** (a) Angell fragility plot showing the viscosity profiles as a function of temperature for typical thermoplastics, vitreous silica, and various vitrimer compositions presented by Leibler et al. Schematic illustration of the change in viscosity at increasing temperature (b) for common thermoplastic polymers following WLF behaviour from  $T_g$ , and (c) for vitrimers with a  $T_g$  lower than the topology freezing transition temperature ( $T_v$ ) following the Arrhenius law. Schemes adopted from literature.<sup>116,123,124</sup>

The first vitrimers were soft, low- $T_g$  epoxy/carboxylic acid and hard, high- $T_g$  epoxy/anhydride networks relying on thermo-activated transesterifications.<sup>116,125</sup> For instance, simple cross-linking of di-functional epoxides with multifunctional carboxylic acids yields  $\beta$ -hydroxyl ester bonds when stoichiometric monomer amounts are used (Figure 15-i). Subsequently, abundant hydroxyl groups and ester functions can undergo transesterifications at elevated temperatures, yielding a new network connectivity while maintaining the average chemical functionality (Figure 14). At room temperature, the exchange reaction rate is negligible and the material behaves like a typical elastomer. To date, most vitrimer systems developed exploit this type of bond exchange mechanism. This is due to both the commercial availability of a wide selection of potential monomers (i.e. epoxides, anhydrides, carboxylic acids) and the simple formation of polymeric materials with rather high  $T_g$ , which is an important requirement for possible structural applications.

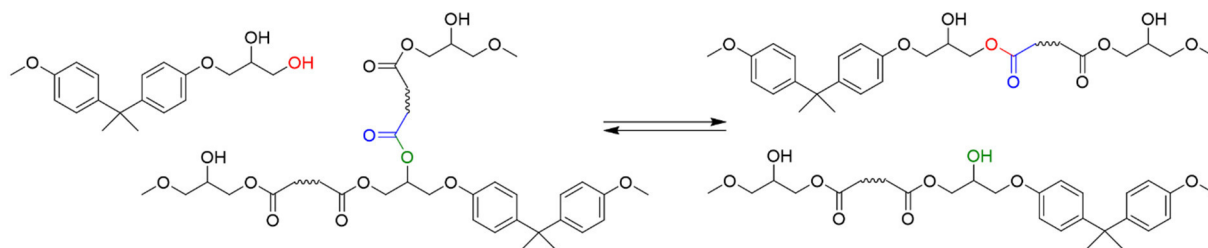


**Figure 14.** Schematic illustration of topology rearrangements in vitrimers on the example of a hydroxy-ester network undergoing thermo-activated catalytic transesterification reactions. Scheme adapted from literature.<sup>116</sup>

These networks are further characterised by relatively high temperatures needed to induce covalent bond shuffling, and often by the requirement of a catalyst. The latter applies in particular to vitrimers relying on transesterifications. At high temperatures, the viscosity behaviour is controlled kinetically by the bond exchange chemistry. Catalysts can efficiently accelerate the exchange reaction kinetics and by this, determine the fragility of the viscoelastic melt (Figure 13a).<sup>124</sup> In fact, only if the bond exchange reactions are sufficiently fast and occur throughout the network, macroscopic flow can be obtained within a reasonable time scale. The most frequently employed and well-studied catalysts in transesterification-based vitrimers are the organic zinc salt zinc acetate<sup>116,124,126–131</sup> and 1,5,7-triazabicyclo[4.4.0]dec-5-ene (TBD)<sup>40,125,132–135</sup>, which is a strong guanidine base. Typical catalyst contents in vitrimers amount to 5-10 mol% with respect to the carboxylic acid groups, although higher loadings have been utilised as well. Other chemical compounds employed as catalysts include  $Zn^{2+}$  ionomer<sup>136</sup>, zinc acetylacetonate<sup>116,137</sup>, tertiary amines<sup>138</sup>, and organic tin salts<sup>139,139,140</sup>. Both catalyst type and quantity strongly influence the vitrification transition.<sup>124</sup> Apart from the efficiency in terms of the bond exchange kinetics, the selection of a suitable catalyst may be guided by parameters like the catalyst (in)solubility, temperature stability, toxicity, corrosivity, as well as long-term issues, such as catalyst ageing, leaching, and hydrolysis.<sup>123,141</sup> Further considerations could include undesirable catalyst migration, which has been addressed either by the covalent attachment of the catalyst to the network<sup>138</sup> or the usage of polymeric catalysts<sup>136</sup>.

Meanwhile, also catalyst-free vitrimers relying on transesterifications have been reported.<sup>138,142,143,144,145</sup> The difficulty in the design of such systems is that not only the bond exchange reactions occur efficiently at high temperatures, but also that full curing of the networks is ensured. Zhang et al. reported catalyst-free vitrimers from hyperbranched epoxy and succinic anhydride.<sup>146</sup> The obtained dynamic in the fully cured networks was attributed to abundant hydroxyl groups, whereby the hydroxyls not only acted as reactive groups participating in transesterifications but also provided catalytic activity for both curing and bond exchange reactions. Interestingly, these networks exhibited relatively high  $T_g$  (up to 87 °C), which is in contrast to a series of catalyst-free vitrimers reported by Williams and co-workers ( $T_g < 70$  °C). The authors obtained transient networks from epoxidised soybean oil and citric acid<sup>145</sup> as well as from DGEBA cured with a mixture of citric and sebacic acid<sup>138,144</sup>. Also here, the vitrimeric nature was explained by the high number of available carboxylic acid groups and hydroxyl functions within the systems. In addition, rather low cross-link densities and the usage of flexible linear monomers yielded

soft matrices (i.e. low  $T_g$ ) with a low backbone stiffness, contributing to polymer chain mobility and consequently the dynamic behaviour.

In this context, it is worth noting that Hillmyer et al. obtained vitrimer behaviour in polylactide-based polyester networks without ample hydroxyl groups, apparently compensated by abundant ester groups and a high activity of the catalyst dioctyltin ( $\text{Sn}(\text{oct})_2$ ).<sup>140</sup>

The role of catalysts in epoxy-acid vitrimers also becomes apparent when considering the chemistry of network formation from epoxides and carboxylic acids (Figure 4, see also section 2.1.2), revealing a benefit towards the generation of the desired network structure. Ideally, the employment of stoichiometric amounts of epoxy groups and carboxylic acid moieties yields only ester bonds and secondary hydroxyl groups by the respective ring opening reaction, i.e. addition esterification (Figure 15-i). However, the secondary hydroxyl groups formed can undergo condensation esterification or etherification with carboxylic acid functions or epoxy, respectively (Figure 15-ii and iii). In terms of full curing and the formation of three-dimensional networks, these “side” reaction pathways are even essential (especially in diepoxy-dicarboxylic acid systems). Importantly, while condensation esterification results in ester functions that can undergo transesterifications, etherification is unwanted because the linkages obtained are inactive towards bond exchange reactions. Catalysts were reported to contribute positively in several respects.<sup>147</sup> Specifically, without catalysis the reactivity of secondary hydroxyl groups is low. In addition, catalysts enhance the initial ring opening reaction between epoxy and carboxylic acid and further promote esterification while etherification is suppressed. Thus, the catalysed networks comprise the relevant functional groups for transesterification exchange reactions, which are ester functions and hydroxyl groups. Noteworthy, common transesterification catalysts typically accelerate the cross-linking reaction (i.e. addition esterification) in epoxy-carboxylic acid networks.<sup>28,116,140,148</sup>

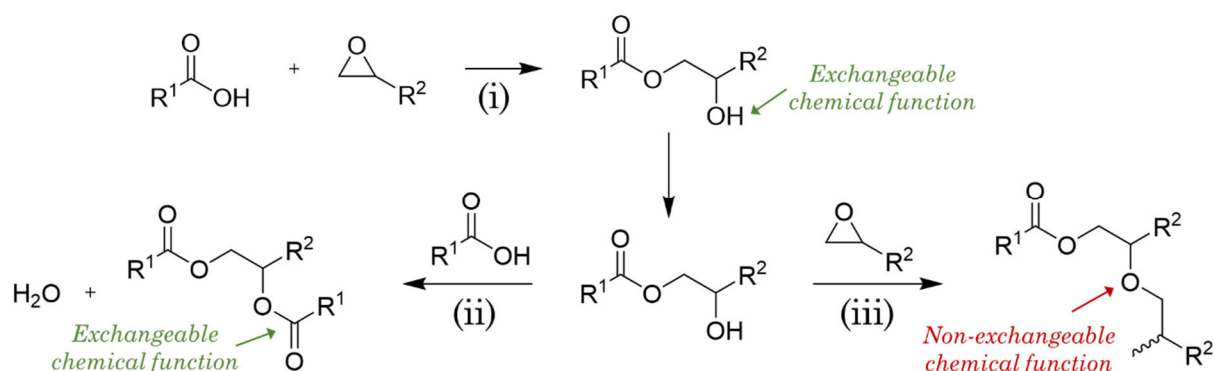


**Figure 15.** Possible reactions in the network formation of epoxy-carboxylic acid vitrimers: (i) Ring opening reaction (addition esterification) of epoxide with carboxylic acid forming  $\beta$ -hydroxyl ester bonds and (ii) subsequent condensation esterification with carboxylic acid giving diesters, both providing exchangeable chemical functions for transesterifications; (iii) etherification of secondary hydroxyls with epoxy yields ether linkages that are inactive towards bond exchange reactions.

Since the introduction of the concept of vitrimers on the example of thermally triggered catalytical transesterifications, several other associative bond exchange reactions have

been introduced. Accordingly, these chemistries were incorporated into a large diversity of polymer matrices. While some of these networks yield full vitrimer characteristics, others only display vitrimer-like features. Moreover, various approaches do not require a catalyst. Catalyst-free vitrimer chemistries are transcarbamoylation<sup>149</sup>, transalkylation of triazolium salts<sup>150</sup>, disulphide exchange<sup>151</sup>, and transamination<sup>152</sup>; whereas imine-amine exchange<sup>153</sup> and transesterification usually require catalysts, although non-catalysed strategies were reported. Figure 16 displays an overview of a variety of bond exchange mechanisms applied in polymeric materials of vitrimeric nature.

It must be emphasised that some covalent exchange mechanisms yield inherently rather vitrimer-like materials than full vitrimers. These are for instance disulphide rearrangements, siloxane-silanol, and imine-amine exchanges.<sup>123</sup> Particularly the rearrangement of disulphide bonds is a complex process. The reversible switching between disulphides and the respective thiols by reduction and oxidation occurs clearly in a dissociative manner.<sup>154</sup> The same applies to the reversible homolytical cleavage of disulphides by UV-light<sup>111</sup> or heat<sup>155</sup> yielding thiyl radicals. A more complex situation is found in networks comprising disulphide bonds and free thiols, with the rearrangements relying on thiol-disulphide exchanges as shown by Klumperman et al.<sup>151</sup> The vitrimeric properties of the networks were primarily attributed to an underlying associative mechanism *via* an addition/elimination pathway. However, Bowman et al. noted that such networks exhibit a hybrid reversible addition-exchange mechanism.<sup>103</sup> In general, dynamic polymer networks involving radical species suffer from a limited dynamic lifetime, which is due to the high reactivity of the radicals, especially towards oxidation at ambient conditions.

Until today there are only a few studies that deal in detail with mechanistic issues of vitrimers, aiming to correlate the chemical reactivity with the macroscopic dynamic behaviour.<sup>37,104,156</sup> Interestingly, there is no set definition of the terms vitrimer and vitrimer-like, meaning that there is an ongoing debate in the field on the properties of a true vitrimeric polymer network.<sup>104,157</sup> This is also because such dynamic networks can display a vitrimeric rheological profile relying on a large variety of chemical reactivities. Moreover, for most vitrimers it is unlikely that the bond dynamic solely occurs through associative exchange reactions. For instance, also transesterifications may proceed *via* a dissociative pathway.<sup>34</sup> In addition, also purely dissociative covalent adaptable networks may exhibit vitrimeric characteristics, depending on the equilibrium between the bonded and de-bonded states.<sup>150</sup> In other words, an associative exchange reaction or a linear Arrhenius-plot are not absolute prerequisites for a polymer network to be referred to as a vitrimer.<sup>104,156</sup> Similar applies to the insolubility of vitrimers, which has been commonly used as a major criterion to assign vitrimer properties to materials.<sup>158</sup> Importantly, the boundaries are blurred and none of the different criteria should be regarded as absolute rather than context-dependent.

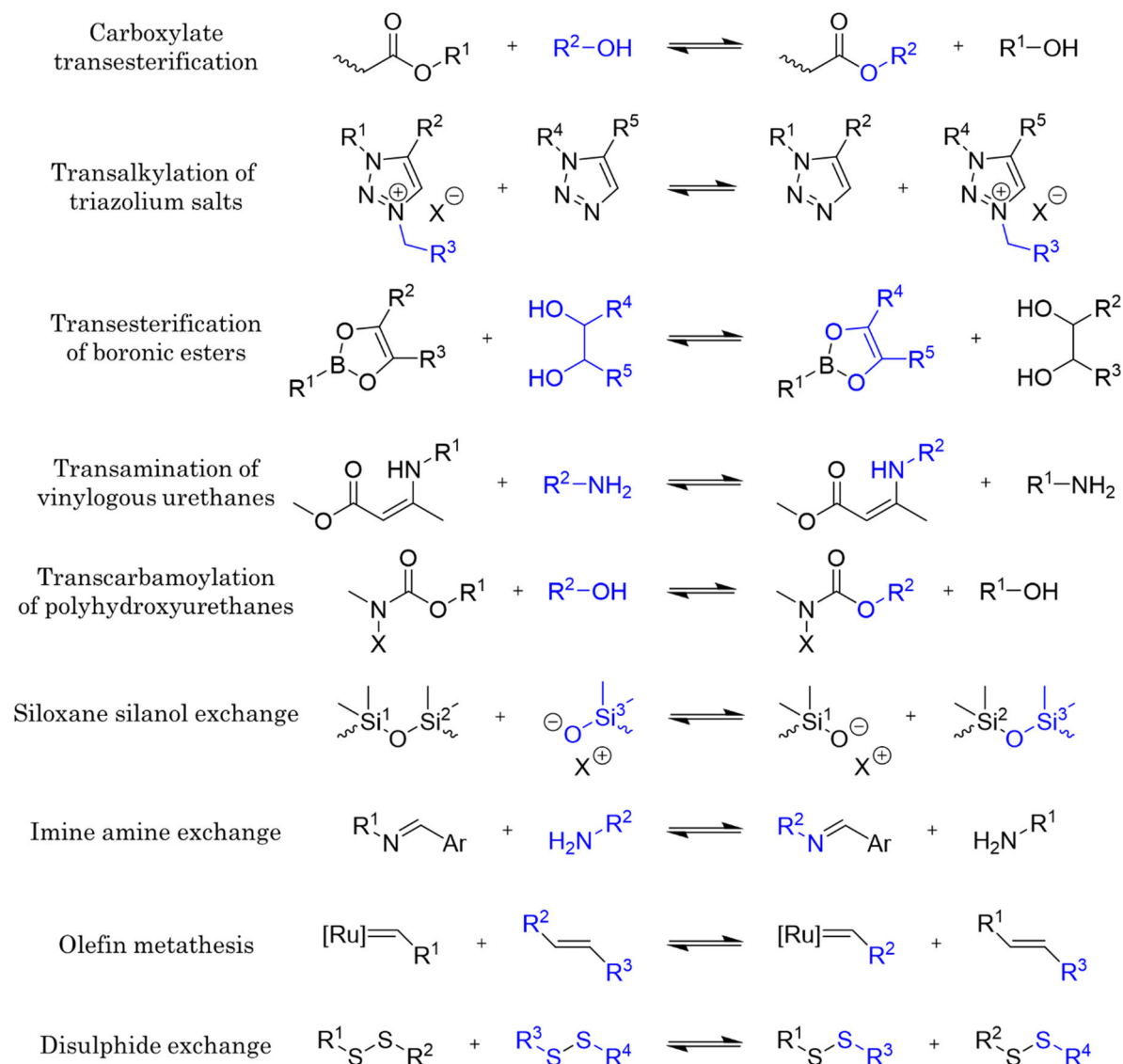


**Figure 16.** Overview of a selection of dynamic exchange reactions applied in vitrimeric polymers.

Besides a classical glass transition temperature ( $T_g$ ), which marks the transition from a glassy to a rubbery state of a cross-linked polymer, vitrimers exhibit a second transition temperature (Figure 13c).<sup>116</sup> The latter is a result of the thermo-activated associative covalent bond exchange reactions in vitrimers. At low temperatures, the bond exchange rate is insignificant and the network topology is quenched. However, upon heating, the reaction kinetics accelerates and the material's viscosity decreases gradually in an Arrhenian manner resulting in macroscopic flow under external force. This transition from a viscoelastic solid to a viscoelastic liquid is referred to as topology freezing transition. By Leibler et al., the corresponding temperature was designated as the topology freezing transition temperature,  $T_v$ .<sup>116</sup> The  $T_v$  indicates the start of the Arrhenius-like dependency of the viscosity, which occurs at a certain temperature where the number of bond exchange reactions becomes relevant. Above  $T_v$ , the viscosity is then kinetically controlled by the bond exchange rate. Noteworthy, the  $T_v$  of a vitrimeric polymer network may be lower (mostly in high  $T_g$  networks) or higher (usually in elastomeric networks) than the

respective  $T_g$ .<sup>123,159</sup> In either case no bond exchange reactions take place before  $T_g$  is reached. The analysis of the  $T_v$  is discussed in detail in section 2.2.7.

The  $T_v$  of vitrimers is governed by the density of (exchangeable) cross-links, the exchange reaction kinetics (e.g. catalyst type and amount), the mobility of the polymer chains, the monomer rigidity, and the abundance of reactive chemical functions (such as hydroxyls in epoxy vitrimers). Of these parameters, the cross-link density (i.e. number of exchangeable linkages) plays a major role. However, its effects in transesterification-based vitrimers are rather unexplored and controversially discussed in the literature. Some reports state that a decrease in cross-link density enhances the bond exchange rate when changing the stoichiometry of a particular network.<sup>131,160</sup> This effect may rather be attributed to the concomitant increase in polymer chain mobility (i.e. decrease in  $T_g$ ) than to the cross-link density itself. It should be considered that varying the stoichiometry of a monomer composition also significantly influences the network structure and the overall number of exchangeable functional groups.<sup>125</sup> Hayashi et al. have even observed the opposite in their polyester vitrimers. With decreasing carboxylic acid equivalent molecular weight ( $M_{COOH}$ ) and thus higher cross-link densities, stress relaxation was more efficient.<sup>161</sup> But here too, the number of exchangeable chemical functions has altered at the same time, which is the increase in free hydroxyl groups. In a more recent report, the same authors assessed a more accurate correlation following an ingenious network design.<sup>162</sup> On the basis of a polyester vitrimer, they were able to vary the cross-link density of the networks while maintaining the overall number of bond exchange carriers. In conclusion, faster stress relaxation was demonstrated for higher densities of exchangeable cross-links when the quantity of hydroxyl functions was kept constant.

Vitrimers, regardless of the underlying bond exchange mechanism, exhibit the unique property of network reorganisation despite being covalently cross-linked. The temperature-induced network dynamic enables stress relaxation and results in macroscopic flow, which is of great interest in the development of more sustainable polymer networks, combining the advantages of both thermosets and thermoplastics. A wide range of possible applications of vitrimers is conceivable, and to date numerous reports have already highlighted the versatility of this new material class. The concept of vitrimers endows polymeric materials with recycling<sup>150,163–166</sup>, reprocessing<sup>116,150,166,167</sup>, (self) repair/healing<sup>137,165,168,169</sup>, reshaping<sup>170</sup>, and welding<sup>125,171</sup> properties. In terms of material types, vitrimer chemistry has been incorporated in polymer composites, either reinforced with fibres<sup>164,168,172–174</sup> (i.e. fibre-reinforced polymers, FRP) or (nano)particles<sup>40,175–177</sup>. There exist high- $T_g$  (epoxy) vitrimers with excellent mechanical and physical properties, resembling classical thermosets. Vitrimer(like) behaviour was also shown in various elastomeric networks, and even in cross-linked thermoplastics<sup>135,160,178</sup>, which were endowed with associative dynamic covalent linkages. Other applications of vitrimers include coatings<sup>142,179</sup>, adhesives<sup>180</sup>, 3D printing<sup>181</sup>, and electronics<sup>182</sup>.

Figure 17 shows two exciting strategies reported in literature towards the preparation of fibre-reinforced polymer composites employing vitrimer matrices. Denissen et al. impregnated glass fibres with vinylogous urea resins to obtain fully cured composites (Figure 18a).<sup>172</sup> Nevertheless, the thermo-activated network dynamics relying on fast amine exchange reactions of the vinylogous urea moieties enabled thermal fusion of

multiple layers of the composites and thermoforming. Odriozola et al. took advantage of aromatic disulphide chemistry as the bond exchange mechanism in the preparation of carbon fibre-reinforced composites from epoxy vitrimers (Figure 17b).<sup>164</sup> At high temperatures, the initially fully cured prepregs were processable into 3D parts by thermoforming, could be hot-pressed into multilayered sheets, and further showed interesting recycling and repair capabilities.

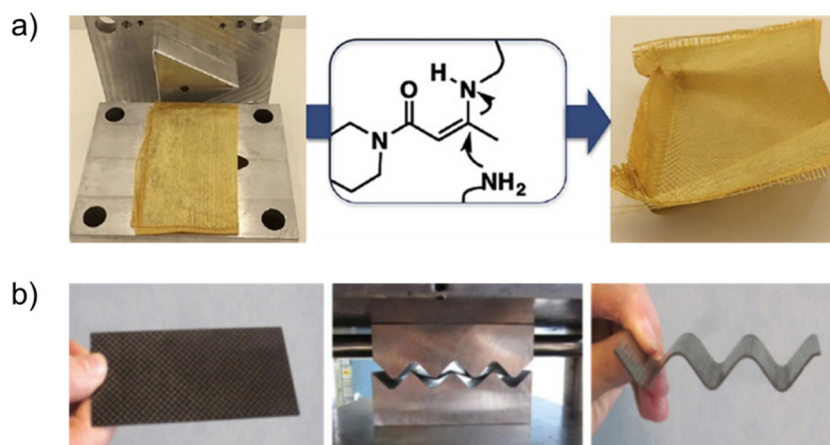


**Figure 17.** (a) Glass fibre-reinforced composites from vinylogous urea vitrimers as demonstrated by Denissen et al. (b) Carbon fibre-reinforced composites from epoxy vitrimers relying on disulphide exchange chemistry as reported by Odriozola et al. Schemes adopted from literature.<sup>164,172</sup>

Clearly, vitrimer chemistry is affected by certain limitations that need to be resolved regarding the potential industrial implementation of these dynamic networks. For instance, transesterification-based vitrimers typically comprise off-stoichiometric amounts with regard to the monomers' chemical functionality, in order to endow the materials with free hydroxyl groups required for bond exchange reactions. Consequently, the chemical and physical properties of the polymer networks are adversely affected.<sup>156</sup> Moreover, the common usage of flexible monomers to enhance the network mobility is detrimental to the thermo-mechanical properties. In general, an increased network rigidity mitigates the bond exchange kinetics, wherefore the synthesis of high- $T_g$  vitrimers is challenging. Indeed, highly dynamic vitrimers often exhibit rather low  $T_g$  that causes an insufficient creep resistance of the materials (at room temperature), which is strongly undesirable in structural applications. Further challenges relate to the usage of large amounts of catalysts, which may be toxic, poorly compatible with the networks, and subject to long-term problems. As a result, many parameters have to be taken into account in the networks design of vitrimers. In general, there is scarce knowledge about the dynamic lifetime of vitrimers, and issues, such as hydrolysis or mechanical stability must be considered.<sup>106</sup> In terms of reprocessing, it should be mentioned that even at elevated temperatures, the viscosity of vitrimers remains relatively high. Therefore, they are only limited (re)processable by industrially relevant continuous processing methods that require very low viscosities, such as compression and injection molding.

## 2.2.5 Vitrimer(-like) chemistry in rubbers

Rubbers are of great importance in the chemical industry and find application in a wide range of products.<sup>183</sup> The covalent cross-linking of rubbers is indispensable to obtain excellent physical and chemical properties, for which permanent elastomers from rubber are well known. This is normally achieved through curing procedures involving sulphur or organic peroxides (see section 2.1.2).<sup>184</sup> However, the permanence of the chemical bonds renders recycling and reclamation of (waste) rubber highly challenging.<sup>185</sup> As for classical thermosets, the issues associated with the irreversibility of the covalent cross-links (see section 2.2.1.) could be addressed by the incorporation of stimuli-responsive dynamic covalent bonds. Considering the vast number of vitrimer systems developed since the introduction of this new material class in 2011, relatively little research has been performed in the context of vitrimer chemistry and rubbers; in particular high molecular weight carbon-based rubbers. To date, synthetic procedures rely on the cross-linking of either epoxidised rubbers or rubbers bearing carboxylic acid groups with cross-linkers possessing carboxylic acid moieties or epoxy functions, respectively (Figure 18). Both approaches make use of transesterification as dynamic bond exchange mechanism and usually require the addition of a suitable catalyst.

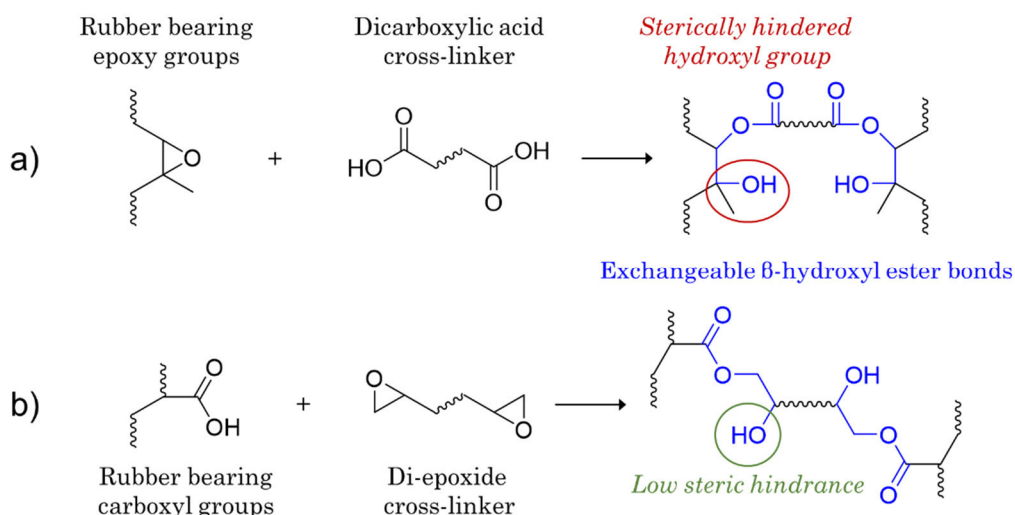


**Figure 18.** Schematic illustration of the preparation of rubber-based elastomeric networks comprising associative exchangeable β-hydroxyl ester bonds. Formation of dynamic covalent cross-links (a) from rubbers bearing epoxy functions and dicarboxylic acid cross-linkers, and (b) from rubbers bearing carboxyl functions cured with di-epoxide cross-linkers. Moreover, visualisation of the obtained network structure, yielding hydroxyl groups with (a) high and (b) low steric hindrance.

Imbernon et al. followed a radical-based strategy in their elastomers from epoxidised natural rubber (ENR) that was cross-linked with a functionalised dicarboxylic acid bearing disulphide bonds.<sup>186</sup> Thermo-activated disulphide rearrangements allowed for a partial relaxation of stresses. Moreover, improved reprocessability and adhesion capabilities were demonstrated. However, due to the radical species involved in the bond exchange reactions, this approach is not considered to be of full vitrimeric nature (see section 2.2.4).



The same authors presented a similar but first non-radical attempt in 2016, relying on the same exchange chemistry that was applied in the classical vitrimers of Leibler et al. Again, ENR was covalently cross-linked with dicarboxylic acids (Figure 19).<sup>127</sup> During curing,  $\beta$ -hydroxyl ester linkages were formed that subsequently enabled thermally and catalytically controlled transesterification exchange reactions in presence of the transesterification catalyst zinc acetate ( $\text{Zn}(\text{OAc})_2$ ). The authors demonstrated the adaptability of the elastomeric networks by stress relaxation experiments and enhanced self-adhesion properties. However, the networks were described only as vitrimer-like rather than full vitrimers. This is due to the incomplete stress relaxation of these elastomers, which was attributed to the lack of exchangeable cross-links (i.e. low cross-link density), the lack and low reactivity of sterically hindered hydroxyl groups, and side reactions such as oxidation forming non-exchangeable cross-links at high temperatures. Consequently, in this ENR-based system, only a restricted change in viscosity by triggering the bond exchange reactions was obtained, which did not enable full reprocessing. It should also be mentioned that the application of inorganic and divalent  $\text{Zn}^{2+}$  as the transesterification catalyst clearly interfered with the cross-linking reaction between the epoxy and carboxylic acid functions, and likely also caused trouble in terms of the stress relaxation behaviour.<sup>127</sup>

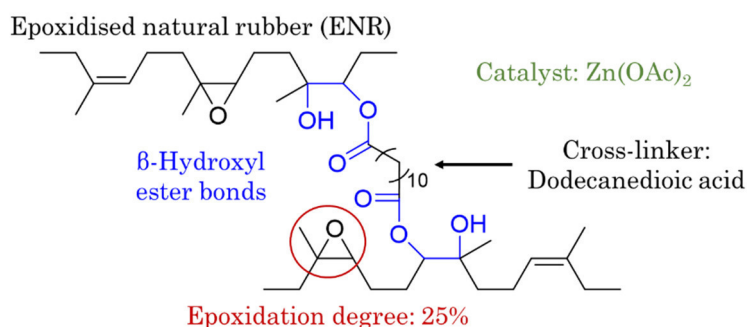


**Figure 19.** Schematic illustration of vitrimer-like elastomers from epoxidised natural rubber (ENR) reported by Imbernon et al.<sup>127</sup> Curing of ENR with di-functional dodecanedioic acid yields  $\beta$ -hydroxyl ester cross-links that are susceptible to thermo-activated transesterification exchange reactions in the presence of the catalyst zinc acetate. Scheme adapted from literature.<sup>127</sup>

Following the study of Imbernon et al., a certain number of publications appeared incorporating vitrimer(-like) chemistries into rubbers. However, almost all are based on ENR rubber as the material of choice, which is due to its straightforward curing employing cross-linkers comprising carboxylic acid moieties, including adequately modified fillers. The latter are an attractive approach to combine curing agent and filler in one chemical (see section 2.2.6). This is of particular interest in the field of rubbers, for which reinforcement is essential to obtain high-performance materials. Furthermore, until now solely transesterification has been used as the underlying bond exchange mechanism. An exception constitutes a study of Liu et al., who introduced dynamic imine bonds into composites from styrene-butadiene rubber (SBR) and graphene.<sup>187</sup> Catalyst-free imine exchange reactions enabled the rearrangement of the network topology, yielding full vitrimer characteristics considering the complete stress relaxation behaviour of the composites.

For instance, Zhang et al. prepared ENR networks with carbon nanodots as high-functionality cross-linking agent, yielding composites with full vitrimer characteristics.<sup>129</sup> The carbon nanodots exhibited surface carboxylic acid groups, allowing the cross-linking of ENR across its epoxy groups. Similar to the work of Imbernon et al., during network formation  $\beta$ -hydroxyl ester linkages were obtained that enabled thermo-activated topology rearrangements through transesterifications at the polymer-filler interface, promoted by the catalyst zinc acetate. Besides almost complete stress relaxation, the dynamic nature of the linkages resulted in recycling, reshaping and welding capabilities of these composites. However, comparatively low filler contents were applied, amounting to a maximum of about 5 phr. Noteworthy, at 50%, the employed ENR had a much higher degree of epoxidation compared to the ENR used by Imbernon et al., which was at 25%.<sup>127</sup> Thus, significantly higher cross-link densities could be achieved, probably enhancing topology rearrangements.

Chen et al. as well as Lin et al. further explored very similar strategies, yet at much higher filler loadings of about 30 wt% in each case. The former prepared elastomeric composites from ENR latex with an epoxidation degree of 40% and TEMPO (2,2,6,6-tetramethylpiperidine-1-oxyl) oxidised cellulose nanocrystals comprising carboxylic acid groups on the filler surface.<sup>128</sup> Lin et al. took advantage of a similar chemistry in their ENR-bentonite composites.<sup>176</sup> ENR rubber at an epoxidation degree of 40% was covalently cross-linked with bentonite as the filler that was previously modified with citric acid, thus possessing surface carboxylic acid moieties. At elevated temperatures, both types of networks revealed interfacial bond exchange reactions of  $\beta$ -hydroxyl esters. While Chen et al. used zinc acetate as transesterification catalyst, the network dynamic in the ENR-bentonite composites of Lin et al. was achieved without the addition of any catalyst. Both approaches resulted in a significant reinforcement and thermal adaptability of the networks at the same time, which was further successfully demonstrated by means of recycling and self-healing experiments. However, also here the materials have to be considered rather as vitrimer-like, since the networks were unable to fully relax stresses.

Going from ENR to ethylene-propylene-diene monomer (EPDM) rubber, but taking advantage of the same chemical functions and bond exchange mechanism, Zhang et al. reported vitrimeric composites from EPDM and carbon black.<sup>130</sup> Here, the filler has not been exploited as both reinforcement and cross-linker. Instead,  $\beta$ -hydroxyl ester bonds were obtained *via* cross-linking with biobased di-functional dodecanedioic acid. Zinc acetate was used as transesterification catalyst and very high filler loadings up to 80 phr were incorporated. Nevertheless, topology rearrangements at elevated temperatures enabled stress relaxation, reshaping and recycling of the rubbery networks.

All aforementioned materials rely on a chemistry with the epoxy groups located at the polymer backbone (e.g. ENR) and the carboxylic acid moieties at the cross-linking agent. In contrast, Guo et al. presented the first synthetic approach involving a reversed reactivity of rubber and cross-linker (Figure 20).<sup>40</sup> The authors implemented full vitrimer characteristics into carboxyl group-grafted SBR using up to 30 phr of epoxy-functionalised nanosilicate, serving as both reinforcing filler and cross-linker. Although following a reversed chemistry, also here the topology rearrangements were achieved through transesterifications of  $\beta$ -hydroxyl ester cross-links at the SBR-silica interface. In this context, it is important to mention that upon cross-linking less sterically hindered

hydroxyl groups are generated compared to curing of epoxidised rubbers with carboxylic acids (see Figure 18). In the latter case, the steric hindrance of free hydroxyl groups necessary for transesterification reactions derives not only from the adjacent methyl group but also from the proximity of the polymer backbone in general. The bond exchange reactions were thermally activated, and organic TBD (1,5,7-triazabicyclo[4.4.0]dec-5-ene) was used for the first time as transesterification catalyst in vitrimeric materials based on rubbers. Along with complete stress relaxation, the ability of the composites to undergo reshaping and recycling was demonstrated. However, the synthetic procedure is solvent-based and therefore not suitable for classical compounding and processing technologies employed in rubber industry.

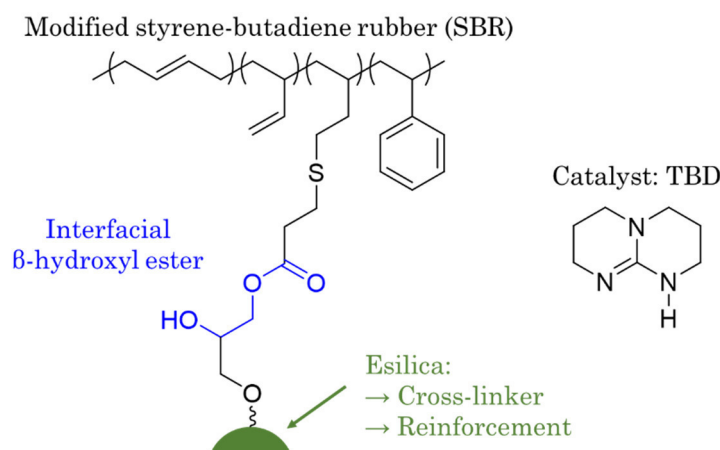


**Figure 20.** Schematic illustration of elastomeric vitrimer composites from carboxyl group-grafted styrene-butadiene rubber (SBR) reported by Guo et al.<sup>40</sup> Curing of the modified rubber with epoxy-functionalised nanosilica (Esilica) yields interfacial β-hydroxyl ester cross-links that are susceptible to thermo-activated transesterification exchange reactions in the presence of the catalyst triazabicyclodecene (TBD). Scheme adapted from literature.<sup>40</sup>

For reasons of completeness, it should be noted that already in 2012 Guan and co-workers obtained dynamic associative covalent networks making use of olefin cross-metathesis exchange reactions in networks from polybutadiene (PBD) rubber.<sup>188</sup> The preparation of the lightly cross-linked materials was carried out in two steps. After covalent cross-linking of the high molecular weight linear PBD *via* oxidation using an organic peroxide, the second-generation Grubbs' Ru metathesis catalyst was introduced by a swelling step. The exchange reaction was found to be highly effective, enabling stress relaxation and quantitative healing already at room temperature. However, creep from low temperatures, the two-step synthesis procedure, and the necessity of organic solvents as well as expensive catalyst are among the drawbacks of this approach.

Another approach based on polybutadiene was reported by Nicolaÿ et al., incorporating exchangeable dioxaborolane moieties.<sup>189</sup> The elastomeric networks showed excellent malleability, even in dual networks comprising a certain number of permanent chemical bonds. Since non-entangled, low molar mass PBD was employed, these networks are not considered as vitrimers from high molecular weight rubber.

In general, the incorporation of dynamic covalent cross-links into rubbers occurs during the cross-linking process only. For these high molecular weight polymers, no exchangeable bonds are initially present in the (linear) polymer chains. Common industrially relevant rubbers exhibit a comparatively small amount of functional groups capable of acting as cross-link sites. Therefore, naturally a much lower number of (dynamic) cross-links is obtained, as opposed to vitrimeric networks from low molecular weight monomers. Thus, it is reasonable to assume that the introduction of full vitrimer characteristics into high molecular weight rubbers is challenging, especially for rubbers with a limited potential in the formation of covalent cross-links. For such networks, similar characteristics should apply as discussed in chapter 2.2.2 on dissociative CANs synthesised following the reversible macromer approach.

### 2.2.6 Fillers in associative dynamic covalent networks

Recently, an increased attention on potential applications of vitrimers can be observed. Taking advantage of their adaptability through associative bond exchange reactions is of particular interest in coatings<sup>142,179</sup>, adhesives<sup>180</sup>, and composites. Vitrimers are promising polymeric materials in the context of reshaping, repairing, (re)processing and recycling. Besides composites from classical thermosetting materials such as epoxy, the application of fillers (at high loadings) is of utmost significance in the field of rubbers (e.g. tires, seals, belts), since unfilled rubbers usually suffer from poor mechanical properties.<sup>190</sup> This section provides a brief overview of vitrimers in the field of composites. More precisely, types of filler particles that have been used to date and the role of the surface chemistry are discussed (Figure 21). Vitrimers have also been employed already as matrices in fiber-reinforced polymer composites (FRPC).<sup>163,164,172–174</sup> This type of composite is not covered here.

Regardless of whether dynamic polymer networks are used as matrix or not, the two key factors determining the final properties of composites are a homogeneous dispersion of the filler and a good interfacial adhesion between filler and matrix.<sup>191</sup> If these conditions are given, an efficient stress transfer from the matrix to the filler is ensured, providing a high reinforcing effect. Both parameters can be improved through the usage of modified fillers.<sup>192</sup> In particular, the covalent attachment of fillers to the polymer chains of a network limits filler aggregation and enhances the stress transfer from matrix to filler, both further improving the interfacial adhesion. However, the incorporation of fillers generally restricts the chain mobility in polymer composites, which especially for the case of dynamic covalent networks causes a detrimental effect on topology rearrangements and the viscous flow properties. Thus, it is of particular importance to align the functionality of the filler surface and the polymer matrix to maintain as much as possible the dynamic nature in composites from associative covalent adaptable networks.

In terms of the network design, practically all vitrimers containing particles as filler rely on transesterification as the bond exchange mechanism. This is mainly due to the ease in availability of fillers comprising either epoxy or carboxylic acid group functionalisation. During network formation, these modified fillers are not only covalently incorporated into the polymer matrix, but even form the same exchangeable linkages at the polymer-filler

interface as existing in the matrix and thus, can participate in topology rearrangements. Following this approach is especially relevant in highly filled vitrimer composites.

Legrand et al. investigated nanofillers within the classical soft vitrimer matrix from Leibler et al., consisting of diglycidyl ether of bisphenol A (DGEBA) and a mixture of tricarboxylic and dicarboxylic fatty acids (Pripol 1040).<sup>126</sup> In detail, the authors were interested in highly filled silica networks, and the impact on both the mechanical and dynamic properties. Interestingly, even at filler contents of up to 40 wt%, all composites still underwent full stress relaxation. However, prolonged relaxation times were found in the presence of filler due to a decreased network mobility. To overcome this issue, epoxy moieties were covalently attached to the silica surface. This modification did not only improve the dispersion state within the network, but also the interfacial adhesion by taking part in the cross-linking reaction and thus, the filler being covalently linked to the polymer matrix. As a result, reinforced yet highly dynamic vitrimer composites were obtained.

Huang et al. drew similar conclusions in their study dealing with the influence of the surface chemistry of silica nanoparticles as filler in disulphide-based vitrimer composites from DGEBA and AFD (4-aminophenyl disulphide).<sup>177</sup> The authors compared epoxy and thiol group functionalised silica nanoparticles with the respective pristine OH-terminated particles. As expected, the reinforcing effect significantly increased upon surface modification due to the covalent attachment of the filler particles to the network. Since these networks relied on disulphide exchange chemistry, epoxy-functionalised silica showed no benefit for an improved stress relaxation. In contrast, nanosilica comprising thiol groups at the particle surface contributed actively to the network dynamics through fast thiol-disulphide exchange reactions.

Both aforementioned studies highlight the importance of aligning the surface chemistry of fillers with the matrix in order to minimise their detrimental effect on the network dynamics in vitrimers. It should be noted that such vitrimers are synthesised from low molecular weight monomers, yielding highly cross-linked networks. Consequently, dynamic covalent bonds are abundantly available throughout the materials. This is not the case for networks based on high molecular weight (linear) polymers, which commonly comprise much lower cross-link densities due to a limited number in chemical functions available as curing sites. Thus, the application of modified fillers is especially interesting in the preparation of dynamic composite networks from rubbers. In rubber-based networks, the modification of fillers not only serves to adapt the chemistries of filler and polymer in terms of good network dynamics, but the filler can be exploited simultaneously as the cross-linking agent. As a result, the filler provides both reinforcement and exchangeable covalent bonds at the polymer-filler interface at the same time. Eventually, no further addition of a cross-linking agent is required. In fact, nearly all studies involving (highly) filled vitrimer(-like) rubbers rely on this strategy for apparent reasons, and were already discussed in detail in section 2.2.5. Vitrimer composites comprising both filler (unmodified or modified) and an additional curing agent are rather based on small monomers, as discussed above. Moreover, in many cases, the fillers were not primarily added for reasons of reinforcement, but for instance as light absorbers subsequently exploited for photothermally triggered bond exchange reactions. This approach allows

spatial control of the topology rearrangements, and has been realised among others<sup>193</sup> using carbon nanotubes<sup>133</sup> (CNTs) or graphene<sup>132</sup> as filler.

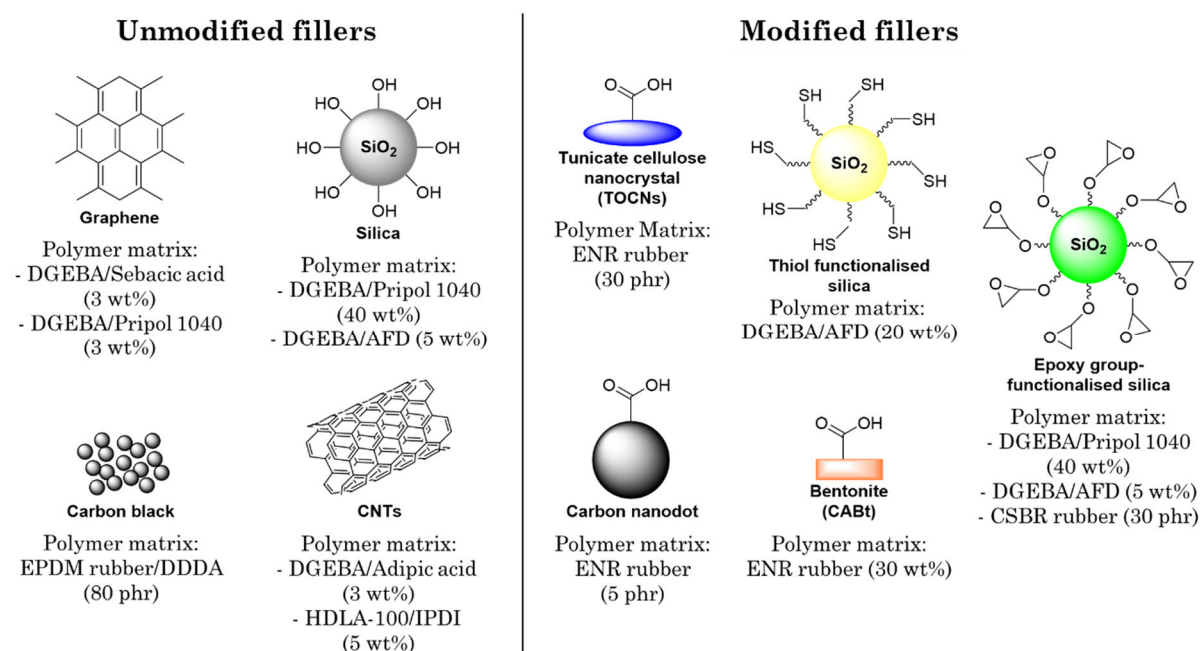


**Figure 21.** Schematic overview of various filler types used for the preparation of vitrimer(-like) composites, including unmodified fillers and modified fillers with tailored surface chemistries. The respective maximum filler contents are given in brackets. *ENR*: epoxidised natural rubber; *DGEBA*: bisphenol A diglycidyl ether, *Pripol 1040*: mixture of C18 fatty acids derivatives; *AFD*: 4-aminophenyl disulphide; *CSBR*: carboxyl group-grafted styrene-butadiene rubber; *CABt*: citric acid-modified bentonite; *EPDM*: ethylene propylene diene monomer rubber; *DDDA*: dodecanedioic acid; *TOCNs*: TEMPO oxidised cellulose nanocrystals; *CNTs*: carbon nanotubes; *HDLA-100*: hindered secondary amide; *IPDI*: isophorone diisocyanate.

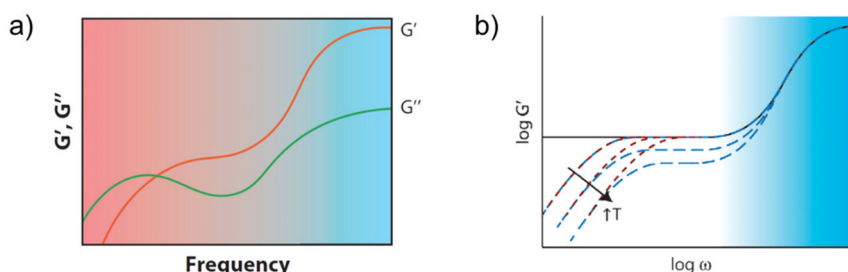
## 2.2.7 Characterisation of dynamic covalent networks

In this section, the characterisation methods commonly applied to demonstrate the dynamic network properties in vitrimers are presented. This relates to the time- and temperature-dependent mechanical behaviour of vitrimers, and in particular to the analysis of the topology freezing transition with its characteristic temperature  $T_v$ . The time- and temperature-dependent properties of vitrimers arise from thermo-activated covalent bond exchanges that occur in an associative manner. When preparing vitrimer (-like) networks, it is not only of interest to simply evidence topology rearrangements, but also to quantify the exchange reaction rate and its temperature-dependence, the activation energy of the exchange chemistry, and the onset of significant bond exchanges (i.e.  $T_v$ ). Particular focus is devoted to the determination of the  $T_v$ , since this temperature is also of great importance for the estimation of the maximum service temperature of vitrimeric polymeric materials, which is crucial for potential applications of this material class. Importantly, it must be noted that the observations made in the characterisation of vitrimers are always related to the observed timeframe of the particular analysis method. Specifically regarding the analysis of  $T_v$ , Guerre et al. emphasised that this temperature value should not be considered as an absolute physical value, but that it is highly

dependent on the applied experiment.<sup>156</sup> Specific and in-depth studies of the rheological behaviour of some vitrimers were reported by Montarnal et al.<sup>194</sup> as well as Terentjev and co-workers<sup>195</sup>.

### *Dynamic mechanical analysis and rheology*

In dynamic analysis methods, the material response (i.e. storage ( $G'$ ) and loss ( $G''$ ) modulus) is measured as a function of time, temperature and frequency of the applied sinusoidal deformation. For permanent polymeric networks, the storage modulus remains larger than the loss modulus at all frequencies and temperatures. For vitrimers, the same is observed at relatively high frequencies (i.e. short time-scales), where the networks behave elastically. However, changing the time-scale by going to lower frequencies (i.e. longer duration of the deformation), the storage modulus becomes lower than the loss modulus (Figure 22a). In order to observe this crossover at high temperatures, the relaxation time that is controlled by the bond exchange rate of the underlying exchange chemistry must be shorter than the experimental time scale.<sup>103,124</sup> Thus, measurements at high frequencies (e.g. conventional DMA analysis) do usually not allow the observation of topology rearrangements. They rather reflect the constant average connectivity (cross-link density) of vitrimers even at temperatures above  $T_v$ , comprising a constant plateau modulus (Figure 22b) that confirms the associative nature of the bond exchange mechanism. The plateau modulus obeys rubber elasticity theory and can be tailored by the cross-link density of a network. Moreover, the relaxation rate of vitrimers significantly accelerates with temperature. Dissociative CANs show a similar frequency- and temperature-dependent stress relaxation as vitrimers.



#### **Thermoset**

- T- and  $\omega$ -independent plateau modulus
- No stress relaxation at all  $\omega$

#### **Dissociative CAN**

- T-dependent plateau modulus
- T- and  $\omega$ -dependent stress relaxation

#### **Vitriimer**

- T- and  $\omega$ -independent plateau modulus
- T- and  $\omega$ -dependent stress relaxation

**Figure 22.** (a) Schematic dynamic rheological graph illustrating the behaviour of storage ( $G'$ ) and loss ( $G''$ ) modulus for vitrimers as a function of frequency ( $\omega$ ) at constant temperature. The phenomenon of crossover of  $G'$  and  $G''$  occurs at low frequency and high temperature, where covalent bond exchanges are significantly fast. (b) Schematic illustration of the frequency- and temperature-dependent behaviour of  $G'$  for thermosets (black), dissociative CANs (blue), and vitrimers (red). Schemes adopted from literature.<sup>103,196</sup>

However, the plateau modulus varies with the temperature, which is due to a decrease in cross-link density, resulting from the displacement of the equilibrium of the reversible cross-linking reaction. In stark contrast, classical thermosets display a temperature- and frequency-independent modulus before undergoing degradation (Figure 22b).

### *Stress relaxation*

Stress relaxation is the ability of a material to decrease internal stresses over time arising from a constant deformation by an external force. Polymers exhibit a stress relaxation behaviour that is depending on various parameters, such as cross-link density, physical interactions (e.g. entanglements and hydrogen bonding), and free volume.<sup>197</sup> Common thermosets show a stress relaxation that strongly depends on the cross-link density, since they are prepared from low molecular weight monomers or oligomers, resulting in highly covalently cross-linked networks.<sup>198</sup> In contrast, in thermoplastics and slightly chemically cross-linked networks stress relaxation is rather controlled by physical interactions. The molecular segmental motion of the polymer chains is strongly influenced by entanglements due to the high molecular weight of the (linear) polymer chains. Consequently, thermosets display very limited stress relaxation, whereas the relaxation behaviour of polymeric materials usually improves with decreasing cross-link density, more physical interactions and higher free volume. The observed stress relaxation is attributed to reptation and the motion of dangling chains and defects.<sup>199</sup> However, the relaxation rate is slow and in principle uncontrolled. Furthermore, the concurrent change in viscosity is rarely sufficient to provide the materials with reprocessability or repairing capabilities. In vitrimers and vitrimer-like polymeric networks, the stress relaxation obtained is owed almost entirely to topology rearrangements enabled by covalent bond exchange reactions above  $T_v$  (or above  $T_g$  for  $T_v < T_g$ ). Thereby, the shape of the sample is permanently altered due to the plastic nature of the deformation. In contrast, permanent and elastic networks would return to the original sample geometry. Importantly, materials with full vitrimer characteristic can completely relax stresses. In contrast, vitrimer-like networks usually display an incomplete stress relaxation behaviour.

The dynamics of vitrimers is practically always studied by stress relaxation experiments (Figure 23a), and the relaxation rate is a measure for the rate of associative bond exchange reactions occurring in the polymer network. The accompanying change in viscosity as a function of temperature follows the Arrhenius law, and so do the relaxation times (Figure 23b). Assuming a Maxwell model of relaxation, the relaxation times ( $\tau$ ) are conventionally determined as the time necessary to relax to 37.8% ( $1/e$ ) of the initial stress.<sup>124</sup> Accordingly, the activation energy ( $E_a$ ) of the underlying bond exchange reaction can be calculated from the Arrhenius equation,  $\tau(T) = \tau_0 \exp(-E_a/RT)$ . When plotting the relaxation times as a function of temperature (Arrhenius plot), theoretical relaxation times for low temperatures can be derived by extrapolation, which would not be experimentally accessible due to unmeasurable long time scales of the viscosity changes.<sup>116</sup> In addition, also through extrapolation of viscosity trends, values for the topology freezing transition temperature ( $T_v$ ) may be extracted from the Arrhenius plot for a viscosity falling below  $10^{12}$  Pa·s. By convention, this viscosity value marks the solid-to-liquid transition of a glass-forming liquid.<sup>116,124,200</sup> Specifically valid for the classical epoxy-acid vitrimer of Leibler et al.<sup>124</sup>, the  $T_v$  could be calculated from the respective Arrhenius plot for a



relaxation time of  $10^6$  s (Figure 23c). This correspondence between the viscosity and the relaxation time was obtained on the basis of the Maxwell equation  $\eta = G \cdot \tau^*$  (with  $G = 1$  MPa).

The experimental approaches for the analysis of the stress relaxation behaviour of vitrimers include rheometry in plate-plate geometry applying shear stresses, and the usage of a dynamic mechanical analyser (DMA) in tensile mode, applying either torsional or elongational static displacements. In any case, the applied deformation must be selected within the linear viscoelastic range of a particular material. For the analysis of  $E_a$  and  $T_v$ , a series of measurements has first to be conducted at different temperatures. The selected temperatures have to be sufficiently above the onset of the topology freezing transition to keep the measurement times reasonably short. Afterwards, following the method described above, the  $T_v$  of a particular vitrimer network can be determined. However, with this approach only theoretical values for  $T_v$  are obtained, wherefore it has to be described rather as an indirect method to access the  $T_v$  of vitrimers.

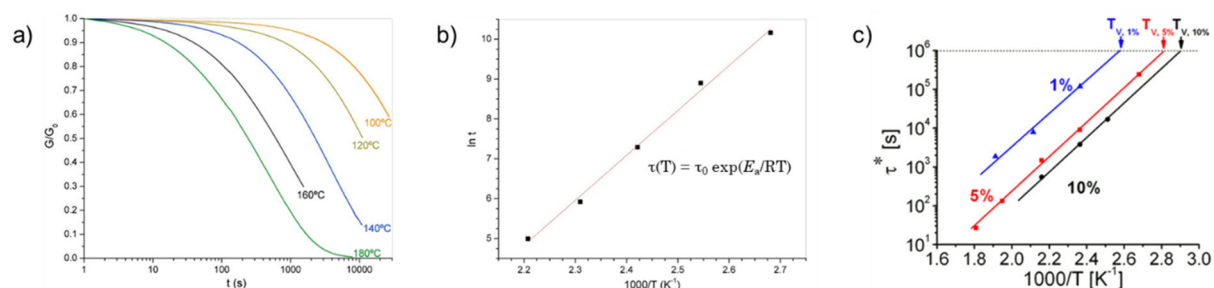


**Figure 23.** (a) Typical series of stress relaxation measurements for a vitrimer at various temperatures showing the normalised relaxation modulus as a function of time, and (b) the corresponding Arrhenius plot of the measured characteristic relaxation times (time to reach  $1/e$  of the initial modulus), allowing the calculation of the activation energy ( $E_a$ ) of the underlying bond exchange chemistry. (c) Illustration of the estimation of  $T_v$  values from the Arrhenius plot by linear extrapolation of the data based on stress relaxation experiments as shown by Leibler et al. Schemes adopted from literature.<sup>124,138</sup>

### Creep measurements

Creep is the progressive deformation of a material over time arising from a constant stress. Creep experiments can be considered as the inverse of stress relaxation and are normally performed at constant temperature. In terms of vitrimers, creep measurements are typically conducted on tensile specimens applying a constant elongational tension. Similar to stress relaxation, the rate of creep is a measure for the rate of associative bond exchange reactions occurring in the particular polymer network. At temperatures above the topology freezing transition, the specimen is in the state of plastic flow and the slope of the steady state creep increases with both the temperature and the efficiency of the bond exchange reactions (e.g. with catalyst type and loading). Importantly, for networks with full vitrimer characteristics the strain increases linearly with time after the initial elastic response. Subsequently, viscosity values ( $\eta$ ) and the relaxation times ( $\tau$ ) can be derived from the measurement curves at different temperatures according to the equations  $\eta = \sigma/\dot{\epsilon}$  and  $\tau = \eta/E$  (with  $\sigma$  the stress,  $\dot{\epsilon}$  the strain rate, and  $E$  the Young's modulus at the measurement temperature). Similar to the methodology for stress relaxation, full vitrimers display an

Arrhenius dependence of the relaxation times, and the activation energy of the particular exchange chemistry can be calculated from the Arrhenius equation accordingly.

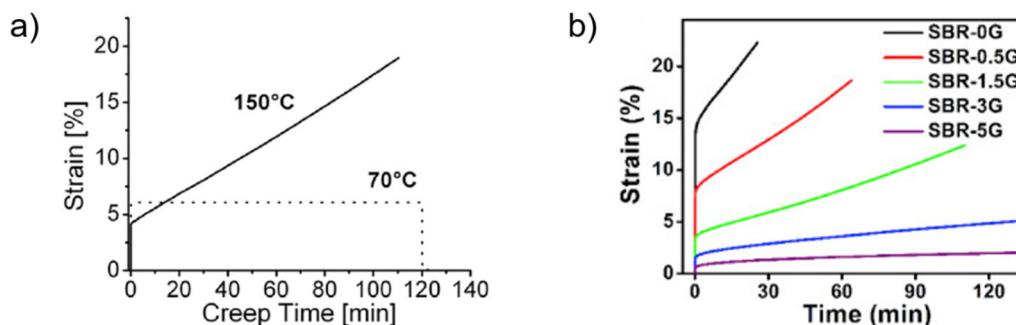


**Figure 24.** Typical elongational creep experiments of vitrimers at constant stresses. (a) Creep measurements below ( $70\text{ }^{\circ}\text{C}$ ) and above ( $150\text{ }^{\circ}\text{C}$ ) the topology freezing transition temperature ( $T_v$ ), showing no plastic deformation and a linearly increasing strain with time, respectively. (b) Creep curves at a constant temperature revealing a decrease in creep rate and increase in initial elastic response with the filler content (i.e. cross-link density). Schemes adopted from literature.<sup>124,187</sup>

### Dilatometry

As an alternative to stress relaxation measurements, dilatometry is regularly encountered in literature to highlight the topology freezing transition in vitrimers.<sup>40,116,124,129,176</sup> In general, dilatometry provides a different perspective on the topology freezing transition than stress relaxation measurements, since the entire relevant temperature range of the transition is covered. With respect to the  $T_v$ , dilatometry offers a direct route towards the determination of this characteristic temperature, as opposed to the procedure *via* stress relaxation data involving an Arrhenius plot, only giving a hypothetical value for  $T_v$  through extrapolation of viscosity trends. Moreover, the latter methodology is not applicable to vitrimer-like materials that exhibit only a partial stress relaxation that is not decreasing to 37.8% of the initial value, at least not for a required series of temperatures.

In a typical dilatometry experiment, the elongational expansion behaviour of a sample is monitored over time at increasing temperature, applying a small stress to avoid buckling (Figure 25). Usually, a first signature in the measurement curve is found due to the classical glass transition ( $T_g$ ). Above  $T_g$ , another increase in strain appears at a certain temperature. This is attributed to the thermo-activated associative bond exchange reactions occurring in the networks, marking the onset of the topology freezing transition.<sup>116</sup> Commonly, the onset is considered as the  $T_v$  of a certain vitrimer. In literature, it is further stated that the topology freezing transition in vitrimers causes an increase in the coefficient of thermal expansion (CTE) because a reorganising network is supposed to have a higher CTE than the respective static network.<sup>124</sup> Above  $T_g$  and below  $T_v$ , the linear expansion coefficient remains constant, reflecting the permanent character of the network in this temperature range.

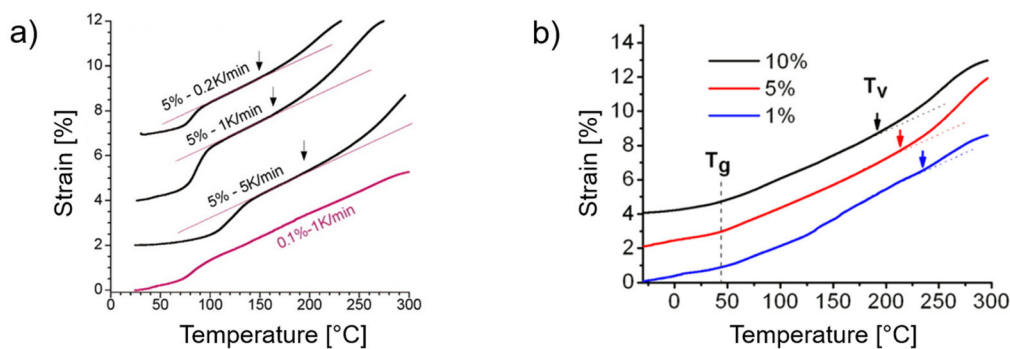


**Figure 25.** Typical dilatometry measurements as performed in literature. Showing (a) the heating rate dependency and (b) the influence of catalyst content on the evolution of the topology freezing transition in the classical vitrimers as demonstrated by Leibler and co-workers. Arrows indicate the onset of the solid-to-liquid transition, which is commonly considered as the  $T_v$  of the material. Schemes adopted from literature.<sup>116,124</sup>

Leibler and co-workers observed a heating rate dependency of the topology freezing transition in dilatometry measurements on their pioneering epoxy vitrimers, which is typical for glass transitions.<sup>116</sup> Moreover, the onset of the transition varies with the type and content of catalyst in transesterification-based vitrimers.<sup>124</sup>

More insights in the context of vitrimers and dilatometry were provided by Pritchard et al.<sup>201</sup> They pointed out that the measurement method is incorrectly referred to as dilatometry rather than creep compliance experiment, since a considerable external force is applied. Specifically, the authors investigated the influence of stress on the onset of the irreversible plastic flow that is the transition from a viscoelastic solid to a viscoelastic liquid. The measurements were conducted at rising temperature and constant tensile stresses on the example of the classical isotropic epoxy-acid vitrimer of Leibler et al. It was concluded that the onset is independent of the applied stress due to the thermally controlled activity of the catalyst determining  $T_v$ , with the  $T_v$  being decoupled from mechanical influences.

It should also be mentioned that dilatometry ideally refers to the measurement of dimensional changes of a sample as a function of temperature without any mechanical constraints. Accordingly, the free movement of a sample can only be ensured in a contact force-free dilatometry measurement in static state.

#### *Aggregation-induced-emission luminogens*

Recently, an entirely different analysis method for the topology freezing transition and its characteristic temperature  $T_v$  was presented. Ji et al. demonstrated the accessibility of  $T_v$  by aggregation-induced-emission (AIE) luminogens (Figure 26).<sup>134</sup> After doping of vitrimers with AIE luminogens, they followed the change in fluorescence of the luminogens at increasing temperature. Approaching the  $T_v$  of a particular vitrimeric network the fluorescence changed significantly. Moreover, the method not only provided a  $T_v$  value but also the estimation of a temperature range of the topology freezing transition was reported, similarly to the detection of a classical  $T_g$ . Interestingly, the authors stated that the method is independent of the catalyst loading. More precisely, an identical  $T_v$  value was found for an epoxy-acid network for both with and without TBD as

transesterification catalyst. This phenomenon was explained by the intrinsic nature of the  $T_v$  of vitrimers. In addition, it is the first analysis method for the determination of  $T_v$  that occurs in static state, thus excluding any interfering effects by external forces.

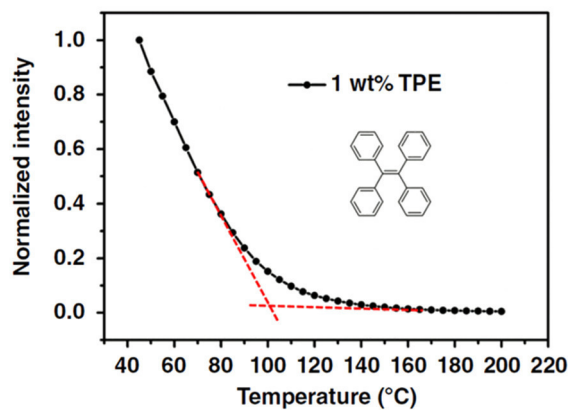


**Figure 26.** Evolution of the fluorescence intensity as a function of temperature for AIE luminogens incorporated into vitrimer matrix as reported by Ji et al. Scheme adopted from literature.<sup>134</sup>

---

### 2.3 References

- 1 S. Sandler, in *Polymer Syntheses VI*, Elsevier Science, Oxford, 1974, vol. 29, 309–342.
- 2 J. G. de Vries and C. J. Elsevier, *The handbook of homogeneous hydrogenation*, Wiley-VCH, Weinheim, 2007.
- 3 D. Mackey and A. H. Jorgensen, in *Encyclopedia of chemical technology*, ed. R. E. Kirk and D. F. Othmer, Wiley, New York, NY, 2003.
- 4 V. C. Chandrasekaran, *Rubber seals for fluid and hydraulic systems*, William Andrew, Amsterdam, 2010.
- 5 V. C. Chandrasekaran, *Essential rubber formulary. Formulas for practitioners*, William Andrew Pub, Norwich, NY, 2007.
- 6 C.R. Kumar and J. Karger–Kocsis, *European Polymer Journal*, 2002, 38, 2231–2237.
- 7 K. Kumeta, I. Nagashima, S. Matsui and K. Mizoguchi, *Journal of Applied Polymer Science*, 2003, 90, 2420–2427.
- 8 H. P. Brown, *Rubber Chemistry and Technology*, 1963, 36, 931–962.
- 9 C. Gürtler and K. Danielmeier, *Tetrahedron Letters*, 2004, 45, 2515–2521.
- 10 P. Ghosh, *Polymer science and technology. Plastics, rubbers, blends and composites*, Tata McGraw-Hill, New Delhi, 2nd edn., 2002.
- 11 J. S. Dick, *Rubber Technology. Compounding and Testing for Performance*, Carl Hanser Fachbuchverlag, s.l., 2nd edn., 2014.
- 12 Przybyszewska, M.; Zaborski, M.; Jakubowski, B.; Zawadiak, J. (2009): Zinc chelates as new activators for sulphur vulcanization of acrylonitrile-butadiene elastomer. In: *Express Polym. Lett.* 3 (4), 256–266.
- 13 a) M. Klueppel and G. Heinrich, *Macromolecules*, 1994, 27, 3596–3603; b) A. Vieyres, R. Pérez-Aparicio, P.-A. Albouy, O. Sanseau, K. Saalwächter, D. R. Long and P. Sotta, *Macromolecules*, 2013, 46, 889–899; c) F. N. Linhares, M. Kersch, U. Niebergall, M. C. A. M. Leite, V. Atlstädt and C. R. G. Furtado, *Fuel*, 2017, 191, 130–139.
- 14 N. J. Morrison and M. Porter, in *Comprehensive polymer science. The synthesis, characterization, reactions et applications of polymers*, ed. G. Allen, Pergamon Press, Oxford, 1989, 115–133.
- 15 S. Oae, ed., *Organic Chemistry of Sulfur*, Springer US, Boston, MA, 1977.
- 16 N. P. Cheremisinoff, in *Condensed Encyclopedia of Polymer Engineering Terms*, ed. N. P. Cheremisinoff, Elsevier Science, Oxford, 169th edn., 2001, 200–255.
- 17 J. Kruželák, R. Sýkora and I. Hudec, *Rubber Chemistry and Technology*, 2017, 90, 60–88.
- 18 S.K. Henning and R. Costin, *Rubber World*, 2006, 233, 28–35.
- 19 P. R. Dlužneski, *Rubber Chemistry and Technology*, 2001, 74, 451–492.
- 20 P. Posadas, M. A. Malmierca, A. Gonzalez-Jimenez, L. Ibarra, A. Rodriguez, J. L. Valentin, T. Nagaoka, H. Yajima, S. Toki, J. Che, L. Rong and B. S. Hsiao, *Express Polym. Lett.*, 2016, 10, 2–14.
- 21 Y. Li, Effect of crosslink density on the tearing of gum natural rubber cured with dicumyl peroxide (DCP), *Master's thesis*, 2013, University of Akron.

- 
- 22 N. Gil-Negrete and A. Alonso, eds., *Constitutive models for rubber VIII. Proceedings of the 8th European Conference on Constitutive Models for Rubber (ECCMR VIII), San Sebastián, Spain, 25 - 28 June 2013*, CRC Press/Balkema, Boca Raton, Fla., 2013.
- 23 L. González, A. Rodríguez, A. Marcos-Fernández, J. L. Valentín and A. Fernández-Torres, *Journal of Applied Polymer Science*, 2007, 103, 3377–3382.
- 24 M. Akiba, *Progress in Polymer Science*, 1997, 22, 475–521.
- 25 a) M. M. Alvarez Grima, *Novel co-agents for improved properties in peroxide cure of saturated elastomers*, 2007; b) R. Rajan, S. Varghese and K. E. George, *Rubber Chemistry and Technology*, 2013, 86, 488–502.
- 26 a) *Arkivoc*, 2002, 2002, 293; b) *Arkivoc*, 2008, 2008, 46; c) D. Li, J. Wang, S. Yu, S. Ye, W. Zou, H. Zhang and J. Chen, *Chemical communications*, 2020, 56, 2256–2259; d) G. Tesoro, *J. Polym. Sci. B Polym. Lett. Ed.*, 1988, 26, 539.
- 27 F. B. Alvey, *J. Polym. Sci. Polym. Chem.*, 1969, 7, 2117–2124.
- 28 W. J. Blank, Z. A. He and M. Picci, *J. Coatings Tech.*, 2002, 74, 33–41.
- 29 F. Ricciardi, M. M. Joullié, W. A. Romanchick and A. A. Griscavage, *J. Polym. Sci. B Polym. Lett. Ed.*, 1982, 20, 127–133.
- 30 C. Wang, L. Luo and H. Yamamoto, *Accounts of chemical research*, 2016, 49, 193–204.
- 31 H. Kakiuchi and Y. Tanaka, *The Journal of organic chemistry*, 1966, 31, 1559–1564.
- 32 L. Shechter and J. Wynstra, *Ind. Eng. Chem.*, 1956, 48, 86–93.
- 33 Libor Matějka, Svatopluk Pokomý and Karel Dušek, *Polymer Bulletin*, 1982, 7, 123–128.
- 34 J. Otera, *Chem. Rev.*, 1993, 93, 1449–1470.
- 35 P. Cassagnau, M. Bert, V. Verney and A. Michel, *Polymer*, 1993, 34, 124–131.
- 36 M. Lamba, J. Druz and A. Bouilloux, *Polym. Eng. Sci.*, 1987, 27, 1221–1228.
- 37 F. Altuna, C. Hoppe and R. Williams, *Polymers*, 2018, 10, 43.
- 38 S. K. Chakraborty and S. K. De, *Journal of Applied Polymer Science*, 1982, 27, 4561–4576.
- 39 G. Zhang, H. Feng, K. Liang, Z. Wang, X. Li, X. Zhou, B. Guo and L. Zhang, *Science Bulletin*, 2020, 65, 889–898.
- 40 Y. Liu, Z. Tang, Y. Chen, C. Zhang and B. Guo, *ACS applied materials & interfaces*, 2018, 10, 2992–3001.
- 41 L. Shechter, J. Wynstra and R. Kurkjy, *Ind. Eng. Chem.*, 1957, 49, 1107–1109.
- 42 A. Bukowska and W. Bukowski, *Org. Process Res. Dev.*, 2002, 6, 234–237.
- 43 A. D. Jenkins, P. Kratochvíl, R. F. T. Stepto and U. W. Suter, *Pure and Applied Chemistry*, 1996, 68, 2287–2311.
- 44 A. Eisenberg and C.-s. Kim, *Introduction to ionomers*, Wiley, New York, 1998.
- 45 A. Eisenberg, *Macromolecules*, 1970, 3, 147–154.
- 46 a) M. A. Malmierca, A. González-Jiménez, I. Mora-Barrantes, P. Posadas, A. Rodríguez, L. Ibarra, A. Nogales, K. Saalwächter and J. L. Valentín, *Macromolecules*, 2014, 47, 5655–5667; b) D. Basu, A. Das, K. W. Stöckelhuber and S. Wießner, in *Designing of Elastomer Nanocomposites: From Theory to Applications*, ed. K. W. Stöckelhuber, A. Das and M. Klüppel, Springer International Publishing, 2017, 235–266.
- 47 A. Eisenberg and M. Navratil, *J. Polym. Sci. B Polym. Lett.*, 1972, 10, 537–542.

- 48 M. Navratil and A. Eisenberg, *Macromolecules*, 1974, 7, 84–89.
- 49 S. Schlick, *Ionomers. Characterization, theory, and applications*, Taylor & Francis, Boca Raton, Fla., 1996.
- 50 Q. Chen, G. J. Tudryn and R. H. Colby, *Journal of Rheology*, 2013, 57, 1441–1462.
- 51 M. Zuliki, S. Zhang, K. Nyamajaro, T. Tomkovic and S. G. Hatzikiriakos, *Physics of Fluids*, 2020, 32, 23104.
- 52 a) A. M. Castagna, W. Wang, K. I. Winey and J. Runt, *Macromolecules*, 2011, 44, 2791–2798; b) Z. R. Hinton and N. J. Alvarez, *Rheol Acta*, 2019, 58, 499–511; c) A. Welty, S. Ooi and B. P. Grady, *Macromolecules*, 1999, 32, 2989–2995; d) K. Sato, *Rubber Chemistry and Technology*, 1983, 56, 942–958.
- 53 M. R. Tant, K. A. Mauritz and G. L. Wilkes, *Ionomers. Synthesis, structure, properties and applications*, Springer Netherlands, Dordrecht, 1997.
- 54 Z. Zhang, C. Huang, R. A. Weiss and Q. Chen, *Journal of Rheology*, 2017, 61, 1199–1207.
- 55 G. R. Hamed and K.-C. Hua, *Rubber Chemistry and Technology*, 2004, 77, 214–226.
- 56 a) G. R. Hamed and K. T. Han, *Rubber Chemistry and Technology*, 1990, 63, 806–824; b) P. Antony, S. Bandyopadhyay and S. K. De, *J Mater Sci*, 1999, 34, 2553–2560.
- 57 U. K. Mandal, *Polym. Int.*, 2000, 49, 1653–1657.
- 58 M. M. Coleman, J. Y. Lee and P. C. Painter, *Macromolecules*, 1990, 23, 2339–2345.
- 59 Y. Gao, N. R. Choudhury and N. K. Dutta, *J. Appl. Polym. Sci.*, 2012, 124, 2908–2918.
- 60 L. Ibarra and M. Alzorriz, *J. Appl. Polym. Sci.*, 2003, 87, 805–813.
- 61 N. Hohlbein, A. Shaaban, A. R. Bras, W. Pyckhout-Hintzen and A. M. Schmidt, *Physical chemistry chemical physics : PCCP*, 2015, 17, 21005–21017.
- 62 A. V. Tobolsky, *Properties and Structure of Polymers*, 1960.
- 63 M. R. Tant, K. A. Mauritz and G. L. Wilkes, *Ionomers. Synthesis, structure, properties and applications*, Springer Netherlands, Dordrecht, 1997.
- 64 S. Bagrodia, G. L. Wilkes and J. P. Kennedy, *Polym. Eng. Sci.*, 1986, 26, 662–672.
- 65 T. Xavier, J. Samuel and T. Kurian, *Macromol. Mater. Eng.*, 2001, 286, 507–512.
- 66 a) A. Das, A. Sallat, F. Böhme, M. Suckow, D. Basu, S. Wiessner, K. W. Stöckelhuber, B. Voit and G. Heinrich, *ACS applied materials & interfaces*, 2015, 7, 20623–20630; b) A. Mordvinkin, M. Suckow, F. Böhme, R. H. Colby, C. Creton and K. Saalwächter, *Macromolecules*, 2019, 52, 4169–4184.
- 67 S. Chatani, C. J. Kloxin and C. N. Bowman, *Polym. Chem.*, 2014, 5, 2187–2201.
- 68 G. Yilmaz and Y. Yagci, *Progress in Polymer Science*, 2020, 100, 101178.
- 69 a) C. Mack, *Fundamental principles of optical lithography. The science of microfabrication*, Wiley, Chichester, 2012; b) W. Schnabel, *Polymers and light. Fundamentals and technical applications*, John Wiley distributor, Weinheim, Chichester, 2007.
- 70 a) M. Yasui and K. Ikuta, *Microsyst Nanoeng*, 2017, 3, 17035; b) T. Scherzer, *Appl Spectrosc*, 2002, 56, 1403–1412; c) J. H. Lee, R. K. Prud'homme and I. A. Aksay, *J. Mater. Res.*, 2001, 16, 3536–3544; d) Y. Otsubo, T. Amari and K. Watanabe, *Journal of Applied Polymer Science*, 1984, 29, 4071–4080; e) Y. Otsubo, T. Amari and K. Watanabe, *Journal of Applied Polymer Science*, 1988, 35, 1651–1660.
- 71 C. P. Holmes, *The Journal of organic chemistry*, 1997, 62, 2370–2380.

- 72 J. A. Warren, J. T. Cabral and J. F. Douglas, *Physical review. E, Statistical, nonlinear, and soft matter physics*, 2005, 72, 21801.
- 73 a) J. Zhao, W. Wu, J. Sun and S. Guo, *Chem. Soc. Rev.*, 2013, 42, 5323–5351; b) Yağci, Yusuf; Reetz, Ivo (1998): Externally stimulated initiator systems for cationic polymerization. In: *Progress in Polymer Science* 23 (8), 1485–1538.
- 74 C. Michelin and N. Hoffmann, *ACS Catal.*, 2018, 8, 12046–12055.
- 75 H. Hadavinia, L. Kawashita, A. J. Kinloch, D. R. Moore and J. G. Williams, *Engineering Fracture Mechanics*, 2006, 73, 2324–2335.
- 76 T. Hughes, G. P. Simon and K. Saito, *Mater. Horiz.*, 2019, 6, 1762–1773.
- 77 T. Hughes, G. P. Simon and K. Saito, *Polym. Chem.*, 2018, 9, 5585–5593.
- 78 D. Tunc, C. Le Coz, M. Alexandre, P. Desbois, P. Lecomte and S. Carloti, *Macromolecules*, 2014, 47, 8247–8254.
- 79 P. Johnston, C. Braybrook and K. Saito, *Chem. Sci.*, 2012, 3, 2301.
- 80 M. Schraub, H. Gray and N. Hampp, *Macromolecules*, 2011, 44, 8755–8762.
- 81 a) J. E. Moses and A. D. Moorhouse, *Chem. Soc. Rev.*, 2007, 36, 1249–1262; b) H. Nandivada, X. Jiang and J. Lahann, *Advanced materials*, 2007, 19, 2197–2208.
- 82 a) A. Gandini, *Polímeros*, 2005, 15, 95–101; b) A. Sanyal, *Macromol. Chem. Phys.*, 2010, 211, 1417–1425; c) J. Zhou, N. K. Guimard, A. J. Inglis, M. Namazian, C. Y. Lin, M. L. Coote, E. Spyrou, S. Hilf, F. G. Schmidt and C. Barner-Kowollik, *Polym. Chem.*, 2012, 3, 628–639.
- 83 A. Gandini, *Progress in Polymer Science*, 2013, 38, 1–29.
- 84 a) J. Shorter, *Biochemical Education*, 1977, 5, 56; b) G. W. Breton and X. Vang, *J. Chem. Educ.*, 1998, 75, 81; c) B. H. Klanderman and T. R. Criswell, *The Journal of organic chemistry*, 1969, 34, 3426–3430.
- 85 E.-Z. M. Ebeid, A.-F. M. Habib and S. A. Azim, *Reactivity of Solids*, 1988, 6, 39–44.
- 86 H. Bouas-Laurent, J.-P. Desvergne, A. Castellan and R. Lapouyade, *Chem. Soc. Rev.*, 2001, 30, 248–263.
- 87 J. van Damme, L. Vlamincx, G. van Assche, B. van Mele, O. van den Berg and F. Du Prez, *Tetrahedron*, 2016, 72, 4303–4311.
- 88 R. R. Islangulov, D. V. Kozlov and F. N. Castellano, *Chemical communications*, 2005, 3776–3778.
- 89 S. V. Radl, M. Roth, M. Gassner, A. Wolfberger, A. Lang, B. Hirschmann, G. Trimmel, W. Kern and T. Griesser, *European Polymer Journal*, 2014, 52, 98–104.
- 90 L. A. Connal, R. Vestberg, C. J. Hawker and G. G. Qiao, *Adv. Funct. Mater.*, 2008, 18, 3315–3322.
- 91 a) S. Tazuke and N. Hayashi, *J. Polym. Sci. Polym. Chem. Ed.*, 1978, 16, 2729–2739; b) J. S. Hargreaves and S. E. Webber, *Macromolecules*, 1984, 17, 235–240.
- 92 N. Kuhl, S. Bode, M. D. Hager and U. S. Schubert, in *Self-healing materials*, ed. M. Hager, S. van der Zwaag and U. S. Schubert, Springer, Cham, Heidelberg, New York, Dordrecht, London, 2016, vol. 273, 1–58.
- 93 T. Hinoue, Y. Shigenoi, M. Sugino, Y. Mizobe, I. Hisaki, M. Miyata and N. Tohnai, *Chemistry*, 2012, 18, 4634–4643.
- 94 a) C. Bratschkov, *European Polymer Journal*, 2001, 37, 1145–1149; b) H. Fidler, A. Lauer, W. Freyer, B. Koeppel and K. Heyne, *The journal of physical chemistry. A*, 2009, 113, 6289–6296.



- 95 J. R. Jones, C. L. Liotta, D. M. Collard and D. A. Schiraldi, *Macromolecules*, 2000, 33, 1640–1645.
- 96 P.-G. de Gennes, *Scaling concepts in polymer physics*, Cornell Univ. Press, Ithaca, NY, ca. 2005.
- 97 G. Odian, in *Advances in Elastomers and Rubber Elasticity*, ed. J. Lal and J. E. Mark, Springer US, Boston, MA, 1986, 1–16.
- 98 In: *The science and technology of rubber*, ed. B. Erman, J. E. Mark and C. M. Roland, Elsevier Acad. Press, Amsterdam, 4th edn., 2013.
- 99 S. Kobayashi and K. Müllen, eds., *Encyclopedia of Polymeric Nanomaterials*, Springer Berlin Heidelberg, Berlin, Heidelberg, 2021.
- 100 A. Eckelt, J. Eckelt and B. Wolf, *Solubility of Polymers*, American Cancer Society, 2011.
- 101 C. J. Kloxin, T. F. Scott, B. J. Adzima and C. N. Bowman, *Macromolecules*, 2010, 43, 2643–2653.
- 102 C. N. Bowman and C. J. Kloxin, *Angewandte Chemie*, 2012, 51, 4272–4274.
- 103 C. J. Kloxin and C. N. Bowman, *Chemical Society reviews*, 2013, 42, 7161–7173.
- 104 J. M. Winne, L. Leibler and F. E. Du Prez, *Polym. Chem.*, 2019, 10, 6091–6108.
- 105 a) W. Post, A. Susa, R. Blaauw, K. Molenveld and R. J. I. Knoop, *Polymer Reviews*, 2019, 11, 1–30; b) D. J. Dobbins, G. M. Scheutz, H. Sun, C. A. Crouse and B. S. Sumerlin, *Journal of Polymer Science*, 2020, 58, 193–203.
- 106 S. Nevejans, N. Ballard, M. Fernández, B. Reck, S. J. García and J. M. Asua, *Polymer*, 2019, 179, 121670.
- 107 X. Chen, M. A. Dam, K. Ono, A. Mal, H. Shen, S. R. Nutt, K. Sheran and F. Wudl, *Science*, 2002, 295, 1698–1702.
- 108 J. Y. Chang, S. K. Do and M. J. Han, *Polymer*, 2001, 42, 7589–7594.
- 109 Y. Higaki, H. Otsuka and A. Takahara, *Macromolecules*, 2006, 39, 2121–2125.
- 110 Y. Amamoto, H. Otsuka, A. Takahara and K. Matyjaszewski, *Advanced materials*, 2012, 24, 3975–3980.
- 111 H. Otsuka, S. Nagano, Y. Kobashi, T. Maeda and A. Takahara, *Chemical communications*, 2010, 46, 1150–1152.
- 112 a) M. Anasagasti, M. Hidalgo and C. Mijangos, *Journal of Applied Polymer Science*, 1999, 72, 621–630; b) V. Bounor-Legaré, I. Ferreira, A. Verbois, P. Cassagnau and A. Michel, *Polymer*, 2002, 43, 6085–6092.
- 113 T. F. Scott, A. D. Schneider, W. D. Cook and C. N. Bowman, *Science*, 2005, 308, 1615–1617.
- 114 C. J. Kloxin, T. F. Scott, H. Y. Park and C. N. Bowman, *Advanced materials*, 2011, 23, 1977–1981.
- 115 a) R. Nicolaÿ, J. Kamada, A. van Wassen and K. Matyjaszewski, *Macromolecules*, 2010, 43, 4355–4361; b) Y. Amamoto, J. Kamada, H. Otsuka, A. Takahara and K. Matyjaszewski, *Angewandte Chemie*, 2011, 50, 1660–1663.
- 116 D. Montarnal, M. Capelot, F. Tournilhac and L. Leibler, *Science*, 2011, 334, 965–968.
- 117 S. Radl, M. Kreimer, T. Griesser, A. Oesterreicher, A. Moser, W. Kern and S. Schlögl, *Polymer*, 2015, 80, 76–87.
- 118 K. Kunal, C. G. Robertson, S. Pawlus, S. F. Hahn and A. P. Sokolov, *Macromolecules*, 2008, 41, 7232–7238.

- 
- 119 J. Manhart, S. Ayalur-Karunakaran, S. Radl, A. Oesterreicher, A. Moser, C. Ganser, C. Teichert, G. Pinter, W. Kern, T. Griesser and S. Schlögl, *Polymer*, 2016, 102, 10–20.
- 120 P. Froimowicz, H. Frey and K. Landfester, *Macromolecular rapid communications*, 2011, 32, 468–473.
- 121 J.-F. Xu, Y.-Z. Chen, L.-Z. Wu, C.-H. Tung and Q.-Z. Yang, *Organic letters*, 2013, 15, 6148–6151.
- 122 L. Kan, H. Cheng, B. Li, X. Zhang, Q. Wang, H. Wei and N. Ma, *New J. Chem.*, 2019, 43, 2658–2664.
- 123 W. Denissen, J. M. Winne and F. E. Du Prez, *Chemical science*, 2016, 7, 30–38.
- 124 M. Capelot, M. M. Unterlass, F. Tournilhac and L. Leibler, *ACS Macro Lett.*, 2012, 1, 789–792.
- 125 M. Capelot, D. Montarnal, F. Tournilhac and L. Leibler, *J. Am. Chem. Soc.*, 2012, 134, 7664–7667.
- 126 A. Legrand and C. Soulié-Ziakovic, *Macromolecules*, 2016, 49, 5893–5902.
- 127 L. Imbernon, S. Norvez and L. Leibler, *Macromolecules*, 2016, 49, 2172–2178.
- 128 L. Cao, J. Fan, J. Huang and Y. Chen, *J. Mater. Chem. A*, 2019, 167, 421.
- 129 Z. Tang, Y. Liu, B. Guo and L. Zhang, *Macromolecules*, 2017, 50, 7584–7592.
- 130 G. Zhang, X. Zhou, K. Liang, B. Guo, X. Li, Z. Wang and L. Zhang, *ACS Sustainable Chem. Eng.*, 2019, 7, 11712–11720.
- 131 K. Yu, P. Taynton, W. Zhang, M. L. Dunn and H. J. Qi, *RSC Adv*, 2014, 4, 48682–48690.
- 132 Z. Yang, Q. Wang and T. Wang, *ACS applied materials & interfaces*, 2016, 8, 21691–21699.
- 133 Y. Yang, Z. Pei, X. Zhang, L. Tao, Y. Wei and Y. Ji, *Chemical science*, 2014, 5, 3486–3492.
- 134 Y. Yang, S. Zhang, X. Zhang, L. Gao, Y. Wei and Y. Ji, *Nature communications*, 2019, 10, 3165.
- 135 F. Ji, X. Liu, C. Lin, Y. Zhou, L. Dong, S. Xu, D. Sheng and Y. Yang, *Macromol. Mater. Eng.*, 2019, 304, 1800528.
- 136 X. Niu, F. Wang, X. Li, R. Zhang, Q. Wu and P. Sun, *Ind. Eng. Chem. Res.*, 2019, 58, 5698–5706.
- 137 X. Yang, L. Guo, X. Xu, S. Shang and H. Liu, *Materials & Design*, 2020, 186, 108248.
- 138 F. I. Altuna, C. E. Hoppe and R. J.J. Williams, *European Polymer Journal*, 2019, 113, 297–304.
- 139 W. Liu, D. F. Schmidt and E. Reynaud, *Ind. Eng. Chem. Res.*, 2017, 56, 2667–2672.
- 140 J. P. Brutman, P. A. Delgado and M. A. Hillmyer, *ACS Macro Lett.*, 2014, 3, 607–610.
- 141 T. Liu, B. Zhao and J. Zhang, *Polymer*, 2020, 194, 122392.
- 142 J. Han, T. Liu, S. Zhang, C. Hao, J. Xin, B. Guo and J. Zhang, *Ind. Eng. Chem. Res.*, 2019, 58, 6466–6475.
- 143 a) T. Liu, S. Zhang, C. Hao, C. Verdi, W. Liu, H. Liu and J. Zhang, *Macromolecular rapid communications*, 2019, 40, e1800889; b) Y. Li, T. Liu, S. Zhang, L. Shao, M. Fei, H. Yu and J. Zhang, *Green Chem.*, 2020, 22, 870–881.
- 144 F. I. Altuna, C. E. Hoppe and R. J. J. Williams, *RSC Adv.*, 2016, 6, 88647–88655.

- 145 F. I. Altuna, V. Pettarin and R. J. J. Williams, *Green Chem.*, 2013, 15, 3360.
- 146 J. Han, T. Liu, C. Hao, S. Zhang, B. Guo and J. Zhang, *Macromolecules*, 2018, 51, 6789–6799.
- 147 D. Montarnal, F. Tournilhac, M. Hidalgo and L. Leibler, *J. Polym. Sci. Part A: Polym. Chem.*, 2010, 48, 1133–1141.
- 148 a) N. Pal, A. Srivastava and J. S. P. Rai, *Int. J. Chem. Kinet.*, 2004, 36, 280–285; b) J. Feltzin, M. K. Barsh, E. J. Peer and I. Petker, *Journal of Macromolecular Science: Part A - Chemistry*, 1969, 3, 261–274; c) M. K. Kiesewetter, M. D. Scholten, N. Kirn, R. L. Weber, J. L. Hedrick and R. M. Waymouth, *The Journal of organic chemistry*, 2009, 74, 9490–9496.
- 149 D. J. Fortman, J. P. Brutman, C. J. Cramer, M. A. Hillmyer and W. R. Dichtel, *J. Am. Chem. Soc.*, 2015, 137, 14019–14022.
- 150 M. M. Obadia, B. P. Mudraboyina, A. Serghei, D. Montarnal and E. Drockenmuller, *J. Am. Chem. Soc.*, 2015, 137, 6078–6083.
- 151 J. Canadell, H. Goossens and B. Klumperman, *Macromolecules*, 2011, 44, 2536–2541.
- 152 W. Denissen, G. Rivero, R. Nicolaÿ, L. Leibler, J. M. Winne and F. E. Du Prez, *Adv. Funct. Mater.*, 2015, 25, 2451–2457.
- 153 P. Taynton, K. Yu, R. K. Shoemaker, Y. Jin, H. J. Qi and W. Zhang, *Advanced materials*, 2014, 26, 3938–3942.
- 154 R. J. Wojtecki, M. A. Meador and S. J. Rowan, *Nature materials*, 2011, 10, 14–27.
- 155 A. V. Tobolsky, W. J. MacKnight and M. Takahashi, *J. Phys. Chem.*, 1964, 68, 787–790.
- 156 M. Guerre, C. Taplan, J. M. Winne and F. Du Prez, *Chem. Sci.*, 2020.
- 157 M. M. Obadia, A. Jourdain, P. Cassagnau, D. Montarnal and E. Drockenmuller, *Adv. Funct. Mater.*, 2017, 27, 1703258.
- 158 N. J. van Zee and R. Nicolaÿ, *Progress in Polymer Science*, 2020, 104, 101233.
- 159 S. Dhers, G. Vantomme and L. Avérous, *Green Chem.*, 2019, 21, 1596–1601.
- 160 R. L. Snyder, D. J. Fortman, G. X. de Hoe, M. A. Hillmyer and W. R. Dichtel, *Macromolecules*, 2018, 51, 389–397.
- 161 M. Hayashi, R. Yano and A. Takasu, *Polym. Chem.*, 2019, 10, 2047–2056.
- 162 M. Hayashi and R. Yano, *Macromolecules*, 2020, 53, 182–189.
- 163 P. Taynton, H. Ni, C. Zhu, K. Yu, S. Loob, Y. Jin, H. J. Qi and W. Zhang, *Advanced materials*, 2016, 28, 2904–2909.
- 164 A. Ruiz de Luzuriaga, R. Martin, N. Markaide, A. Rekondo, G. Cabañero, J. Rodríguez and I. Odriozola, *Mater. Horiz.*, 2016, 3, 241–247.
- 165 J. Chen, H. Huang, J. Fan, Y. Wang, J. Yu, J. Zhu and Z. Hu, *Frontiers in chemistry*, 2019, 7, 632.
- 166 L. Yue, V. S. Bonab, D. Yuan, A. Patel, V. Karimkhani and I. Manas Zloczower, *Global Challenges*, 2019, 1800076.
- 167 a) H. Zheng, Q. Liu, X. Lei, Y. Chen, B. Zhang and Q. Zhang, *J Mater Sci*, 2019, 54, 2690–2698; b) C. Taplan, M. Guerre, J. M. Winne and F. E. Du Prez, *Mater. Horiz.*, 2019, 1, 46.
- 168 W. Post, A. Cohades, V. Michaud, S. van der Zwaag and S. J. Garcia, *Composites Science and Technology*, 2017, 152, 85–93.

- 169 a) X. Wu, X. Yang, R. Yu, X.-J. Zhao, Y. Zhang and W. Huang, *J. Mater. Chem. A*, 2018, 6, 10184–10188; b) V. Solouki Bonab, V. Karimkhani and I. Manas-Zloczower, *Macromol. Mater. Eng.*, 2019, 304, 1800405;
- 170 a) Y. Yang, E. M. Terentjev, Y. Wei and Y. Ji, *Nature communications*, 9, 1906; b) Q. Chen, X. Yu, Z. Pei, Y. Yang, Y. Wei and Y. Ji, *Chemical science*, 2017, 8, 724–733.
- 171 Q. Shi, K. Yu, M. L. Dunn, T. Wang and H. J. Qi, *Macromolecules*, 2016, 49, 5527–5537.
- 172 W. Denissen, I. de Baere, W. van Paepegem, L. Leibler, J. Winne and F. E. Du Prez, *Macromolecules*, 2018, 51, 2054–2064.
- 173 K. Yu, Q. Shi, M. L. Dunn, T. Wang and H. J. Qi, *Adv. Funct. Mater.*, 2016, 26, 6098–6106.
- 174 E. Chabert, J. Vial, J.-P. Cauchois, M. Mihaluta and F. Tournilhac, *Soft Matter*, 2016, 12, 4838–4845.
- 175 Y. Spiesschaert, M. Guerre, L. Imbernon, J. M. Winne and F. Du Prez, *Polymer*, 2019, 172, 239–246.
- 176 C. Xu, R. Cui, L. Fu and B. Lin, *Composites Science and Technology*, 2018, 167, 421–430.
- 177 Z. Huang, Y. Wang, J. Zhu, J. Yu and Z. Hu, *Composites Science and Technology*, 2018, 154, 18–27.
- 178 a) A. Demongeot, R. Groote, H. Goossens, T. Hoeks, F. Tournilhac and L. Leibler, *Macromolecules*, 2017, 50, 6117–6127; b) Y. Gao, W. Liu and S. Zhu, *Macromolecules*, 2018, 51, 8956–8963; c) M. Röttger, T. Domenech, R. van der Weegen, A. Breuillac, R. Nicolaÿ and L. Leibler, *Science*, 2017, 356, 62–65.
- 179 C. Hao, T. Liu, S. Zhang, L. Brown, R. Li, J. Xin, T. Zhong, L. Jiang and J. Zhang, *ChemSusChem*, 2019, 12, 1049–1058.
- 180 S. Zhang, T. Liu, C. Hao, L. Wang, J. Han, H. Liu and J. Zhang, *Green Chem.*, 2018, 20, 2995–3000.
- 181 a) Q. Shi, K. Yu, X. Kuang, X. Mu, C. K. Dunn, M. L. Dunn, T. Wang and H. Jerry Qi, *Mater. Horiz.*, 2017, 4, 598–607; b) B. Zhang, K. Kowsari, A. Serjouei, M. L. Dunn and Q. Ge, *Nature communications*, 2018, 9, 1831.
- 182 a) H. Zhang, H. Han and X. Xu, *Composites Science and Technology*, 2018, 158, 61–66; b) J. Deng, X. Kuang, R. Liu, W. Ding, A. C. Wang, Y.-C. Lai, K. Dong, Z. Wen, Y. Wang, L. Wang, H. J. Qi, T. Zhang and Z. L. Wang, *Advanced materials*, 2018.
- 183 M. Morton, *Rubber Technology*, Springer Netherlands, Dordrecht, 2010.
- 184 J.-M. Vergnaud and I.-D. Rosca, *Rubber Curing and Properties*, CRC Press, 2016.
- 185 a) B. Adhikari, *Progress in Polymer Science*, 2000, 25, 909–948; b) V. V. Rajan, W. K. Dierkes, R. Joseph and J.W.M. Noordermeer, *Progress in Polymer Science*, 2006, 31, 811–834.
- 186 L. Imbernon, E. K. Oikonomou, S. Norvez and L. Leibler, *Polym. Chem.*, 2015, 6, 4271–4278.
- 187 Y. Liu, Z. Tang, Y. Chen, S. Wu and B. Guo, *Composites Science and Technology*, 2018, 168, 214–223.
- 188 Y.-X. Lu, F. Tournilhac, L. Leibler and Z. Guan, *J. Am. Chem. Soc.*, 2012, 134, 8424–8427.
- 189 A. Breuillac, A. Kassalias and R. Nicolaÿ, *Macromolecules*, 2019, 52, 7102–7113.

- 190 a) D. C. Edwards, *J Mater Sci*, 1990, 25, 4175–4185; b) K. Roy, S. C. Debnath and P. Potiyaraj, *Journal of Elastomers & Plastics*, 2020, 52, 167–193.
- 191 a) S.-Y. Fu, X.-Q. Feng, B. Lauke and Y.-W. Mai, *Composites Part B: Engineering*, 2008, 39, 933–961; b) K. W. Stöckelhuber, A. S. Svistkov, A. G. Pelevin and G. Heinrich, *Macromolecules*, 2011, 44, 4366–4381.
- 192 a) C. Alzina, N. Sbirrazzuoli and A. Mija, *J. Phys. Chem. C*, 2011, 115, 22789–22795; b) J.-H. Ma, L.-Q. Zhang and Y.-P. Wu, *Journal of Macromolecular Science, Part B*, 2013, 52, 1128–1141; c) R. L. Sala, T. M. Arantes, E. Longo, E. R. Leite, C. M. Paranhos and E. R. Camargo, *Colloids and Surfaces A: Physicochemical and Engineering Aspects*, 2014, 462, 45–51.
- 193 F. Lossada, J. Guo, D. Jiao, S. Groeer, E. Bourgeat-Lami, D. Montarnal and A. Walther, *Biomacromolecules*, 2019, 20, 1045–1055.
- 194 A. Jourdain, R. Asbai, O. Anaya, M. M. Chehimi, E. Drockenmuller and D. Montarnal, *Macromolecules*, 2020, 53, 1884–1900.
- 195 F. Meng, M. O. Saed and E. M. Terentjev, *Macromolecules*, 2019, 52, 7423–7429.
- 196 M. K. McBride, B. T. Worrell, T. Brown, L. M. Cox, N. Sowan, C. Wang, M. Podgorski, A. M. Martinez and C. N. Bowman, *Annual review of chemical and biomolecular engineering*, 2019, 10, 175–198.
- 197 C. M. Neely and P. J. Graham, *Polymer relaxation*, Nova Science Publishers, Hauppauge, N.Y, 2012.
- 198 R. Chasset and P. Thirion, *Physics of non-crystalline solids. Proceedings of the International Conference*, North Holland Publishing Co., Amsterdam, 1965.
- 199 J. G. Curro and P. Pincus, *Macromolecules*, 1983, 16, 559–562.
- 200 a) C. A. Angell, *Science*, 1995, 267, 1924–1935; b) J. C. Dyre, *Rev. Mod. Phys.*, 2006, 78, 953–972.
- 201 R. H. Pritchard, A.-L. Redmann, Z. Pei, Y. Ji and E. M. Terentjev, *Polymer*, 2016, 95, 45–51.

# Chapter 3

## SWITCHABLE ADHESION IN ELASTOMERS FROM HXNBR

### 3.1 Bibliographic information

#### Published in:

Kaiser, S.; Radl, S. V.; Manhart, J.; Ayalur-Karunakaran, S.; Griesser, T.; Moser, A.; Ganser, C.; Teichert, C.; Kern, W.; Schlögl, S. Switching "on" and "off" the adhesion in stimuli-responsive elastomers. *Soft Matter*. DOI: 10.1039/c8sm00284c.

#### Author contributions:

Simon Kaiser: Conceptualisation; Methodology; Investigation; Data curation; Formal analysis; Validation; Original draft; Review and editing

Simone Radl: Investigation; Data curation; Original draft

Jakob Manhart: Investigation; Data curation

Santhosh Ayalur-Karunakaran: Investigation; Data curation

Thomas Griesser: Review and editing

Andreas Moser: Investigation; Data curation

Christian Ganser: Investigation; Data curation

Christian Teichert: Data curation; Validation

Wolfgang Kern: Funding acquisition; Resources

Sandra Schlögl: Funding acquisition; Project administration; Resources; Supervision; Conceptualisation; Methodology; Validation; Original draft; Review and editing

The manuscript presented here is an adapted accepted manuscript in order to correspond to the formatting of this thesis and does not necessarily reflect the actual published version.

## SWITCHING “ON” AND “OFF” THE ADHESION IN STIMULI-RESPONSIVE ELASTOMERS

S. Kaiser<sup>a</sup>, S. V. Radl<sup>a</sup>, J. Manhart<sup>a</sup>, S. Ayalur-Karunakaran<sup>a</sup>, T. Griesser<sup>b,c</sup>, A. Moser<sup>d</sup>, C. Gansere<sup>e</sup>, C. Teichert<sup>e</sup>, W. Kern<sup>a,c</sup> and S. Schlögl<sup>a,†</sup>

<sup>a</sup> Polymer Competence Center Leoben GmbH, Roseggerstraße 12, A-8700 Leoben, Austria.

<sup>†</sup>E-mail: sandra.schloegl@pccl.at

<sup>b</sup> Christian Doppler Laboratory for Functional and Polymer Based Ink-Jet Inks, Otto Glöckel-Straße 2, A-8700 Leoben, Austria.

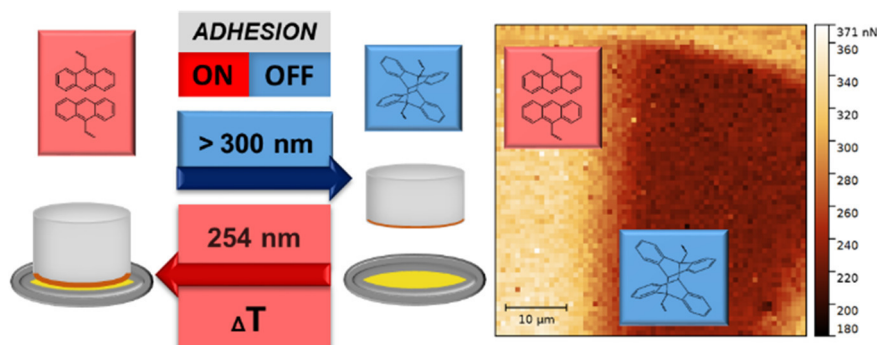
<sup>c</sup> Chair in Chemistry of Polymeric Materials, Montanuniversität Leoben, Otto Glöckel-Straße 2, A-8700 Leoben, Austria.

<sup>d</sup> Chair in Materials Science and Testing of Plastics, Montanuniversität Leoben, Otto Glöckel-Straße 2, A-8700 Leoben, Austria.

<sup>e</sup> Institute of Physics, Montanuniversität Leoben, Franz Josef-Straße 18, A-8700 Leoben, Austria.

### 3.2 Abstract

The present work aims at the preparation of dry adhesives with switchable bonding properties by using the reversible nature of the  $[4\pi_s+4\pi_s]$  cycloaddition of anthracenes. Photo-responsive hydrogenated carboxylated nitrile butadiene rubber with photo-responsive pendant anthracene groups is prepared by one-pot synthesis. The formation of 3D networks relies on the photodimerisation of the anthracene moieties upon UV exposure ( $\lambda > 300$  nm). Controlled cleavage of the cross-link sites is achieved by either deep UV exposure ( $\lambda = 254$  nm) or thermal dissociation at 70 °C. The kinetics of the optical and thermal cleavage route are compared in thin films using UV-Vis spectroscopy and their influence on the reversibility of the network is detailed. Going from thin films to free standing samples the modulation of the network structure and thermo-mechanical properties over repeated cross-linking and cleavage cycles are characterised by low-field NMR spectroscopy and dynamic mechanical analysis. The applicability of the stimuli-responsive networks as adhesives with reversible bonding properties is demonstrated. The results evidence that the reversibility of the cross-linking reaction enables a controlled switching “on” and “off” of adhesion properties. The recovery of the adhesion force amounts to 75 and 80% for photo- and thermal dissociation, respectively. Spatial control of adhesion properties is evidenced by adhesion force mapping experiments of photo-patterned films.





### 3.3 Introduction

Over the last ten years optically triggered cycloaddition reactions have inspired researchers to develop photo-reversible polymer materials, since they open promising routes for spatially controlled tuning of material properties at room temperature.<sup>1</sup> As pericyclic reactions these cycloaddition reactions follow the Woodward-Hoffmann rules and form  $[2\pi_s+2\pi_s]$  and  $[4\pi_s+4\pi_s]$  adducts *via* light induced dimerisation.<sup>2</sup> Whilst  $[2\pi_s+2\pi_s]$  photocycloaddition reactions proceed at shorter wavelengths ( $\lambda < 350$  nm), the  $[4\pi_s+4\pi_s]$  photodimerisation of anthracenes has an extended spectral window up to a wavelength of 400 nm.<sup>3</sup>

The photoreactivity of anthracene was discovered in 1866 by Fritzsche, who exposed a solution of anthracene to sunlight and observed the formation of a colourless precipitate. In a further experiment, Fritzsche was able to regenerate anthracene by heating the precipitate to its melting point.<sup>4</sup> The structure of the solid photoproduct – the anthracene photodimer – was then identified in 1891.<sup>2</sup> Subsequent studies on the reaction mechanism revealed that the photodimerisation of anthracene is a pericyclic reaction that proceeds *via* a head-to-tail or head-to-head  $[4\pi_s+4\pi_s]$  cycloaddition reaction across the central ring of the conjugated  $\pi$ -system. Pericyclic reactions of anthracene and its derivatives are highly versatile since they undergo photo-induced and thermally triggered cycloaddition reactions with numerous dienophiles across the 9- and 10-positions.<sup>5</sup> The photodimerisation of anthracene and its derivatives can be reversed, and free anthracene is regained by either deep UV exposure or by thermal annealing (Figure 1). The reversible character of the cycloaddition reaction of anthracenes has led to advanced polymer architectures, which were applied in the fabrication of stimuli-responsive polymers.<sup>7-9</sup>

In a recent work, we demonstrated the feasibility of the  $[4\pi_s+4\pi_s]$  photodimerisation of anthracene derivatives for the development of reversible and mendable epoxy based materials.<sup>10</sup> Since no significant regeneration of free anthracene groups was achieved upon deep UV exposure, a thermal dissociation of the dimers was carried out at 130 °C for 90 min. The functional epoxy based materials were repeatedly healed at the same damage site by a combined treatment of heat and UV exposure ( $\lambda > 300$  nm). To obtain fully photo-reversible networks, we introduced anthracene groups in elastomeric networks based on hydrogenated carboxylated nitrile butadiene rubber (anth-HXNBR).<sup>11</sup> In the rubbery state, a distinctive recovery of the anthracene groups upon photocleavage was obtained, which was exploited for the design of reversible photoresists.

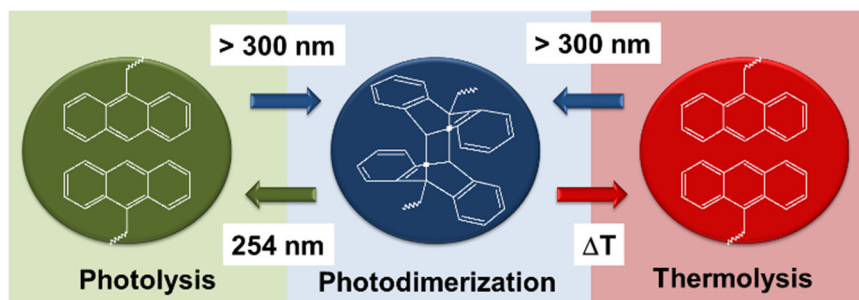


**Figure 1** – Reversible photodimerisation of anthracenes.<sup>6</sup>

In the present work, the reversibility of this photo-responsive elastomer is used to prepare a dry adhesive with switchable bonding properties. The controlled bonding and debonding relies on the light and thermally induced modulation of polymer chain dynamics. In the non-cross-linked state, stimuli-responsive elastomers provide a high adhesion force to rigid polar surfaces, which can be reduced significantly upon UV-induced cross-linking at wavelengths above 300 nm. Regeneration of the adhesion force is accomplished either by a UV-induced ( $\lambda = 254$  nm) or by a thermally triggered cleavage reaction demonstrating the reversibility of the adhesion strength.

The design of polymer materials, which exhibit reversible dry adhesion, is often strongly inspired by nature.<sup>12</sup> One of the most prominent examples is the fine structure of hierarchically arranged fibrils of gecko foot pads, which efficiently make use of van der Waals and capillary forces to switch adhesion and friction properties.<sup>13</sup> Synthesis strategies to re-engineer the structure of gecko pads involve patterning methods such as soft-lithography using poly(dimethylsiloxane), hot-embossing techniques employing thermoplastic materials or multistep photolithography to obtain hierarchical structures.<sup>14</sup> By combining patterning techniques with shape memory materials Reddy and del Campo have prepared stimuli-responsive structures, that regained their adherence by reheating the materials above their glass transition temperatures.<sup>15</sup> In terms of thermally triggered reversible adhesives, further routes exploit the phase separation of initially miscible blends of poly(3-caprolactone) and diglycidyl ether of bisphenol-A cured with diaminodiphenylsulfone or a detachment based on reversible Diels-Alder chemistry of epoxy based networks, that bear furan and maleimide pendant groups.<sup>16</sup>

With respect to optically triggered adhesion, Weder et al. reported the synthesis of metallosupramolecular polymers comprising metal-coordinate and hydrogen-bonding motifs that facilitated reversible bonding upon either heating or UV exposure at wavelengths between 320 and 390 nm.<sup>17</sup> In terms of light induced debonding the absorbed UV-light was converted to heat, which caused a temporary dissociation of the supramolecular polymer structure leading to a strong decrease of the viscosity. The polymers were capable of re-assembling when the light was switched off and the bonding properties were regained. Light induced changes in viscosity were also employed by Akiyama et al. for the preparation of photo-reversible adhesives.<sup>18</sup> They synthesised sugar-alcohol derivatives with photo-responsive azobenzene moieties that are well known for their reversible *cis-trans* isomerisation upon irradiation. Due to the photo-induced phase transition, a liquefaction of the material (debonding step) was obtained *via* UV exposure, whilst subsequent illumination with visible light led to a solidification again (bonding step).

Recently, Chung and co-workers described the design of bioinspired acrylic terpolymers comprising anthracene pendant groups.<sup>19</sup> They exploited the cross-linking reaction across the anthracene moieties after interfacial adhesion between substrates and adhesive polymers to enhance the bonding strength of the adhesive. However, this strategy allows only for a one-time switching of adhesive properties.

In contrast, the herein described design of photo-reversible elastomers paves the way towards a repeated switching “on“ and “off“ of the adhesion and enables a spatial control of adhesion properties.

### 3.4 Results and discussion

#### *Synthesis of a stimuli-responsive elastomer*

Anth-HXNBR was conveniently accessed by side chain functionalisation of a hydrogenated carboxylated acrylonitrile butadiene rubber (HXNBR). The one-pot synthesis was carried out by a ring opening reaction between an epoxy functionalised anthracene derivative and the carboxylic acid pendant groups of the rubber (Figure 2). The derivatisation reaction was carried out at room temperature since the acidity of the carboxylic acid groups catalysed the ring-opening reaction of the epoxy moieties.

Cross-linking of anth-HXNBR was then accomplished by the photodimerisation of the attached pendant anthracene groups using UV-light with wavelengths above 300 nm. In a previous work, we performed a comparative study on the influence of the amount of attached anthracene pendant groups on the cross-linking performance and related thermo-mechanical properties of the stimuli-responsive elastomer networks.<sup>11</sup> We observed that the change in the mechanical properties (e.g. dissipation factor and  $T_g$ ) due to the cross-linking process was more pronounced in rubber materials with a higher amount of anthracene pendant groups. In particular, for HXNBR modified with 1.3 mol% anthracene groups, the  $T_g$  shifted from -7 to +7 °C upon UV cross-linking, whilst the difference in  $T_g$  did not exceed 1 °C if the modification yield was below 0.5 mol%. This behaviour was attributed to a varying cross-link density, since at a higher modification yield it is expected that more cross-links are formed by the dimerisation reaction. It should be noted that 1.3 mol% was the maximum modification yield that was achieved with the described one-pot synthesis. Thus, this stimuli-responsive rubber (anth-HXNBR) has been applied in the current study.

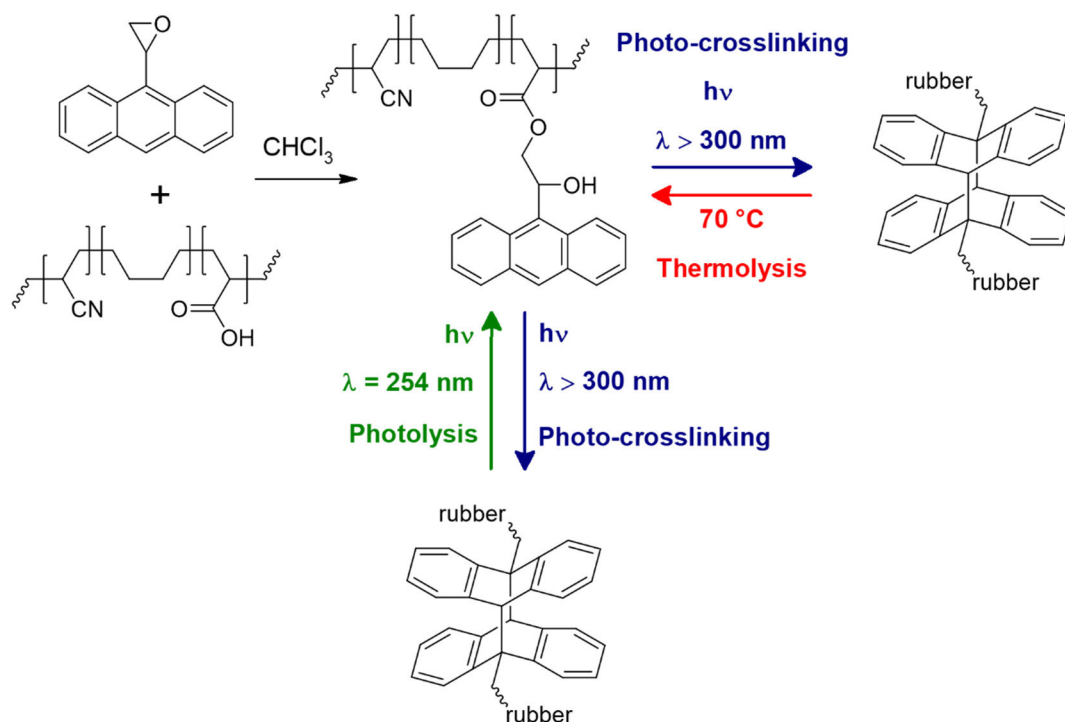


**Figure 2** – One-pot synthesis of anth-HXNBR *via* ring opening reaction and reversible cross-linking of anth-HXNBR networks.

For characterising the reversible dimerisation of anth-HXNBR, de-crosslinking of the photodimers was carried out by thermolysis as well as by photolysis at 254 nm. Regarding the photocleavage, free anthracene groups are regenerated by a photochemically allowed cycloreversion reaction. The photodissociation of the anthracene dimers yields two anthracene moieties, which can re-dimerise under the illumination conditions reaching an equilibrium between the free anthracene groups and their dimers. In contrast, the thermal cycloreversion is forbidden and the generally accepted mechanism involves a homolytic bond cleavage of one of the strained carbon bridgehead–bridgehead bonds upon the formation of a transient di-radical intermediate.<sup>6</sup> A homolytic scission of the second carbon bridgehead–bridgehead bond results in a re-aromatisation and a regeneration of the anthracene structure. Thus, contrary to the photolysis, thermolysis does not lead to an equilibrium between the free anthracene groups and their dimers.

### *Reversibility of stimuli-responsive elastomer networks in thin films*

In thin spin-cast rubber layers (layer thickness amounted to a few micrometers), the reversibility of the  $[4\pi_s+4\pi_s]$  photocycloaddition across the pendant anthracene groups was determined by UV-Vis spectroscopy following the changes of the characteristic absorption profile of anthracenes between 330 and 400 nm. It has to be considered that the irradiation with UV-light was carried out under a nitrogen atmosphere to avoid the formation of endoperoxides. In previous work it has already been demonstrated that the photo-cross-linking proceeds efficiently upon UV illumination at wavelengths above 300 nm corresponding to a distinctive decrease of the anthracene absorption bands at 336, 350, 370 and 390 nm (Figure 3 replotted from ref. 11). Besides the depletion of the anthracene signals, an increase in the absorbance between 290 and 310 nm is observed, which is associated with the formation of benzene based by-products.<sup>10</sup>

The subsequent thermolysis of the photodimers was monitored at different temperatures (45, 70 and 100 °C) to assess the optimum temperature for maximum bond dissociation. Along with the photo-cross-linking, the thermolysis was also carried out under inert

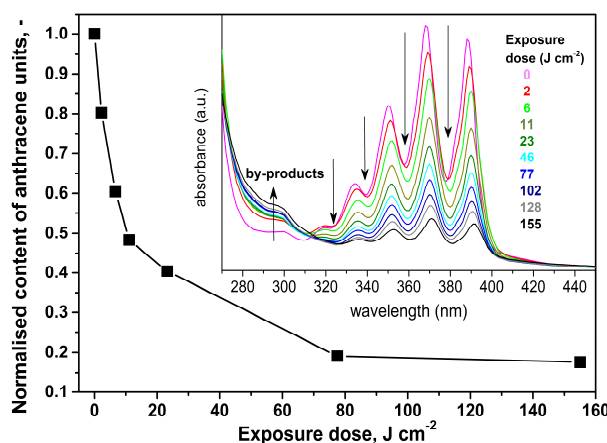


**Figure 3** – Conversion of anthracene moieties in spin-cast anth-HXNBR films (film thickness of a few micrometers) upon prolonged UV exposure ( $\lambda > 300$  nm,  $N_2$ ). The inset depicts the time-dependent UV-Vis spectra of anth-HXNBR upon photo-cross-linking ( $\lambda > 300$  nm,  $N_2$ ). Graphs have been replotted from ref. 11 and lines are a guide to the eye.

atmosphere to avoid the irreversible formation of endoperoxides. At 45 °C, the UV-Vis spectra did not show any significant regeneration of free anthracene groups.

Thus, 45 °C was applied as measurement temperature in solid state NMR experiments, which are described in the following section. By treating the photo-cross-linked anth-HXNBR at 70 °C, a distinctive increase of the anthracene absorption profile was observed. This evidences the thermolysis of the photodimers and the regeneration of free anthracene moieties (Figure 4a). However, only a part of the free anthracene groups is regenerated, which might be attributed to side reactions of thermally formed di-radical intermediates yielding irreversible by-products. In particular, the additional increase of the absorbance between 290 and 310 nm suggests a further formation of benzene based by-products during the thermal treatment. From the results of the UV-Vis experiments it can be concluded that by-products formed during the cross-linking and cleavage step will limit the reversibility of the photodimerisation reaction.

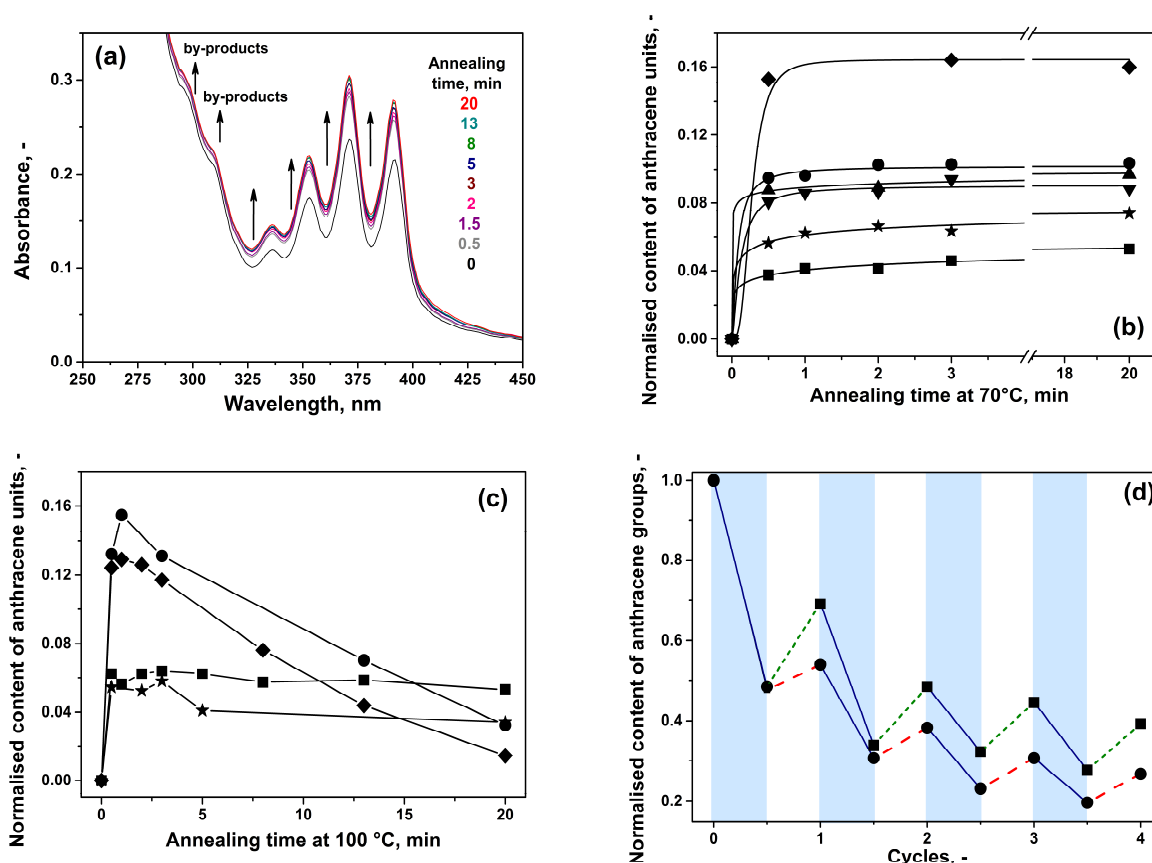


**Figure 4** – (a) Time-dependent UV-Vis spectra of the thermal dissociation of anthracene dimers in spin-cast anth-HXNBR films with a film thickness of a few micrometers (prior cross-linked with 11 J cm<sup>-2</sup>,  $\lambda > 300$  nm, N<sub>2</sub>) at 70 °C. Thermal dissociation of anthracene dimers in spin-cast anth-HXNBR films *versus* thermal annealing time at (b) 70 and (c) 100 °C. Anth-HXNBR was prior cross-linked at different UV exposure doses: 6.6 (full diamonds), 11 (full circles), 23.1 (full triangles down), 64.2 (full triangles up), 77 (full stars) and 154 J cm<sup>-2</sup> (full squares). (d) Remaining anthracene groups in reversibly cross-linked anth-HXNBR (spin-cast films with a thickness in the range of a few micrometers) over repeated cycles of photo-cross-linking (11 J cm<sup>-2</sup>,  $\lambda > 300$  nm, N<sub>2</sub>) – solid lines – and thermal dissociation (70 °C, 20 min, N<sub>2</sub>) – long dashed lines – *versus* photo-induced dissociation (9.7 J cm<sup>-2</sup>,  $\lambda = 254$  nm, N<sub>2</sub>) – short dashed lines.

Figure 4b illustrates the kinetics of the thermal dissociation in dependence on the exposure dose used in the photo-cross-linking of spin-cast anth-HXNBR films. It should be noted that a varying exposure dose influences the conversion of the anthracene groups (Figure 3) and thus, the cross-link densities in the stimuli-responsive elastomers. In all samples, the maximum dissociation yields are achieved within three minutes of thermal annealing at 70 °C.

Furthermore, the results reveal that a thermal annealing provides a larger process window than a photolysis process since, even in slightly cross-linked anth-HXNBR films, the regained anthracene signals do not decrease significantly within twenty minutes at 70 °C. It is also observed that the cross-link density of anth-HXNBR, which is related to the exposure dose used in the photo-cross-linking step, clearly affects the maximum regeneration of anthracene absorbance (i.e. maximum yield of thermal dissociation). In particular, it amounts to 17% in films with a low cross-link density (exposure dose: 6.6 J cm<sup>-2</sup>) and decreases to 5% in networks with a higher cross-link density (exposure dose: 154 J cm<sup>-2</sup>).

By increasing the annealing temperature from 70 to 100 °C, the regeneration of the anthracene absorbance as a function of the cross-link density followed a similar trend (Figure 4c). In spin-cast anth-HXNBR films, which have been previously illuminated with a lower exposure dose, the regeneration was more pronounced than in films that have been previously illuminated with a higher dose. However, the influence of the temperature (70 *versus* 100 °C) on the maximum yield of thermal dissociation, obtained at a selected exposure dose used in the photo-cross-linking step, does not follow a clear trend (see also Table 1). A thermal annealing at 100 °C gives higher cleavage yields in films prior cross-linked at 11 or 154 J cm<sup>-2</sup>, whilst a thermal annealing at 70 °C gives superior cleavage yields in films prior cross-linked at 6.6 or 77 J cm<sup>-2</sup>.

By following the regeneration of the anthracene signals over the annealing time at 100 °C, it is observed that in lower cross-linked elastomer networks the regained anthracene signals rapidly decrease if the annealing time exceeds 2 min. At a higher cross-link density (154 J cm<sup>-2</sup>), the absorption band areas of the regenerated anthracene groups reach a plateau between 2 and 20 min of thermal annealing at 100 °C. Thus, the results suggest that lower cross-linked elastomer networks are more susceptible to irreversible side reactions at higher annealing temperatures, which narrows the process window of the thermolysis at 100 °C. Based on these results, subsequent studies on the reversibility of the network formation and the reversible switching of mechanical and adhesion properties were carried out with an annealing temperature of 70 °C.

In Table 1, the maximum regeneration of the anthracene absorbance *versus* the exposure dose used in the photo-cross-linking step is compared for the thermolysis and the photolysis route. Regarding the thermolysis (performed either at 70 °C or 100 °C), the maximum regeneration of the anthracene absorbance decreases with increasing cross-link density of the elastomer network, whilst for the photolysis the opposite effect is observed: enhanced regeneration of the anthracene absorbance at a higher initial cross-link density. Contrary to the findings of Tazuke and co-workers<sup>2,20</sup>, who described the superiority of the thermolysis of the anthracene dimers to the photolysis, the results suggest that in spin-cast elastomer layers, the photo-dissociation is more efficient.

Although the thermally induced regeneration of the anthracene groups is limited, the results clearly show that the thermolysis proceeds within a short time and at moderate reaction temperatures (70 °C). The rapid thermolysis of the photodimers might be mainly related to the high mobility of the anthracene pendant groups in the elastomer network. Tazuke and co-workers demonstrated that the local mobility of dianthracene units is important in the course of vibrational thermal activation. In polymers with identical functional groups, the thermolysis rate can be directly correlated with the  $T_g$  as the  $T_g$  is affected by main-chain rigidity and interpolymer interactions, which are both influenced by segment mobility. However, if comparing different polymer systems with each other, also other interactions (e.g. hydrogen bonds) have to be considered since they have the ability to influence the local mobility of the photoreactive pendant groups. Along with network mobility, Du Prez and co-workers recently demonstrated in a comparative study of functional 9-substituted anthracenes that the dissociation temperature of the photodimers is also affected by the substituents at the 9-position.<sup>21</sup>

In a previous work, we studied the reversible cross-linking in an epoxy based material by employing the same epoxy functional anthracene derivative used in the elastomer networks under investigation.<sup>10</sup> By pursuing a thermal curing reaction in the presence of an anhydride hardener, the epoxy functional anthracene derivative was directly incorporated into the polymer backbone across its epoxy groups (Figure 5b). Compared to the stimuli-responsive elastomer, the epoxy based network was characterised by a higher rigidity ( $T_g = 55$  °C). In addition, the anthracene groups were directly attached to the polymer chain in 9-position, whilst in the elastomer networks the anthracene pendant groups were linked *via* a spacer (anth-HCOH-CH<sub>2</sub>-O-CO) in the 9-position to the rubber chain (Figure 5a). The differences in spacer length and network mobility had a distinctive influence on the conditions of the thermolysis of the photodimers. Whilst in the elastomer networks the thermal dissociation of the anthracene dimers already proceeded at 70 °C, a temperature of 130 °C was required to cleave the photodimers in the rigid epoxy based material.

**Table 1** – Comparison of the maximum cleavage yields obtained from UV-Vis experiments in spin-cast anth-HXNBR films (film thickness in the range of a few micrometers) prior cross-linked with varying UV exposure doses ( $\lambda > 300$  nm, N<sub>2</sub>).

Exposure dose cross-linking (J cm <sup>-2</sup> )	Maximum yield of thermal dissociation <sup>1</sup> at 70 °C (%)	Maximum yield of thermal dissociation <sup>1</sup> at 100 °C (%)	Maximum yield of photo-dissociation <sup>1</sup> ( $\lambda = 254$ nm, N <sub>2</sub> ) (%) <sup>2</sup>
6.6	16 [3] <sup>3</sup>	13 [3] <sup>3</sup>	17 [0.4] <sup>4</sup>
11	10 [3]	15 [1]	20 [1.9]
77	7 [20]	6 [3]	20 [7.3]
154	5 [20]	6 [1]	24 [9.1]

<sup>1</sup> Maximum regeneration of anthracene absorbance at 336, 350, 370 and 390 nm obtained from UV-Vis experiments.

<sup>2</sup> Values are obtained from ref. 11.

<sup>3</sup> Values in brackets provide the reaction time in min at which the maximum yield of dissociation was observed.

<sup>4</sup> Values in brackets provide the exposure dose in J cm<sup>-2</sup> at which the maximum yield of dissociation was observed.

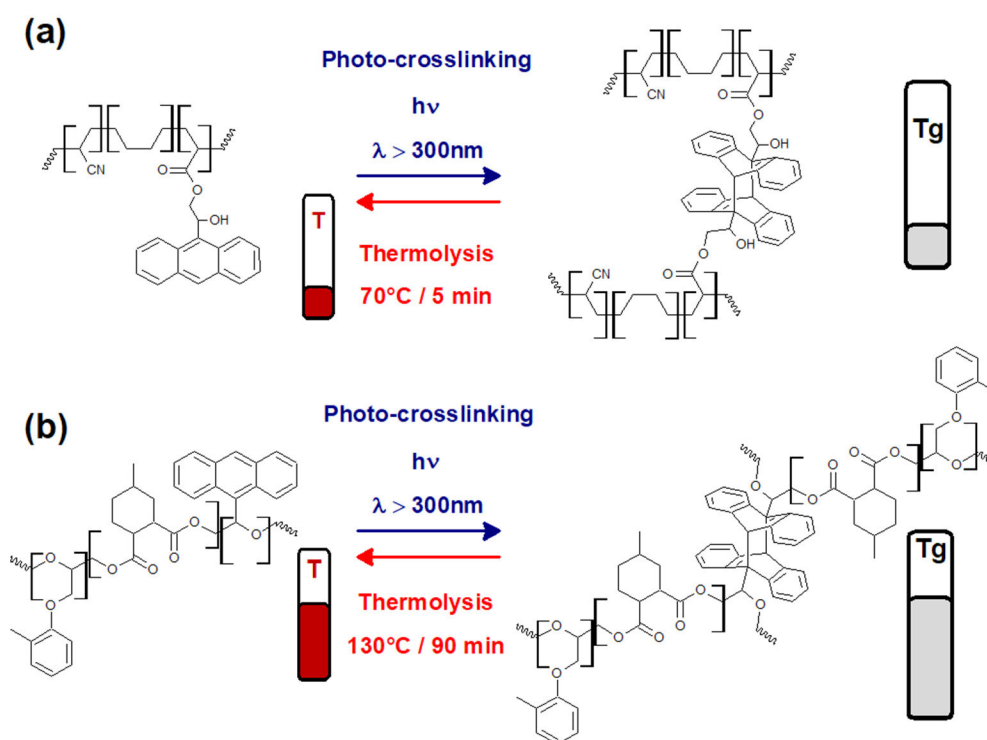


**Figure 5** – Comparing the temperature conditions for the thermolysis of anthracene photodimers in (a) flexible elastomer networks and (b) rigid epoxy based materials.

At lower temperatures, no significant regeneration of the anthracene signals was observed. Along with the higher temperature, an extended annealing time of 90 min had to be applied to reach the maximum regeneration of the anthracene signals. The comparison of both materials clearly shows that reaction rate and cleavage temperature are strongly governed by the mobility of the anthracene groups in the polymer network.

Going a step beyond the characterisation of a one-time switching of the cross-link state, the reversibility of the dimerisation reaction in anth-HXNBR networks was further studied over repeated cycles of photochemical bond formation and thermal dissociation or photocleavage by means of UV-Vis spectroscopy (Figure 4d). In thin spin-cast films it can be seen that the reversibility of the networks is mainly limited by the cleavage step since only a part of the original anthracene signals can be recovered during either thermolysis or photolysis. Since a higher number of anthracene moieties are regenerated by the photolysis route, the reversibility achieved *via* photolysis is higher compared to thermolysis.

#### *Reversible mechanical properties of stimuli-responsive elastomer networks*

Along with spin-cast films comprising a film thickness of a few micrometers, reversible changes of network characteristics were also studied in free-standing anth-HXNBR films that comprised a thickness in the range of  $100\ \mu\text{m}$ . Figure 6a illustrates the elastic storage modulus over one cycle of UV-induced cross-linking ( $\lambda > 300\ \text{nm}$ ,  $46\ \text{J cm}^{-2}$ ) and subsequent thermal cleavage ( $70^\circ\text{C}$ , 20 min). Data over four repeating cycles of cross-linking and thermolysis and the related loss moduli are shown in the ESI (Figure S1). From Figure 6a it can be seen that the storage modulus is very high below the glass



transition temperature, which is typical for an elastomeric material, as the rubber chains are frozen in the glassy state. Since the mobility of the rubber chains is limited, the material is brittle and does not have any surface tack. Besides the  $T_g$ , no other relaxation phenomena were observed within a temperature range of -60 to +25 °C. By increasing the temperature above the glass transition temperature, the rubber chains are able to move and the storage modulus decreases significantly until the rubbery plateau is reached. With a storage modulus of 1.95 MPa at 21 °C, free-standing anth-HXNBR films are not applicable as a classic pressure sensitive adhesive (without adding some selected tackifiers).<sup>22</sup> Previous work showed, that at a frequency of 1 Hz, the storage modulus for a pressure sensitive adhesive should range between 10 and 300 kPa (at application temperature) to ensure that the polymers are compliant enough to form a good contact within a short contact time and at a low contact pressure.<sup>23</sup>

The DMA results further revealed that photo-cross-linking of anth-HXNBR does only lead to a slight increase of the storage modulus above  $T_g$ . A subsequent thermolysis leads to a slight decrease of the storage modulus but the original values of the pristine and non-cross-linked anth-HXNBR are not reached.

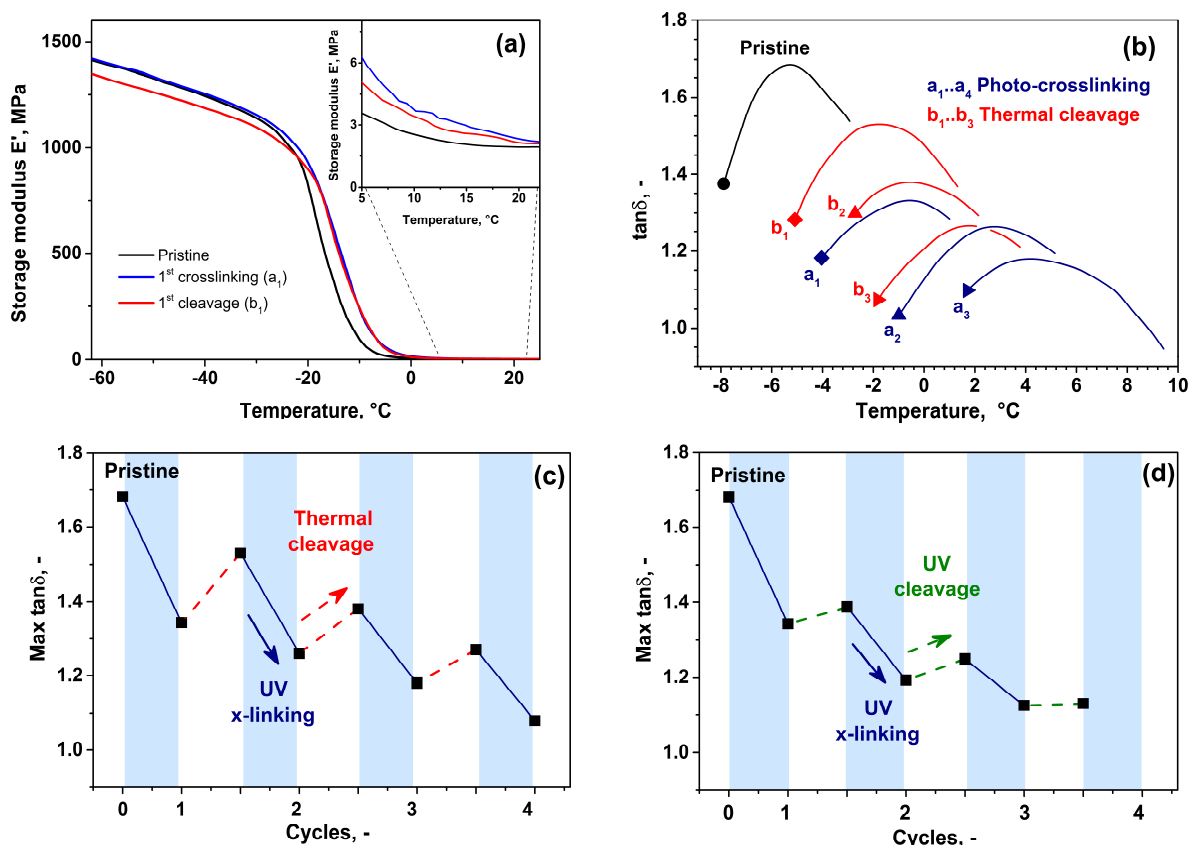


**Figure 6** – (a) Elastic storage modulus ( $E'$ ) versus temperature of free-standing anth-HXNBR films (film thickness in the range of 100  $\mu\text{m}$ ) over one cycle of photo-cross-linking ( $a_1$ ) with 46  $\text{J cm}^{-2}$  ( $\lambda > 300 \text{ nm}$ ,  $\text{N}_2$ ) and thermal dissociation ( $b_1$ ) at 70 °C (20 min,  $\text{N}_2$ ). (b) Dissipation factor of free-standing anth-HXNBR films over repeated cycles of photo-cross-linking ( $a_1, a_2, a_3$ ) with 46  $\text{J cm}^{-2}$  ( $\lambda > 300 \text{ nm}$ ,  $\text{N}_2$ ) and thermal dissociation ( $b_1, b_2, b_3$ ) at 70 °C (20 min,  $\text{N}_2$ ). Maximum  $\tan\delta$  values (c) over three cycles of photo-cross-linking (solid lines) and thermal dissociation (dashed lines), and (d) over three cycles of photo-cross-linking (solid lines) and photo-cleavage (9.7  $\text{J cm}^{-2}$ ,  $\lambda = 254 \text{ nm}$ ,  $\text{N}_2$ ) (dashed lines) – replotted from ref. 11.

Contrary to the storage modulus, the influence of the reversible cross-linking on the dissipation factor and  $T_g$  is more pronounced. Photo-cross-linking facilitates a distinctive decrease of the dissipation factor, and a significant shift of the  $T_g$  to higher values (Figure 6b). This is related to the restricted movement of the molecular chains and the decreasing energy dissipation of the anth-HXNBR films by the cross-linking reaction. In particular, the  $T_g$  increases from -5 to -0.5 °C, whilst the maximum dissipation factor decreases from 1.68 to 1.33. Controlled thermal cleavage of the photodimers leads to the opposite effect as network points are broken and the mobility of the rubber chains increases. Thus, upon thermolysis the  $T_g$  decreases from -0.5 to -2 °C and the maximum dissipation factor rises from 1.33 to 1.53.

The reversibility of the thermo-mechanical properties over four repeating cycles of cross-linking and thermolysis are provided in Figure 6b and 6c. 56% of the maximum  $\tan\delta$  value are recovered during the first thermal cleavage step (see  $b_1$  in Figure 6b). Even after the third cleavage step (see  $b_3$  in Figure 6b) still 50 % of the maximum  $\tan\delta$  value are regained, demonstrating the high reversibility of the photocycloaddition reaction in free-standing samples.

In contrast, the photo-dissociation yield is rather low in free-standing films. Whilst the thermal annealing enables a repeated switching between different cross-linking states over four cycles, the maximum  $\tan\delta$  value could not be recovered at all after the second cycle *via* photolysis (Figure 6d replotted from ref.<sup>11</sup>). This difference between thermolysis and photolysis is mainly related to the film thickness of the free-standing samples, which is roughly two magnitudes higher than the spin-cast films used in the UV-Vis experiments. Deep UV-light has only a low penetration depth, which limits the efficiency of the photolysis in thicker samples.

#### *Reversible network properties of stimuli-responsive elastomer networks*

This is also confirmed by NMR relaxometry measurements, which were performed to characterise the reversible network dynamics (Figure 7a and 7b). The  $1/T_{2,\text{avg}}$  values are related to the average mobility of the elastomer networks and increase upon photo-induced cross-linking corresponding to an increased cross-link density. The subsequent cleavage of the anthracene photodimers is indicated by the significant decrease of  $1/T_{2,\text{avg}}$ . It is obvious that the higher cleavage yield of the thermolysis compared to the photolysis of the anthracene photodimers follows the same trend as observed by DMA measurements. However, the difference in the efficiency of the two cleavage processes is more pronounced, which is attributed to the higher sensitivity of the NMR analysis towards changes in the network structure in comparison to the DMA experiments.

The related distribution curves of the NMR relaxometry experiments are shown in Figure 7c. The mobility and chain motion in reversible elastomer networks are derived by the peak maxima corresponding to the modal relaxation time and the width of the peaks, which is associated with the relaxation time distribution. In the pristine state (see 1 in Figure 7c), three relaxation times ( $T_2^{\text{eff}}$ : 0.08-0.2 ms, 0.5-0.8 ms and 1.0-3.0 ms) are observed. The three fractions possibly rely on chain length distribution effects and different molecular interactions. The least mobile chains with the shortest relaxation times exhibit the highest contributions (i.e. the weight fraction calculated from peak area).

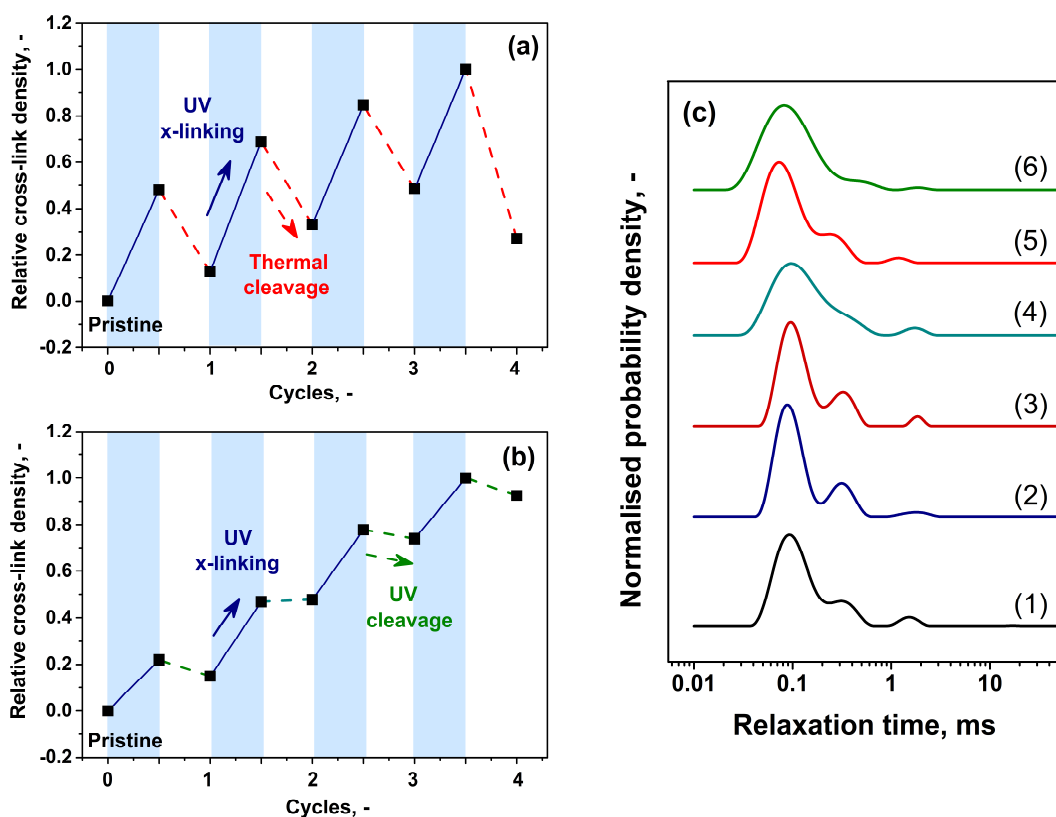


**Figure 7** – Relative  $1/T_{2,avg}$  values (a) of free-standing anth-HXNBR films (film thickness in the range of 100  $\mu\text{m}$ ) over several cycles of photo-cross-linking ( $46 \text{ J cm}^{-2}$ ,  $\lambda > 300 \text{ nm}$ ,  $\text{N}_2$ ) (solid lines) and thermal cleavage ( $70^\circ\text{C}$ , 20 min,  $\text{N}_2$ ) (dashed lines). (b) Replotted<sup>11</sup> relative  $1/T_{2,avg}$  values of anth-HXNBR films over several cycles of photo-cross-linking ( $46 \text{ J cm}^{-2}$ ,  $\lambda > 300 \text{ nm}$ ,  $\text{N}_2$ ) (solid lines) and photo-cleavage ( $9.7 \text{ J cm}^{-2}$ ,  $\lambda = 254 \text{ nm}$ ,  $\text{N}_2$ ) (dashed lines). (c) NMR relaxation distribution curves of (1) pristine, (2) photo-cross-linked ( $46 \text{ J cm}^{-2}$ ,  $\lambda > 300 \text{ nm}$ ,  $\text{N}_2$ ), (3) thermally cleaved after the first cycle ( $70^\circ\text{C}$ , 20 min,  $\text{N}_2$ ), (4) photochemically cleaved after the first cycle ( $9.7 \text{ J cm}^{-2}$ ,  $\lambda = 254 \text{ nm}$ ,  $\text{N}_2$ ), (5) thermally cleaved after the fourth cycle and (6) photochemically cleaved after the fourth cycle anth-HXNBR.

A relaxation time between 0.08 and 0.2 ms typically corresponds to rigid segments as has been observed on filler surfaces.<sup>24</sup> Although the results indicate that the majority of the rubber chains have restricted mobility, the short relaxation times are likely due to the low temperature at which the measurements were performed. Higher measurement temperatures were not applied to avoid any thermolysis of the photodimers during the experiments.

Photo-cross-linking leads to a slight shift of the peaks to lower relaxation times (see 2 in Figure 7c) indicating a decrease in chain mobility, which is typical for cross-linking reactions. The subsequent cleavage of the photodimers is also evidenced by the decay curves, as the peak maxima shift to longer relaxation times again (see 3 and 4 in Figure 7c). This shift is related to faster chain dynamics and an increased motional freedom of the polymer chains in the network. Along with confirming the cleavage of cross-link points, the decay curves give also an insight into the homogeneity of the networks after the cleavage reaction.

In particular, photo-induced bond cleavage leads to a more heterogeneous network structure compared to the thermal dissociation as the relaxation distribution of the decay curves become significantly broader (see 4 and 6 in Figure 7c). The results suggest that the photodimers located at the surface predominantly cleave upon deep UV exposure, whilst those in the bulk remain largely unreacted due to the low penetration depth of the short wavelength UV-light and the high optical density of the regenerated anthracene groups. As NMR techniques average the behaviour of the whole sample, the heterogeneity of the network increases.

In contrast, a more homogenous network density profile is obtained after the thermolysis, which is evidenced by the narrower relaxation distribution widths (see 3 and 5 in Figure 7c). This result is expected since a thermally induced process is less limited by the film thickness than a photo-induced one. Although the photolysis is superior in very thin films (spin-cast films with a thickness of a few micrometers), the results clearly confirm that the thermolysis is far more efficient and homogeneous in free standing samples with a thickness in the range of 100  $\mu\text{m}$ .

#### *Characterisation of reversible adhesion properties*

Carboxylated rubber materials have a long tradition in adhesion technology and their application ranges from pressure sensitive adhesives and structural adhesives to adhesives for polar rigid surfaces involving metal-to-rubber adhesives and metal-to-metal adhesives.<sup>26</sup> In the present study, the photo-responsive nature of the modified carboxylated rubber was exploited to prepare films with reversible surface tack properties (Figure 8a). Along with the type of measurement and interfacial properties, surface tack is strongly influenced by the viscoelastic properties of a material.<sup>27</sup> For a high surface tack, the  $\tan\delta$  value should be high since the material has to resist elastic deformation and energy dissipation during the debonding step.<sup>23</sup> Thus, for a more viscoelastic material more energy will be dissipated leading to an increased adhesion strength. In addition, the rubbery plateau should be low to ensure sufficient wetting of the substrate during the bonding step.

DMA experiments have already revealed that the reversible cross-linking significantly influences the dissipation factor and the  $T_g$  of free-standing anth-HXNBR films. Thus, a reversible switching of the surface tack and adhesion properties as a function of the cross-link state of the anthracene pendant groups in the stimuli-responsive anth-HXNBR samples is expected.

To evaluate the reversibility of the surface tack properties, the adhesion force between anth-HXNBR and aluminium was measured with an experimental set-up similar to a probe tack test.<sup>30</sup> It should be noted that various parameters such, as stiffness of the testing machine, initial load, temperature or haul-off speed influence the surface tack values of elastomers in a probe tack test experiment.<sup>31</sup> In the current set-up, reproducible aligning of the samples was ensured by preparing anth-HXNBR films in metal molds (Figure S3 in the ESI). The molds were fixed in the specimen holder and the samples were kept in the molds during the measurements. For the probe tack test, a relatively fast haul-off speed (50  $\text{mm s}^{-1}$ ) and a short contact time (5 s) were applied. Previous studies showed that under these conditions an interfacial failure mechanism occurs which can be

described by the propagation of a crack at the interface between a rigid surface and a viscoelastic medium.<sup>30,33</sup>

As shown in Figure 8b photo-cross-linking of pristine anth-HXNBR leads to a distinctive decrease of the adhesion force from  $209.7 \pm 7.8$  to  $116.5 \pm 7.5$  N. The adhesion force is successfully recovered by subsequent thermal annealing or photocleavage, and amounts to  $166.8 \pm 5.5$  N and  $157.0 \pm 1.4$  N, respectively. The related load-displacement curves are provided in the ESI (Figure S2). Over one cycle of photo-cross-linking and cleavage (either thermal or photochemical) the shape of the load-displacement curves during the debonding stage of the probe tack measurement does not change significantly. A single peak maximum in force is observed that sharply drops during the debonding stage, which indicates an interfacial crack propagation as failure mode.<sup>30</sup>

The adhesion properties of carboxylated rubbers to hard surfaces such as glass or metals are governed by both the chemical surface composition as well as the viscoelastic state of the bulk material. It is well known that an increasing content of carboxylic groups in the rubber chain directly correlates with improved bond strength to polar surfaces since hydrogen bonding and dipolar forces increase at the interface between adhesive and

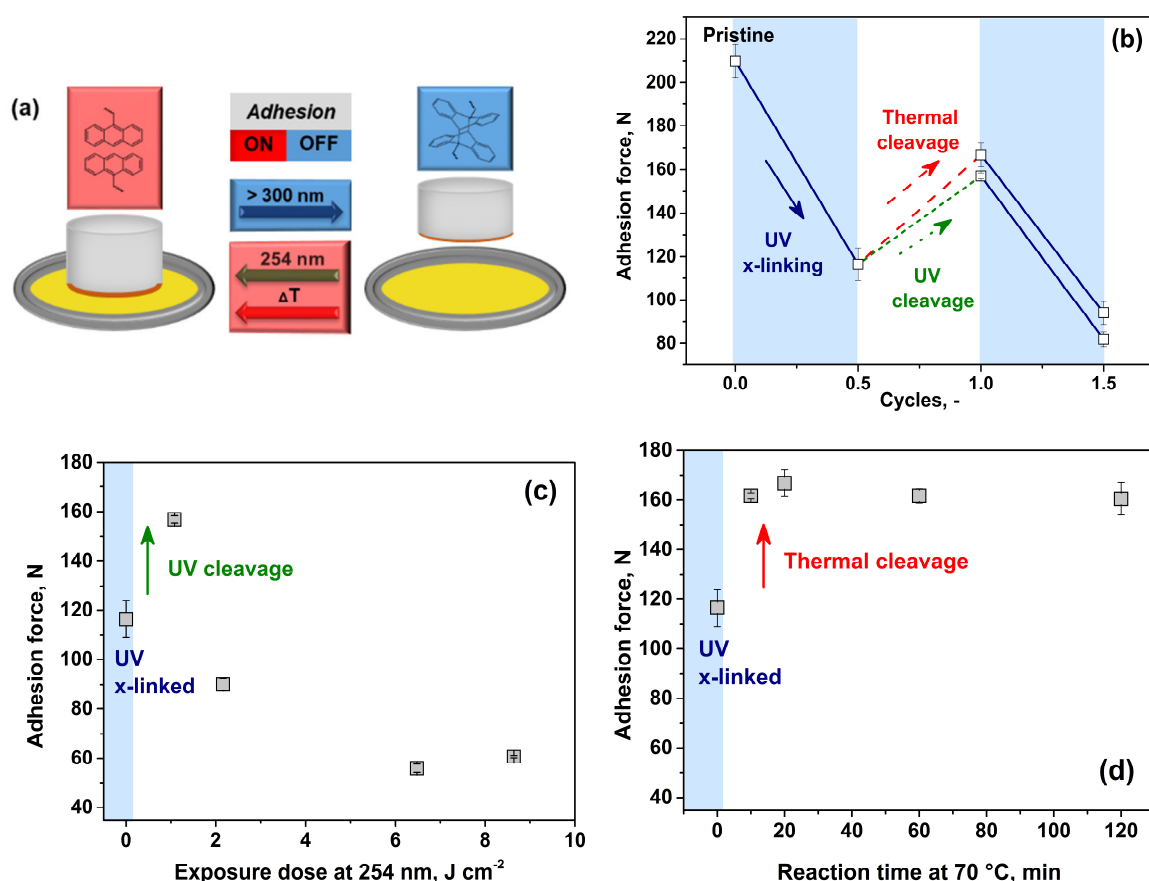


**Figure 8** – (a) Schematic representation of the reversible switching of adhesion properties in anth-HXNBR. (b) Adhesion force of anth-HXNBR films over a cycle of photo-cross-linking ( $46\ J\ cm^{-2}$ ,  $\lambda > 300\ nm$ ,  $N_2$ ) – solid lines – and thermal cleavage ( $70\ ^\circ C$ , 20 min,  $N_2$ ) – long dashed lines – versus photo-induced cleavage ( $\lambda = 254\ nm$ ,  $1.1\ J\ cm^{-2}$ ,  $N_2$ ) – short dashed lines. Adhesion force of anth-HXNBR as a function of (c) the exposure dose at 254 nm and (d) the thermal annealing time at  $70\ ^\circ C$ .

substrate.<sup>28</sup> However, it is expected that surface effects play a minor role in the reversible adhesion properties of anth-HXNBR. On the one hand, a major part of the free carboxylic acids has been already consumed during the derivatisation reaction with 2-(anthracene-9-yl)oxirane. Thus, pristine anth-HXNBR is rather hydrophobic, displaying a water contact angle of  $94.8 \pm 1.6^\circ$  and a diodomethane contact angle of  $40.4 \pm 0.7^\circ$ . Vaidya and co-workers described that the influence of ionic interactions on the adhesion force of a polymer-aluminium interface is negligible if the water contact angle of the polymer is above  $80^\circ$ .<sup>29</sup> On the other hand, the contact angle of anth-HXNBR does not change upon the photo-cross-linking reaction (contact angle of water:  $93.6 \pm 1.0^\circ$ ; contact angle of diodomethane:  $40.7 \pm 0.1^\circ$ ), which suggests that the different cross-linking states of anth-HXNBR do not significantly affect chemical surface interactions between elastomer and aluminium.

Thus, the controlled change in the adhesion force of anth-HXNBR can be mainly associated with the UV and thermally induced changes in the viscoelastic properties of the elastomer, which have been confirmed by the DMA experiments. Several studies describe the influence of viscoelasticity on adhesion and surface tack of pressure sensitive adhesives.<sup>32</sup> In particular, Keddie et al. switched off the surface tack of polymer based composites by a thermally triggered change of the elastic modulus.<sup>34</sup> Whilst Keddie et al. described an irreversible one-way switching, the reversible nature of anth-HXNBR enables a repeated switching of the adhesion force (Figure 8b).

The results are in good agreement with the NMR and DMA experiments, as the thermally induced recovery of the adhesion strength is more pronounced in free-standing samples than the photochemically induced one. The strong correlation between the dimerisation reaction of the pendant anthracene groups and the adhesion force is also demonstrated in Figure 8c and 8d, in which the change of the adhesion force is plotted against the exposure dose of the photolysis and the reaction time of the thermolysis, respectively. In terms of the photo-induced regeneration of the adhesion properties, the results reveal that the recovered adhesion force decreases if the exposure dose exceeds  $1.1 \text{ J cm}^{-2}$  (Figure 8c). In previous UV-Vis studies it was shown that prolonged UV exposure at 254 nm leads to a decrease of the anthracene signals, which has been attributed to an irreversible formation of by-products and the re-dimerisation of the anthracene groups.<sup>11</sup> The adhesion tests give an indication that these reactions facilitates a decrease of the adhesion force. In contrast, no distinctive change in the recovered adhesion force is observed between 10 and 120 min of thermal annealing at  $70^\circ\text{C}$ . The data correlate well with the UV-Vis experiments that demonstrated that the regenerated anthracene groups stay constant for a longer time period during the thermolysis.

Photo-induced processes further enable a spatially controlled switching of adhesion properties. This is demonstrated by employing AFM based adhesion mapping. The results are presented in Figure 9. Photolithography was applied to inscribe micro-sized patterns within spin-cast anth-HXNBR films, which have prior been cross-linked by flood UV exposure (illumination conditions and inscribed pattern are provided in Figure 9a). The patterning was carried out with deep UV exposure, which induced a cleavage of the photodimers and thus, a regeneration of the adhesion force in the exposed areas was expected. The topography image of the patterned film and the related profile are provided in Figure 9b and 9c. The cross-linked area, which has not been exposed during the

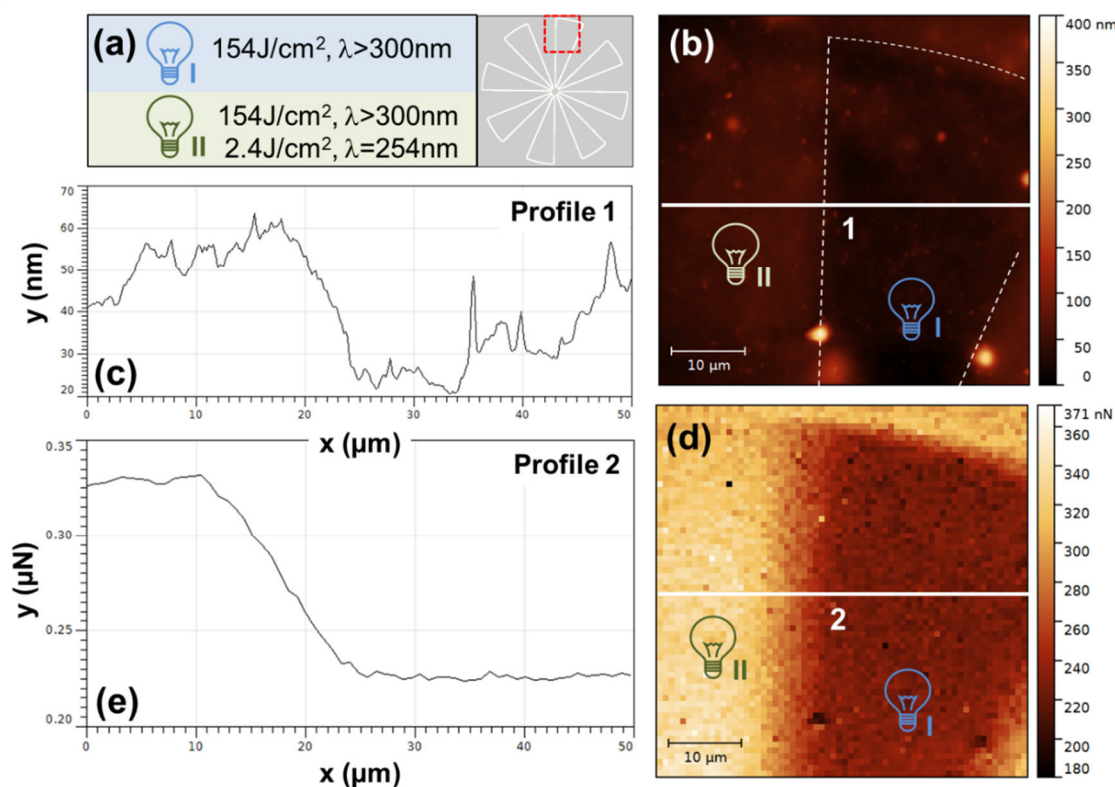


**Figure 9** – (a) Irradiation states and schematic representation of the micropatterns inscribed within spin-cast anth-HXNBR films by photolithography. The marked region in the pattern indicates the area, which has been studied by AFM experiments. (b) 50 μm × 50 μm AFM micrograph of the topography of the patterned anth-HXNBR film. The dashed white lines mark the area which has been blocked for illumination II. The bulb symbols indicate the areas that have been exposed to the illumination procedures I and II as indicated in (a). (c) Height profile along the horizontal line 1 shown in (b). (d) 50 μm × 50 μm AFM force map (64 × 64 pixel) of the patterned anth-HXNBR film. (e) Adhesion force profile along the horizontal line 2 shown in (d).

photolithography step, is roughly 20 nm lower than the regions additionally illuminated with UV-light at 254 nm. Whilst cross-linking reactions typically involve a volume shrinkage of the bulk material and a decrease of the film thickness, the subsequent partial cleavage of the network induces a slight increase of the film thickness again.<sup>11,35</sup> The corresponding image and profile of the adhesion force mapping experiments are shown in Figure 9d and 9e, respectively. The results provide clear evidence that the cross-linked (i.e. non-exposed) area exhibits an adhesion, which is around 100 nN lower than the de-crosslinked (i.e. exposed) area.

### 3.5 Conclusions

A stimuli-responsive rubber with pendant anthracene groups was exploited for the preparation of dry adhesives with reversible adhesion strength. The reversible dimerisation of the anthracene moieties was confirmed by UV-Vis spectroscopy. It was found that in the flexible anth-HXNBR networks, the thermolysis proceeds at a moderate temperature (70 °C) and within short reaction times (< 5 min). An increase in the annealing temperature (from 70 to 100 °C) did not enhance the cleavage yield of the

photodimers but accelerated irreversible side reactions in networks with a lower cross-link density. The UV-Vis experiments further revealed that for thin spin-cast films (thickness of a few micrometers), photo-induced dissociation of the anthracene dimers is superior to thermal dissociation. In contrast, DMA and solid state NMR measurements showed that the thermolysis is more efficient in free-standing films with a thickness in the range of 100  $\mu\text{m}$ . At a higher film thickness the photo-induced recovery of free anthracene units and thus, the reversibility of the cross-linking process, is limited by the low penetration depth of the deep UV-light. However, during the thermal annealing the heat is distributed over the sample thickness more homogeneously, which enables an efficient regeneration of the free anthracene groups. The repeated switching of cross-link state and related material properties such as dissipation factor and  $T_g$  over several cycles of cross-linking and bond cleavage was demonstrated.

Owed to a high  $\tan\delta$  value (high energy dissipation) and a low elasticity storage modulus in the rubbery plateau (wettability of the substrate during the bonding step), pristine anth-HXNBR exhibits a significant surface tack ( $209.7 \pm 7.8$  N) at room temperature. Photo-cross-linking led to a distinctive decrease of the adhesion force (from  $209.7 \pm 7.8$  to  $116.5 \pm 7.5$  N) due to the restricted movement of the molecular chains and the decreasing energy dissipation of the cross-linked anth-HXNBR films. This is in good agreement with the increase in the cross-link density and the decrease in the  $\tan\delta$  values that were observed in NMR and DMA experiments, respectively. 75 and 80% of the original adhesion force was recovered by subsequent cleavage of the photodimer links employing either photolysis or thermolysis. Due to the controlled cleavage of the photodimer cross-links, which was confirmed by NMR and UV-Vis experiments, the viscoelasticity of the anth-HXNBR films increased again and more energy was dissipated, which resulted in an increase in the adhesion strength.

In addition, the spatial control of the adhesion force was evidenced by adhesion force mapping experiments of photo-patterned anth-HXNBR films. From the results it can be concluded that not only is a repeatable and relatively fast switching of adhesion properties feasible but the photo-responsive nature of the elastomer allows for a switching of the adhesion force within a defined region.

### 3.6 Experimental

#### *Materials*

Hydrogenated carboxylated nitrile butadiene rubber (HXNBR) with a molecular weight of 370,000 g/mol and with  $5 \pm 1$  wt% carboxylic acid content,  $33 \pm 1.5$  wt% acrylonitrile content and  $3.5 \pm 1$  wt% residual C=C double bonds was provided by Arlanxeo (Cologne, Germany) under the trade name Therban XT VPKA 88892. (Anthracene-9-yl)oxirane was synthesised as previously reported.<sup>10</sup> All other chemicals were supplied by Sigma-Aldrich (St. Louis, USA) unless otherwise stated and were used without further purification.



*Synthesis of anth-HXNBR*

Hydrogenated carboxylated nitrile butadiene rubber with 1.3 mol% pendant anthracene groups (anth-HXNBR) per repeating unit was synthesised as previously reported.<sup>11</sup> For the synthesis, 1.0 g HXNBR was purified by dissolving the rubber in 100 mL chloroform. The solution was stirred over night at room temperature and the rubber was then precipitated with cold methanol. The precipitate was filtered, washed thoroughly with chloroform and dried at 40°C under vacuum.

The purified HXNBR (100 mg) was dissolved in chloroform (10 mL) and an excess of 2-(anthracene-9-yl)oxirane (150 mg) was added. The solution was stirred for 12 h at room temperature and precipitated again with cold methanol. The bright yellow precipitate was purified by two precipitation steps to remove any non-covalently bond 2-(anthracene-9-yl)oxirane.

*Reversible cross-linking of anth-HXNBR*

Thin films were prepared by spin casting a solution of anth-HXNBR (2 wt% in chloroform) on CaF<sub>2</sub> platelets (film thickness was in the range of several micrometers) and UV-induced cross-linking was realised by UV irradiation with a medium pressure Hg lamp (Omicure S1000) equipped with a filter to exclude UV-light below 300 nm. The power density ( $P$ ; in mW cm<sup>-2</sup>) at the sample surface was measured with an integrating radiometer (Powerpuck II, EIT Instrument Markets, USA) and amounted to 222 mW cm<sup>-2</sup> ( $\lambda = 300\text{-}450$  nm). The UV illumination was carried out under inert atmosphere to avoid any formation of endoperoxides. Photo-dissociation was accomplished by deep UV exposure under inert atmosphere employing a low pressure Hg lamp ( $\lambda = 254$  nm, 1.2 mW cm<sup>-2</sup>). Thermal dissociation was performed by heating the cross-linked samples to 70 °C on a heating plate under nitrogen atmosphere. Measurements of the heating rate with high sensitive fast-response thermocouple proved that the desired temperature was reached within 3 s. The reversibility of the photocycloaddition reaction was monitored during four cycles of photo-cross-linking and dissociation by UV-Vis measurements using a Varian Cary 50 UV-Vis spectrophotometer in absorption mode.

*Characterisation of reversible network characteristics and thermo-mechanical properties*

Free standing films were prepared by pouring a solution of anth-HXNBR (3.5 wt% in chloroform) in glass petri dishes ( $d=7$  cm). The solvent was removed (21 °C for 12 h under atmospheric pressure) and films with a thickness in the range of 100  $\mu\text{m}$  were obtained. For NMR experiments, the free standing films were cut into 10 mm wide strips, rolled into a cylinder without strain and placed vertically inside an NMR tube. Cross-linking and dissociation were then performed as described in the previous section.

Low field NMR measurements were carried out on a Bruker minispec mq20 equipment operating at <sup>1</sup>H Larmor frequency of 19.5 MHz. The probe dead time was 9  $\mu\text{s}$ ,  $\pi/2$  and  $\pi$  pulses were optimised for each sample but were generally in the range from 2.8-2.9  $\mu\text{s}$  and 5.4-5.6  $\mu\text{s}$ , respectively. The samples were heated with dry air and a BVT3000 temperature regulator was used for temperature control. The measurements were carried out at  $45 \pm 0.1$  °C after equilibrating the samples at least for a minimum of 30 min.

$T_2$  relaxation measurements were carried out with a Hahn echo pulse sequence [ $\pi/2$ - $\tau$ - $\pi$ -( $\tau$ -dead time)-acquisition]. This way acquisition started at the top of the echo and was acquired for 1 ms. The echo time ( $2\tau$ ) was varied from 60  $\mu$ s to about 20 ms and care was taken that the signal had decayed at least to 0.05% of its initial intensity. The intensity of the echo from about 5-100  $\mu$ s was numerically integrated and was taken as the echo intensity of the corresponding echo time ( $2\tau$ ).

For the analysis of the relaxation curves, a three-component exponential fit was done to the decay and a single average parameter was extracted. To avoid inter-parameter dependencies, the long tail of the signal was first fitted and the shape parameters were determined. The whole curve was fitted after fixing the shape parameters of the long tail and the remaining parameters were allowed to vary. Then, a single parameter, *viz.* an average relaxation rate ( $R_2^{\text{avg}}$  or  $1/T_2^{\text{avg}}$ ) was derived from the fit to describe the chain dynamics, by weighing each relaxation rate by its component fraction.<sup>11,36</sup> Further details of the NMR experiments are given in the ESI.

Regarding DMA measurements, test specimens with 25 mm in length and 7 mm in width were cut from the free standing films with a razor blade. The test specimens were fixed in the grips with 19.5 mm clamping length and positioned within the DMA analyser set up in tensile mode. The DMA experiments were carried out between -60 °C and 25 °C by using a heating rate of 2 K min<sup>-1</sup>. The measurement frequency was 1 Hz and the amplitude amounted to 20  $\mu$ m. The measurement data were processed with Origin 9 software.

#### *Characterisation of the reversible adhesion force*

For measuring the reversible adhesion properties of anth-HXNBR films a measuring method based on a compression-tensile test combination as previously reported was adapted.<sup>37</sup> Originally developed for measuring the surface tack of polymer surfaces, this method offers an easily implementable setup and yields reproducible results within short measurement times. Herein, the experiments were performed on a MTS servo-hydraulic tensile testing machine (MTS 831/15 kN, MTS Systems Corporation, Eden Prairie, USA). The setup consisted of an aluminium die tip ( $d=3$  cm,  $R_a=0.36$   $\mu$ m) mounted on the upper crosshead of the tensile tester, which was then brought into contact with the sample being clamped at the lower crosshead (Figure S3 in the ESI). Aluminium was chosen as the die tip material, since the reproducibility of the procedure is increased for multiple reasons. The die tip can be cleaned easily (the risk of transferring surface components from one specimen to another is minimised) and therefore it is not necessary to exchange the die tip prior to each measurement. Furthermore, the mechanical properties of the die tip can be considered as constant for repeating measurements, since ageing of the aluminium surface can be neglected and swelling of the die tip by the cleaning solvent does not occur. Test specimens were prepared by pouring a solution of anth-HXNBR (3.9 mL, 3.5 wt% in chloroform) in round aluminium molds ( $d=5$  cm) yielding layer thicknesses of  $72\pm 2.8$   $\mu$ m. Before testing the adhesion strength, all specimens were conditioned for 1 h at 23 °C and 50% relative humidity. The test procedure and parameters for all performed measurements were defined as follows. Firstly, the aluminium die tip was, in a force controlled way, vertically pressed onto the specimen surface with a constant controlled compressive force of -100 N. After a holding time of 5 s, the die tip was then, in a

displacement controlled way, pulled up away from the sample at a constant haul-off speed of 50 mm s<sup>-1</sup>. The force-displacement curve was recorded and its maximum force was taken as a measure of the adhesion strength, i.e. the force necessary to remove the aluminium die tip vertically from the anth-HXNBR surface.

#### *Spatial control of adhesion force*

Thin films were prepared by spin casting a solution of anth-HXNBR (2 wt% in chloroform) on a Si wafer. Flood exposure of the samples was carried out as described in the previous section using a medium pressure Hg lamp (Omnicure S1000). The exposure dose was 154 J cm<sup>-2</sup> ( $\lambda=300-450$  nm). Micro-sized patterns were then inscribed by photolithographic techniques using a mask aligner (MJB4, SUSS, Germany) in soft contact mode. Irradiation was carried out with an external light source, which was a low pressure mercury lamp (2.4 J cm<sup>-2</sup>,  $\lambda=254$  nm). The patterned films were characterised by adhesion force mapping experiments employing atomic force microscopy (AFM). The atomic force microscope was an Asylum Research MFP-3D, equipped with a closed loop scanner. An NT-MDT NSG 30 silicon AFM probe was used for all measurements, with a typical tip radius of 6 nm and a resonant frequency of 335 kHz. The cantilever's spring constant determined – using the thermal sweep method<sup>38</sup> – to be 40 N m<sup>-1</sup>. Measurements were conducted at a temperature and relative humidity of 23 °C and 20%, respectively. The area of interest was first scanned in tapping mode to record a reliable topography image at 512×512 pixels. Then, adhesion force mapping<sup>39</sup> was applied, where at a grid of 64×64 pixels a force *vs.* distance curve was recorded at each point with a speed of 1  $\mu\text{m s}^{-1}$ . This yielded a map of the adhesion forces between AFM tip and sample at each position. The adhesion force was defined as the minimum force in the curve.

### **3.7 Acknowledgements**

This research work was performed at the Polymer Competence Center Leoben GmbH (PCCL, Austria) within the framework of the COMET-program of the Federal Ministry for Transport, Innovation and Technology and Federal Ministry for Economy, Family and Youth with contributions by the Chair of Chemistry of Polymeric Materials (Montanuniversitaet Leoben, Austria). The PCCL is funded by the Austrian Government and the State Governments of Styria, Upper and Lower Austria. T. Griesser thanks the Christian Doppler research association and the Austrian Ministry for Economy, Family and Youth (BMWFJ) for financial support. In addition, the authors thank Andreas Oesterreicher (Christian Doppler Laboratory for Functional and Polymer Based Ink-Jet Inks) for support in the synthesis of the anthracene monomer and Florian Arbeiter (Montanuniversitaet Leoben) for support in the interpretation of the DMA data.

### 3.8 References

- 1 E. Blasco, M. Wegener and C. Barner-Kowollik, *Advanced materials*, 2017, 29, 1604005.
- 2 H. D. Becker, *Chem. Rev.*, 1993, 93, 145–172.
- 3 a) N. K. Guimard, K. K. Oehlenschlaeger, J. Zhou, S. Hilf, F. G. Schmidt and C. Barner-Kowollik, *Macromol. Chem. Phys.*, 2012, 213, 131–143; b) V. Amendola and M. Meneghetti, *J. Mater. Chem.*, 2012, 22, 24501; c) G. L. Fiore, S. J. Rowan and C. Weder, *Chemical Society reviews*, 2013, 42, 7278–7288.
- 4 H. Kaden, ed., *Studien zu Carl Julius Fritzsche (1808-1871) und Il'ja Il'ič Mečnikov (1845-1916). Quellenarbeit in der Wissenschaftsgeschichte*, Shaker, Aachen, 2008, vol. 1.
- 5 J. Atherton and S. Jones, *Tetrahedron*, 2003, 59, 9039–9057.
- 6 H. Bouas-Laurent, J.-P. Desvergne, A. Castellan and R. Lapouyade, *Chemical Society reviews*, 2001, 30, 248–263.
- 7 P. Madhavan, B. Sutisna, R. Sougrat and S. P. Nunes, *RSC Adv*, 2016, 6, 75594–75601.
- 8 T. Yamamoto, S. Yagyū and Y. Tezuka, *J. Am. Chem. Soc.*, 2016, 138, 3904–3911.
- 9 P. G. Frank, B. T. Tuten, A. Prasher, D. Chao and E. B. Berda, *Macromol. Rapid Commun.*, 2014, 35, 249–253.
- 10 S. Radl, M. Kreimer, T. Griesser, A. Oesterreicher, A. Moser, W. Kern and S. Schlögl, *Polymer*, 2015, 80, 76–87.
- 11 J. Manhart, S. Ayalur-Karunakaran, S. Radl, A. Oesterreicher, A. Moser, C. Ganser, C. Teichert, G. Pinter, W. Kern, T. Griesser and S. Schlögl, *Polymer*, 2016, 102, 10–20.
- 12 H. Lee, B. P. Lee and P. B. Messersmith, *Nature*, 2007, 448, 338–341.
- 13 L. F. Boesel, C. Greiner, E. Arzt and A. del Campo, *Advanced materials*, 2010, 22, 2125–2137.
- 14 a) A. K. Geim, S. V. Dubonos, I. V. Grigorieva, K. S. Novoselov, A. A. Zhukov and S. Y. Shapoval, *Nat Mater*, 2003, 2, 461–463; b) B. Bhushan, *J. Adhes. Sci. Technol.*, 2007, 21, 1213–1258; c) K. Autumn, Y. A. Liang, S. T. Hsieh, W. Zesch, W. P. Chan, T. W. Kenny, R. Fearing and R. J. Full, *Nature*, 2000, 405, 681–685.
- 15 S. Reddy, E. Arzt and A. del Campo, *Adv. Mater.*, 2007, 19, 3833–3837.
- 16 J. H. Aubert, *The Journal of Adhesion*, 2010, 79, 609–616.
- 17 C. Heinzmann, S. Coulibaly, A. Roulin, G. L. Fiore and C. Weder, *ACS Appl. Mater. Interfaces*, 2014, 6, 4713–4719.
- 18 H. Akiyama, S. Kanazawa, Y. Okuyama, M. Yoshida, H. Kihara, H. Nagai, Y. Norikane and R. Azumi, *ACS Appl. Mater. Interfaces*, 2014, 6, 7933–7941.
- 19 T. Harper, R. Slegeris, I. Pramudya and H. Chung, *ACS Appl. Mater. Interfaces*, 2017, 9, 1830–1839.
- 20 S. Tazuke and N. Hayashi, *J. Polym. Sci. Polym. Chem. Ed.*, 1978, 16, 2729–2739.
- 21 J. van Damme, L. Vlamincx, G. van Assche, B. van Mele, van den Berg, Otto and F. Du Prez, *Tetrahedron*, 2016, 72, 4303–4311.
- 22 A. Pocius, *Adhesion and Adhesives Technology*, 3rd edn., 2012.
- 23 I. Benedek, *Pressure-sensitive adhesives and applications*, Marcel Dekker, New York, 2nd edn., 2004.

- 
- 24 V. M. Litvinov, R. A. Orza, M. Klüppel, M. van Duin and Magusin, P. C. M. M., *Macromolecules*, 2011, 44, 4887–4900.
- 25 R. I. Chelcea, R. Fechete, E. Culea, D. E. Demco and B. Blümich, *Journal of magnetic resonance*, 2009, 196, 178–190.
- 26 a) C. E. Frank, G. Kraus and A. J. Haefner, *Ind. Eng. Chem.*, 1952, 44, 1600–1603;  
b) I. Skeist, *Handbook of Adhesives*, Springer US, Boston, MA, 1990;
- 27 a) K. Brown, J. C. Hooker and C. Creton, *Macromol. Mater. Eng.*, 2002, 287, 163;  
b) A. V. Pocius and D. A. Dillard, eds., *The mechanics of adhesion*, Elsevier, Amsterdam, Boston, 2002, I.
- 28 D. W. Aubrey and S. Ginosatis, *The Journal of Adhesion*, 2006, 12, 189–198.
- 29 C. Ochoa-Putman and U. K. Vaidya, *Composites Part A: Applied Science and Manufacturing*, 2011, 42, 906–915.
- 30 I. Benedek and M. M. Feldstein, *Handbook of pressure-sensitive adhesives and products*, CRC Press, Boca Raton, Fla., London, 2009.
- 31 M. Barquins and D. Maugis, *The Journal of Adhesion*, 2006, 13, 53–65.
- 32 a) H.-H. Chu, C.-K. Wang, K. S. Chuang and C.-Y. Chang, *J Polym Res*, 2014, 21;  
b) K. Ebe, H. Seno and K. Horigome, *J. Appl. Polym. Sci.*, 2003, 90, 436–441; c) I. Webster, *Int. J. Adhes. Adhes.*, 1999, 19, 29–34.
- 33 R. Schach and C. Creton, *Journal of Rheology*, 2008, 52, 749–767.
- 34 R. S. Gurney, D. Dupin, J. S. Nunes, K. Ouzineb, E. Siband, J. M. Asua, S. P. Armes and J. L. Keddie, *ACS Appl. Mater. Interfaces*, 2012, 4, 5442–5452.
- 35 J. E. Dietz and N. A. Peppas, *Polymer*, 1997, 38, 3767–3781.
- 36 V. M. Litvinov, R. A. Orza, M. Klüppel, M. van Duin and Magusin, P. C. M. M., *Macromolecules*, 2011, 44, 4887–4900.
- 37 U. D. Cakmak, G. Grestenberger and Z. Major, *Express Polym. Lett.*, 2011, 5, 1009–1016.
- 38 J. L. Hutter and J. Bechhoefer, *Rev. Sci. Instrum.*, 1993, 64, 1868–1873.
- 39 Van der Werf, Kees O., Putman, Constant A. J., de Grooth, Bart G. and J. Greve, *Appl. Phys. Lett.*, 1994, 65, 1195–1197.

## 3.9 Supporting information

## SWITCHING “ON” AND “OFF” THE ADHESION IN STIMULI-RESPONSIVE ELASTOMERS

S. Kaiser<sup>a</sup>, S. V. Radl<sup>a</sup>, J. Manhart<sup>a</sup>, S. Ayalur-Karunakaran<sup>a</sup>, T. Griesser<sup>b,c</sup>, A. Moser<sup>d</sup>, C. Ganser<sup>e</sup>, C. Teichert<sup>e</sup>, W. Kern<sup>a,c</sup> and S. Schlögl<sup>a†</sup>

<sup>a</sup> Polymer Competence Center Leoben GmbH, Roseggerstraße 12, A-8700 Leoben, Austria.

†E-mail: sandra.schloegl@pccl.at

<sup>b</sup> Christian Doppler Laboratory for Functional and Polymer Based Ink-Jet Inks, Otto Glöckel-Straße 2, A-8700 Leoben, Austria.

<sup>c</sup> Chair in Chemistry of Polymeric Materials, Montanuniversitaet Leoben, Otto Glöckel-Straße 2, A-8700 Leoben, Austria.

<sup>d</sup> Chair in Materials Science and Testing of Plastics, Montanuniversitaet Leoben, Otto Glöckel-Straße 2, A-8700 Leoben, Austria.

<sup>e</sup> Institute of Physics, Montanuniversitaet Leoben, Franz Josef-Straße 18, A-8700 Leoben, Austria.

## DMA data on anth-HXNBR

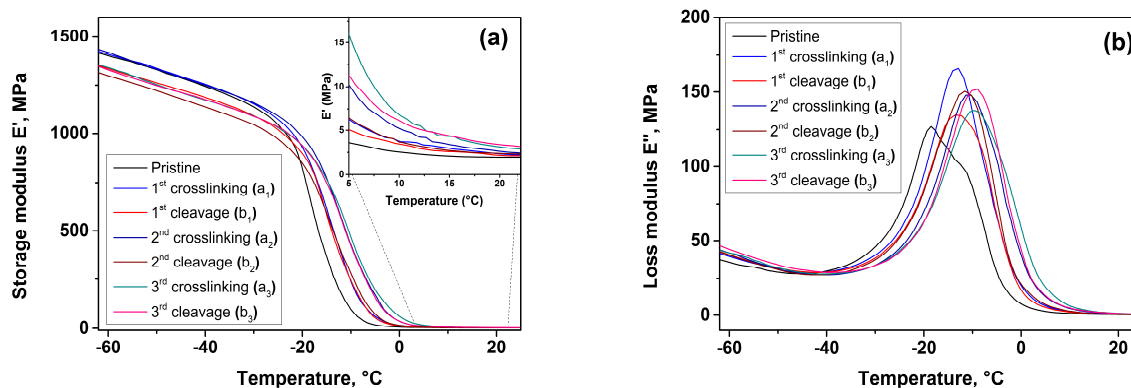


**Figure S1** – (a) Elastic storage modulus ( $E'$ ) and (b) loss modulus ( $E''$ ) versus temperature of free-standing anth-HXNBR films over repeated cycles of photo-cross-linking ( $a_1$ ,  $a_2$ ,  $a_3$ ) with  $46 \text{ J cm}^{-2}$  ( $\lambda > 300 \text{ nm}$ ,  $\text{N}_2$ ) and thermal dissociation ( $b_1$ ,  $b_2$ ,  $b_3$ ) at  $70 \text{ °C}$  (20 min,  $\text{N}_2$ ).

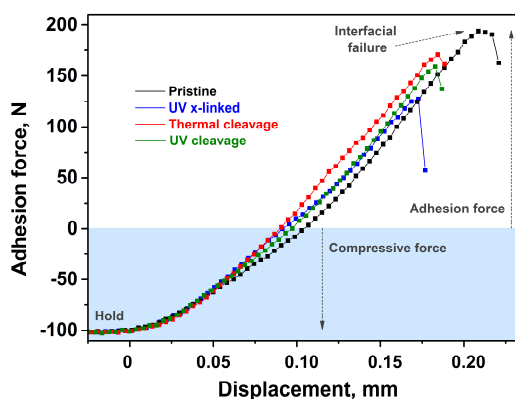


**Figure S2** – Load-displacement curves of probe tack measurements of anth-HXNBR films over one cycle of photo-cross-linking ( $46 \text{ J cm}^{-2}$ ,  $\lambda > 300 \text{ nm}$ ,  $\text{N}_2$ ) and subsequent dissociation of the formed photodimers. Dissociation was performed either by thermal annealing at  $70 \text{ °C}$  (20 min,  $\text{N}_2$ ) or by exposure with deep UV-light ( $1.1 \text{ J cm}^{-2}$ ,  $\lambda = 254 \text{ nm}$ ,  $\text{N}_2$ ).

### Background to NMR relaxometry as a tool to quantify reversibility in stimuli-responsive elastomers

NMR relaxometry is a popular technique to study network structure in elastomers. This method is governed by dipolar dephasing brought about by residual dipolar couplings and which is only partially averaged due to non-isotropically fluctuating network segments. The magnitude of  $D_{\text{res}}$  being directly proportional to non-isotropic nature of motion, which in turn is directly related to the cross-link density (or inverse network chain length,  $M_c^{-1}$ ) allows a determination of the cross-link density by measuring the corresponding relaxation rates. One of the prerequisites for such a study is that  $T_2$  should be measured in conditions where the network segments have completely explored the available conformational space such that the anisotropy is a function of motional restriction. This is usually achieved by measuring at 50-100 K above the glass transition temperature. This is clearly at crossroads for the samples under investigation, since higher temperatures changes the cross-linked state of the system during the course of the experiment due to cleavage reaction of anthracene dimers. Noting this fact, we have intentionally used  $T_2$  relaxometry as a qualitative tool giving no significance to the absolute parameter values and taking only the relative changes in the parameters into account. This is sufficient for the purpose of the study and shows excellent correlation with other characterisation methods, at the same time being complimentary to it.

The experiments were carried out at 45 °C, which is 50 K above  $T_g$  of the elastomers. It is also worth mentioning that no Gaussian shape was seen neither in a simple FID nor a magic-sandwich echo refocused FID, which is an indication of absence of any rigid sub-species at the measured temperature. Relaxometry curves were measured with Hahn echo as a function of echo times. The echo curves were analysed as mentioned above to arrive at a single parameter ( $R_2^{\text{avg}}$ ). Further, the maximum value of  $R_2^{\text{avg}}$  during the cycle was normalised to '1' symbolising the maximum cross-linked state and the minimum to '0' to symbolise be the least cross-linked state, which happened to be the uncrosslinked state. The changes in the overall cross-link density of the sample is shown for the thermally cleaved sample and UV-cleaved sample. It has to be once again pointed out that these values are representative and have no physical significance.

### Adhesion force measurement

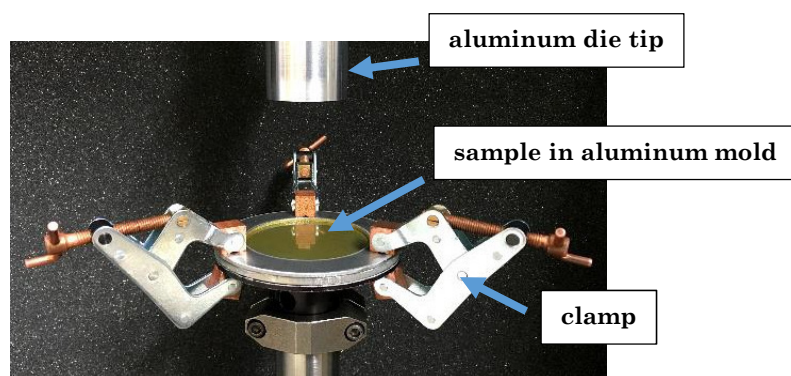


Figure S3 – Experimental set-up for determining the adhesion force of anth-HXNBR films.

# Chapter 4

## VITRIMER-LIKE ELASTOMERS FROM HXNBR RUBBER



#### 4.1 Bibliographic information

##### Published in:

Kaiser, S.; Wurzer, S.; Pilz, G.; Kern, W.; Schlögl, S. Stress relaxation and thermally adaptable properties in vitrimer-like elastomers from HXNBR rubber with covalent bonds. *Soft Matter*. DOI: 10.1039/C9SM00856J.

##### Author contributions:

Simon Kaiser: Conceptualisation; Methodology; Investigation; Data curation; Formal analysis; Validation; Visualisation; Original draft; Review and editing

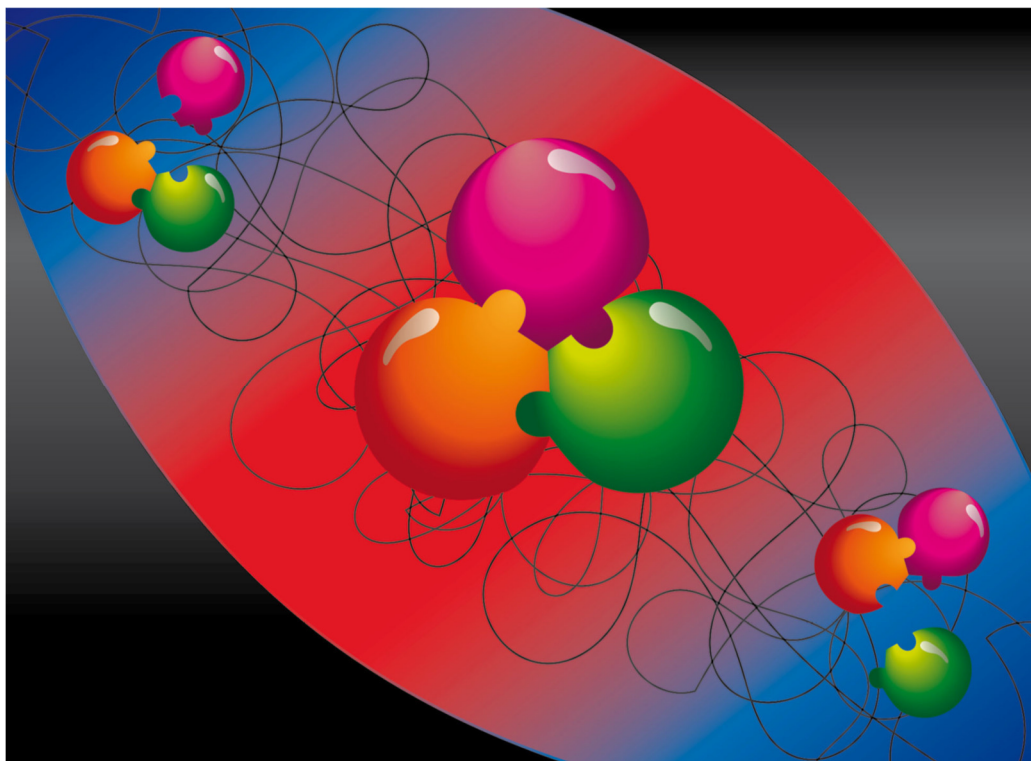
Stefan Wurzer: Investigation; Data curation

Gerald Pilz: Resources; Methodology

Wolfgang Kern: Funding acquisition; Resources

Sandra Schlögl: Funding acquisition; Project administration; Resources; Supervision; Conceptualisation; Methodology; Validation; Original draft; Review and editing

The manuscript presented here is an adapted accepted manuscript in order to correspond to the formatting of this thesis and does not necessarily reflect the actual published version. The graphic below depicts the back cover of Issue 30 (14 August 2019, Page 6029 to 6248) of the journal *Soft Matter*. The concept for the graphic originates from Simon Kaiser.



# STRESS RELAXATION AND THERMALLY ADAPTABLE PROPERTIES IN VITRIMER-LIKE ELASTOMERS FROM HXNBR RUBBER WITH COVALENT BONDS

Simon Kaiser<sup>a</sup>, Stefan Wurzer<sup>a</sup>, Gerald Pilz<sup>a</sup>, Wolfgang Kern<sup>a,c</sup> and Sandra Schlögl<sup>a,†</sup>

<sup>a</sup> Polymer Competence Center Leoben GmbH, Roseggerstrasse 12, A-8700 Leoben, Austria.

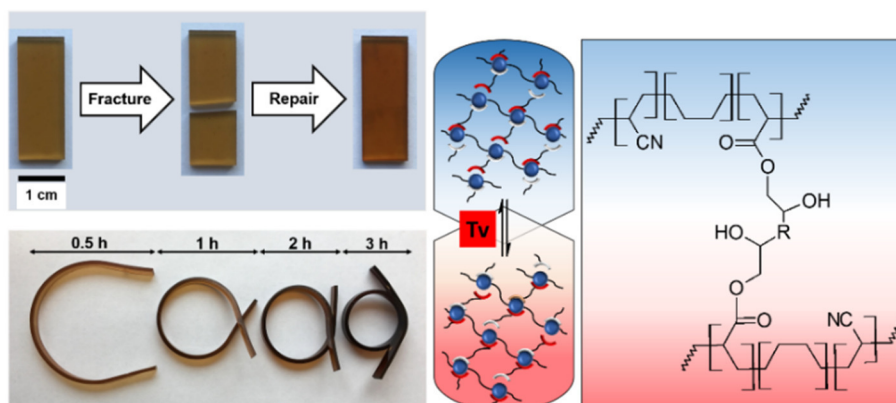
<sup>†</sup>E-mail: sandra.schloegl@pccl.at

<sup>b</sup> Institute of Materials Science and Testing of Polymers, Montanuniversitaet Leoben, Otto Glöckel-Strasse 2, A-8700 Leoben, Austria.

<sup>c</sup> Institute of Chemistry of Polymeric Materials, Montanuniversitaet Leoben, Otto Glöckel-Strasse 2, A-8700 Leoben, Austria.

## 4.2 Abstract

Widening the scope of skeletons in the chemistry of vitrimer(-like) high molecular weight rubbers, the present study highlights the preparation of vitrimer-like elastomers based on a technically relevant rubber that is characterised by high thermal and oxidation stability. In particular, we prepared covalently cross-linked hydrogenated carboxylated nitrile butadiene rubber (HXNBR) networks that can rearrange their topology due to the exchangeable nature of the cross-links. By cross-linking with a di-functional epoxide,  $\beta$ -hydroxyl ester linkages are incorporated into the rubber, enabling thermo-activated transesterifications in the presence of the catalyst triazabicyclodecene. At moderate temperatures, the covalent linkages ensure good mechanical properties as well as chemical and thermal stability of the rubber, which is essential for most applications. In addition, bond exchange reactions allow for fast and distinctive stress relaxation at elevated temperatures. Due to the enhanced network mobility above the vitrification transition temperature, the materials exhibit thermally adaptable properties. A comparative study throughout all experiments with catalyst-free samples serving as a reference is made. Shape change experiments reveal a certain malleability of the HXNBR elastomers and improved adhesion properties are shown by means of lap shear tests. In the presence of catalyst, the failure mechanism changes from adhesive to cohesive failure proving the weldability of the material. Furthermore, the samples exhibit thermally triggered repair capabilities as demonstrated by stress-rupture tests. In general, it is shown that already low quantities of exchangeable cross-links of associative nature impart a promising thermal adaptability into high molecular weight HXNBR rubber.



### 4.3 Introduction

First described by Leibler and co-workers, vitrimers are recently gaining increased attention in the design of functional polymer networks with adaptable properties.<sup>1</sup> Vitrimers contain exchangeable chemical bonds and belong to the group of covalent adaptable networks (CANs). In contrast to classical thermo-reversible reactions such as Diels-Alder chemistry, the dynamic nature of the cross-links in vitrimers relies on a thermo-activated associative exchange mechanism.<sup>2</sup> Thus, vitrimers do not depolymerise at elevated temperature, but retain their network integrity.<sup>1,3</sup> In other words, vitrimeric materials can rearrange their topology but remain insoluble since the number of cross-links is preserved.<sup>1</sup> To date, vitrimeric networks have been realised using a vast variety of materials as well as underlying associative exchange reactions.<sup>4</sup> Along with the catalytic transesterification of polyester/polyols,<sup>1</sup> synthesis routes for vitrimers rely on the transalkylation of trialkylsulfonium salts,<sup>5</sup> the transesterification of boronic esters<sup>6</sup> and polycarbonates<sup>7</sup> or the exchange of vinylogous urethanes<sup>8</sup> and amines.<sup>9</sup> Most of the reported vitrimer systems require the addition of a catalyst. Among the regularly used and well-studied catalysts are zinc acetate and zinc acetylacetonate<sup>1</sup> as well as the strong guanidine base triazabicyclodecene.<sup>10</sup>

The viscoelastic properties of vitrimers are determined by two different transition temperatures: (i) the typical glass transition temperature ( $T_g$ ) and (ii) the topology freezing transition temperature ( $T_v$ ), which describes the transition from a viscoelastic solid to a viscoelastic liquid.<sup>2</sup> Below  $T_v$ , the bond exchange reactions are slow and the topology of the network is frozen, therefore the material behaves like a classical thermoset.<sup>11</sup> The  $T_v$  is governed by the density of exchangeable cross-links, the exchange reaction kinetics and the mobility of the polymer chains.<sup>2</sup> Due to the dynamic nature of the cross-links and the related controlled macroscopic flow at elevated temperatures, vitrimers are promising materials for reshaping,<sup>12</sup> self-healing,<sup>13</sup> reprocessing<sup>14</sup> and recycling.<sup>15</sup>

The majority of the reported vitrimeric materials are thermosets based on low molecular weight monomers such as epoxy-anhydride, epoxy-carboxylic acid networks, polyurethanes or polycarbonates. Only recently, publications introducing vitrimeric or vitrimer-like properties into rubbers have emerged.<sup>16-20</sup> Leibler et al. studied an elastomer network based on epoxidised natural rubber (ENR) cross-linked with a dicarboxylic acid. In the presence of zinc acetate an adaptable network due to transesterification reactions was obtained, enabling partial stress relaxation and enhanced self-adhesion properties at elevated temperatures.<sup>21</sup> The authors have described this network only as vitrimer-like rather than a full vitrimer. Incomplete stress relaxation was observed because of the lack of exchangeable cross-links and the low reactivity of sterically hindered hydroxyl groups as well as side reactions such as oxidation. Recently, Guo and co-workers prepared vitrimeric nanocomposites based on carboxyl group-grafted styrene-butadiene rubber, which was cross-linked with silica particles bearing functional epoxy groups.<sup>16</sup> They further transferred the concept of vitrimers to filled ENR compounds by exploiting  $\beta$ -hydroxyl ester linkages between ENR and carbon nanodots.<sup>20</sup>

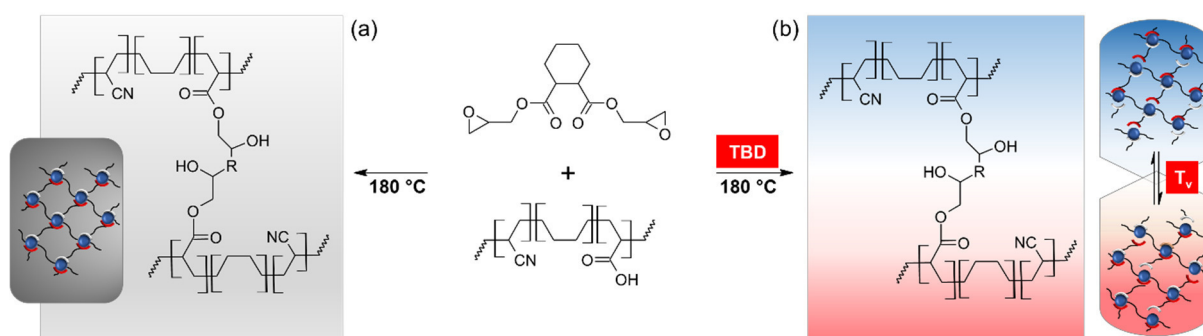


**Figure 1** – Schematic representation of the cross-linking of HXNBR with a di-functional epoxy cross-linker yielding  $\beta$ -hydroxyl ester linkages. (a) Formation of a permanent network and (b) formation of a covalently cross-linked network enabling bond exchange reactions in the presence of the transesterification catalyst triazabicyclodecene (TBD).

Inspired by these studies, we followed a vitrimeric approach to introduce exchangeable covalent cross-links into an industrially relevant rubber by synthesising an adaptable network from hydrogenated carboxylated nitrile-butadiene rubber (HXNBR). Whilst vitrimer chemistry has been incorporated into rubbers using epoxidised natural rubber or styrene-butadiene rubber, the concept – to the best of our knowledge – has not yet been transferred to hydrogenated and carboxylated nitrile-butadiene rubbers. HXNBR is a terpolymer from the monomers butadiene, acrylonitrile and an unsaturated carboxylic acid and displays several advanced properties over nitrile-butadiene rubber (NBR). The introduction of carboxyl groups to NBR increases the mechanical strength and further enhances the abrasion and wear resistance. Additional hydrogenation improves the thermal and oxidative stability of the rubber as well as the resistance to heat, oil and chemicals.<sup>22</sup> This is due to the replacement of radical-susceptive carbon-carbon double bonds with saturated hydrocarbon bonds.<sup>23</sup> Natural rubber networks, for instance, lack from oxidative and ozone stability and are further not resistant to oil. It has been reported that these properties can be significantly improved by using a coating from HXNBR rubber.<sup>24</sup> Carboxylated HNBR rubbers are polar and thus have a long tradition in adhesion technology such as adhesives for polar rigid surfaces.<sup>25,26</sup> Further fields of application are found in oil well specialisations<sup>27</sup> and the automotive sector as oil-resistant elastomers.<sup>28,29</sup> HXNBR is also employed in blends with other rubbers and the combination with polar or non-polar resin materials is common.<sup>26</sup> A well-known procedure is the blending with ethylene propylene diene monomer rubber (EPDM). While EPDM provides low-temperature flexibility, the modified NBR ensures resistance to heat, ozone and hydrocarbon fluids.<sup>29</sup> In the current study, the choice of a classic carboxylated NBR rather than a telechelic carboxyl-terminated butadiene-acrylonitrile rubber (CTBN) was made because of the higher industrial relevance of the former due to the production in bulk and the ease of availability. As CTBN types are not produced in abundance and are commonly of low molecular weight, and therefore liquid, classic XNBR rubbers are produced on a kiloton scale and the conventional rubber compounding procedures can be applied.<sup>30</sup>

Our group recently reported a stimuli-responsive HXNBR network with reversible cross-link sites, being dissociative in nature.<sup>31</sup> By introducing anthracene moieties *via* side chain modification, a photo-responsive dry adhesive was obtained enabling a (photo)reversible switching of adhesion properties as a function of the cross-linking state. Along with a

bonding and de-bonding on demand, the reversible network characteristics were further exploited for a reversible switching of solubility properties, the inscription of micropatterns and the development of self-repair concepts for HXNBR compounds.<sup>32</sup>

In this study, we go from a dissociative to an associative bond exchange mechanism and demonstrate vitrimer-like behaviour of a HXNBR network that undergoes thermally triggered bond exchange reactions. As HXNBR contains carboxylic acid functions, exchangeable cross-links can be easily introduced by curing the rubber with an epoxy-based cross-linker (Figure 1). Along with the formation of esters, hydroxyl groups in the  $\beta$ -position are generated by the nucleophilic ring opening reaction between carboxyl functions and the epoxy groups.<sup>33</sup> In the presence of an appropriate catalyst, the formed  $\beta$ -hydroxyl esters, in turn, become susceptible to transesterification exchange reactions.<sup>1</sup> Since it has been reported that zinc acetate is likely to hamper the cross-linking reaction between epoxy functions and carboxylic acid groups in ENR,<sup>21</sup> we choose triazabicyclodecene (TBD) as catalyst. TBD is a well proven, metal-free catalyst for transesterification reactions.<sup>10</sup> In this work, the reversible network is compared to a reference network comprising identical but permanent, non-reversible cross-links. Adaptability of the rubber through thermo-activated transesterification reactions is studied by stress relaxation and creep measurements. The results reveal that the synthesised elastomers are characterised by fast and substantial stress relaxation whilst showing low creep, which are beneficial properties when it comes to the use of these networks in technical applications.<sup>34</sup> The bond exchange reactions at elevated temperature are exploited for inducing shape changes of the covalently cross-linked HXNBR elastomers, thermally controlled changes in adhesion properties and the introduction of repair capabilities, evidencing the versatility of the developed vitrimer-like rubber.

## 4.4 Results and discussion

### *Covalent cross-linking of HXNBR with di-functional epoxide and acceleration by TBD*

Rubber networks exhibit unique mechanical properties such as high elasticity and high toughness. Along with the mechanical performance, the thermal and chemical stability, such as solvent resistance, are ensured by covalent cross-links. However, if the covalent cross-links are permanent, the rubbers are neither malleable, recyclable nor reprocessible, once cured. Implementing the concept of vitrimers into rubbers enables large stress relaxation and improves the adhesion properties even in highly cross-linked rubbers.<sup>21</sup>

To obtain networks with covalent but exchangeable cross-links, compounds of hydrogenated carboxylated nitrile butadiene rubber (HXNBR) and a di-functional epoxy-based cross-linker (Epalloy 5200, E5200) were prepared, with the amount of epoxy functions being in stoichiometry with the carboxyl group functions in all cases. Along with a catalyst-free sample (HXNBR-E5200), from which permanent network characteristics are expected, two compounds containing the transesterification catalyst triazabicyclodecene (TBD) at 10 (HXNBR-E5200-TBD10) and 20 mol% (HXNBR-E5200-TBD20), relative to the carboxylic acid groups, were prepared.

The cure behaviour of the different compounds was followed at 180 °C in a moving die rheometer (Figure 2a). The results show that within the first seconds of the thermal curing, the elastic torque ( $S'$ ) decreases due to softening of the rubber. This is followed by a rapid increase in  $S'$ , which is observed in all three compounds, indicating that the cross-linking reaction is proceeding. For HXNBR-E5200 (green curve in Figure 2a), the further course of  $S'$  reveals a comparatively slow cross-linking reaction, with 95% of the ultimate state of cure ( $t_{95}$ ) being reached after 39 min. However,  $S'$  reaches a plateau value, revealing that the nucleophilic ring opening reaction of the epoxy groups with the carboxylic acid moieties is complete. In the presence of TBD, the cross-linking reaction is accelerated considerably as proven by the much steeper initial slopes of  $S'$ . With 10 and 20 mol% of TBD,  $t_{95}$  is reached after only 2.56 and 1.28 min, respectively. The acceleration of the cross-linking reaction was expected, since TBD is a known base catalyst facilitating various reactions<sup>35</sup> such as the ring opening reaction of epoxides with anhydrides.<sup>36</sup> The results further give rise to a high network stability for all compounds, since almost no reversion is observed upon extended curing (80 min) at 180 °C. Despite the slow curing reaction of the catalyst-free sample, the similar plateau value compared to the compounds containing the catalyst indicates not only a complete cross-linking reaction, but also suggests a comparable cross-link density.<sup>37</sup> It should be noted, that the cross-link density is one of the parameters that determine  $T_v$ , wherefore the reference material should exhibit a cross-link density as similar as possible to the compounds with TBD.<sup>2</sup>

To confirm the comparable cross-link densities, equilibrium swelling measurements in chloroform were conducted with samples after curing to the respective  $S'$  plateau values. For HXNBR-E5200, HXNBR-E5200-TBD10 and HXNBR-E5200-TBD20 mass swelling ratios of  $6.04 \pm 0.01$ ,  $5.72 \pm 0.04$  and  $5.61 \pm 0.03$  were found, respectively. The data suggests a similar network integrity for all three compounds, which means that the network as schematically illustrated in Figure 1 should have been formed. The equilibrium swelling experiments further revealed that the gel contents are consistently high and amount to 96%. It should be noted that the mass swelling ratios are significantly higher than for conventional peroxide or sulfur cured nitrile butadiene rubber (NBR) networks.<sup>38</sup> This is related to the low amount of carboxyl groups present in the rubber chains (5 mol%), limiting the number of possible cross-links. Permanently cross-linked rubbers are known to display a stress relaxation behaviour depending on the cross-link density, whereby the lower the density of cross-links, the faster the stress relaxation.<sup>39</sup> Thus, due to a sufficiently high molecular mobility, slightly cross-linked elastomers are promising candidates in applications where self-healing or good adhesion properties are demanded.<sup>40</sup>

The chemical nature of the cross-links was studied by FTIR spectroscopy. Comparing the IR spectra of HXNBR-E5200 (Figure S1a in ESI), prior to and after thermal curing at 180 °C, a depletion of the characteristic epoxy bands at 909 and 848  $\text{cm}^{-1}$  is observed. Furthermore, the carbonyl absorption band at 1698  $\text{cm}^{-1}$ , representing carboxylic acid groups, disappears. On the other hand, the absorption band corresponding to ester groups increases and shifts to 1731  $\text{cm}^{-1}$ . The results confirm the nucleophilic ring opening reaction involving the conversion of carboxyl groups to ester moieties. Moreover, a broad band appears at 3489  $\text{cm}^{-1}$ , which is associated with the formation of (free) hydroxyl groups

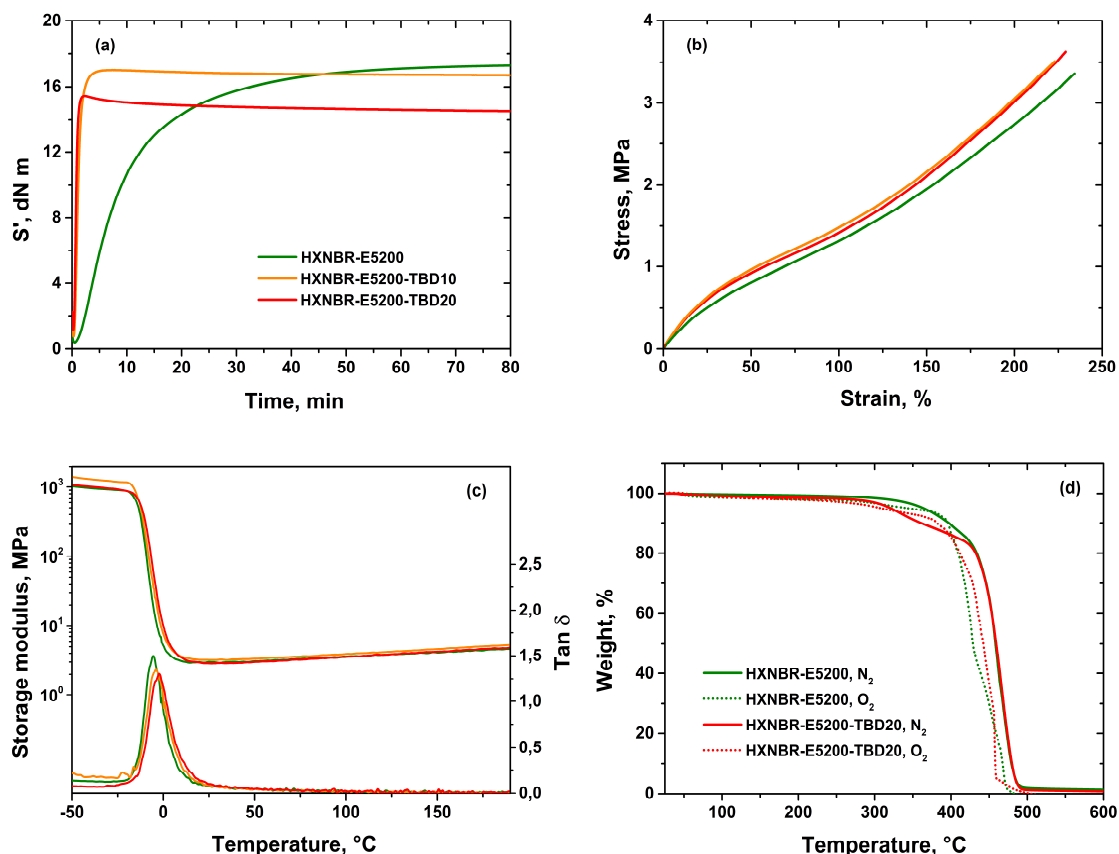


**Figure 2** – (a) Cross-linking kinetics of the different HXNBR compounds at 180 °C followed in the moving die rheometer, (b) typical stress-strain curves, (c) DMA analysis showing the storage modulus  $E'$  and the mechanical loss factor ( $\tan \delta$ ) of HXNBR compounds with permanent and exchangeable cross-links (green: HXNBR-E5200; orange: HXNBR-E5200-TBD10; red: HXNBR-E5200-TBD20), and (d) thermogravimetric analysis under both atmospheres, nitrogen and oxygen.

from  $\beta$ -hydroxyl esters. Identical observations were made for HXNBR-E5200-TBD10 and HXNBR-E5200-TBD20 (Figures S1b and c in ESI).

The possible formation of additional covalent bonds due to thermal cross-linking of residual carbon-carbon double bonds in HXNBR was examined by the absorption band at  $972\text{ cm}^{-1}$  (Figure S1d in ESI). The band corresponds to the vibration of 1,4-trans double bonds.<sup>41</sup> No decrease in absorption was observed for any of the compounds when comparing the spectra before and after curing, as well as compared to the spectrum of the pristine HXNBR. Consequently, we assume that no covalent bonds across the carbon-carbon double bonds have formed in the prepared HXNBR networks.

This issue was further addressed by means of decomposition experiments (Figure S8 in ESI). A sample of HXNBR-E5200-TBD20 was immersed in a 1:1 mixture of ethylene glycol and trichlorobenzene and stirred at 180 °C. After 6 h the sample was completely dissolved, confirming the incorporation of the alcohol through transesterification exchange reactions causing a total depolymerisation of the network. The experiment indicates the absence of permanent cross-links, therefore the HXNBR network should contain only reversible  $\beta$ -hydroxyl ester linkages.

It has been reported, that a prolonged heat treatment can be detrimental to the mechanical properties of rubbers.<sup>42</sup> Thus, the distinctive acceleration of the cure kinetics by the addition of TBD does not only provide a promising route towards cure time reduction but might also be beneficial with respect to the mechanical properties. Typical stress-strain curves of the compounds under investigation are presented in Figure 2b, and the mechanical properties are summarised in Table S1 in ESI. From the data, it can be derived that the longer curing time necessary for HXNBR-E5200 to complete the cross-linking reaction does not negatively affect the mechanical properties, since the tensile testing data is similar to the materials containing TBD. Figure 2c shows the storage modulus ( $E'$ ) and the mechanical loss factor ( $\tan\delta$ ) as a function of temperature obtained by DMA analysis. The data reveal very similar  $E'$  and  $\tan\delta$  values over the measured temperature region for all compounds. The glass transition temperatures were found to be -5.5, -4.0 and -2.2 °C for HXNBR-E5200, HXNBR-E5200-TBD10 and HXNBR-E5200-TBD20, respectively. In addition, slightly increasing moduli are observed at temperatures above  $T_g$ . This is attributed to the distinctive thermally induced entropic rubber-elastic contraction found for the prepared HXNBR networks (see Figure 4). For verification, equilibrium swelling experiments in a good solvent were carried out (Figure S7 in ESI). Cured samples of HXNBR-E5200 and HXNBR-E5200-TBD20 were immersed in chloroform before and after storage at 180 °C for 2 h. In the case of the formation of additional cross-links at elevated temperature, the swelling degrees would be expected to decrease. The data reveal very similar swelling factors for both compounds before and after storage at 180 °C, proving a constant network connectivity in the investigated, and for DMA measurements relevant, time and temperature range. The DMA data is consistent with the rheological studies, equilibrium swelling experiments as well as tensile testing, and confirms the similar network properties of the different compounds. Thus, HXNBR-E5200 comprising permanent covalent cross-links is considered a suitable reference system for the following investigations. Moreover, the thermal and oxidative stability of the prepared compounds was studied using thermogravimetric analysis and FTIR spectroscopy. The TGA curves are shown in Figure 2d. The HXNBR samples were investigated under both nitrogen and oxygen atmosphere and the data show a high thermal oxidative stability of the samples. FTIR spectra of HXNBR-E5200-TBD20 were recorded over time of a sample stored at 180 °C and ambient atmosphere (Figure S1e in ESI). The spectra show no change within 5 h, demonstrating that no relevant amount of degradation products was formed.

To further prove the permanence and the resistance to chemical solvents of the HXNBR networks containing TBD, dissolution experiments in trichlorobenzene (TCB) were performed (Figure S6 in ESI). HXNBR-E5200-TBD20 was submerged in TCB and the swelling degree was followed at high temperature over time. The sample swells but remains undissolved, even after immersion for 20 h at 180 °C. The soluble fraction amounts to 6%.

#### *Network rearrangements due to thermo-activated bond exchange reactions*

Stress relaxation measurements of all compounds were performed in a moving die rheometer directly upon curing at 180 °C. After allowing the samples to equilibrate to the selected measurement temperatures for 15 min, a step strain of 1% was applied and the



evolution of the stress was monitored over time. Previously conducted amplitude sweep measurements ensured that the applied strain was within the linear viscoelastic region of the samples (Figure S2 in ESI). At 30 °C, no significant stress relaxation takes place for any of the samples, as indicated by essentially flat curves (Figure 3a). Since the rate of transesterifications is very slow at such a low temperature, the topology of the networks is frozen. At an elevated temperature of 180 °C, the compounds containing the catalyst (orange and red curve in Figure 3b) can rearrange their network topology through transesterification exchange reactions of  $\beta$ -hydroxyl ester linkages and the curves reveal a substantial stress relaxation. This also indicates that the vitrification transition temperature,  $T_v$ , has clearly been exceeded. The results further show that bond exchange reactions are more pronounced with increasing catalyst content. In the absence of TBD (HXNBR-E5200) transesterification reactions do not occur, even at 180 °C (green curve in Figure 3b). Such behaviour can be expected for a permanently cross-linked network without exchangeable linkages. This also suggests that thermally induced exchange reactions do not take place in HXNBR-E5200, for instance as previously reported for catalyst-free vitrimeric epoxy networks.<sup>43</sup> In other words, the behaviour of the reference compound proves that the observed stress relaxation can be attributed to the rearrangement of the network topology due to thermo-activated and catalytically controlled bond exchange reactions. Furthermore, stress relaxation experiments were

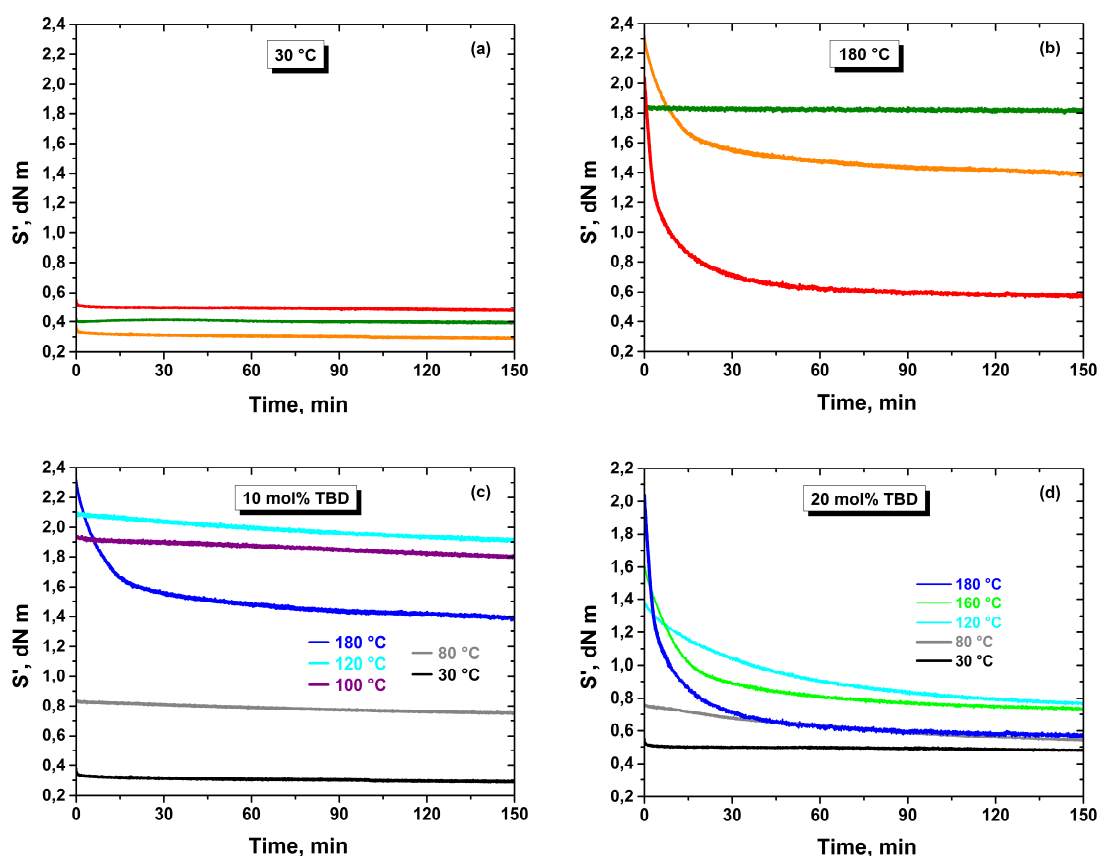


**Figure 3** – Stress relaxation experiments at (a) 30 °C and (b) 180 °C for the different HXNBR compounds (green: HXNBR-E5200; orange: HXNBR-E5200-TBD10; red: HXNBR-E5200-TBD20). Stress relaxation data of (c) HXNBR-E5200-TBD10 and (d) HXNBR-E5200-TBD20 at various temperatures.

conducted at various temperatures ranging between 30 and 180 °C for samples containing the catalyst (Figure 3c and d). The initial relaxation modulus increases with temperature, which is in accordance with the well-known proportional increase of the elastic modulus with temperature.<sup>44</sup> In terms of HXNBR-E5200-TBD10, the onset of  $T_v$  appears to be at about 100-120 °C, since the respective relaxation curves show a slight slope. In contrast, the addition of 20 mol% TBD already enables significant stress relaxation at such a temperature. For both compounds, the stress relaxation rate further accelerates with increasing temperature. From the data, it can be derived that the onset of  $T_v$  is at approximately 80 °C for HXNBR-E5200-TBD20. The increased catalyst concentration shifts the vitrification transition to lower temperatures. However, full stress relaxation is not achieved, which might be related to the following effects. On the one hand, the HXNBR-E5200 networks exhibit a comparatively low cross-link density, which is limited by the low content of carboxylic acid groups in the rubber under investigation. This narrows the probability of collision between  $\beta$ -hydroxyl ester linkages to undergo associative exchange reactions. On the other hand, the polymer chains are very long in the high molecular weight HXNBR ( $M_w = 370,000$  g/mol) and it is highly likely that entanglements are present in the samples, restricting the network dynamics and preventing the material to flow as observed for true vitrimers.

Nevertheless, the stress relaxation is reasonably efficient and the observed initial stress relaxation at 180 °C of the compound containing 20 mol% TBD is fast. HXNBR-E5200-TBD20 is capable of relaxing 74% (within 150 min) of the initial stress at 180 °C and with 50% of it being relaxed after only 8 min (see red curve in Figure 3b). This is quite remarkable considering the low cross-link density of the rubber network and, to the best of our knowledge, no faster stress relaxation has been reported yet in a high molecular weight rubber exhibiting associative bond exchange reactions.<sup>16-19,21</sup> It should also be mentioned that in contrast to ENR cross-linked with dicarboxylic acids, the free hydroxyl groups in HXNBR are less sterically hindered (Figure 1).<sup>45</sup> Steric hindrance has been reported to impede transesterification exchange reactions.<sup>21</sup> In the HXNBR compounds under investigation, the hydroxyl ester groups are located on the side chain and are not sterically hindered by adjacent methyl groups, which is expected to significantly increase the mobility of the exchangeable bonds in the network. Leibler et al. have also noted that side reactions such as oxidation limit the applicability of vitrimer-like ENR.<sup>21</sup> Due to the high number of carbon-carbon double bonds, natural rubber based compounds are highly susceptible to oxidation reactions.<sup>24</sup> In contrast, most of the double bonds in HXNBR are hydrogenated which makes this class of rubber less prone to oxidation reactions<sup>24</sup> and thus, a promising base material for vitrimer-like elastomers.

Along with stress relaxation studies, creep measurements were carried out to study the effect of exchangeable cross-links on the time dependent deformation behaviour at various temperatures (Figure 4). The experiments were conducted for the different compounds at both 80 (about at  $T_v$ ) and 160 °C (above  $T_v$ ). At 80 °C, only a small amount of creep is observed for the compounds containing TBD, as indicated by the essentially flat curves (orange and red dashed curves in Figure 4). This can be expected for a measuring temperature in the vitrification transition temperature range, since transesterifications are slow. Catalyst-free HXNBR-E5200 even shows a declining curve after the initial elastic response (green dashed curve in Figure 4). This observation can be attributed to

the entropic rubber-elastic contraction.<sup>47</sup> In contrast, when 10 and 20 mol% TBD are present, the entropic contraction is compensated by the more pronounced creep elongation enabled by bond exchange reactions. As previously shown in stress relaxation experiments, the onset of bond exchange reactions is at about 80 and 100 °C for HXNBR-E5200-TBD 20 and HXNBR-E5200-TBD10, respectively. Going to 160 °C, which is above  $T_v$ , the picture clearly changes. While in HXNBR-E5200 entropic rubber-elastic contraction still predominates and is even more pronounced than at 80 °C (green solid curve in Figure 4), due to more extensive entropy elastic effects at higher temperature, a distinctive creep is observed in compounds containing TBD. In particular, the creep increases with rising catalyst concentration. This enhanced elongation is associated with the larger number of transesterification rearrangements due to the higher catalyst loading. The entropic rubber-elastic contraction turns into the irreversible plastic deformation because of associative bond exchange reactions. Considering the ability of HXNBR-E5200-TBD20 to substantially relax stress (Figure 3d), the total measured creep (within 180 min) is low. This can mainly be attributed to the counteractive effect of entropic contraction, which is most pronounced at high temperatures and hence, significantly hinders creep deformation. It has to be noticed that the shown creep curves only reflect the portion of pure creep deformation without the instantaneous elastic deformation in the loading phase. It should further be noted that in typical applications of elastomers (e.g. seals) creep is not desired, since it induces a viscous flow that causes permanent deformation and geometry changes and often leads to product failure.<sup>34</sup> Thus, the prepared vitrimer-like HXNBR networks are interesting candidates for technical applications since they are capable of large stress relaxation but at the same time can hold stress with little creep for the reasons stated.

The permanent plastic extension generated by bond exchange reactions at elevated temperature and by the application of an external force can also be demonstrated by shape change experiments. Cured rubber strips were subjected to helical- or fusilli-shaped deformations (Figure 5a and 5b). The objects were then exposed to 180 °C for different times. For samples containing TBD, thermo-activated transesterifications enable a

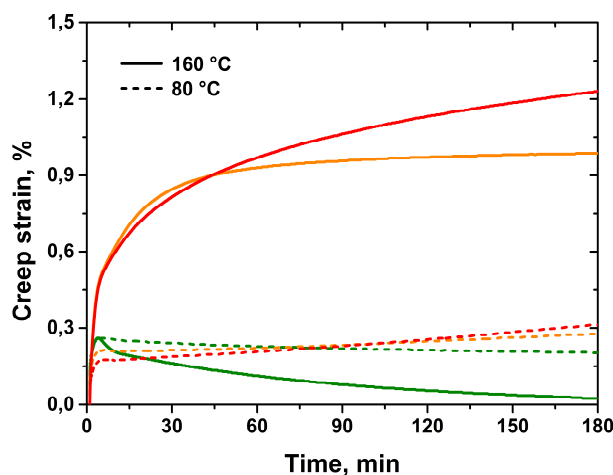


**Figure 4** – Creep experiments for the different HXNBR compounds at 80 °C (dashed lines) and 160 °C (solid lines) with a nominal stress of 0.1 MPa (green: HXNBR-E5200; orange: HXNBR-E5200-TBD10; red: HXNBR-E5200-TBD20).

relaxation of the applied stress to some extent and the effect increases with time. After cooling down to room temperature, the new shapes are partially retained. Partial recovery of the initial shape was shown for fusilli-shaped samples, and is more effective the smaller the shape change in the previous step. The catalyst-free compound, on the other hand, shows only minor permanent deformation and therefore is not susceptible to shape changes. The results clearly show that the ability towards reshaping of the material requires the presence of the catalyst and improves with both rising reaction time (at 180 °C) and TBD content.

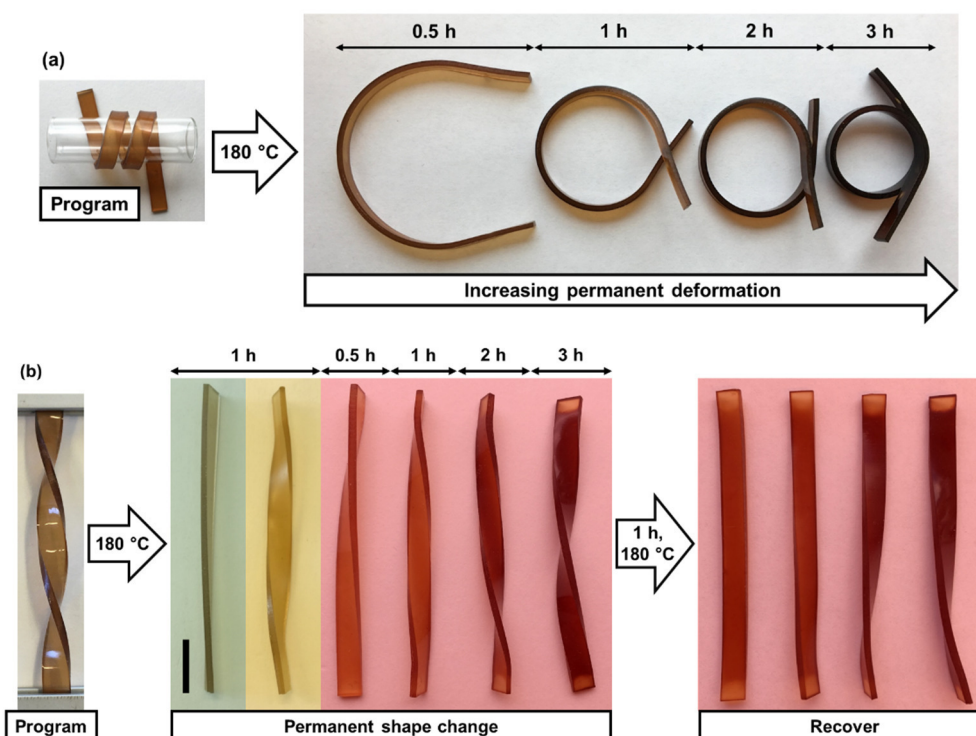


**Figure 5** – Photographs of (a) reconfiguration towards helical-shaped samples for different times at 180 °C (length of the strips 15 cm). (b) Shape recovery process on the example of fusilli-shaped elastomer strips (highlighted green: HXNBR-E5200; highlighted orange: HXNBR-E5200-TBD10; highlighted red: HXNBR-E5200-TBD20). The scale bar corresponds to 1 cm.

#### *Transesterification reaction induced adhesion improvement*

In further experiments, the adaptable adhesion of the elastomers was studied. As the catalyst enables transesterification exchange reactions in the HXNBR networks at elevated temperatures, thermally mendable adhesion properties were expected.

In order to quantify self-adhesion properties of the different compounds, lap shear tests were performed as described in the experimental part and previously in literature.<sup>21,48</sup> The effect of catalyst loading, time and temperature on the adhesion performance was investigated. The forces necessary to peel the samples were used to calculate the corresponding adhesion energies according to eqn 1. Figure 6a shows the obtained data of the different compounds for various adhesion times at 180 °C. In terms of HXNBR-E5200, complete peeling (adhesive failure) is observed for all investigated times. The adhesion energy increases from 5 to 15 min of adhesion time and does not increase any further for longer times. For the specimens containing the transesterification catalyst the adhesion

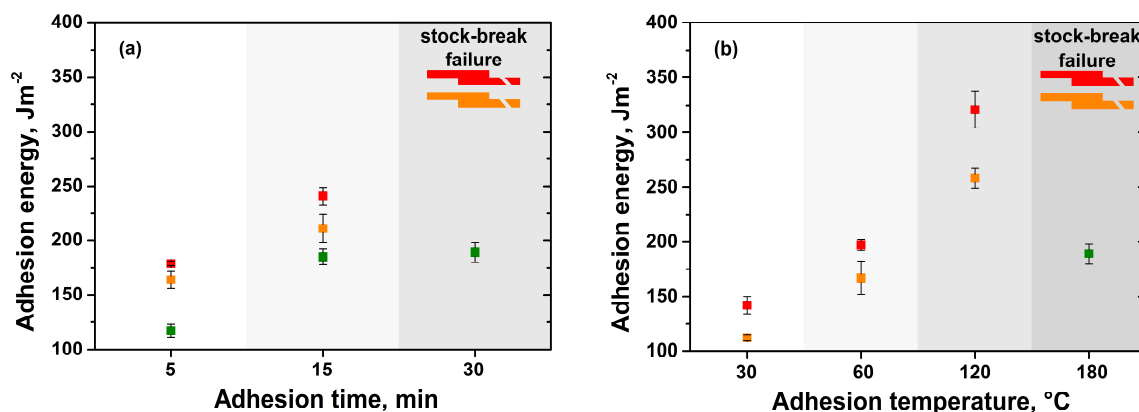


**Figure 6** – Adhesion energies calculated from lap shear tests for the different HXNBR compounds: (a) adhered for various adhesion times at 180 °C and (b) adhered for 30 min at selected temperatures (green: HXNBR-E5200; orange: HXNBR-E5200-TBD10; red: HXNBR-E5200-TBD20).

energies increase in a similar manner when rising the adhesion time from 5 to 15 min. Already at these short times, the adhesion energies are slightly higher than for the reference material, indicating a generally higher self-sticky nature of the compounds with TBD. A further increase of the adhesion time to 30 min causes stock-break (cohesive) failure for both compounds. The catalyst clearly improves the interfacial adhesion of the samples and cohesive failure becomes the predominant failure mechanism. Since no catalyst is present in HXNBR-E5200, the adhesion obtained can only originate from physical interactions at the interface of the two adhered samples, such as chain inter-diffusion and dipolar interactions between polar groups like hydroxyl groups and esters. The contribution of thermally induced transesterification reactions in the absence of the catalyst can be excluded, as demonstrated previously by stress relaxation measurements (green curve in Figure 3b). In contrast, the significant increase of adhesion energies for compounds with TBD (for adhesion times longer than 15 min) is obviously the result of bond exchange reactions. Both, enhanced chain inter-diffusion by an increased chain mobility, as well as transesterification exchange reactions across the interface most likely contribute to the observed adhesion improvement. Furthermore, the contribution of side reactions can be excluded, because prolonged curing experiments have proven a high network stability for all compounds even at 180 °C. No reversion was observed in the rheological measurements (Figure 2a). The equilibrium swelling data (Figure S7 in the ESI) and decomposition experiments (Figure S8 in the ESI) as described above in the text support this assumption. In Figure 6b the adhesion energies as a function of the temperature at a constant adhesion time of 30 min are plotted. It appears that for 30 and 60 °C adhesion can be attributed to the self-stickiness and to chain inter-diffusion at the interface of the joint for the compounds containing TBD. The similar adhesion energy of about  $190 \text{ Jm}^{-2}$  for the catalyst-free reference material obtained at 180 °C supports this assumption. At 120 °C, adhesion clearly improves when TBD is present, apparently in a non-linear manner. The effect is more pronounced for higher catalyst concentrations. These observations are consistent with the stress relaxation measurements. Note that for HXNBR-E5200-TBD20 the onset of  $T_v$  was found to be at about 80 °C, while at 120 °C

transesterification exchange reactions already take place noticeably (see grey and cyan curve in Figure 3d, respectively). At 180 °C the joint becomes stronger than the material itself and cohesive failure occurs as already observed in Figure 6a. Despite the small number of exchangeable cross-links in the prepared materials, a clear thermal adaptability is obtained when TBD is present. Thus, not only the bulk but also the surface properties of the HXNBR networks are mendable which also paves the way towards a welding of the covalently cross-linked elastomers.

#### *Thermal repair capabilities in vitrimer-like HXNBR*

Along with stress-relaxation, shape changing and adaptable adhesion properties, the enhanced network mobility enabled by bond exchange reactions resulted in thermally induced repair capabilities of the elastomers. The thermal repair behaviour of HXNBR-E5200 and HXNBR-E5200-TBD20 was studied by means of stress-rupture tests of repaired strips of rubber as described in the experimental part and shown in Figure 7a. The calculated stresses are plotted against the respective failure times in Figure 7b. In the absence of the catalyst, for instance, the specimens are able to withstand a stress of 0.39 MPa for 2 min after exposure to 180 °C for 1 h. Although the material does not contain exchangeable cross-links, some adhesion across the teared sample planes is obtained due to physical entanglement and dipolar interactions of the rubber chains. The contribution of transesterifications can be clearly seen in the stress-rupture performance of HXNBR-E5200-TBD20. At 0.42 MPa for instance, failure occurs after much longer time (82 min) under the same repair conditions. The effect significantly improves when the adhesion time is increased from 1 to 2 h. The data confirms a distinctive enhancement of the repair capability for the compound containing TBD. It should again be considered that despite the low cross-link density and therefore small number of available  $\beta$ -hydroxyl ester linkages, thermally mendable HXNBR elastomers are obtained with less than two phr of TBD.

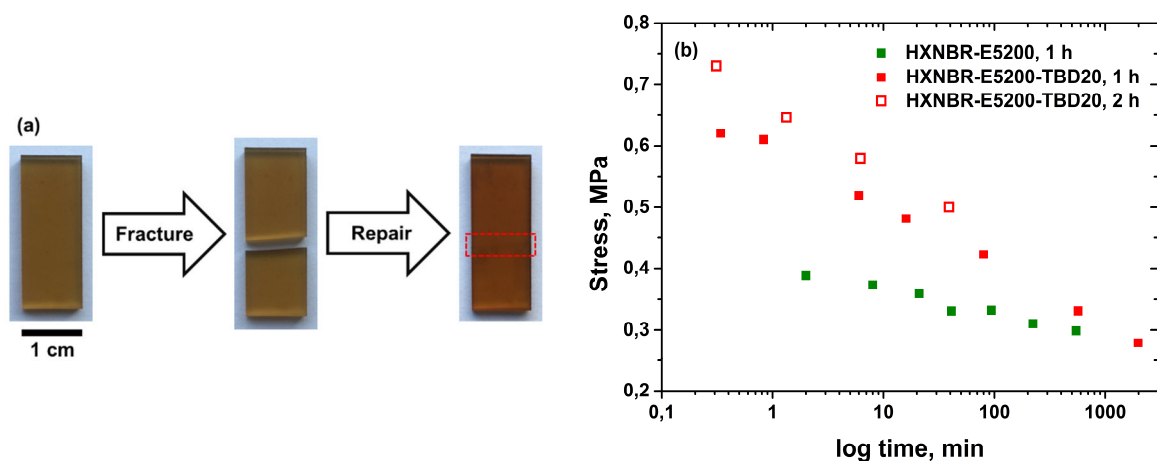


**Figure 7** – (a) Photographs of the repair process of HXNBR samples. (b) Stress-rupture curves for HXNBR-E5200 (green squares) and HXNBR-E5200-TBD20 (full red squares: healed for 1 h; open red squares: healed for 2 h) samples after rupture and subsequent exposure to 180 °C.

## 4.5 Experimental

### *Materials and chemicals*

Therban® XT KA 8889 VP, a hydrogenated carboxylated nitrile butadiene rubber (HXNBR) with a molecular weight of 370,000 g/mol ( $M_w$ ) and with 5 mol% carboxylic acid content, 33 mol% acrylonitrile content and 3.5 mol% residual carbon-carbon double bonds, was provided by Arlanxeo (Cologne, Germany). Diglycidyl hexahydrophthalate (Epalloy 5200) was purchased from CVC Thermoset Specialities (Moorestown, USA). 1,5,7-triazabicyclo[4.4.0]dec-5-ene (TBD) and all other chemicals were obtained from Sigma-Aldrich (St. Louis, USA) and were used as received.

### *Preparation of rubber compounds*

The rubber compounds were masticated by means of a Collin (Ebersberg, Germany) W 150 P two-roll mill at 40 °C for 20 min. During the mixing process, the temperature did not exceed 50 °C. TBD, which is solid under the mixing conditions ( $m_p \approx 125$  °C), was dissolved in the cross-linker Epalloy 5200 in order to facilitate its incorporation into the rubber and to ensure a homogeneous distribution in the compound. Subsequently, the rubber compounds were cured in a Collin P 200 PV platen press at 120 bar and 180 °C for the appropriate times, which were determined by the rheology experiments. The amount of cross-linker was fixed to one molecule of di-epoxide per two carboxylic acid groups of the rubber, i.e. the quantity of epoxy groups was in stoichiometry with carboxylic acid functions. Assuming a complete reaction, a maximum degree of cross-linking should be achieved. This is desirable as only a limited number of cross-linking points are available (5 mol% of carboxylic acids in the rubber). The TBD contents were 10 and 20 mol% relative to the carboxylic acid groups. In the context, sample code HXNBR-E5200- $x$  refers to Epalloy 5200-cross-linked HXNBR with  $x$  mol% TBD. The compositions of the rubber compounds are shown in Table 1.

**Table 1** – Compositions of the rubber compounds.

Rubber compound notation	HXNBR, phr	Epalloy 5200, phr	TBD, phr (mol% <sup>a</sup> )
HXNBR-E5200	100	11.8	
HXNBR-E5200-TBD10	100	11.8	0.97 (10)
HXNBR-E5200-TBD20	100	11.8	1.93 (20)

<sup>a</sup> Relative to the number of carboxylic acid functions.

### *Characterisation methods*

*Curing kinetics.* Curing kinetics was determined at 180 °C using a MonTech (Buchen, Germany) D-RPA 3000 moving die rheometer (1.67 Hz frequency, 0.5% strain).

*FTIR spectroscopy.* Fourier transform infrared spectra were taken with a Bruker (Billerica, USA) Vertex 70 FT-IR spectrometer equipped with a reflection diamond attenuated total reflection (ATR) accessory (Platinum ATR). 16 scans were accumulated with a resolution of 4 cm<sup>-1</sup>.

*Tensile properties.* Tensile testing was carried out on a ZwickRoell (Ulm, Germany) Z1.0 static materials testing machine with a crosshead speed of 250 mm min<sup>-1</sup>. Standard dumbbell specimens with an initial measuring length of 50 mm and 4 mm width were punched out of the cured rubber sheets. A minimum of five specimens was tested for each compound.

*Equilibrium swelling.* Rectangular-shaped samples with a weight of about 100 mg were cut from the cured rubber compounds. The samples were immersed in chloroform at 23 °C for 48 h. After the weight of the swollen gel was determined the samples were dried at 50 °C until constant weight and reweighed to obtain the gel contents. Mass swelling ratios were calculated as  $Q_m=(m_s-m_d)/m_d$  with  $m_s$  being the mass of the swollen sample and  $m_d$  its initial mass. Five samples were tested for each series and the arithmetic average was taken.

*Thermal gravimetric analysis.* TGA experiments were carried out using a Mettler Toledo (Columbus, USA) TGA/DSC1 thermogravimetric analyser. Measurements were performed under both atmospheres, nitrogen and oxygen. The samples were heated from room temperature to 700 °C at a heating rate of 10 °C/min.

*Dynamic mechanical analysis.* DMA experiments were conducted on a Mettler Toledo SDTA861e dynamic mechanical analyser in tensile mode. Rectangular strips (width: 3.5 mm, thickness: 1.5 mm, clamping distance: 12.5 mm) were tested in displacement controlled oscillation of 5 µm amplitude at 1 Hz. Heating ramps were applied at 2 K/min from -50 to 200 °C.

*Stress relaxation.* Stress relaxation experiments at different temperatures were performed in the moving die rheometer right after curing of the samples up to 98% of the ultimate state of cure (t<sub>98</sub>) at 180 °C. After curing, the samples were allowed to equilibrate to the selected measurement temperature for 15 min. Subsequently, a 1% step strain was applied, which was within the linear viscoelastic region of the samples (Figure S2 in ESI), and the decrease in stress was recorded over time.

*Creep test.* Creep experiments were performed using an Anton Paar (Graz, Austria) modular compact rheometer MCR 702 multi drive in tensile mode. Rectangular samples (width: 10.5 mm, thickness: 2.5 mm, clamping distance: 36 mm) were cut out of a sheet of cured HXNBR. After heating up to the desired test temperature, the specimen was held unloaded for a further minute before a constant stress of 0.1 MPa was applied rapidly and held constant for 180 min. The respective strain profiles were recorded over time. In order to show the pure creep strain curves for each test condition, the portion of instantaneous elastic response was skipped. This was done by setting the origin of each strain curve to a starting point when full load was applied.

#### *Shape change experiments*

To investigate the temperature-induced shape changing behaviour, strips of 0.5 cm width were cut from cured rubber sheets. Helical-shaped objects were prepared from strips of 15 cm length by wrapping the samples around glass vials and fixation by clamps. Moreover, strips of 6 cm length were rotated 360 degrees to obtain fusilli-shaped samples and clamped into place to preserve the deformation. The shaped objects were left in a vacuum



oven at 180 °C for different times. Recovery was tested by clamping the strips in the turned back positions.

#### *Adhesion measurements*

Lap shear tests were performed to evaluate the self-adhesion behaviour of the HXNBR networks by adapting a previously reported method.<sup>21,48</sup> Single-lap joint specimens were produced by cutting rectangular samples (10 × 40 mm) from cured rubber sheets and placing the test specimen on top of each other with an overlap length of 20 mm (Figure S3 in ESI). The lap joints were fixed and slightly compressed (20%) by applying a pressure on the overlap area with a home-made device. The clamped lap joints were then placed under vacuum, either for different adhesion times at 180 °C, or at different temperatures whilst keeping the adhesion time constant at 30 min. The adhered specimens were allowed to cool down to room temperature and at least three samples were tested for each condition. Tests were performed at room temperature on a ZwickRoell (Ulm, Germany) Z1.0 static materials testing machine with a crosshead speed of 100 mm min<sup>-1</sup> until complete peeling or stock-break failure. The force-displacement curve was recorded and its maximum force was taken as a measure of the adhesion strength and subsequently applied to calculate adhesion energies according to Kendall's formula:<sup>49</sup>

$$G = \frac{F^2}{4w^2Eh} \quad \text{eqn 1}$$

where  $F$  is the maximum of the measured force,  $E$  the Young's modulus,  $w$  the width and  $h$  the thickness of the sample (the joint is thus  $2h$  thick). Determination of the Young's modulus  $E$  of the rubber compounds was carried out at the same conditions with cut samples of the same geometry as for lap shear tests, but without overlapping area.  $E$  was taken as the slope of the stress-strain curve between 0.1 and 0.3% elongation (Figure S4 in ESI).

#### *Thermal repair experiments*

The thermal repair capabilities were studied with rectangular (28 × 10 mm) samples cut from cured rubber sheets. The specimens were torn and subsequently the fragments were aligned and placed together. In a home-made device the fractured samples were then uniaxially compressed to 10% of displacement and treated at 180 °C in a vacuum oven. The extent of repair was evaluated by attaching weights of different masses to the samples and measuring the time to failure (Figure S5 in ESI). The calculated stresses were then plotted against the respective failure times.

## 4.6 Conclusions

Vitrimer-like chemistry has been successfully incorporated into hydrogenated carboxylated nitrile butadiene rubber. In the absence of a catalyst, thermal curing of the technically relevant rubber across its carboxylic acid groups was reasonably efficient when using a di-functional epoxy cross-linker. By adding the guanidine base triazabicyclodecene (TBD) the cross-linking reaction was accelerated tremendously and the curing was accomplished within less than two minutes. Along with fast curing rates, TBD allowed for

thermally triggered transesterification exchange reactions of the formed  $\beta$ -hydroxyl esters linkages. The obtained network dynamic at elevated temperature was studied by stress relaxation experiments, revealing that the extent of stress relaxation increases with catalyst loading and with rising temperature. The experiments further showed that the vitrification transition temperature was distinctly shifted to lower values when more TBD was present. An outstanding feature of the newly developed vitrimer-like HXNBR compounds is the speed of stress relaxation. A catalyst content of 1.7 wt% (1.9 phr) enabled 74% of the initial stress to relax, with 50% of it being relaxed after only 8 min. Despite the pronounced stress relaxation behaviour, creep tests revealed only little creep even at elevated temperature. This was attributed to the strong entropic rubber-elastic contraction observed for the material when heated. Thermally mendable rubbers with low creep at the same time may be a desired combination for industrial applications. The capability of topology rearrangements above the vitrification transition temperature further resulted in an adaptability of the rubber networks, which was not observed in the catalyst-free reference material. Along with the ability towards shape changing, an improved self-adhesion was demonstrated. Lap shear tests revealed enhanced adhesion properties when the catalyst TBD was present and have been shown to be achieved in different time-temperature windows. Furthermore, the mendable nature of the elastomers showed potential in thermal repairing. In terms of recovering the initial material properties, a clear improvement was achieved for the samples containing exchangeable cross-links. With this study we enlarged the scope of vitrimer-like elastomers based on rubbers of high molecular weight and paved the way towards the introduction of dynamic properties into technically relevant rubber.

#### 4.7 Acknowledgements

The research work of this paper was performed at the Polymer Competence Center Leoben GmbH (PCCL, Austria) within the framework of the COMET-program (project VI-1.02) of the Federal Ministry for Transport, Innovation and Technology and Federal Ministry for Economy, Family and Youth with contributions by the Chair of Chemistry of Polymeric Materials (Montanuniversitaet Leoben, Austria). The PCCL is funded by the Austrian Government and the State Governments of Styria, Lower and Upper Austria. The authors also thank Michael Giebler for helpful discussions on vitrimer chemistry as well as Bernhard Lechner for his support in the rubber compounding and processing procedures. Further Sebastian Stieger is acknowledged for helpful discussions on rheological experiments.

## 4.8 References

- 1 D. Montarnal, M. Capelot, F. Tournilhac and L. Leibler, *Science*, 2011, 334, 965–968.
- 2 W. Denissen, J. M. Winne and F. E. Du Prez, *Chemical science*, 2016, 7, 30–38.
- 3 C. J. Kloxin and C. N. Bowman, *Chemical Society reviews*, 2013, 42, 7161–7173.
- 4 P. Chakma and D. Konkolewicz, *Angewandte Chemie*, 2019.
- 5 B. Hendriks, J. Waelkens, J. M. Winne and F. E. Du Prez, *ACS Macro Lett.*, 2017, 6, 930–934.
- 6 O. R. Cromwell, J. Chung and Z. Guan, *J. Am. Chem. Soc.*, 2015, 137, 6492–6495.
- 7 R. L. Snyder, D. J. Fortman, G. X. de Hoe, M. A. Hillmyer and W. R. Dichtel, *Macromolecules*, 2018, 51, 389–397.
- 8 W. Denissen, G. Rivero, R. Nicolaÿ, L. Leibler, J. M. Winne and F. E. Du Prez, *Adv. Funct. Mater.*, 2015, 25, 2451–2457.
- 9 W. Denissen, I. de Baere, W. van Paepegem, L. Leibler, J. Winne and F. E. Du Prez, *Macromolecules*, 2018, 51, 2054–2064.
- 10 M. Capelot, M. M. Unterlass, F. Tournilhac and L. Leibler, *ACS Macro Lett.*, 2012, 1, 789–792.
- 11 M. Capelot, D. Montarnal, F. Tournilhac and L. Leibler, *J. Am. Chem. Soc.*, 2012, 134, 7664–7667.
- 12 Z. Wang, Z. Li, Y. Wei and Y. Ji, *Polymers*, 2018, 10, 65.
- 13 Y. Yang, E. M. Terentjev, Y. Wei and Y. Ji, *Nature communications*, 2018, 9, 1906.
- 14 a) J. P. Brutman, P. A. Delgado and M. A. Hillmyer, *ACS Macro Lett.*, 2014, 3, 607–610; b) D. J. Fortman, J. P. Brutman, C. J. Cramer, M. A. Hillmyer and W. R. Dichtel, *J. Am. Chem. Soc.*, 2015, 137, 14019–14022.
- 15 L. Imbernon and S. Norvez, *European Polymer Journal*, 2016, 82, 347–376.
- 16 Y. Liu, Z. Tang, Y. Chen, C. Zhang and B. Guo, *ACS applied materials & interfaces*, 2018, 10, 2992–3001.
- 17 C. Xu, R. Cui, L. Fu and B. Lin, *Composites Science and Technology*, 2018, 167, 421–430.
- 18 Z. Tang, Y. Liu, B. Guo and L. Zhang, *Macromolecules*, 2017, 50, 7584–7592.
- 19 L. Cao, J. Fan, J. Huang and Y. Chen, *J. Mater. Chem. A*, 2019, 167, 421.
- 20 M. Qiu, S. Wu, S. Fang, Z. Tang and B. Guo, *J. Mater. Chem. A*, 2018, 6, 13607–13612.
- 21 L. Imbernon, S. Norvez and L. Leibler, *Macromolecules*, 2016, 49, 2172–2178.
- 22 H.-Q. Xie, X.-D. Li and J.-S. Guo, *J. Appl. Polym. Sci.*, 2003, 90, 1026–1031.
- 23 a) Y. Han, L. Mao, H. Meng, L. Zhang and D. Yue, *J. Appl. Polym. Sci.*, 2014, 131; b) N. K. Singha, S. Bhattacharjee and S. Sivaram, *Rubber Chemistry and Technology*, 1997, 70, 309–367.
- 24 R. Joseph, *Rubber Chemistry and Technology*, 2006, 79, 553–560.
- 25 C. E. Frank, G. Kraus and A. J. Haefner, *Ind. Eng. Chem.*, 1952, 44, 1600–1603.
- 26 I. Skeist, *Handbook of Adhesives*, Springer US, Boston, MA, 1990.
- 27 L. Ferrari, R. J. Pazur and E. C. Campomizzi, *Rubber World*, 2004, 230.
- 28 R. J. Pazur and E. C. Campomizzi, *Blends of HXNBR and low viscosity HNBR for automotive applications*, 2007, vol. 235.
- 29 R. C. Klingender, *Handbook of Specialty Elastomers*, CRC Press, 2008.

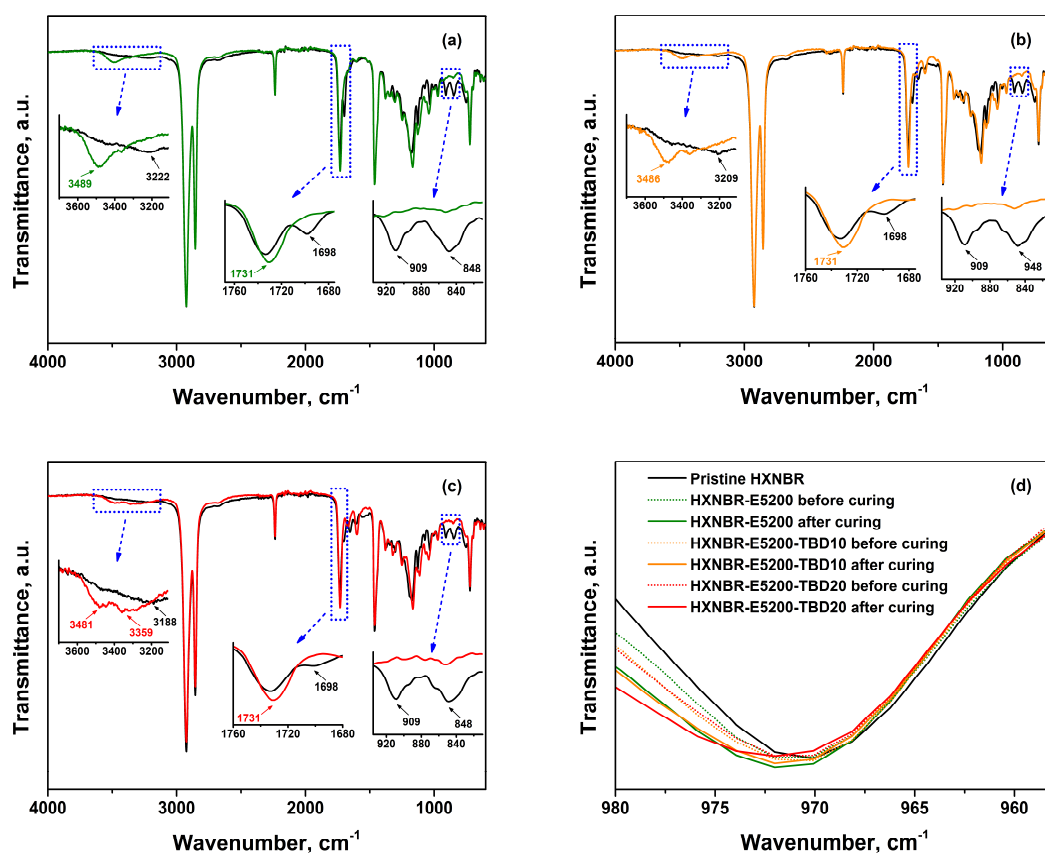
- 30 K. W. Stöckelhuber, A. Das and M. Klüppel, *Designing of Elastomer Nanocomposites: From Theory to Applications*, Springer International Publishing, 2016.
- 31 S. Kaiser, S. V. Radl, J. Manhart, S. Ayalur-Karunakaran, T. Griesser, A. Moser, C. Ganser, C. Teichert, W. Kern and S. Schlögl, *Soft Matter*, 2018.
- 32 a) J. Manhart, S. Ayalur-Karunakaran, S. Radl, A. Oesterreicher, A. Moser, C. Ganser, C. Teichert, G. Pinter, W. Kern, T. Griesser and S. Schlögl, *Polymer*, 2016, 102, 10–20; b) J. Manhart, S. Schlögl and W. Kern, *Kautschuk Gummi Kunststoffe*, 71, 2012, 30–32.
- 33 Y. Liu, Z. Du, C. Zhang, C. Li and H. Li, *J. Appl. Polym. Sci.*, 2007, 103, 2041–2048.
- 34 B. Slay and W. Webber, *Sealing Technology*, 2011, 2011, 9–12.
- 35 M. P. Coles, *Chemical communications*, 2009, 3659–3676.
- 36 A. Kummari, S. Pappuru and D. Chakraborty, *Polym. Chem.*, 2018, 9, 4052–4062.
- 37 J. S. Dick, *Rubber Technology: Compounding and Testing for Performance*, Carl Hanser Verlag GmbH & Company KG, 2014.
- 38 K. F. El-Nemr, *Materials & Design*, 2011, 32, 3361–3369.
- 39 R. Chasset and P. Thirion, *"Physics of non-crystalline solids"*. Proceedings of the International Conference, North Holland Publishing Co., Amsterdam, 1965.
- 40 A. Rahman, L. Sartore, F. Bignotti and L. Di Landro, *ACS applied materials & interfaces*, 2013, 5, 1494–1502.
- 41 Y. Liu, H. Kim, Q. Pan and G. L. Rempel, *Catal. Sci. Technol.*, 2013, 3, 2689.
- 42 M. Pire, S. Norvez, I. Iliopoulos, B. Le Rossignol and L. Leibler, *Polymer*, 2011, 52, 5243–5249.
- 43 J. Han, T. Liu, C. Hao, S. Zhang, B. Guo and J. Zhang, *Macromolecules*, 2018, 51, 6789–6799.
- 44 D. W. van Krevelen, *Properties of Polymers. Their Correlation with Chemical Structure; Their Numerical Estimation and Prediction from Additive Group Contributions*, Elsevier Science, Oxford, 3rd edn., 1997.
- 45 M. Pire, C. Lorthioir, E. K. Oikonomou, S. Norvez, I. Iliopoulos, B. Le Rossignol and L. Leibler, *Polym. Chem.*, 2012, 3, 946.
- 46 M. Edge, N. S. Allen, R. Gonzalez-Sanchez, C. M. Liauw, S. J. Read and R. B. Whitehouse, *Polymer Degradation and Stability*, 1999, 64, 197–205.
- 47 W. Hu, *Polymer Physics: A Molecular Approach*, Springer Vienna, 2012.
- 48 L. Imbernon, E. K. Oikonomou, S. Norvez and L. Leibler, *Polym. Chem.*, 2015, 6, 4271–4278.
- 49 K. Kendall, *J. Phys. D: Appl. Phys.*, 1975, 8, 512–522.

## 4.9 Supporting information

## STRESS RELAXATION AND THERMALLY ADAPTABLE PROPERTIES IN VITRIMER-LIKE ELASTOMERS FROM HXNBR RUBBER WITH COVALENT BONDS

Simon Kaiser<sup>a</sup>, Stefan Wurzer<sup>a</sup>, Gerald Pilz<sup>a</sup>, Wolfgang Kern<sup>a,c</sup> and Sandra Schlögl<sup>a,†</sup><sup>a</sup> Polymer Competence Center Leoben GmbH, Roseggerstrasse 12, A-8700 Leoben, Austria.<sup>†</sup>E-mail: sandra.schloegl@pccl.at<sup>b</sup> Institute of Materials Science and Testing of Polymers, Montanuniversitaet Leoben, Otto Glöckel-Strasse 2, 8700 Leoben, Austria.<sup>c</sup> Institute of Chemistry of Polymeric Materials, Montanuniversitaet Leoben, Otto Glöckel-Strasse 2, 8700 Leoben, Austria.

## FTIR spectroscopy



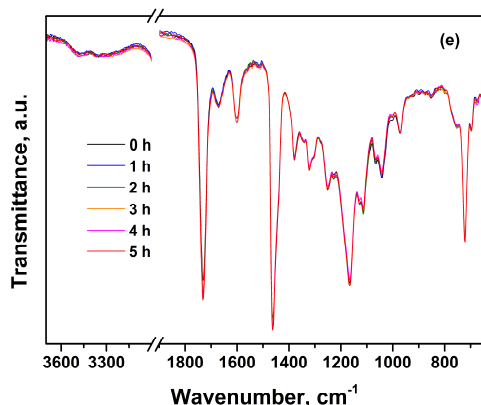


**Figure S1** – FTIR spectra of (a) HXNBR-E5200, (b) HXNBR-E5200-TBD10 and (c) HXNBR-E5200-TBD20 before (black curves) and after (coloured curves) curing at 180 °C to the respective  $t_{95}$  values. (d) Comparison of the absorption band at 972  $\text{cm}^{-1}$ , corresponding to the vibration of 1,4-trans double bonds in HXNBR, for the three different compounds before and after curing, and the spectrum of the pristine HXNBR. (e) Evolution of the spectrum of a sample of HXNBR-E5200-TBD20 over time for storage at 180 °C at ambient atmosphere.

## Tensile testing

**Table S1** - Mechanical properties of the different HXNBR compounds obtained from tensile testing.

Rubber compound notation	Tensile strength, MPa	Elongation at break, %	Modul, MPa
HXNBR-E5200	3.36	234	2.93
HXNBR-E5200-TBD10	3.51	223	3.60
HXNBR-E5200-TBD20	3.62	229	3.48

## Amplitude sweep measurements

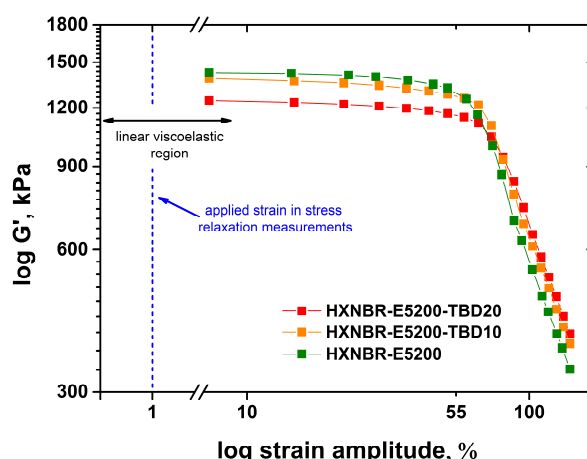


**Figure S2** – Amplitude sweep measurements at 180 °C for the different compounds directly after curing up to the respective  $S'$  plateau values in the moving die rheometer (green: HXNBR-E5200; orange: HXNBR-E5200-TBD10; red: HXNBR-E5200-TBD20).

### Lap shear tests

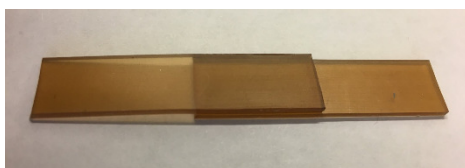


**Figure S3** – Photograph of a single-lap joint specimen (an individual strip has a size of  $10 \times 40$  mm) used for lap shear tests to evaluate the HXNBR self-adhesion properties. The overlap length is 20 mm.

### Determination of Young's moduli to calculate adhesion energies

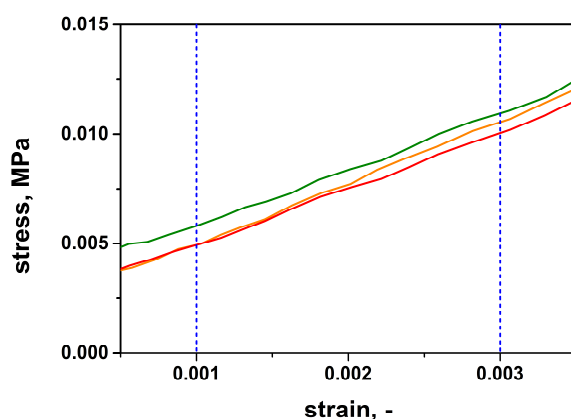


**Figure S4** – Stress-strain curves between 0.1 and 0.3% strain of rectangular samples ( $10 \times 40$  mm) cut from cured rubber sheets. Tests were performed with a crosshead speed of  $100 \text{ mm min}^{-1}$ . The Young's moduli were determined as the slope of the respective stress-strain curve between 0.1 and 0.3% elongation.

### Experimental setup to investigate the repair capabilities



**Figure S5** – Photograph of a typical repaired elastomer sample fixed between two clamps used for stress-rupture tests. To the lower clamp the respective weights with different masses were attached.

### Dissolution experiments

Dissolution tests of HXNBR-E5200-TBD20 in trichlorobenzene were performed on rectangular samples with a weight of about 350 mg cut from the cured rubber compound.

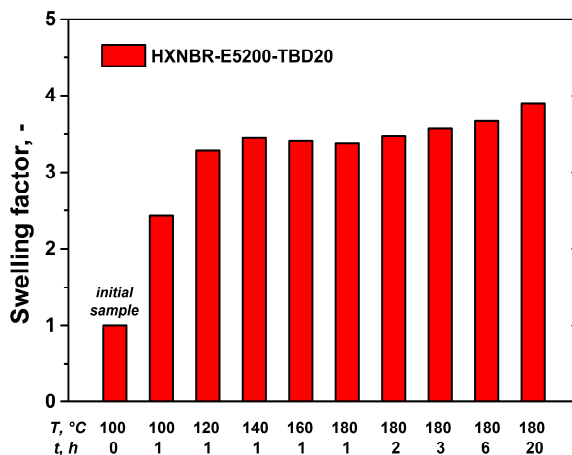


**Figure S6** – Swelling data obtained for the immersion of HXNBR-E5200-TBD20 in trichlorobenzene. The temperature was gradually increased from 100 to 180 °C by 20 °C steps and then kept at this temperature for varying times.

### Equilibrium swelling experiments

Equilibrium swelling tests in chloroform were performed on rectangular samples with a weight of about 100 mg cut from the cured rubber compounds.

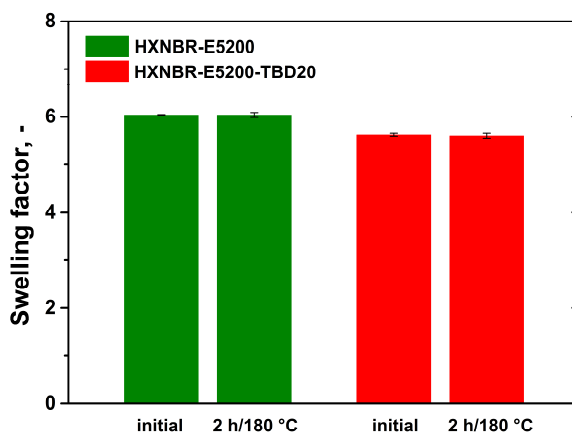


**Figure S7** – Equilibrium swelling data obtained for the immersion of HXNBR-E5200 and HXNBR-E5200-TBD20 in chloroform for 48 h. The experiments were conducted with samples before and after storage for 2 h at 180 °C. For each compound and condition, five samples were used and the arithmetic mean value was taken.



### Decomposition experiments

Decomposition experiments of HXNBR-E5200-TBD20 were carried out to verify whether the network contains permanent covalent cross-links besides the exchangeable  $\beta$ -hydroxyl ester linkages. Since the HXNBR rubber under investigation contains about 3.5 mol% residual carbon-carbon double bonds, thermal cross-linking across these bonds could occur. In case that the HXNBR network contains only exchangeable cross-links, the material should dissolve fully in an excess of ethylene glycol (EG) above the vitrification transition temperature. Since EG is a poor solvent for HXNBR, a 1:1 mixture of EG and trichlorobenzene has been chosen to induce swelling of the sample at the same time and therefore facilitate the incorporation of the alcohol via transesterification exchange reactions. Additionally, triazabicyclodecene was added to accelerate the reaction. For HXNBR-E5200-TBD20, TBD was added in a quantity to obtain a molar ratio of 1:1 with respect to the  $\beta$ -hydroxyl ester linkages. Rectangular samples with a weight of about 150 mg were cut from the cured rubber compound. Figure S8 shows the reaction mixture after stirring for 6 h at 180 °C. The mixture was then poured over a sieve and no gel was found, indicating the absence of permanent, non-reversible cross-links in the HXNBR.

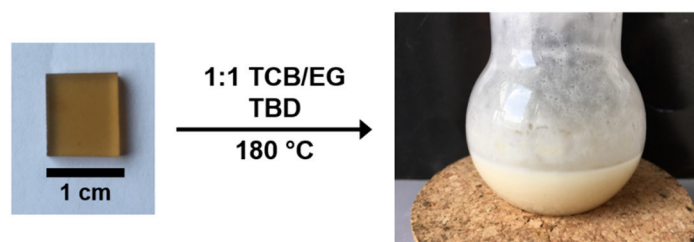


**Figure S8** – Photograph of the decomposition experiment of HXNBR-E5200-TBD20 performed in 1:1 ethylene glycol and trichlorobenzene. The photograph shows the reaction mixture after stirring for 6 h at 180 °C.

# Chapter 5

## VITRIMER-LIKE ELASTOMERIC COMPOSITES FROM HXNBR RUBBER

## 5.1 Bibliographic information

### Published in:

Kaiser, S.; Jandl, J.; Novak, P.; and Schlögl, S. Design and characterisation of vitrimer-like elastomeric composites from HXNBR rubber. *Soft Matter*. DOI: 10.1039/D0SM00362J.

### Author contributions:

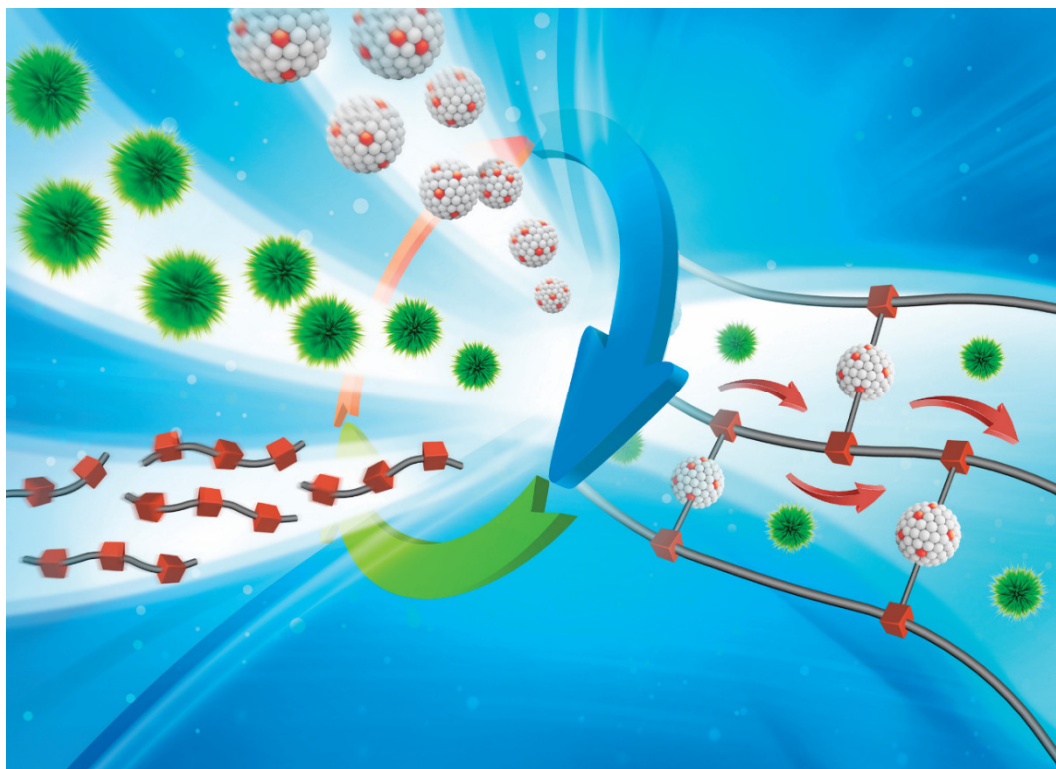
Simon Kaiser: Conceptualisation; Methodology; Investigation; Data curation; Formal analysis; Validation; Visualisation; Original draft; Review and editing

Julius Jandl: Investigation; Data curation; Formal analysis

Patrick Novak: Investigation; Data curation

Sandra Schlögl: Funding acquisition; Project administration; Resources; Supervision; Conceptualisation; Methodology; Validation; Original draft; Review and editing

The manuscript presented here is an adapted accepted manuscript in order to correspond to the formatting of this thesis and does not necessarily reflect the actual published version. This chapter contains results of the bachelor thesis of Julius Jandl. The graphic below depicts the back cover of Issue 37 (7 October 2020, Page 8517 to 8726) of the journal *Soft Matter*. The concept for the graphic originates from Simon Kaiser.



## DESIGN AND CHARACTERISATION OF VITRIMER-LIKE ELASTOMERIC COMPOSITES FROM HXNBR RUBBER

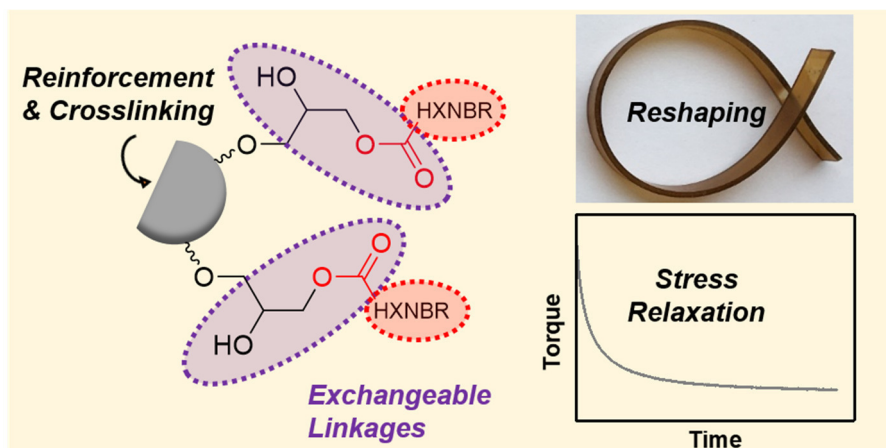
Simon Kaiser<sup>a</sup>, Julius Jandl<sup>a</sup>, Patrick Novak<sup>a</sup>, and Sandra Schlögl<sup>a†</sup>

<sup>a</sup> Polymer Competence Center Leoben GmbH, Roseggerstrasse 12, A-8700 Leoben, Austria.

<sup>†</sup>E-mail: sandra.schloegl@pccl.at

### 5.2 Abstract

The present study aims at the incorporation of vitrimer-like properties into elastomeric composites as a promising approach towards the sustainable production of rubber-based materials. In particular, hydrogenated carboxylated nitrile butadiene rubber (HXNBR), as a technically relevant high-performance rubber, is covalently cross-linked with epoxy group-functionalised calcium silicate (Esilicate) across its pending carboxylic acid moieties. Reaction with the reactive functions attached on the filler surface results in the formation of  $\beta$ -hydroxyl ester linkages at the HXNBR-Esilicate interface, which undergo thermo-activated transesterifications in the presence of a suitable catalyst. Topology rearrangements in the composites are confirmed by stress relaxation measurements at elevated temperatures. Comparison with an unfilled reference network reveals that the extent of stress relaxation can be mostly maintained upon the addition of the reactive filler even at large quantities. The Esilicate serves as both cross-linker and reinforcing filler, leading to a significant enhancement of the mechanical properties.



### 5.3 Introduction

Sulphur vulcanisation and peroxide cross-linking are currently the most applied curing methods for elastomers. Although the permanent covalent bonds provide the materials with high elasticity and solvent resistance, they pose a challenge when it comes to the (re)processing and recycling of the networks.<sup>1</sup>

An elegant concept to maintain the network connectivity but still ensure malleability/processability of covalently cross-linked polymers was introduced by Leibler and co-workers in 2011.<sup>2</sup> The authors obtained dynamic covalent epoxy-acid networks through topology rearrangements, which were associative in nature and the reaction kinetics was controlled thermally and catalytically. Upon the application of an external stimulus, a bond-forming/bond-breaking process occurred, causing a temporary macroscopic flow of the networks. The chemistry of this novel class of polymers, coined vitrimers, has recently been extended to rubbers, with most of the networks relying on transesterification exchange reactions.<sup>3-7</sup> Due to the high molecular weight of the polymer chains, the presence of entanglements acting as physical cross-links, and an often limited number of potential cross-linking sites, it is not trivial to achieve full vitrimer characteristics in rubbers. In many cases only a vitrimer-like behaviour is obtained, indicated by incomplete stress relaxation of the materials.<sup>6,8</sup> It should also be mentioned that the cross-link density in rubber networks is naturally significantly lower compared to typical (epoxy-based) thermosets. The cross-link density is among the parameters governing the topology freezing transition with its temperature  $T_v$ .<sup>9</sup> On the example of a transesterification-based polyester vitrimer, Hayashi et al. recently showed that the higher the cross-link density the faster the stress relaxation, if the quantity of reactive functional groups such as free hydroxyl moieties is kept constant.<sup>10</sup>

Vitrimers and vitrimer-like materials relying on transesterifications usually require a suitable catalyst to enhance the thermally activated bond exchange reactions.<sup>2,11</sup> Both, catalyst type and concentration strongly influence the vitrification transition and its related temperature  $T_v$ .<sup>11</sup> The most frequently used transesterification catalyst is  $Zn(OAc)_2$ .<sup>2</sup> On the other hand, the organic guanidine base 1,5,7-triazabicyclo[4.4.0]dec-5-ene (TBD) was shown as an effective catalyst in composites from DGEBA and adipic acid filled with carbon nanotubes<sup>12</sup> or in epoxy-based composites containing graphene.<sup>13</sup>

Along with catalysis, further key parameters controlling the exchange reaction kinetics are the number of hydroxyl and ester groups in the materials.<sup>10,14</sup> In epoxy-anhydride networks, no transesterification reactions occur when stoichiometric amounts of epoxy groups and anhydrides are used due to the formation of solely diesters.<sup>15</sup> Hillmyer et al. in turn showed that the abundance of esters throughout a polylactide-based polyester network can also strongly influence the exchange reaction kinetics without ample hydroxyl groups.<sup>16</sup>

The network dynamics of vitrimers is further affected by the addition of fillers, which could impede topology rearrangements. However, to enhance the mechanical properties of vitrimers the addition of fillers is essential.<sup>12,13,17</sup> Legrand et al. investigated silica-epoxy vitrimer nanocomposites.<sup>18</sup> The addition of up to 40 wt% of nano-filler (OH-terminated) clearly enhanced the mechanical properties while maintaining the ability of the networks to fully relax stresses by thermo-activated and catalysed transesterifications, albeit at a

smaller reaction rate compared to the unfilled analogue. Thus, the authors further investigated the effect of the surface chemistry of the filler. Epoxide-functionalisation allowed for a covalent linkage of the particles to the network forming  $\beta$ -hydroxyl ester bonds, enabling bond exchange reactions at the polymer-particle interface. Accordingly, networks containing modified particles showed an improved stress relaxation compared to samples prepared with non-functionalised particles. It should be noted that the matrix itself is already of vitrimeric nature of these composites, meaning that the exchangeable bonds are not only formed at the polymer-filler interface but are abundantly available in the bulk of the material. Other studies covered the introduction of carbon nanotubes<sup>12</sup> or graphene<sup>13</sup> into epoxy vitrimers, but at much lower filler loadings.

The application of fillers at high contents (>20 phr)<sup>19</sup> is of fundamental importance in the field of rubbers, since unfilled networks usually suffer from poor mechanical properties.<sup>20,21</sup> The matrix-filler interactions are a key parameter determining the final composite properties.<sup>22</sup> The covalent attachment of fillers to the matrix is considered to improve both the filler dispersion and the reinforcing efficiency due to an increased interfacial adhesion.<sup>23,24</sup>

The first reported elastomer composite showing vitrimer characteristics was prepared from epoxidised natural rubber (ENR) and carbon nanodots<sup>5</sup> with surface carboxyl groups at a maximum filler content of 5 wt%. Xu et al. presented reinforced vitrimer-like composites from ENR without the addition of a catalyst, employing citric acid-modified bentonite as the cross-linker at 30 wt%.<sup>4</sup> In contrast to the work of Legrand et al., in these networks no dynamic covalent bonds are present in the matrix. The covalent linkages carrying the exchangeable groups are solely formed at the polymer-filler interface during the network formation. While most networks rely on a chemistry with the epoxy groups located at the polymer backbone (e.g. ENR) and the carboxylic acid moieties at the filler surface, Liu et al. studied the first approach following a reversed reactivity of rubber and filler towards dynamic and reinforced vitrimer composites. The authors implemented vitrimer behaviour into carboxyl group-grafted styrene-butadiene rubber (SBR), using up to 30 phr of epoxy-functionalised nanosilicate.<sup>3</sup> The  $\beta$ -hydroxyl ester bonds formed at the rubber-particle interface were exploited for TBD-catalysed thermally triggered transesterifications allowing full stress relaxation. However, the approach is solvent-based and therefore not suitable for classical rubber compounding procedures.

Our group recently reported vitrimer-like elastomers from a high molecular weight hydrogenated carboxylated nitrile butadiene rubber (HXNBR) with a low number of reactive curing sites (5 mol%).<sup>25</sup> HXNBR is a high-performance rubber with superior mechanical and physical properties compared to either regular HNBR or XNBR.<sup>26</sup> The level of monomer containing the carboxyl functions in carboxylated rubbers is typically not exceeding 7 mol% for reasons of processability, which strongly limits the amount of potential cross-link sites. For the first time,  $\beta$ -hydroxyl ester linkages were incorporated into HXNBR rubber, which were susceptible to thermo-activated transesterifications in presence of the catalyst TBD. Despite the low cross-link density of the networks, thermal adaptability was proven by stress relaxation experiments, and exploited for improved adhesion properties and thermally triggered repairing. However, the unfilled networks revealed unsatisfactory mechanical properties regarding tensile strength and Young's

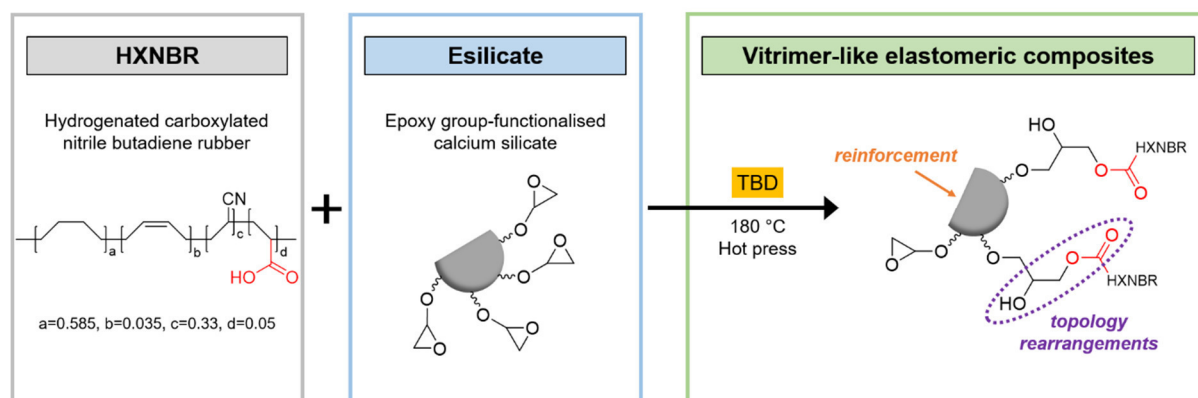


**Figure 1** – Illustration of the network design for the preparation of vitrimer-like elastomeric composites from HXNBR rubber.

modulus compared to other reported vitrimer elastomers from rubbers that were reinforced using fillers.<sup>3,4,8</sup>

In this work, we significantly improve the mechanical properties by preparing HXNBR composites using a calcium silicate-based filler bearing epoxy groups (Figure 1). Due to the reactive surface sites, the filler shows a dual performance acting as cross-linker and providing reinforcement at the same time. The cross-linking reaction results in the formation of covalent exchangeable bonds at the rubber-filler interface. The approach clearly shows that thermally adaptable properties can be introduced in highly filled composites from a technically relevant rubber that is characterised by a good mechanical performance.

## 5.4 Results and discussion

### *Covalent cross-linking of HXNBR with epoxy group-functionalised silicate particles*

In the first step, the morphology, chemical surface structure and thermo-oxidative properties of epoxy group-functionalised silicate particles (Esilicate) were characterised by scanning electron microscopy (SEM), ATR-FTIR spectroscopy and thermogravimetric analysis. Figure S1a in ESI shows the SEM micrograph received from pristine Esilicate, which is composed of small but agglomerated particles in the micrometer range. The ATR-FTIR spectrum (Figure S1b in ESI) confirms the presence of epoxy groups on the particle surface, indicated by the characteristic epoxy absorption bands at 909 and 854  $\text{cm}^{-1}$ . The absorption bands at 2939 and 2841  $\text{cm}^{-1}$  arise from  $-\text{CH}_2$  of the silane coupling agent, which is bearing the epoxy groups. The absorption bands observed at 1021 and 787  $\text{cm}^{-1}$  are attributed to Si-O-Si and Si-O groups of the silicate carrier, respectively. The broad absorption band at around 3462  $\text{cm}^{-1}$  arises from Si-OH groups. Figure S1c in ESI depicts the TGA curve of pristine Esilicate particles obtained under a thermal oxidative atmosphere. The weight loss below 190  $^{\circ}\text{C}$  is due to the removal of physically absorbed water, and the weight loss from 190  $^{\circ}\text{C}$  is associated with the decomposition of the silane coupling agent grafted on the inorganic carrier.

Compounds from HXNBR and Esilicate were prepared with filler contents of 15 phr (HXNBR-Esilicate15-TBD20) and 30 phr (HXNBR-Esilicate30-TBD20) in the presence of

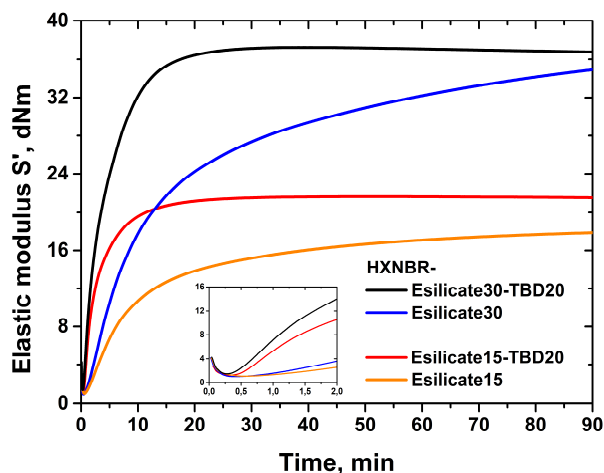


**Figure 2** – Elastic component of the torque ( $S'$ ) as a function of time followed in the moving die rheometer at 180 °C for the HXNBR composites with 15 and 30 phr of Esilicate each with and without TBD.

**Table 1** – Rheometric properties of HXNBR-Esilicate composites obtained from rheological experiments at 180 °C in comparison to the compound cured with liquid di-epoxide E5200.

Sample code, HXNBR-	$S'_{\min}$ , dNm	$S'_{\max}$ , dNm	$\Delta S'$ , dNm	t95, min
E5200	0.4	17.3	16.9	38
E5200-TBD20	1.2	15.4	14.2	1.3
Esilicate15	1.0	17.8	16.8	56
Esilicate15-TBD20	1.2	21.6	20.4	14
Esilicate30	1.0	34.9	33.9	69 <sup>a</sup>
Esilicate30-TBD20	1.4	37.2	35.8	9.4

<sup>a</sup> For 90 min of curing.

20 mol% (related to the COOH groups) of the transesterification catalyst triazabicyclodecene (TBD). Moreover, the respective catalyst-free networks were prepared serving as references for the following characterisations (HXNBR-Esilicate15 and HXNBR-Esilicate30). The cure characteristics of the different compounds were followed in a moving die rheometer (MDR) at 180 °C and the rheographs are displayed in Figure 2, showing the evolution of the elastic component of the torque ( $S'$ ) versus time. After a short initial softening of the rubber, indicated by a decrease in  $S'$ , a rapid increase in  $S'$  is observed for all compounds, revealing a proceeding cross-linking reaction. However, the catalyst-free samples exhibit a significantly slower curing reaction than their TBD containing analogues, which is attributed to the catalytic activity of TBD in the reaction of carboxylic acids with epoxides.<sup>27</sup> In the elastomer composites under investigation, TBD accelerates the cross-linking kinetics tremendously. A complete cross-linking reaction for the compounds with TBD is indicated by reaching a plateau value of  $S'$ . While the compounds with TBD achieve a plateau after only a few minutes, HXNBR-Esilicate15



requires about 90 minutes and HXNBR-Esilicate30 does not yield a plateau in the measurement period investigated. The data further show a high network stability for the composites containing TBD, since no significant reversion is observed during prolonged curing (90 min) at 180 °C.

This issue was further verified for even longer curing times and higher temperatures as shown in Figure S5. The rheometric properties of the composites are summarised in Table 1 and compared to a compound cured with 11.8 phr of diglycidyl hexahydrophthalate (Epalloy 5200, E5200), a low molecular weight di-epoxide. While the  $S'_{\max}$  of HXNBR-Esilicate15-TBD20 is only little bigger than for the compound cross-linked with the di-epoxide (HXNBR-E5200-TBD20, Figure S4a in ESI), the compound containing 30 phr of Esilicate yields a substantially higher  $S'_{\max}$ . Both a higher cross-link density and the typical increase in viscosity when using fillers due to a restricted rubber chain mobility explain this effect.<sup>24,28</sup> It is important to note that no covalent cross-links can be formed in the matrix of the present networks, but solely at the polymer-filler interface by the reaction of pending carboxylic acid moieties of HXNBR with surface epoxy groups of Esilicate. Consequently, all existing exchangeable chemical bonds (i.e. esters) in both filled composites, each with and without TBD, are naturally located at the HXNBR-Esilicate interface.

To analyse the cross-link densities, equilibrium swelling measurements were carried out in chloroform. Table 2 shows the mass swelling ratios and sol fractions of the HXNBR composites in comparison with unfilled networks from HXNBR and di-epoxide. All compositions containing TBD exhibit a slightly lower swelling degree than the respective catalyst-free networks, which indicates a more efficient curing process in the presence of TBD, yielding higher cross-link densities. This data is consistent with the observations of the rheological measurements considering the values of  $S'_{\max}$  (Figure 2 and Table 1). Assuming that all covalent bonds formed during cross-linking are esters, and therefore of exchangeable nature, the dynamic bond density is assumed to be higher in the catalysed systems. Moreover, the data show a decrease in swelling degree going from the di-epoxide cross-linker to Esilicate, and a further decrease with the filler loading. Apparently, higher Esilicate contents provide more potential cross-linking sites and thus, yield higher cross-link densities by reacting with more carboxylic acid groups of HXNBR during the curing reaction. An interesting aspect is the obviously lower cross-link density of unfilled HXNBR-E5200-TBD20, although the number of epoxy groups was in stoichiometry with the carboxylic acid functions of HXNBR. Apparently, not all –COOH groups were involved in the network formation, possibly due to their poor accessibility and/or side reactions of the epoxy groups of the cross-linker such as epoxy homopolymerisation. On the other hand, consecutive etherification of  $\beta$ -hydroxyl groups formed in the initial ring-opening reaction could occur and contribute to the higher number of chemical bonds in the composites. However, the swelling behaviour of the networks with TBD and their respective catalyst-free references suggest similar network properties, making the latter suitable references. The sol fractions are low for all investigated networks.

In the analysis of the equilibrium swelling data as a measure of the cross-link density, it is assumed that the mass swelling ratios reflect only the covalent bonds of the networks. However, the possible contribution of physical interactions such as polymer chain adsorption at the Esilicate surface is unclear. To address this issue, swelling/dissolution

experiments of the compounds containing TBD were conducted in trichlorobenzene (TCB) as a function of temperature and immersion time (Figure 3). It is expected that physical interactions contributing to the network integrity are released under these conditions, with only the covalent cross-links remaining. For all samples, the swelling degree rises strongly in the beginning of the immersion at 120 °C, and only slowly thereafter. Interestingly, the composites display a temporary decrease in mass swelling ratio with the gradual increase of the temperature to 180 °C. This observation is attributed to entropic elasticity effects in these networks leading to sample contraction, which is more pronounced at elevated temperatures. In particular, two key findings can be derived from the experiments. First, the results confirm the different densities of covalent cross-links in the various rubber compositions prepared, as already indicated in the previous swelling experiments in chloroform.

**Table 2** – Equilibrium swelling data obtained for HXNBR-Esilicate composites in comparison to a compound cured with liquid di-epoxide E5200.

HXNBR-	Mass swelling ratio, -	Sol fraction, %
E5200	6.11	4.1
E5200-TBD20	5.80	4.2
Esilicate15	5.53	2.8
Esilicate15-TBD20	4.90	2.6
Esilicate30	3.82	2.2
Esilicate30-TBD20	3.56	2.8

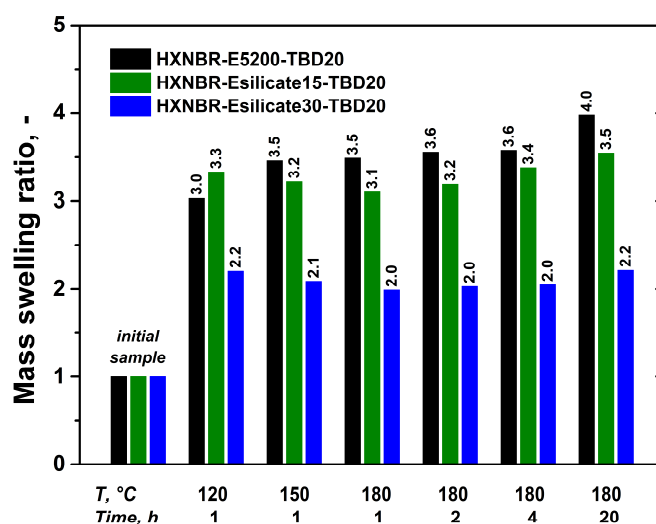


**Figure 3** – Swelling/dissolution experiments of HXNBR-Esilicate composites and the unfilled reference (all containing 20 mol% of TBD related to COOH) in trichlorobenzene (TCB) at increasing temperature and as a function of time.

We conclude that physical interactions do not contribute decisively to the swelling behaviour of these materials. Second, all samples remain undissolved even after 20 h at 180 °C, where transesterifications are active. Thereby the data prove that the networks are of permanent nature and resistant to chemical solvents even in the presence of TBD. The sol fractions amounted to 8% for HXNBR-E5200-TBD20, and 6% each for the composites.

In order to gain further insight into the role of physical interactions in the swelling properties of the composites, a TBD-free compound containing 30 phr of Esilicate was prepared without applying high temperature curing. After compounding, the blend was hot pressed for 10 min at 60 °C. Previously conducted rheological measurements in the moving die rheometer have shown no increase in torque over time, indicating that no covalent cross-links are formed at this temperature (Figure S7). Moreover, FTIR spectroscopy was carried out. No significant difference was observed in the spectra before and after treatment at 60 °C in the hot press (Figure S6), which evidences the absence of curing reactions under these conditions. In the next step, we were interested in the swelling behaviour of this compound, which obviously comprises only physical interactions such as polymer chain adsorption on the Esilicate's surface. After immersion for 48 h in chloroform (at room temperature), the samples formed a highly swollen rubber-filler gel, which immediately dissolved entirely upon gentle mechanical stirring. The experiment confirms the release of physical cross-links in the composites during equilibrium swelling in chloroform (and in trichlorobenzene at 180 °C).

To evidence the nucleophilic ring opening reaction between the carboxylic acid groups of HXNBR and surface epoxy groups of Esilicate, ATR-FTIR spectroscopy was conducted before and after curing at 180 °C. As an example, the spectrum of HXNBR-Esilicate30-TBD20 is shown in Figure 4, and the spectra of HXNBR-Esilicate15-TBD20 and HXNBR-E5200-TBD20 are displayed in Figure S2 in ESI. Prior to thermal curing, the spectra show the carbonyl absorption band of carboxylic acid moieties at 1701  $\text{cm}^{-1}$  and the absorption bands of epoxy groups (attached to the silicate filler) at 909 and 855  $\text{cm}^{-1}$ . After curing, the depletion of the characteristic epoxy absorptions at 909 and 855  $\text{cm}^{-1}$  prove the consumption of surface epoxy groups. However, the latter does not disappear completely,

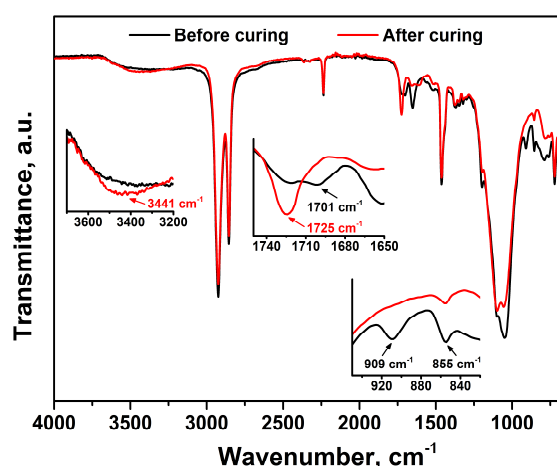


**Figure 4** – ATR-FTIR spectra of HXNBR-Esilicate30-TBD20 before (black) and after (red) curing at 180 °C.

indicating residual epoxy groups on the filler surface. This is to be expected since it is unlikely that all epoxy functions react with carboxylic acid moieties owing to limited accessibility, and due to the epoxy groups likely being in excess to  $-\text{COOH}$ . Furthermore, the absorption at  $1701\text{ cm}^{-1}$  related to the carbonyl of carboxylic acid groups disappeared. This is accompanied by an absorption band emerging at  $1725\text{ cm}^{-1}$ , which is associated with the formation of carbonyl groups of esters. The increase of the absorption band at about  $3441\text{ cm}^{-1}$  is attributed to the generation of secondary hydroxyl groups. The data confirm the formation of  $\beta$ -hydroxyl ester bonds at the HXNBR-Esilicate interface and thus, the successful covalent cross-linking of the present HXNBR rubber with the modified filler. The possible formation of permanent covalent bonds in the present HXNBR due to self-cross-linking at high temperatures could be excluded by rheological experiments and FTIR spectroscopy on neat rubber (Figure S4 in ESI).

#### *Network rearrangements in HXNBR-Esilicate composites*

To evidence thermo-activated bond exchange reactions in the Esilicate-filled networks, stress relaxation measurements were performed. After *in situ* curing in the moving die rheometer, a constant deformation of 1% was applied and the evolution of the stress was monitored over time. Previously conducted strain sweep experiments confirmed that the applied strain was within the linear viscoelastic region of the samples (Figure S3 in ESI). Figure 6a and 6b show the stress relaxation behaviour of the composites filled with 15 phr (HXNBR-Esilicate15-TBD20) and 30 phr (HXNBR-Esilicate30-TBD20) of Esilicate in the presence of 20 mol% (related to the COOH groups) of TBD at various temperatures. Both compositions exhibit substantial stress relaxation over time at high temperatures. In order to compare and to identify possible contributions (i.e. of physical nature) of the matrix to stress relaxation, measurements were conducted on the TBD-free references at  $180\text{ }^{\circ}\text{C}$ . The small relaxation observed (8 and 11% of the initial stress after 150 min for composites with 15 and 30 phr of Esilicate, respectively) is attributed to the rearrangements of flexible parts of the networks, reptation, and adsorption/desorption processes at the HXNBR-particle interface as a result of non covalent interactions between Esilicate and the rubber matrix.<sup>18</sup> The extent of the latter naturally increases with the Esilicate content, and its contribution to the observed stress relaxation is also demonstrated by comparison with the relaxation behaviour of the TBD-free and unfilled network cross-linked with di-epoxide (HXNBR-E5200). This network shows a relaxation of only 1.7% of the initial stress after 150 min at  $180\text{ }^{\circ}\text{C}$  (Figure 6c), further indicating that no thermally activated transesterifications or network degradation takes place in the references. In general, all references prepared behave like permanent covalent networks in the absence of catalyst. Therefore, it is obvious that the substantial stress relaxation over time measured for the composites containing TBD is a result of covalent topology rearrangements. More precisely, due to catalysed transesterifications at the HXNBR-Esilicate interface as illustrated in Figure 5. Despite the lower number of (exchangeable) ester bonds in the particular TBD-free compositions compared to the materials with TBD, we consider these as adequate systems in order to show the crucial role of the catalyst for bond exchange reactions. Anyway, a smaller density of covalent cross-links would rather enhance stress relaxation.<sup>29</sup> For instance, low covalent cross-link densities are usually

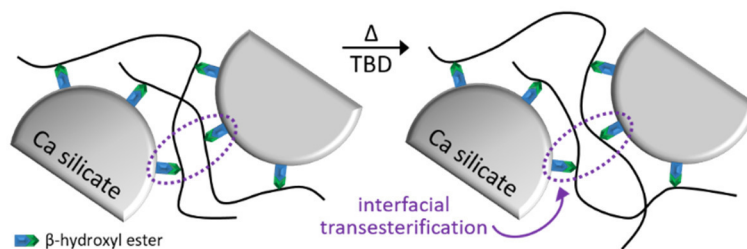


**Figure 5** – Schematic illustration of thermo-activated and TBD-catalysed transesterifications at the HXNBR-Esilicate interface.

exploited in (self-)healable polymer networks to ensure a high chain mobility. The lower the cross-link density, the stronger this effect and thus also the stress relaxation.

In this context, we were interested in the sensitivity of the stress relaxation capabilities of the HXNBR under investigation towards the presence of chemical bonds in the network structure. Figure S7 in ESI shows that already a small amount of covalent cross-links between the rubber chains and Esilicate prevents full stress relaxation, which is inherently given for the raw rubber. The data confirm that the significant number of chemical bonds generated in the present HXNBR networks by either the di-epoxide or epoxy group-functionalised filler almost completely prevents any stress relaxation in

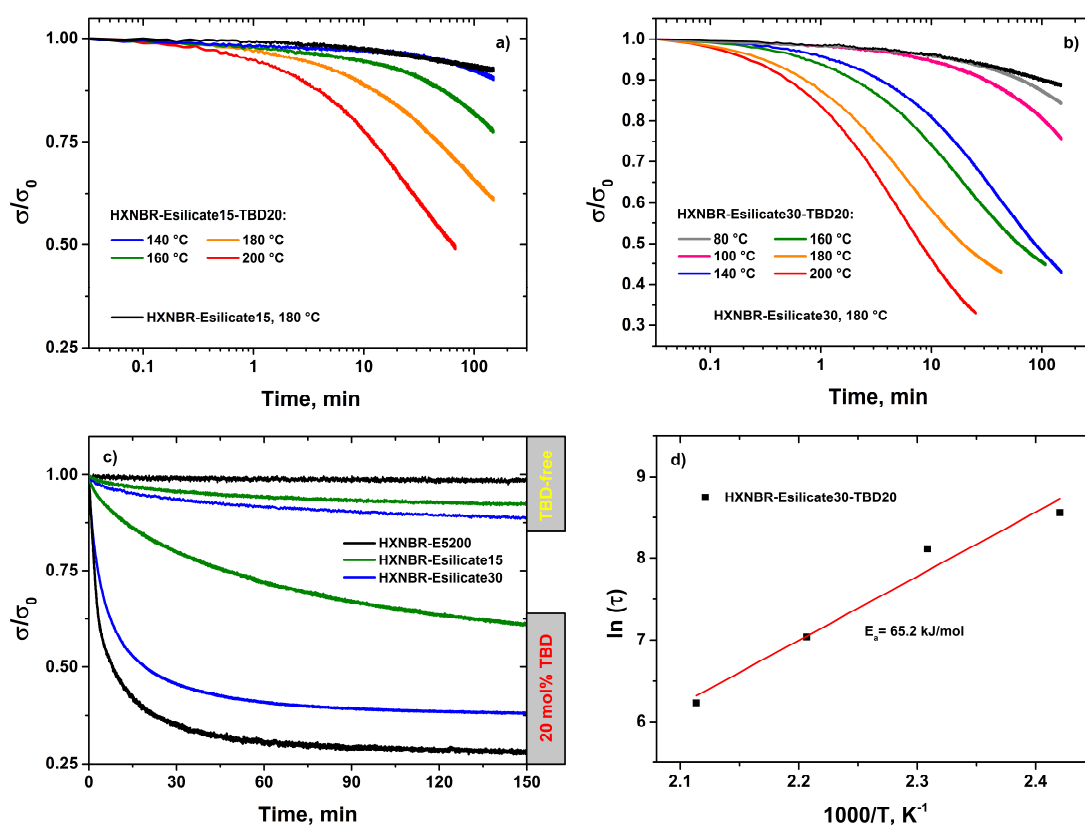


**Figure 6** – Normalised stress relaxation experiments of HXNBR networks comprising (a) 15 and (b) 30 phr of Esilicate in the presence of 20 mol% (related to the COOH groups) of TBD measured at various temperatures. (c) Normalised stress relaxation curves of HXNBR composites and unfilled HXNBR cross-linked with di-epoxide (measured at 180 °C). (d) Arrhenius plot of the measured relaxation times for HXNBR-Esilicate30-TBD20.

absence of TBD, with negligible physical long-term relaxation. In conclusion, the chemical stress relaxation observed in the highly cross-linked networks containing TBD is clearly related to thermally triggered and catalytically controlled bond exchange reactions.

The relaxation rate is small at low temperatures and increases with temperature, since interfacial bond exchange reactions involving ester linkages and free hydroxyl groups are accelerated at higher temperatures. In particular, 62 and 79% of the initial stress in HXNBR-Esilicate15-TBD20 and HXNBR-Esilicate30-TBD20 are relaxed within 150 min at 200 °C, respectively. To correlate the relaxation time and the temperature in the composite with 30 phr Esilicate, characteristic relaxation times were determined as the time required to relax to 50% of the initial stress. The data satisfies the Arrhenius law, and based on the slope ( $m = -E_a/R$ ) of the straight line fitted to the data an activation energy ( $E_a$ ) of 65.2 kJ/mol was calculated (Figure 6d). This value is similar to activation energies reported in literature for transesterification-based dynamic networks from rubbers.<sup>5,7</sup> Interestingly, the network with higher Esilicate loading exhibits a faster and more pronounced stress relaxation (Figure 6c), highlighting the role of the dynamic bond density on the transesterification kinetics. Usually the opposite effect is observed in literature because the incorporation of fillers restricts the polymer chain mobility and thus slows down topology rearrangements by associative bond exchanges.<sup>3,8,18</sup> We attribute this effect to the low content of carboxylic acid groups in the present HXNBR (5 mol% of COOH containing monomer), which strongly limits the number of possible covalent cross-links.

Therefore, the incorporation of a certain amount of filler (i.e. surface epoxy groups) seems necessary to address all carboxyl moieties in the cross-linking process. Only in this case, a maximum number of reactive COOH groups along the rubber backbone is cross-linked with the reactive filler, which is supported by the swelling data (Table 2 and Figure 3) that clearly indicate a higher density of exchangeable cross-links for the composite with 30 phr of Esilicate. Figure 6c also shows that the addition of Esilicate increases the relaxation time compared to the unfilled network cross-linked with di-epoxide, which is in accordance with the literature.<sup>3,18</sup> The incomplete stress relaxation observed for all types of networks (Figure 6c), either cured with liquid di-epoxide or reactive filler is attributed to two main effects. First, the low cross-link density narrows the probability of meeting between exchangeable  $\beta$ -hydroxyl ester linkages. Secondly, this effect is further enhanced by the presence of entanglements in the high molecular weight HXNBR under investigation. It should also be mentioned that the formation of irreversible (i.e. non-exchangeable) covalent bonds cannot be entirely excluded. Nevertheless, the materials relax substantially, especially in view of the small number of exchangeable ester cross-links (and hydroxyl functions).

For further characterisation of the composites, cyclic strain-recovery profiles of HXNBR-Esilicate30-TBD20 were recorded at different temperatures, and the data is displayed in Figure 7a. At 30 °C, no increase in creep strain occurs during the application of the external force. Moreover, the residual deformation remains unchanged when comparing the strains after removal of the force in cycles 1 and 2. At this temperature, the bond exchange reaction rate is very slow and the sample performs like a permanent network without exchangeable covalent cross-links. The residual strain generated in the initial loading step is owed to the high stress applied, and may be due to both the rupture of covalent bonds and/or irreversible physical rearrangements. Yet, the application of such a

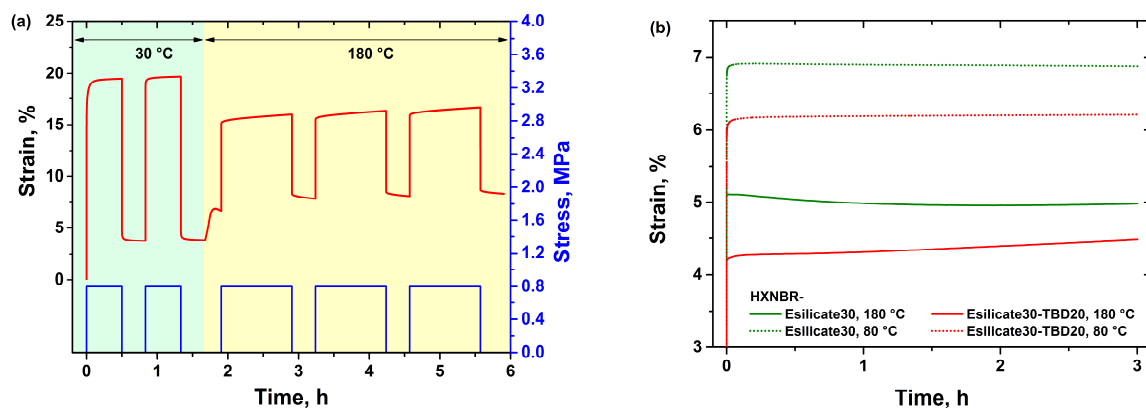


**Figure 7** – (a) Cyclic strain-recovery profile of HXNBR-Esilicate30-TBD20 containing 20 mol% (related to COOH) of TBD at 30 and 180 °C. (b) Creep measurements at 80 (dashed curves) and 180 °C (solid curves) for catalyst-free HXNBR-Esilicate30 and HXNBR-Esilicate30-TBD20 containing 20 mol% (related to COOH) of TBD. A constant stress of 0.4 MPa was applied for 3 h.

high stress is necessary, since covalent networks from the present HXNBR exhibit a distinctive entropic rubber-elastic contraction at high temperatures.<sup>25</sup> With insufficient external forces, it is difficult to overcome the entropic contraction to reveal the dynamic nature of the cross-links. This effect is clearly demonstrated by the measurement curves at 180 °C. During force-free heating to 180 °C, the specimen undergoes thermal expansion and the subsequent slight decrease in strain during temperature equilibration is attributed to entropic effects that are triggered by the high temperature. Interestingly, application of the same stress at 180 °C induces a much smaller instantaneous strain than at 30 °C because of strong entropy elasticity effects. Nevertheless, the strain-recovery cycles reveal an irreversible plastic deformation of the specimen for all three cycles during application of the stress, which does not recover after the release of the external force. The permanent viscous deformation is a response to the applied stress, and the network partially adopted to the new state by topology rearrangements that are enabled by thermo-activated and catalytically controlled interfacial transesterifications.

In contrast, for TBD-free HXNBR-Esilicate30 the picture clearly changes at high temperatures (Figure S8 in ESI). While at 30 °C a similar behaviour is found as for the composite with TBD, at 180 °C only minor plastic deformation over time is detected upon the application of the external force. The absence of TBD prevents any bond exchange reactions. The larger initial strain of HXNBR-Esilicate30 is explained by the lower cross-link density of the network due to the absence of TBD in the curing process, which was shown previously by equilibrium swelling experiments (Table 2). Figure S8 summarises the exact values of residual strain after each cycle and the overall creep strain over three cycles for both investigated materials derived from the measurement curves at 180 °C.

To complement the cyclic strain-recovery data, elongational creep experiments were conducted on the composites containing 30 phr of Esilicate with and without TBD. Figure 7b displays the time dependent deformation behaviour of both compounds at different temperatures as a function of time. At 80 °C (dashed curves in Fig. 7b), no creep is detected for any of the compositions after the initial elastic response, as indicated by the essentially flat curves. In fact, catalyst-free HXNBR-Esilicate30 shows a slightly declining curve,

which is due to entropic rubber-elastic contraction of the sample at elevated temperature. Going to 180 °C, similar characteristics in strain are found as previously observed in the cyclic strain-recovery profiles. The instantaneous strains generated by application of the external force are significantly smaller compared to the measurements at 80 °C because entropy elasticity effects are more pronounced at higher temperatures. Consequently, for HXNBR-Esilicate30, a decrease in strain is detected over time and the measurement further reveals a long-term effect of the entropic contraction. In contrast, in the presence of TBD (HXNBR-Esilicate30-TBD20) the entropic contraction is compensated by the viscous deformation of the specimen under external force enabled by thermo-activated transesterifications. Hence, the sample displays a distinctive creep over time.

The data of the cyclic strain-recovery measurements and creep experiments is consistent with the stress relaxation results. The measurements prove the occurrence of associative interfacial bond exchange reactions in the HXNBR-Esilicate networks. The transesterifications are triggered at elevated temperatures and, importantly, are solely enabled by the catalyst TBD. Further supported by the swelling behaviour in TCB, the results confirm vitrimer-like properties of the composites under investigation. Despite the incomplete stress relaxation, distinct topology rearrangements are achieved. Considering the stress relaxation characteristics of the unfilled compound cured with di-epoxide, the adaptability is largely preserved in the filled networks.

Shape change experiments allow for a simple demonstration of the adaptability of macroscopic samples from networks comprising exchangeable covalent bonds. Taking advantage of topology rearrangements at elevated temperatures, the introduction of new shapes to samples of HXNBR-Esilicate30-TBD20 is feasible (Figure 8b). Following 360 degree bending of cured rubber strips at 180 °C, the network largely adopts to the newly formed shape without losing its good elasticity. The extent of irreversible plastic deformation increases with time, and without catalyst, only minor shape adaptation is found (Figure 8a). The shape change observed for the TBD-free composition is attributed to the rearrangements of flexible parts of the network, adsorption/desorption processes at the polymer-filler interface, and reptation. However, the behaviour of the sample without catalyst clearly illustrates the major contribution of catalysed interfacial transesterifications to the extent of deformation in samples from HXNBR-Esilicate30-TBD20. The results prove the ability towards easy reshaping of vitrimer-like HXNBR-Esilicate composites, which is impossible for permanent covalent networks.

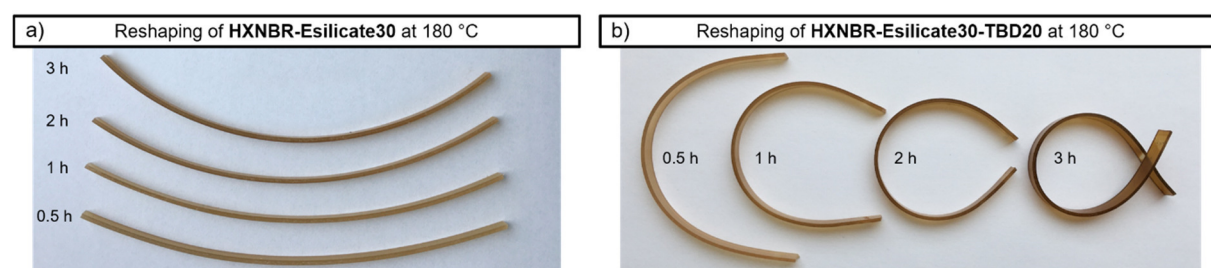


**Figure 8** – Photographs of shape change experiments conducted at 180 °C for different times on (a) catalyst-free HXNBR-Esilicate30 and (b) HXNBR-Esilicate30-TBD20 comprising 20 mol% (related to COOH) of TBD.

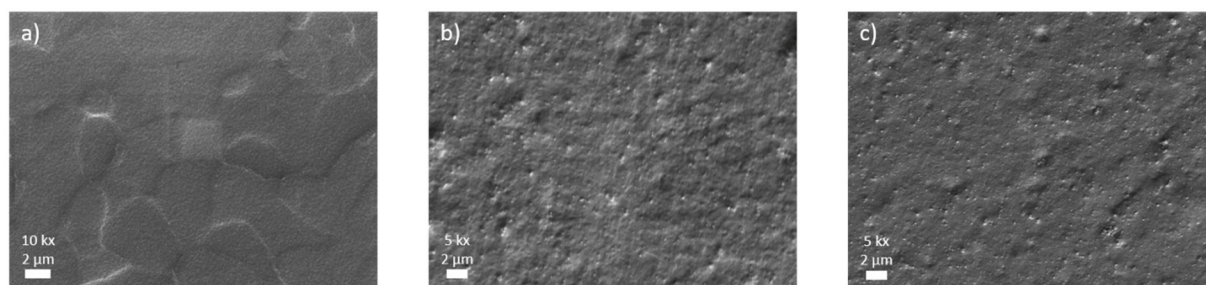


*Structure, mechanical and thermo-oxidative properties of HXNBR-Esilicate composites*

To reveal the dispersion state of the modified filler in the HXNBR matrix, cross-sections of the Esilicate-filled composites were investigated by scanning electron microscopy (SEM). Figure 9 displays the micrographs obtained for the composite filled with 30 phr of Esilicate with and without TBD, and of HXNBR-E5200-TBD20 as unfilled reference. The white points are identified as the filler particles and the micrograph shows that the Esilicate is uniformly distributed over the sample's cross-section without forming a significant quantity of aggregates. Moreover, there is no obvious influence of TBD on the state of dispersion of the Esilicate particles. It is anticipated that the distribution of the reactive filler in HXNBR benefits from its surface modification. In general, tailoring the surface chemistry of fillers is a common procedure to improve their quality of dispersion (and interfacial adhesion) in polymers<sup>23,24</sup>, which has also been shown in the context of vitrimers.<sup>18,30</sup> In the present study, the investigation of the influence of the surface modification of Esilicate, for instance by comparison with non-functionalised silicate, was beyond the scope of the paper. In this context, it must also be noted that the Esilicate serves as the cross-linker, wherefore no covalent cross-linked network would be obtained without surface epoxy groups.

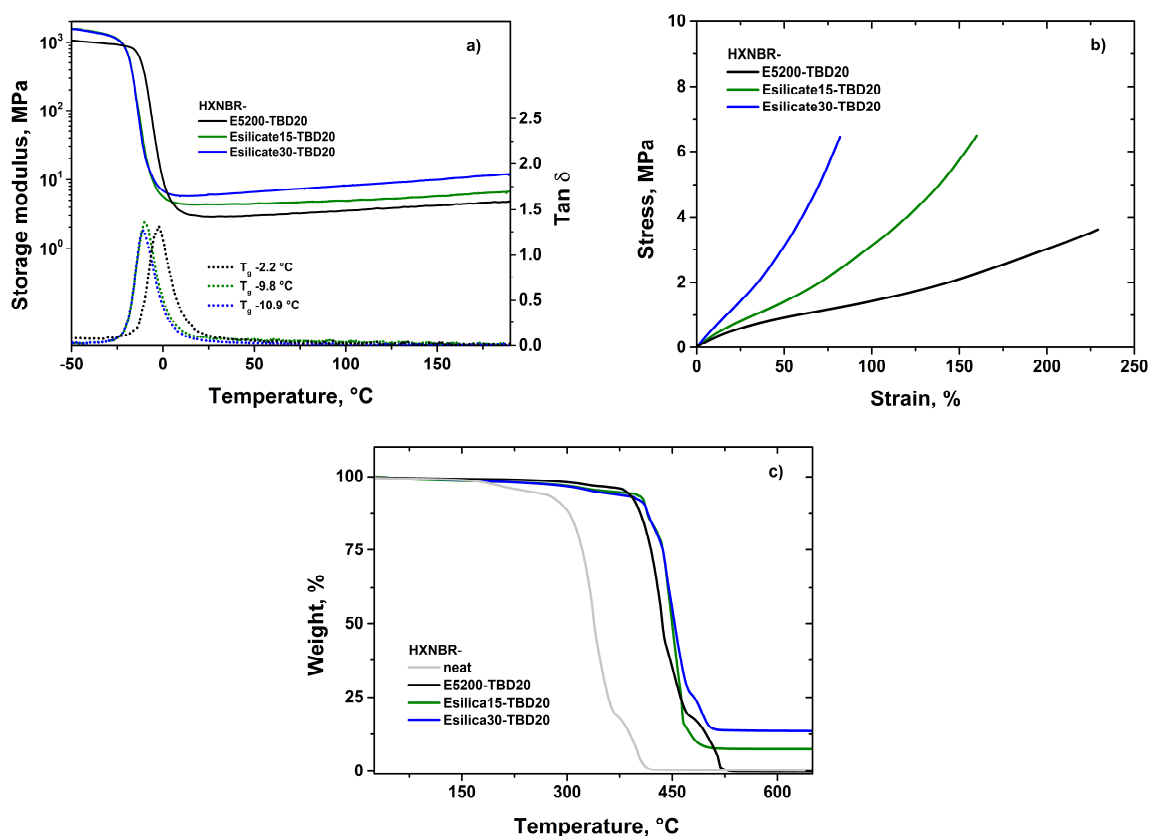
The expected reinforcement effect of covalently bonded and uniformly distributed Esilicate in HXNBR was evaluated by means of DMA measurements and tensile testing. The DMA data show that the storage modulus ( $E'$ ) improves in both the glassy and rubbery region by the addition of the reactive filler and further increases with the Esilicate loading (Figure 10a). The enhanced storage modulus is attributed to the good polymer-filler interactions, which are of physical and chemical nature in the present composites. Moreover, the higher cross-link density of the filled compounds, which was shown by equilibrium swelling measurements (Table 2), is likely to contribute to the increase in storage modulus. This is due to a reduced mobility of the rubber chains, and the effect further increases with the filler content.<sup>31</sup> Interestingly,  $T_g$  decreases upon the addition of Esilicate. This behaviour is associated with the high proportion of organic coupling agent on the particle surface, characterised by a low  $T_g$ , and thus causing a plasticising effect around  $T_g$ .<sup>32</sup>

Figure 10b displays representative stress-strain curves of the Esilicate composites and of HXNBR-E5200-TBD20 as unfilled reference network, and the mechanical properties are summarised in Table 3. The addition of Esilicate leads to a marked improvement in tensile



**Figure 9** – SEM micrographs of cross-sections of a) unfilled HXNBR-E5200-TBD20, and the composite HXNBR-Esilicate30 (b) with and (c) without TBD obtained by fracturing the samples under liquid nitrogen.

strength when comparing the filled compounds to the unfilled reference network cross-linked with the di-epoxide. The tensile strength almost doubles going from HXNBR-E5200-TBD20 to HXNBR-Esilicate30-TBD20, revealing a strong reinforcing capability of the present Esilicate. The distinct reinforcement effect observed indicates a good rubber-filler adhesion<sup>33</sup>, which benefits from the homogeneous dispersion of the functionalised filler in the matrix, and of both physical and chemical interactions with the polymer chains. On the other hand, the incorporation of Esilicate and the resulting interactions with the rubber matrix, especially of covalent nature, strongly reduce the mobility of the macromolecular chains. Consequently, a substantial decrease in elongation at break is observed. Furthermore, the filler remarkably improves the tensile modulus, indicating an increased stiffness. Both effects increase with the filler content. In order to gain more insight into the role of physical and chemical rubber-filler interactions in the mechanical properties of the present composites, we also conducted tensile testing on the non-cross-linked blend from HXNBR and 30 phr of Esilicate, which was previously introduced in the equilibrium swelling section. The respective stress-strain curve is displayed in Figure S9c in ESI in comparison to the curve of fully cured HXNBR-Esilicate30-TBD20. Interestingly, the uncured compound exhibits the highest tensile strength of all networks under investigation. In absence of any covalent cross-links, the rubber-filler adhesion is entirely characterised by physical interactions (physisorption). Obviously, these interactions provide the high tensile strength, and at the same time maintain good elastic properties of the matrix.



**Figure 10** – a) Storage modulus  $E'$  and  $\tan \delta$  as a function of temperature, b) typical stress-strain curves, and c) TGA experiments of HXNBR-E5200-TBD20 (black), HXNBR-Esilicate15-TBD20 (green) and HXNBR-Esilicate30-TBD20 (blue).

**Table 3** – Mechanical properties obtained from tensile testing of HXNBR-Esilicate composites in comparison to the compound cured with the liquid di-epoxide E5200.

Sample code, HXNBR-	Tensile strength, MPa	Elongation at break, %	Young's modulus, MPa
E5200-TBD20	3.64	230	3.33
Esilicate15-TBD20	6.53	161	4.58
Esilicate30-TBD20	6.50	82	6.83

The elasticity is governed by so-called interfacial slippage, which allows for stress delocalisation within the polymer network.<sup>20</sup> If polymer-filler slippage is prevented, for instance by the introduction of chemical bonds, the elasticity of rubbers is reduced.<sup>33</sup> This is apparently the case in the present composites that were fully cured at high temperature, subsequently forming covalent cross-links between the epoxy groups on Esilicate and pending carboxylic acid moieties in HXNBR. In general, rubber-filler interactions largely determine the reinforcing effect in rubbers, and the amount of physical and chemical interactions plays an important role in the final material properties. Optimal reinforcement usually involves both types of interactions, and in literature, there is evidence that only a minor amount of strong (i.e. covalent) bonds is desirable in the reinforcement of rubbers with fillers.<sup>20</sup> The tensile strength of a particular rubber composite normally finds its optimal value at a certain filler content as well as ratio of physical and chemical interactions. However, the optimisation of the mechanical properties was beyond the scope of the paper. Yet, it is interesting that although the number of covalent cross-link sites is rather limited in the present HXNBR (5 mol% of COOH containing monomer), the density of covalent bonds in the cured composites clearly restricts polymer/filler slippage. The data indicates the formation of comparatively short rubber chains that are covalently attached to neighbouring Esilicate particles as a result of the cross-linking reaction. The strong increase of the Young's modulus and the substantial decrease of the elongation at break in the filled and cross-linked networks is ascribed to this effect. The comparison between the non-cross-linked compound and the cured composite highlights that the final mechanical properties of the composites under investigation are largely governed by the polymer-filler interactions of covalent nature.

Compared to other reported vitrimer(-like) elastomers from rubbers, the present HXNBR composites exhibit similar tensile strengths, higher tensile moduli, and reduced elongations at break.<sup>3,4,8</sup> The mechanical properties are also similar with regard to composites from XNBR, however, comprising significantly lower elongations at break.<sup>34</sup> This is attributed to the covalent attachment of the polymer chains on the filler, an approach that is usually not employed in rubber industry.

The thermo-oxidative stability of the compounds was studied using thermogravimetric analysis (TGA). The TGA data is shown in Figure 10c and shows a thermal oxidative stability up to 190 °C for the HXNBR-Esilicate composites. In comparison to unfilled HXNBR-E5200-TBD20, the onset of network degradation shifts to lower temperatures, despite the higher cross-link density. This is attributed to the relatively low thermo-oxidative stability of the silane coupling agent ( $\approx 190$  °C), which is grafted on the inorganic silicate (Figure S1c in ESI).

The covalent attachment of reactive fillers with multiple cross-link sites to polymer chains in rubbers may lead to the formation of chains with non-uniform length.<sup>3,5,8</sup> This notion has already been discussed before in the context of the tensile tests. On stretching, these comparatively short chains are exposed to higher stresses and preferentially rupture, providing the desired reinforcement effect. On the other hand, the longer chains ensure the elasticity and structural integrity of the material. The ruptures cause energy dissipation and cyclic loading-unloading experiments can illustrate this process. Figures 11a-c display the respective measurements performed on unfilled HXNBR-E5200-TBD20 and the HXNBR-Esilicate composites containing 15 and 30 phr of filler. Figure 11d depicts the dissipated energies calculated from the hysteresis loops for the different compositions as a function of the applied strain and the cycle number. In addition, the detailed values for the hysteresis losses and residual strains of each cycle are summarised in Table 4.

Without Esilicate (Figure 11a), stretching to 40% allows the sample to fully recover to the first loading-unloading cycle after a resting time of 1 h. The hysteresis energy loss is already small in the first cycle and remains almost unchanged for the subsequent cycles 2 and 3. From the data, we conclude that the observed energy dissipation is mainly due to reversible physical processes such as the breakage of non-covalent interactions, while the

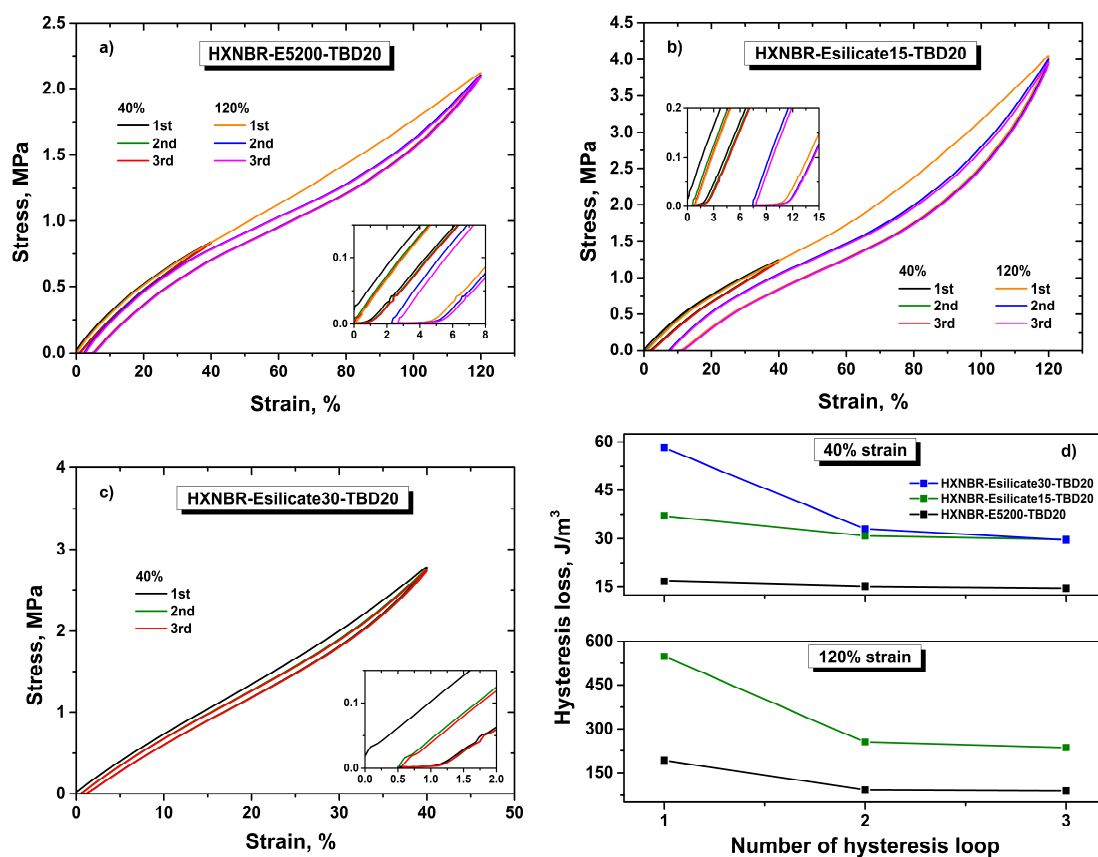


**Figure 11** – Cyclic hysteresis curves of (a) unfilled HXNBR-E5200-TBD20 and the composites (b) HXNBR-Esilicate15-TBD20 and (c) HXNBR-Esilicate30-TBD20 at different strains. d) Hysteresis loss of HXNBR composites with 15 and 30 phr of Esilicate and of unfilled HXNBR-E5200-TBD20 derived from the loading-unloading curves as a function of strain and number of hysteresis loop.

**Table 4** – Hysteresis losses and residual strains derived from cyclic hysteresis curves of cured HXNBR composites with 15 and 30 phr of Esilicate, of uncured HXNBR-Esilicate30, and of unfilled HXNBR-E5200-TBD20 during three tensile cycles at different strains.

Sample code, HXNBR-	Hysteresis loss, mJ m <sup>-3</sup> ; Residual strain, %		
	<i>1<sup>st</sup> cycle</i>	<i>2<sup>nd</sup> cycle</i>	<i>3<sup>rd</sup> cycle</i>
	40% strain		
E5200-TBD20	16.7; 0	15.1; 0	14.5; 0
Esilicate15-TBD20	37.0; 0.6	30.8; 0.8	29.7; 1.0
Esilicate30-TBD20	58.2; 0.5	33.0; 0.6	29.6; 0.6
Esilicate30 uncured	70.7; 0	67.3; 0	66.8; 0
	120% strain		
E5200-TBD20	193; 2.3	91.4; 2.7	88.7; 2.8
Esilicate15-TBD20	548; 7.4	255; 7.8	235; 7.8

rupture of covalent bonds apparently does not occur. When the sample is stretched to 120%, significantly larger hysteresis losses are observed, especially in the first cycle. After unloading, the sample does not return to its initial length within the resting time of 1 h, and a permanent set of 2.3% remains after the first cycle. The calculated energy dissipation of cycles 2 and 3 is similar, but much smaller compared to cycle 1. The data show that in the absence of filler significant hysteresis occurs at high strains. While the irreversible portion of the dissipated energy is attributed to the breakage of covalent bonds and disentanglements by reptation, the reversible portion is assigned to physical processes.

Going from the unfilled network to the composite HXNBR-Esilicate15-TBD20, a different behaviour is observed (Figure 11b). Already at a strain of 40% a residual deformation after the resting time in cycle 1 remains, which amounts to 0.6%. The successive loading curves cannot recover to the first one. This behaviour evidences that at least two processes contribute to the energy dissipation. On the one hand, hysteresis associated with reversible physical processes such as desorption of polymer chains from Esilicate surface. On the other hand, the dissipated energy partly originates from the irreversible breakage of short rubber chains that are covalently attached to neighbouring Esilicate particles. The latter process is more pronounced by stretching the specimen to 120%, where a significantly larger hysteresis in the first loading-unloading cycle is measured. After unloading, the hysteresis cannot recover within the resting time, and a residual strain of 7.4% remains. Here again, the following hysteresis loops are similar regarding the quantity of dissipated energy and the residual deformation increases only slightly. The measurements confirm the irreversible breakage of short rubber chains between Esilicate particles in the filled network under external force.

For the composite with a filler loading of 30 phr, HXNBR-Esilicate15-TBD20, cyclic loading-unloading curves were only performed at 40% elongation (Figure 11c). The composite is not capable of undergoing equally high strains such as 120% because the

elongation at break is considerably reduced due to the covalent polymer-filler interactions (Table 3).

At an elongation of 40%, the residual strain after the resting time is similar to the composite containing 15 phr of Esilicate. However, a more pronounced hysteresis is obtained (58.2 vs. 37.0 mJ m<sup>-3</sup>). The larger amount of dissipated energy indicates an increased number of bond breakages of short rubber chains for the composite with the higher filler content. This notion is supported by the higher cross-link density of the composite with 30 phr of Esilicate compared to the network with 15 phr, reflected by the smaller mass swelling ratio of the former (Table 2). It can also be assumed that the contribution of (reversible) physical processes to the observed hysteresis is higher in the material containing more filler. In general, the hysteresis loops reveal low residual deformations at 40% elongation for the present composites even at high filler loadings, confirming a good elasticity likely ensured by the longer polymer chains in the matrix. This is expectable considering the low number of covalent cross-links achievable in the present networks (5 mol% of COOH containing monomer in HXNBR). Compared to other highly filled composites from XNBR rubber, the present networks display low hysteresis energy losses as well as low permanent deformations after the stress-strain cycles.<sup>35</sup>

In addition, we conducted similar measurements on non-cross-linked HXNBR-Esilicate30 to assess the influence of covalent polymer-filler interactions in the hysteresis behaviour of the cured compounds. Figure S9a shows the cyclic loading-unloading curves at 40% elongation, and the respective hysteresis losses and residual strains are given in Table 4. Moreover, Figure S9b displays the dissipated energies in each cycle compared to HXNBR-Esilicate30-TBD20. Interestingly, the hysteresis found for the specimen comprising solely physical polymer-filler interactions is larger than for HXNBR-Esilicate30-TBD20. Despite this fact, the sample can recover to the first loading-unloading curve in the subsequent cycles, and no residual deformation is observed. This is in striking contrast to the cured composite with 30 phr of Esilicate. It should also be noted that the recovery of the strain after the first unloading phase proceeded faster than for the cured compounds. The data reveals that in the absence of covalent cross-links, the observed hysteresis is only due to reversible physical processes, which is supported by the similar values for the dissipated energies in cycles 1-3. The hysteresis is primarily attributed to polymer adsorption/desorption processes at the filler surface. Apparently, irreversible energy dissipation that could be assigned to reptation does not occur at this strain. This control experiment confirms the contribution of the breakage of covalent HXNBR-Esilicate interactions to the hysteresis in the cured composites upon stretching.

## 5.5 Conclusions

Vitrimer-like chemistry in technically relevant HXNBR rubber has been successfully extended to composites on the example of a calcium silicate-based filler (Esilicate). The modified filler was covalently incorporated into the rubber matrix via surface epoxy groups forming  $\beta$ -hydroxyl ester bonds at the rubber-Esilicate interface, which are capable to undergo transesterification reactions. In presence of the catalyst triazabicyclodecene (TBD), interfacial thermo-activated bond exchange reactions enabled a substantial stress relaxation of the composites. The data revealed that the network dynamics can be largely

maintained in the filled network, when comparing to an unfilled compound cross-linked with a liquid di-epoxide. The Esilicate did not only serve as the cross-linker, but at the same time provided a distinct reinforcement effect enhancing the mechanical properties, such as the tensile strength and Young's modulus. The presented straightforward solvent-free approach towards adaptable filled elastomers uses easily available commercial materials and demonstrates that vitrimer-like chemistry is scalable and can be readily implemented in HXNBR rubber at an industrial level.

## 5.6 Experimental

### *Materials*

Therban® XT KA 8889 VP, a hydrogenated carboxylated nitrile butadiene rubber (HXNBR) with a molecular weight ( $M_w$ ) of 370,000 g/mol and with 5 mol% carboxylic acid content, 33 wt% acrylonitrile content and 3.5 wt% residual carbon-carbon double bonds, was provided by Arlanxeo (Cologne, Germany). Calcium silicate particles (Rima Sil 1200) modified with CoatOSil MP 200 (Momentive Performance Materials, Waterford, USA), an epoxy functional silane oligomer, and a  $d_{50}$  of 2  $\mu\text{m}$  were obtained from Grolman (Neuss, Germany). The silane proportion on the particle surface is approximately 50 wt%. Diglycidyl hexahydrophthalate (Epalloy 5200) was obtained from CVC Thermoset Specialities (Moorestown, USA). 1,5,7-Triazabicyclo[4.4.0]dec-5-ene (TBD) was purchased from Sigma-Aldrich and used as received.

### *Preparation of HXNBR compounds*

The rubber compounds were masticated using a Collin (Ebersberg, Germany) W 150 P two-roll mill at 40 °C. During the mixing process the temperature did not exceed 50 °C. For the reference compound cross-linked with the di-epoxide Epalloy 5200 (WPE=170 g/mol), the number of epoxy groups was in stoichiometry with carboxylic acid functions of HXNBR. The catalyst TBD, which is solid under the mixing conditions, was previously mixed with the liquid cross-linker in order to facilitate its homogeneous distribution in the rubber. In the second step, the liquid cross-linker/TBD formulation was added to the rubber compound during mastication. For the Esilicate-filled composites, the desired amounts of filler and TBD were pre-mixed and subsequently incorporated into the rubber. The given catalyst quantities in mol% are related to the number of carboxylic acid groups of HXNBR. In the context, sample code HXNBR- $x$ - $y$  refers to HXNBR cross-linked with  $x$  in the presence of the catalyst  $y$ . The coding and composition of the rubber compounds are displayed in Table 5.

### *Characterisation methods*

*Curing kinetics.* The cure characteristics were determined using a MonTech (Buchen, Germany) D-RPA 3000 moving die rheometer (MDR) (1.67 Hz frequency, 0.5% strain).

*Stress relaxation.* Stress relaxation experiments at different temperatures were performed in the moving die rheometer right after curing of the samples up to 95% of the final state of cure ( $t_{95}$ ) at 180 °C. After curing, the samples were allowed to equilibrate to the selected measurement temperature for 10 min. Subsequently, a 1% step strain was applied, which

was within the linear viscoelastic region of the samples (Figure S3 in ESI), and the decrease in torque was recorded over time.

*ATR-FTIR spectroscopy.* Fourier transform infrared spectra were taken with a Bruker (Billerica, USA) Vertex 70 FT-IR spectrometer equipped with a reflection diamond attenuated total reflection (ATR) accessory (Platinum ATR). 16 scans were accumulated with a resolution of 4 cm<sup>-1</sup>.

*Swelling experiments.* Rectangular-shaped samples with a weight of about 100 mg were cut from the cured rubber compounds. The samples were immersed in chloroform for 48 h at 23 °C. After the weight of the swollen gel was determined, the samples were dried at 50 °C until constant weight and reweighed. Mass swelling ratios were calculated as  $(m_s - m_d)/m_d$ , and sol fraction was determined as  $(m_i - m_d)/m_i$ , where  $m_i$  is the initial mass of the sample,  $m_s$  and  $m_d$  are the mass of the swollen and deswollen sample, respectively. Five samples were tested for each series and the arithmetic average was taken. In the composites, the filler particles were considered as non-swelling, and the measured volume changes were corrected based on the matrix:filler ratio. The same applies to the swelling experiments in trichlorobenzene.

*Tensile testing and cyclic loading-unloading tests.* Uniaxial tensile tests were carried out on a ZwickRoell (Ulm, Germany) Z1.0 static materials testing machine with a crosshead speed of 250 mm min<sup>-1</sup> at room temperature. Dumbbell specimens with an initial measuring length of 50 mm (gauge length 25 mm) and 4 mm width were punched out of cured rubber sheets. Five specimens were tested for each compound. The tensile moduli were calculated by taking the slope of the stress-strain curves from 0.5-3% strain. Cyclic loading-unloading curves were carried out at a strain rate of 100 mm/min for both loading and unloading, and an initial preload of 0.02 MPa was applied. After stretching to the desired strain, the sample underwent immediate unloading. After three cycles, the sample was subjected to the next higher elongation for another three cycles. The specimens were allowed to relax for 60 min after each cycle.

*Thermal gravimetric analysis (TGA).* TGA experiments were carried out using a Mettler Toledo (Columbus, USA) TGA/DSC1 thermogravimetric analyser. Measurements were performed under oxygen atmosphere. The samples were heated from room temperature to 700 °C at a heating rate of 10 °C/min.

*Dynamic mechanical analysis (DMA).* DMA experiments were conducted on a Mettler Toledo (Columbus, USA) SDTA861e dynamic mechanical analyser in tensile mode. Rectangular rubber strips (width: 3.5 mm, thickness: 1.0 mm, clamping distance: 12.5 mm) were tested in displacement controlled oscillation of 5 µm amplitude at 1 Hz. Heating ramps were applied at 2 K/min from -50 to 200 °C.

*Cyclic strain-recovery profiles and creep experiments.* The tests were performed on rectangular specimens (30 mm × 4 mm × 1.0 mm and a gauge length of 20 mm) using an Anton Paar (Graz, Austria) modular compact rheometer MCR 702 MultiDrive in tensile mode. In the cyclic measurements, during temperature equilibration at 30 °C, the specimens were held unloaded before the external force was applied. The stress was alternated between 0.8 MPa for 60 min and 0 MPa for 10 min in each cycle and the corresponding strain was monitored over time. During the heating step to 180 °C and the subsequent temperature equilibration for 10 min, the specimens were again held



unloaded. For elongational creep measurements, after force-free heating up to the desired test temperature and following temperature equilibration for 10 min, a stress of 0.4 MPa was applied and held constant for 3 h. The corresponding strain was recorded over time.

*Scanning electron microscopy (SEM).* SEM measurements were conducted using a scanning electron microscope Tescan (Brno, Czech Republic) VEGA-II. The liquid nitrogen-fractured cross-sections were sputter coated with gold.

**Table 5** – Sample coding and composition of the rubber compounds prepared.

Compound code	HXNBR, phr <sup>a</sup>	Cross-linker, phr	TBD, phr (mol% <sup>b</sup> )
HXNBR-E5200	100	11.8	-
HXNBR-E5200-TBD20	100	11.8	1.93 (20)
HXNBR-Esilicate15	100	15	-
HXNBR-Esilicate15-TBD20	100	15	1.93 (20)
HXNBR-Esilicate30	100	30	-
HXNBR-Esilicate30-TBD20	100	30	1.93 (20)

<sup>a</sup> phr = parts per hundred rubber; <sup>b</sup> related to COOH.

## 5.7 Acknowledgements

The research work was performed within the COMET-Module “Chemitecture“ (project-no.: 21647048) at the Polymer Competence Center Leoben GmbH (PCCL, Austria) within the framework of the COMET-program of the Federal Ministry for Transport, Innovation and Technology and the Federal Ministry for Digital and Economic Affairs with contributions by Montanuniversitaet Leoben. The PCCL is funded by the Austrian Government and the State Governments of Styria, Upper and Lower Austria. The authors also thank Bernhard Lechner for the assistance in DMA measurements, Nicole Zarfl for conducting SEM experiments, and Jürgen Grosser for support in cyclic loading-unloading tests.

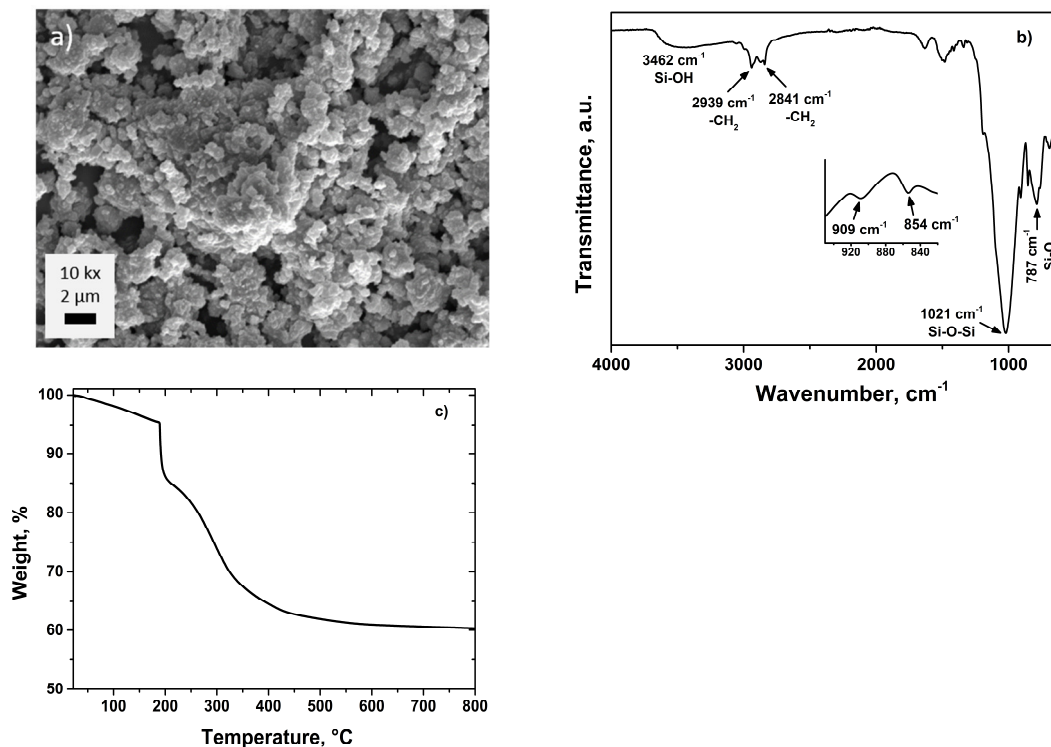
## 5.8 References

- 1 a) B. Erman, J. E. Mark and C. M. Roland, *The science and technology of rubber*, Elsevier Acad. Press, Amsterdam, 4th edn., 2013; b) J. Kruželák, R. Sýkora and I. Hudec, *Rubber Chemistry and Technology*, 2017, 90, 60–88.
- 2 D. Montarnal, M. Capelot, F. Tournilhac and L. Leibler, *Science*, 2011, 334, 965–968.
- 3 Y. Liu, Z. Tang, Y. Chen, C. Zhang and B. Guo, *ACS applied materials & interfaces*, 2018, 10, 2992–3001.
- 4 C. Xu, R. Cui, L. Fu and B. Lin, *Composites Science and Technology*, 2018, 167, 421–430.
- 5 Z. Tang, Y. Liu, B. Guo and L. Zhang, *Macromolecules*, 2017, 50, 7584–7592.
- 6 L. Imbernon, S. Norvez and L. Leibler, *Macromolecules*, 2016, 49, 2172–2178.
- 7 Z. Feng, J. Hu, H. Zuo, N. Ning, L. Zhang, B. Yu and M. Tian, *ACS applied materials & interfaces*, 2019, 11, 1469–1479.
- 8 L. Cao, J. Fan, J. Huang and Y. Chen, *J. Mater. Chem. A*, 2019, 167, 421.
- 9 W. Denissen, J. M. Winne and F. E. Du Prez, *Chemical science*, 2016, 7, 30–38.
- 10 M. Hayashi and R. Yano, *Macromolecules*, 2020, 53, 182–189.
- 11 M. Capelot, M. M. Unterlass, F. Tournilhac and L. Leibler, *ACS Macro Lett.*, 2012, 1, 789–792.
- 12 Y. Yang, Z. Pei, X. Zhang, L. Tao, Y. Wei and Y. Ji, *Chemical science*, 2014, 5, 3486–3492.
- 13 Z. Yang, Q. Wang and T. Wang, *ACS applied materials & interfaces*, 2016, 8, 21691–21699.
- 14 D. J. Fortman, J. P. Brutman, C. J. Cramer, M. A. Hillmyer and W. R. Dichtel, *J. Am. Chem. Soc.*, 2015, 137, 14019–14022.
- 15 M. Capelot, D. Montarnal, F. Tournilhac and L. Leibler, *J. Am. Chem. Soc.*, 2012, 134, 7664–7667.
- 16 J. P. Brutman, P. A. Delgado and M. A. Hillmyer, *ACS Macro Lett.*, 2014, 3, 607–610.
- 17 a) W. Zhao, Z. Feng, Z. Liang, Y. Lv, F. Xiang, C. Xiong, C. Duan, L. Dai and Y. Ni, *ACS applied materials & interfaces*, 2019, 11, 36090–36099; b) L. Jiang, Q. Liu, Y. Lei, Y. Wang, Y. Zhao and J. Lei, *Mater. Chem. Front.*, 2019, 3, 1601–1612; c) J. Chen, H. Huang, J. Fan, Y. Wang, J. Yu, J. Zhu and Z. Hu, *Frontiers in chemistry*, 2019, 7, 632; d) E. Chabert, J. Vial, J.-P. Cauchois, M. Mihaluta and F. Tournilhac, *Soft Matter*, 2016, 12, 4838–4845; e) W. Denissen, I. de Baere, W. van Paepegem, L. Leibler, J. Winne and F. E. Du Prez, *Macromolecules*, 2018, 51, 2054–2064.
- 18 A. Legrand and C. Soulié-Ziakovic, *Macromolecules*, 2016, 49, 5893–5902.
- 19 S. Sasmaz, *Filler Materials in Rubber Industry*, *Conference Paper*, 2015.
- 20 D. C. Edwards, *J Mater Sci*, 1990, 25, 4175–4185.
- 21 K. Roy, S. C. Debnath and P. Potiyaraj, *Journal of Elastomers & Plastics*, 2020, 52, 167–193.
- 22 S.-Y. Fu, X.-Q. Feng, B. Lauke and Y.-W. Mai, *Composites Part B: Engineering*, 2008, 39, 933–961.

- 
- 23 R. L. Sala, T. M. Arantes, E. Longo, E. R. Leite, C. M. Paranhos and E. R. Camargo, *Colloids and Surfaces A: Physicochemical and Engineering Aspects*, 2014, 462, 45–51.
- 24 L. Qu, G. Yu, L. Wang, C. Li, Q. Zhao and J. Li, *J. Appl. Polym. Sci.*, 2012, 126, 116–126.
- 25 S. Kaiser, S. Wurzer, G. Pilz, W. Kern and S. Schlögl, *Soft Matter*, 2019, 15, 6062–6072.
- 26 H.-Q. Xie, X.-D. Li and J.-S. Guo, *J. Appl. Polym. Sci.*, 2003, 90, 1026–1031.
- 27 a) M. P. Coles, *Chemical communications*, 2009, 3659–3676; b) W. J. Blank, Z. A. He and M. Picci, *J. Coatings Tech.*, 2002, 74, 33–41.
- 28 A. Laskowska, M. Zaborski, G. Boiteux, O. Gain, A. Marzec and W. Maniukiewicz, *Express Polym. Lett.*, 2014, 8, 374–386.
- 29 R. Chasset and P. Thirion, *"Physics of non-crystalline solids". Proceedings of the International Conference*, North Holland Publishing Co., Amsterdam, 1965.
- 30 Z. Huang, Y. Wang, J. Zhu, J. Yu and Z. Hu, *Composites Science and Technology*, 2018, 154, 18–27.
- 31 C. G. Robertson, C. J. Lin, M. Rackaitis and C. M. Roland, *Macromolecules*, 2008, 41, 2727–2731.
- 32 C. Corcione and M. Frigione, *Materials*, 2012, 5, 2960–2980.
- 33 M. R. Mitchell, R. E. Link, A. Mostafa, A. Abouel-Kasem, M. R. Bayoumi and M. G. El-Sebaie, *J. Test. Eval.*, 2010, 38, 101942.
- 34 a) A. Mousa, G. Heinrich, F. Simon, U. Wagenknecht, K.-W. Stöckelhuber and R. Dweiri, *Mat. Res.*, 2012, 15, 671–678; b) Ahmad Mousa, Gert Heinrich and Udo Wagenknecht, *Cure Characteristics and Mechanical Properties of Carboxylated Nitrile Butadiene Rubber (XNBR) Vulcanizate Reinforced by Organic Filler*, 2013.
- 35 a) K. Sasikumar, P. Jayesh, N. R. Manoj, T. Mukundan and D. Khastgir, *Polym. Compos.*, 2018, 39, E1269-E1279; b) S. K. Chakraborty and S. K. De, *Polymer*, 1983, 24, 1055–1062.

## 5.9 Supporting information

## DESIGN AND CHARACTERISATION OF VITRIMER-LIKE ELASTOMERIC COMPOSITES FROM HXNBR RUBBER

Simon Kaiser<sup>a</sup>, Julius Jandl<sup>a</sup>, Patrick Novak<sup>a</sup>, and Sandra Schlögl<sup>a†</sup><sup>a</sup> Polymer Competence Center Leoben GmbH, Roseggerstrasse 12, A-8700 Leoben, Austria.<sup>†</sup>E-mail: sandra.schloegl@pccl.at

**Figure S1** – Characterisation of epoxy group-functionalised calcium silicate particles: (a) SEM micrograph, (b) ATR-FTIR spectrum, and (c) TGA curve of pristine epoxy group-functionalised calcium silicate particles Rima Sil 1200.

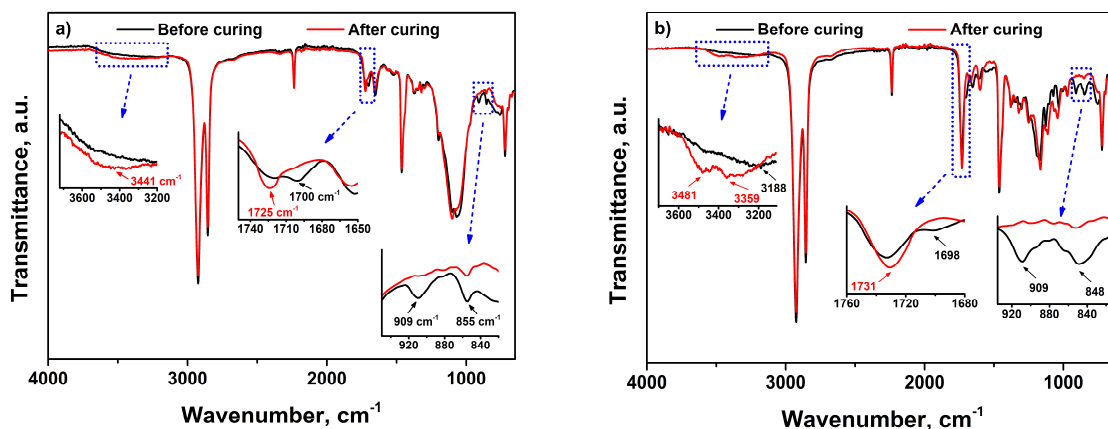


**Figure S2** – ATR-FTIR spectra of (a) HXNBR-Esilicate15-TBD20 and (b) HXNBR-E5200-TBD20 before (black curve) and after (red curve) curing at 180 °C.

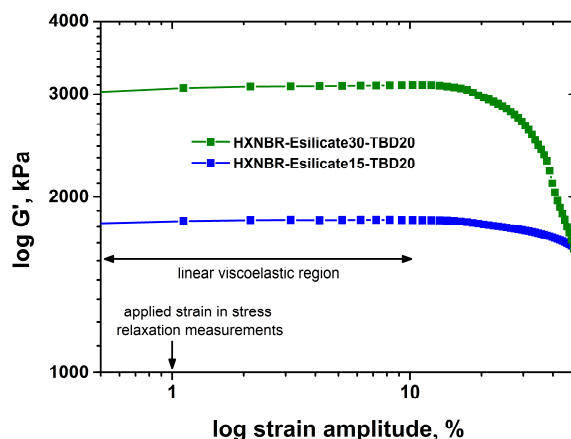


**Figure S3** – Strain sweep measurements of HXNBR-Esilicate composites HXNBR-Esilicate15-TBD20 (blue) and HXNBR-Esilicate30-TBD20 (green). The measurements were performed at 180 °C in the moving die rheometer directly after curing.

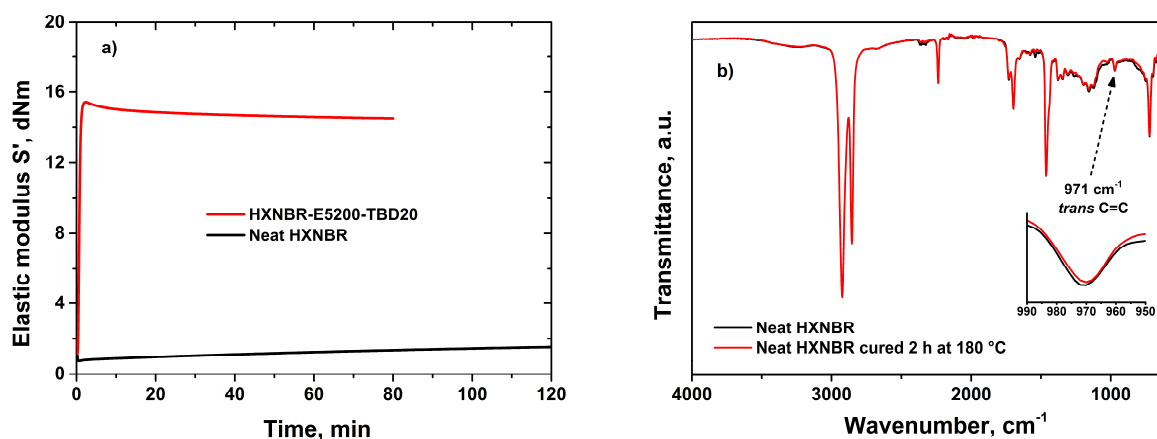


**Figure S4** – The possible formation of permanent covalent bonds due to thermally induced self-cross-linking of the present HXNBR, by either residual carbon-carbon double bonds or the formation of anhydride linkages between two carboxylic acid groups, was examined by rheology and ATR-FTIR spectroscopy. The rheological measurement of neat rubber in the moving die rheometer for 2 h at 180 °C does not indicate the formation of such cross-links. Moreover, ATR-FTIR spectra of neat HXNBR before and after the treatment in the rheometer were recorded. The absorption band at 971  $\text{cm}^{-1}$  corresponds to the vibration of 1,4-trans double bonds of the rubber backbone, and no decrease in absorption is observed. The formation of characteristic absorption bands related to anhydrides is also not apparent. Consequently, we assume that no self-cross-linking of the present HXNBR occurs under the conditions applied.

(a) Rheograms of neat HXNBR rubber measured for 2 h at 180 °C in the moving die rheometer and of HXNBR cross-linked with the di-epoxide Epalloy 5200 in the presence of 20 mol% (related to COOH) of TBD (HXNBR-E5200-TBD20).

(b) ATR-FTIR spectra of neat HXNBR rubber before (black) and after (red) the rheological measurement for 2 h at 180 °C in the moving die rheometer.

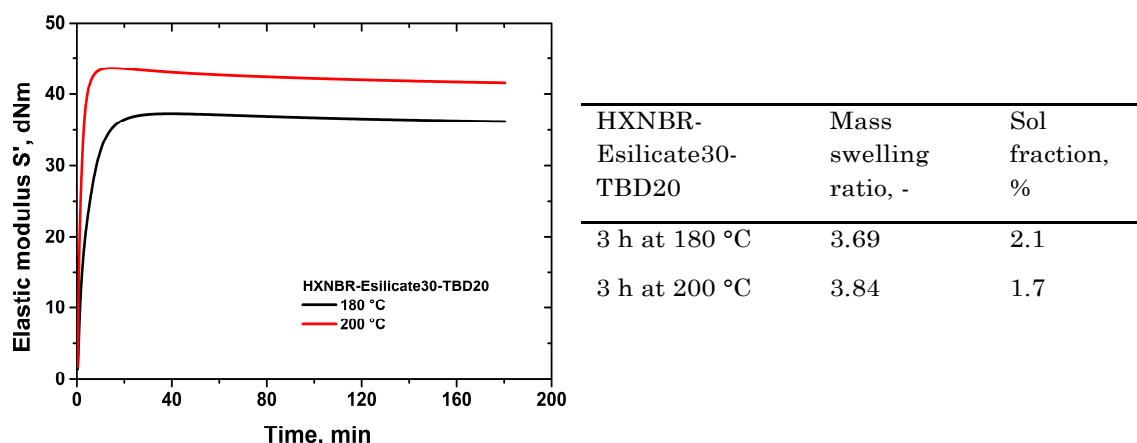


**Figure S5** – Left: prolonged rheological measurements of HXNBR-Esilicate30-TBD20 at 180 and 200 °C performed in the moving die rheometer. The rheograms reveal only minor reversion for the composite under investigation even at very high temperatures, whereby the reversion is slightly more pronounced at 200 °C compared to 180 °C. Right: data obtained from swelling experiments (chloroform, 48 h, at room temperature) of the samples from the prolonged rheological measurements. The results show that the  $S'$  plateau value does not precisely correlate with the mass swelling ratio, i.e. with the density of covalent cross-links. This is probably due to the effect of the different measurement temperatures on the shear modulus, which is typically increasing with temperature in elastomers from rubbers.

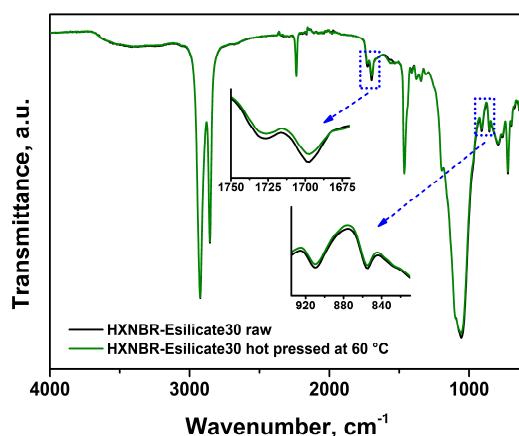


**Figure S6** – ATR-FTIR spectra of a compound from HXNBR containing 30 phr of Esilicate (HXNBR-Esilicate30) before and after treatment in the hot press at 60 °C for 10 min. The spectra are nearly identical, showing only a slight decrease of the absorption bands associated with the epoxy groups on Esilicate (909 and 855  $\text{cm}^{-1}$ ) and with the carboxylic acid groups of HXNBR (1725 and 1701  $\text{cm}^{-1}$ ). These changes may be associated with the formation of few covalent cross-links between HXNBR and Esilicate via the epoxy-carboxyl reaction at this low temperature, which is consistent with the swelling data displayed in Figure S7.

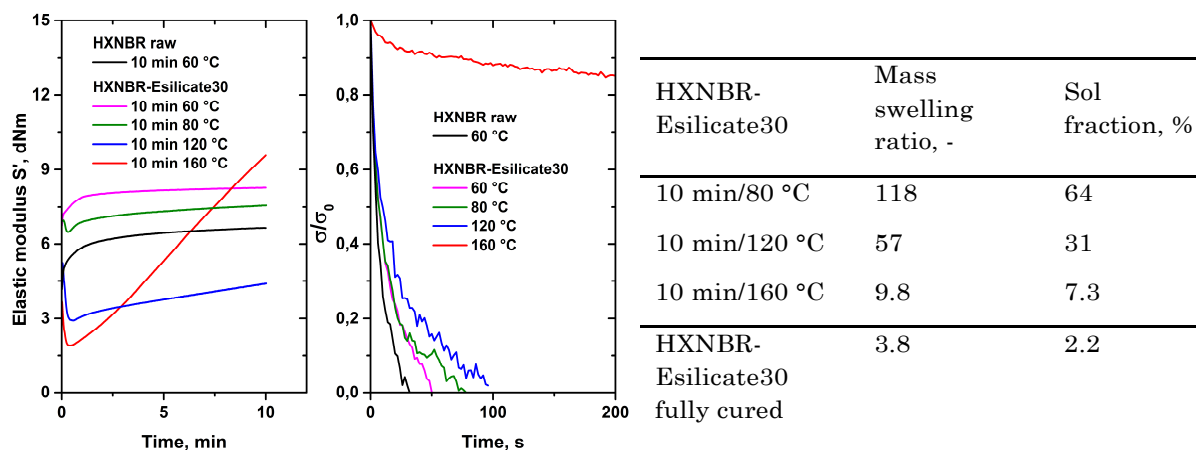


**Figure S7** – Left: rheological measurements of raw HXNBR (black curve) and a composition from HXNBR and 30 phr of Esilicate (HXNBR-Esilicate30) performed in the moving die rheometer for 10 min each. For HXNBR-Esilicate30, a stepwise increase of the measurement temperature was carried out to reveal the onset of significant covalent cross-linking. The data shows that the formation of chemical bonds via the epoxy-carboxyl reaction only accelerates considerably from curing temperatures higher than 120 °C.

Center: shear stress relaxation measurements of raw HXNBR (black curve) and HXNBR-Esilicate30 performed directly after the respective curing step in the moving die rheometer. A constant deformation of 1% was applied. From the data, it can be concluded that raw HXNBR undergoes full and extremely fast stress relaxation even at low temperatures, what is to be expected for a rubber without covalent cross-links. Moreover, exposure of the reactive composition HXNBR-Esilicate30 to relatively low temperatures for 10 min still allows for full and fast stress relaxation, as probably only few covalent bonds have been formed yet in these samples. However, the stress relaxation time already significantly increases when raising the temperature from 60 to 120 °C in the previous curing step. After a further increase to 160 °C, the subsequent stress relaxation experiment reveals only minor relaxation capabilities of the sample. This control experiment clearly shows that already small quantities of covalent cross-links between the polymer chains of HXNBR and Esilicate are sufficient to prevent stress relaxation of the composites.

Right: to estimate the number of covalent cross-links formed at the different curing temperatures, additional swelling experiments were carried out (chloroform, 48 h, at room temperature). The data shows the different mass swelling ratios obtained in comparison to the value measured for fully cured HXNBR-Esilicate30. As expected, the mass swelling ratio and the soluble fraction decrease with rising curing temperature. The data confirms that at low temperatures only few covalent cross-links were formed within 10 min of curing, reflected by the very high values for the mass swelling ratios and soluble fractions. Importantly, the sample of HXNBR-Esilicate30 cured for 10 min at 160 °C still exhibits a rather low cross-link density compared to the fully cured compound. Nevertheless, substantial stress relaxation is already prevented.

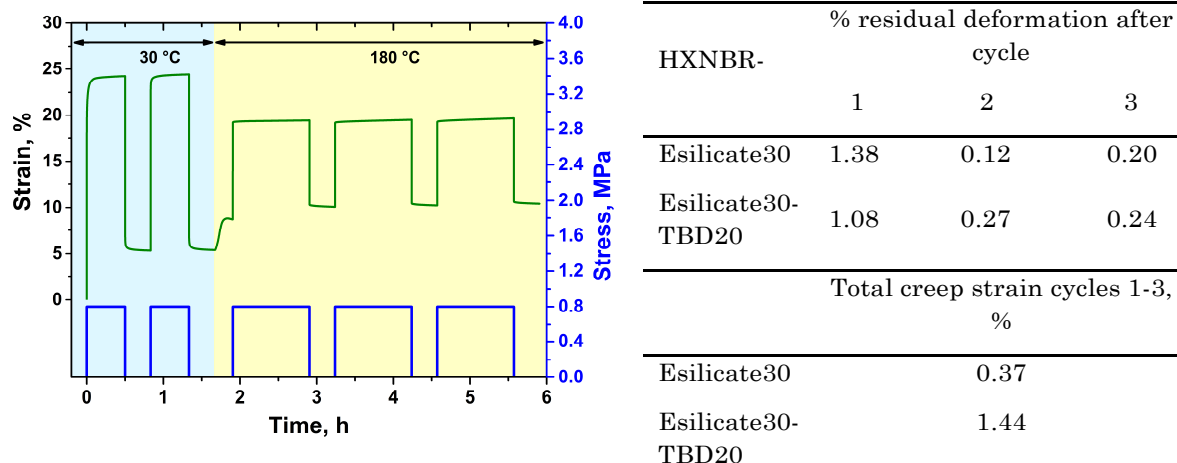


**Figure S8** – Left: cyclic strain-recovery profile of HXNBR-Esilicate30 at 30 and 180 °C. Right: summary of the values for residual strain and total creep strain over three strain-recovery cycles at 180 °C derived from cyclic strain-recovery profiles of HXNBR-Esilicate30 and HXNBR-Esilicate30-TBD20 (Figure 7a in the manuscript).

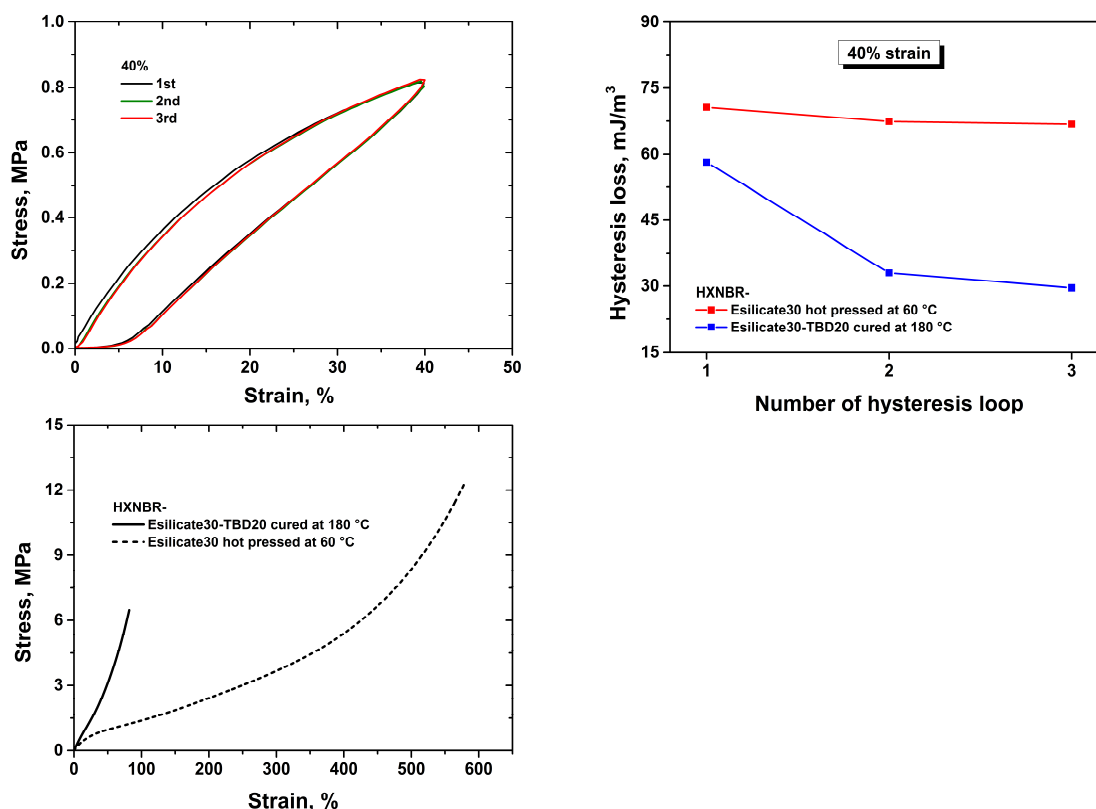


**Figure S9** – Top left: loading-unloading curves of HXNBR containing 30 phr of Esilicate (HXNBR-Esilicate30) applying a strain of 40%. The composite was hot pressed at 60 °C to avoid the formation of covalent cross-links. Top right: comparison of the calculated hysteresis losses for each hysteresis loop of HXNBR-Esilicate30 that was hot pressed at 60 °C and HXNBR-Esilicate30-TBD20 (see Figure 11c in the manuscript) that was fully cured at 180 °C. The data was derived from the loading-unloading curves at a strain of 40%. Left bottom: comparison of representative stress-strain curves of HXNBR-Esilicate30 hot pressed at 60 °C and HXNBR-Esilicate30-TBD20 fully cured at 180 °C.



# Chapter 6

## ANALYSIS OF THE $T_v$ OF VITRIMERS BY CREEP MEASUREMENTS

## 6.1 Bibliographic information

### Published in:

Kaiser, S.; Novak, P.; Giebler, M.; Gschwandl, M.; Novak, P.; Pilz, G.; Morak, M. and Schlögl, S. The crucial role of external force in the estimation of the topology freezing transition temperature of vitrimers by elongational creep measurements. *Polymer*. DOI: 10.1016/j.polymer.2020.122804.

### Author contributions:

Simon Kaiser: Conceptualisation; Methodology; Investigation; Data curation; Formal analysis; Validation; Visualisation; Original draft; Review and editing

Patrick Novak: Investigation; Data curation

Michael Giebler: Investigation; Methodology

Mario Gschwandl: Data curation; Formal analysis; Visualisation

Philipp Novak: Investigation; Data curation; Formal analysis; Visualisation

Gerald Pilz: Resources; Methodology

Matthias Morak: Methodology; Data curation; Software; Validation; Visualisation

Sandra Schlögl: Funding acquisition; Project administration; Resources; Supervision; Conceptualisation; Methodology; Validation; Original draft; Review and editing

The manuscript presented here is an adapted accepted manuscript in order to correspond to the formatting of this thesis and does not necessarily reflect the actual published version. This chapter contains results of the bachelor thesis of Julius Jandl.

# THE CRUCIAL ROLE OF EXTERNAL FORCE IN THE ESTIMATION OF THE TOPOLOGY FREEZING TRANSITION TEMPERATURE OF VITRIMERS BY ELONGATIONAL CREEP MEASUREMENTS

Simon Kaiser<sup>a</sup>, Patrick Novak<sup>a</sup>, Michael Giebler<sup>a</sup>, Mario Gschwandl<sup>a</sup>, Philipp Novak<sup>a</sup>, Gerald Pilz<sup>b</sup>, Matthias Morak<sup>a</sup> and Sandra Schlögl<sup>a†</sup>

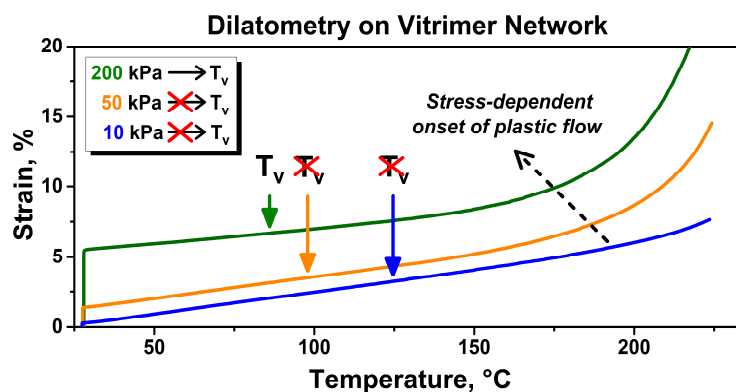
<sup>a</sup> Polymer Competence Center Leoben GmbH, Roseggerstrasse 12, A-8700 Leoben, Austria.

<sup>†</sup>E-mail: sandra.schloegl@pccl.at

<sup>b</sup> Institute of Materials Science and Testing of Polymers, Montanuniversitaet Leoben, Otto Glöckel-Strasse 2, A-8700 Leoben, Austria.

## 6.2 Abstract

Vitrimers are covalent adaptable networks that rely on associative bond exchange reactions. Along with the glass transition temperature, the service temperature of thermally activated vitrimers is strongly governed by the topology freezing transition temperature ( $T_v$ ), at which the covalent bond exchange reactions become significantly fast. Despite the vast number of developed vitrimer systems, there is a serious lack in direct methods for the determination of the  $T_v$ . In the present work, we highlight a versatile and facile measurement routine, which enables a precise estimation of the  $T_v$  in epoxy-acid vitrimers undergoing thermo-activated transesterifications. In particular, elongational creep of the networks is measured as a function of temperature and the applied stress. The results show that the onset temperature of the plastic flow regime is clearly stress-dependent, possibly leading to an inaccuracy of  $T_v$  data in the existing literature obtained from so-called dilatometry measurements. We demonstrate that with increasing external force on the specimens, the onset of macroscopic flow is gradually shifted to lower temperatures and approaches the accurate  $T_v$  of the material at a particular stress level. This behaviour is found in different epoxy-acid vitrimers with varying  $T_g$ . The data is in very good accordance with (theoretical)  $T_v$  values, which are reported in literature and were received from stress relaxation data, confirming the validity and equivalence of the method presented.



### 6.3 Introduction

Covalent adaptable networks (CANs) are a promising material class to combine the advantages of thermoplastics and thermosets.<sup>1</sup> An extraordinary type of CAN, coined vitrimers, was introduced by Leibler and co-workers in 2011.<sup>2</sup> Vitrimers are permanent yet dynamic networks that rely on an associative exchange mechanism of the covalent bonds. This ensures that the network connectivity in thermally triggered vitrimers is preserved at all temperatures, wherefore vitrimers do not undergo a gel-to-sol transition and in principle remain insoluble.<sup>3</sup> Despite being covalently cross-linked, the topology rearrangements render vitrimers (re)processable, recyclable, self-healable, and weldable.<sup>2,4-8</sup>

The viscoelastic properties of vitrimers are not only governed by the classical glass transition temperature ( $T_g$ ) but also by the topology freezing transition, with its temperature denoted as  $T_v$ .<sup>2</sup> The latter transition is a unique characteristic of vitrimers that distinguishes them not only from thermosets with permanent chemical bonds but also from CANs relying on a dissociative cross-link exchange mechanism. When heating vitrimers, the bond exchange reaction rate increases following the Arrhenius law, allowing the networks to flow macroscopically in an Arrhenian dependence with temperature and to fully relax stresses.<sup>2</sup> Since the associative exchange reactions are thermo-activated, the exchange reaction is quenched at temperatures below  $T_v$  and the network topology is essentially frozen. More precisely, the timescale of bond exchanges is then longer than the timescale of the observation. With increasing temperature, the topology rearrangements become significantly fast from  $T_v$ , and thereafter the gradual transition from a viscoelastic solid to a viscoelastic liquid occurs. The transition was described to resemble a classical  $T_g$ , since it is of continuous nature and shows a heating rate dependency.<sup>2</sup> The topology freezing transition temperature is governed by the density of (exchangeable) cross-links, the exchange reaction kinetics, the mobility of the polymer chains, and the abundance of reactive chemical functions.<sup>3</sup> Furthermore, and particularly in the case of transesterification-based vitrimers, the  $T_v$  and the temperature range of the transition are often controlled by the nature and content of a suitable catalyst.<sup>9</sup>

When it comes to a possible structural application of vitrimers, the onset temperature of distinctive bond exchange reactions (i.e.  $T_v$ ) and the corresponding macroscopic effects induced by an external force are of great importance, since they strongly affect the suitable service temperature of these materials. In polymer industry, a frequently encountered parameter for the estimation of the maximum service temperature of polymeric materials is the heat distortion temperature (HDT, ASTM D648 and ISO 75).<sup>10</sup> The HDT indicates the temperature at which a sample in a three-point bend test setup deflects by a preset value when exposed to a fixed load. However, to the best of our knowledge, this method has not yet been investigated in the context of vitrimers. Currently, the most common methods used to assess the  $T_v$  of vitrimers are stress relaxation, dilatometry, and creep experiments. These techniques are all based on the application of an external force. The further improvement of current analysis methods and the development of new ones to gain more detailed insight into the dynamics of vitrimers, especially regarding the intrinsic properties, is still of great interest to the community.<sup>11</sup> For instance, until recently there was no method for determining the  $T_v$  of vitrimers in static state. Ji et al. presented the contact force-free detection of the  $T_v$  using aggregation-induced-emission (AIE)

luminogens.<sup>12</sup> Following a doping of vitrimers with AIE luminogens, the change of the fluorescence of the luminogens was measured as a function of temperature and correlated with the topology freezing transition. The method allowed the authors not only to determine a  $T_v$  value in a direct way, but also to access a temperature range of the topology freezing transition, similar to classical  $T_g$  analysis. Apart from the work of Ji et al., the dynamics of vitrimers is commonly studied by stress relaxation experiments, either applying rheometry<sup>2,9</sup>, or using a dynamic mechanical analyser (DMA) in tensile mode<sup>13,14</sup> with static displacement. Conventionally, a viscosity equal to  $10^{12}$  Pa·s describes the liquid-to-solid transition of a glass-forming liquid.<sup>15,16</sup> Specifically valid for the classical epoxy-acid vitrimer of Leibler et al.<sup>2</sup>, following stress relaxation measurements at various (high) temperatures, the  $T_v$  could be determined from the respective Arrhenius plot for a relaxation time of  $10^6$  s. This correspondence between the viscosity and the relaxation time was obtained on the basis of the Maxwell relation  $\eta = G \cdot \tau^*$  (with  $G = 1$  MPa).<sup>9</sup> However, with this approach only theoretical  $T_v$  values are obtained because it is based on the extrapolation of experimental data acquired at temperatures well above  $T_v$ . Therefore, this procedure can rather be described as an indirect methodology to access the  $T_v$  of vitrimers.

A more direct route towards the determination of the  $T_v$  is dilatometry, which is regularly encountered in literature to monitor the topology freezing transition as a function of temperature and thereby confirming the existence of the solid-to-liquid transition in vitrimers.<sup>2,5,9,17–20</sup> In general, dilatometry provides a different perspective on the topology freezing transition of vitrimers compared to stress relaxation measurements, since the entire relevant temperature range of the transition (including the  $T_v$ ) is covered. Both dilatometry measurements and stress relaxation experiments are frequently conducted on the same material. Importantly, we have noticed profound discrepancies when comparing the  $T_v$  values obtained from these two testing methods. Table S1 in the supporting information provides an overview of publications and shows the respective values of  $T_v$  received either from dilatometry measurements or stress relaxation data. Considering these discrepancies, it could be assumed that dilatometry is more of a qualitative method confirming the transient nature of vitrimers, rather than giving accurate values for  $T_v$ . Nevertheless, the onset temperature of plastic flow in dilatometry curves is frequently labelled as  $T_v$  although significant stress relaxation already occurs at substantially lower temperatures. In this context it should also be mentioned that no clear evaluation method of the onset of plastic flow has been reported so far. In a typical dilatometry measurement, the elongational expansion behaviour of the sample is monitored over time applying a constantly increasing heat (e.g. 5 K/min) and a small stress to avoid buckling (mostly 10 kPa).<sup>9</sup> Pritchard et al. pointed out that the measurement method is often incorrectly referred to as dilatometry rather than creep compliance experiment.<sup>21</sup> The authors investigated the influence of stress on the onset of irreversible plastic flow, i.e. the transition from a viscoelastic solid to a viscoelastic liquid, at rising temperature and constant tensile stresses for the classical isotropic epoxy-acid vitrimer of Leibler et al. They concluded that the onset temperature is independent of the applied stress due to the thermally-controlled activity of the catalyst determining  $T_v$ , with the  $T_v$  being decoupled from external mechanical influences. It should be noted that only two different stresses (100 and 200 kPa) were applied in their experiments. No measurements were conducted going to lower stresses approaching the 10 kPa commonly used in literature, or even contact force-free measurement conditions (i.e. dilatometry).

When comparing the  $T_v$  with the data from Leibler et al.<sup>2,9</sup>, a significantly lower value was reported ( $\approx 100$  vs.  $\approx 200$  °C). Apparently, the results were compared with dilatometry measurements, which were conducted applying a stress of only 10 kPa. From the Arrhenius plot, Leibler et al. indeed have derived a  $T_v$  of about 100 °C for the material, which again demonstrates the discrepancy of  $T_v$  data already discussed above (see Table S1). Furthermore, no variation of the heating rate was performed, and the applied 5 K/min have to be considered as rather fast, since Leibler et al. have described a distinct heating rate dependency of the topology freezing transition on the basis of dilatometry experiments.<sup>2</sup>

In this paper, inspired by the work of Pritchard et al.<sup>21</sup>, we aim to conduct a more comprehensive study on the role of external force on the topology freezing transition and the estimation of the  $T_v$  in elongational creep experiments as a function of temperature and stress level. The studies were carried out on the two classical vitrimers of Leibler et al. and two further epoxy-acid vitrimers (Figure 1), all of them isotropic and amorphous in nature and well described in literature, using triazabicyclodecene (TBD) as the transesterification catalyst.<sup>2,9,12</sup> To further validate the method and illustrate its resolution capabilities in terms of slightly varying vitrification transition temperatures, DGEBA-Prisol 1040 networks with different catalyst quantity (5 and 10 mol% of TBD) and type of catalyst (TBD and zinc acetate) were studied. The topology freezing transition temperatures obtained are compared with the values for  $T_v$  reported in literature. The results suggest that an accurate estimation of  $T_v$  from elongational creep measurements at rising temperature is feasible for epoxy-acid vitrimers. We found that the onset temperature of the solid-to-liquid transition is clearly force-dependent. By gradually increasing the stress on the sample, the onset is shifted to a temperature suggesting a  $T_v$  in accordance with the theoretical value obtained through stress relaxation measurements. For the high- $T_g$  vitrimer, composed of DGEBA and glutaric anhydride, however, a less pronounced force dependency was found.

Besides the  $T_v$ , we were also able to show the role of external force in the context the thermal expansion coefficient (CTE) of vitrimers by using optical thermal strain analysis based on digital image correlation (DIC) under contact force-free conditions. In static state, the investigated vitrimers show no change of the CTE in the temperature range of  $T_v$ , which is in striking contrast to what is reported in literature.<sup>2,9</sup>

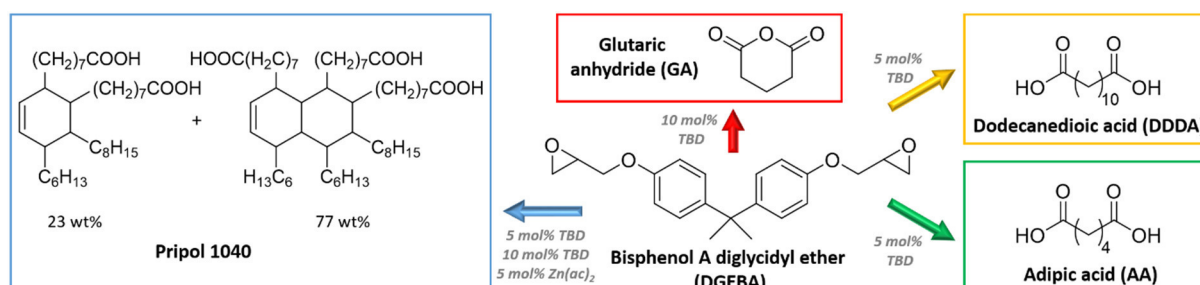


**Figure 1** – Selected epoxy-acid vitrimers with varying  $T_g$  used for elongational creep experiments and optical thermal strain measurements in the present study.

## 6.4 Results and discussion

### *Stress-dependent onset of the plastic flow in epoxy-acid vitrimers*

The well characterised epoxy-acid vitrimer introduced by Leibler and co-workers was used as model system for the first test series.<sup>2</sup> The network was synthesised from diglycidyl ether of bisphenol A (DGEBA) and a mixture of dicarboxylic and tricarboxylic fatty acids (Pripol 1040), with the carboxylic acid functions and the epoxy groups in stoichiometry. On the example of 5 mol% (related to the COOH groups) of 1,5,7-triazabicyclo[4.4.0]dec-5-ene (TBD) as transesterification catalyst, elongational creep experiments were performed applying stresses of 10 and 100 kPa. 10 kPa are usually applied in literature to avoid buckling and 100 kPa is in the range of stresses which have been examined by Pritchard et al. in their creep experiments.<sup>21</sup> Moreover, the elongational creep was measured at two heating rates (1 and 3 K/min), since the vitrification transition was reported to be heating rate dependent.<sup>2</sup>

The effect of different stresses and of the variation of the heating rate on the creep behaviour and onset of plastic flow at increasing temperature are shown in Figure 2a. The application of the stress at 27 °C induces an instantaneous strain, which increases with the applied load. After that, with rising temperature, the measurement curves show a distinctive steady-state region in strain comprising thermal expansion, stress-dependent creep, and entropy-elastic processes. At a certain temperature, the data deviates from this nearly linear behaviour. We consider this point as the onset of the irreversible plastic flow regime, where chemical bond exchanges become macroscopically apparent due to the loss of cross-links contributing to the material's elasticity. Beyond this point the sample changes gradually to the state of plastic flow and the strain increases rapidly with temperature and stress, indicating the transition from a viscoelastic solid to a viscoelastic liquid. This is due to the molecular network rearrangements, which in the vitrimer under investigation are a result of thermo-activated and catalytically controlled transesterifications. In the context of vitrimers and dilatometry, this temperature is usually denoted as the topology freezing transition temperature,  $T_v$ .<sup>9</sup>

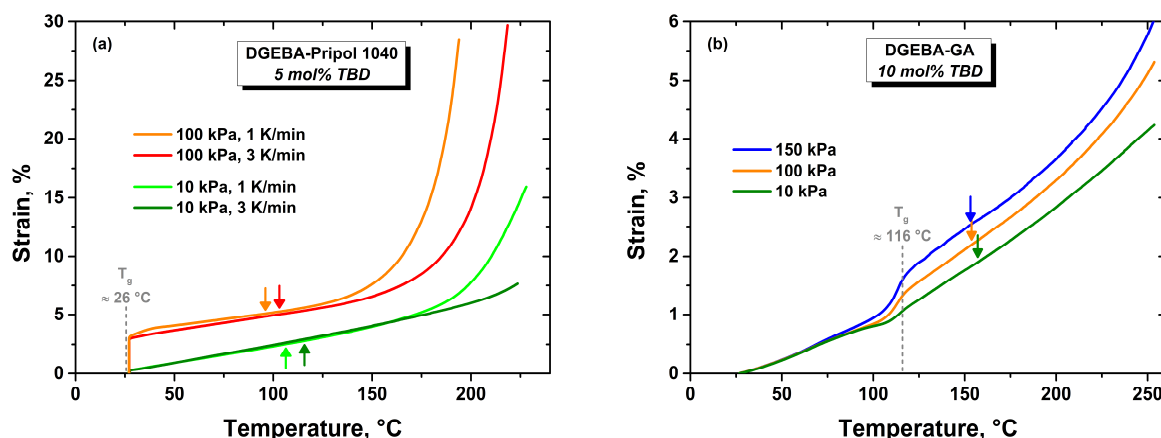


**Figure 2** – Elongational creep curves of the (a) DGEBA-Pripol 1040 vitrimer (containing 5 mol% of TBD related to the COOH groups) and (b) DGEBA-GA vitrimer (containing 10 mol% of TBD related to the acyl groups) obtained at various stress levels and heating rates of 1 and 3 K/min. The arrows indicate the respective onset of plastic flow.

The proper analysis of the onset temperature of plastic flow of the creep data is challenging due to the continuous changes in the measurement curves. Therefore, simply fitting a straight line to the only approximately linear parts of the curve followed by the analysis of the first deviation of the creep data from this extrapolated straight line does not appear sufficient. However, this is usually the practice found in literature.<sup>2,5,9,17–19,21–24</sup> With this method the identification of an accurate temperature value for the onset of the plastic flow regime is already strongly governed by the selection of the relevant (non-linear) data range within a particular creep curve that is considered for the linear fit. The selection has a significant influence on the slope of the obtained straight line, so that the criterion of deviation from linearity does not appear to be suitable for determining the onset temperature. In addition, the temperature range of this nearly linear region changes considerably with the external force applied on the sample and also with the type of material, which leads to a distinct user dependency in the data analysis. While building a physical model to fit the data was beyond the scope of this work, a mathematical approach has been defined and applied to all elongational creep measurements conducted in order to systematically process and evaluate the creep data. Based on an exponential fitting of the data, the criteria defined in this mathematical concept facilitate a consistent analysis of the onset temperatures of plastic flow of the creep curves, especially within the measurement series of a particular material, which is of great importance to reliably identify eventual trends. Furthermore, the method enables the comparability of the acquired  $T_v$  values of the different materials under investigation by minimising the user influence in the selection of the relevant part of the measurement data by considering the entire data of the creep curves. The established analysis method is described in detail in the experimental part and further graphically displayed in Figure 8.

From the creep data of the TBD-catalysed DGEBA-Prisol 1040 network, it can be derived that there is a shift of the onset of plastic flow to lower temperatures with decreasing heating rate. This is in accordance with the heating rate dependency of the  $T_v$  already described in literature.<sup>2</sup> However, the extent of the shift decreases with the stress level. Along with the heating rate, the results further reveal that the applied stress influences the onset temperature of plastic flow. When comparing the creep curves for 10 and 100 kPa at a heating rate of 3 K/min, the onset deviates by 22 °C. This is in contrast to the independence of the onset from the applied stress previously reported for the same vitrimer.<sup>21</sup> The authors conducted measurements at 100 and 200 kPa, but did not investigate loads lower than 100 kPa, for which we find a strong shift of the onset to higher temperature.<sup>21</sup>

We further studied the other classical vitrimer of Leibler et al. The “hard” network was synthesised from DGEBA and glutaric anhydride (GA), with the epoxy groups and the acyl groups in stoichiometry and in the presence of 10 mol% (related to the acyl groups) of TBD as transesterification catalyst. Screening a series of elongational stresses, signatures for  $T_g$  and the topology freezing transition were detected. The material was not able to withstand stresses higher than 150 kPa. In this high- $T_g$  vitrimer, the shift in the onset of plastic flow to lower temperature is less pronounced with increasing load compared to the more flexible epoxy-acid network and the  $T_v$  is 153 °C, measured at 150 kPa (Figure 2b).

The data suggest that the onset of plastic flow is indeed shifting to lower temperatures with increasing external force, levelling at a certain characteristic temperature. We



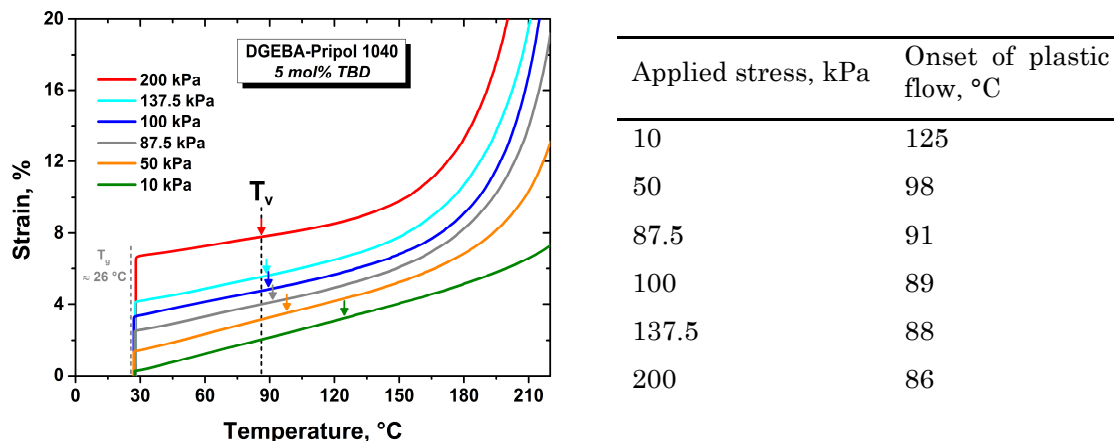


**Figure 3** – Elongational creep curves of the DGEBA-Prisol 1040 vitrimer comprising 5 mol% (related to the COOH groups) of TBD as transesterification catalyst for various stresses at a heating rate of 3 K/min. The arrows indicate the respective onset of plastic flow.

hypothesise that this temperature corresponds to the  $T_v$  of a particular vitrimer, reflected by the macroscopically emerging onset of the transition from a viscoelastic solid to a viscoelastic liquid. In the following, we verify the correctness of this assumption by systematically studying a variety of vitrimers by conducting elongational creep measurements at various stresses.

#### *Accurate estimation of the $T_v$ in epoxy-acid vitrimers by selecting suitable measurement conditions*

To confirm this hypothesis, a more detailed analysis of the DGEBA-Prisol 1040 vitrimer with 5 mol% TBD was conducted. Stresses ranging from 10 to 200 kPa were applied to the specimens and the obtained elongational creep curves are displayed in Figure 3. It should be noted that the material was not able to withstand stresses higher than 200 kPa.

The slope (i.e. creep rate) of the measurement curves in the region of nearly linear steady-state creep decreases slightly with increasing stress. This is due to a more pronounced entropic rubber-elastic contraction upon heating for samples with a higher instantaneous strain after applying the particular stress. Going from 10 to 50 kPa the onset temperature of plastic flow shifts strongly from 125 to 98 °C. With a further increase in stress to 87.5 kPa the onset continues to shift to 91 °C. Interestingly, if the stress exceeds 87.5 kPa, the onset shifts only slightly to lower temperatures and appears to reach a limit temperature. Table 1 summarises the onset temperatures derived from Figure 3.

From the data, we deduce that by going to a sufficiently high stress in elongational creep experiments the onset temperature of plastic flow of this vitrimer levels at about 86 °C, which is considered as the  $T_v$  of the material. Apparently, from a certain level of strain, the onset of plastic flow is solely controlled by thermally activated and catalytically controlled bond exchange reactions and is not further sensitive to the external force. We assume that a certain degree of pre-stretching (i.e. adequate stress level) of the sample is required to identify already small changes (i.e. cross-link exchanges) at the molecular level due to network rearrangements using a macroscopic testing method. While at small strains no signature in the creep curve emerges until the exchange reaction kinetics is

already fast, high pre-stretching promotes entropy-elastic effects, which could interfere with a precise detection of the  $T_v$ . It seems obvious that rather “hard” vitrimers (see Figure 2b) with a high Young's modulus as a result of a high cross-link density exhibit a less pronounced stress dependency of the onset of plastic flow. Such networks are subject to comparatively high strains already at low stresses due to their overall low elasticity, and energy-elastic behaviour dominates over entropy elasticity even above  $T_g$ .<sup>25</sup> Thus, already at low strains a reasonable degree of pre-stretching is given. The  $T_v$  of the investigated epoxy-acid vitrimer with 5 mol% of TBD was previously reported to be approximately 97 °C.<sup>9</sup> The authors determined this value from the Arrhenius plot based on shear stress relaxation experiments. Therefore, we conclude that the selection of suitable measurement conditions in elongational creep experiments indeed enables the direct and accurate determination of  $T_v$  for the vitrimer under investigation.

For a similar vitrimer with zinc acetate instead of TBD as the catalyst, dilatometry measurements at 10 kPa revealed a  $T_v$  higher than 200 °C, while shear stress relaxation data gave about 83 °C.<sup>9</sup> Thus, the discrepancy between the values of  $T_v$ , on the one hand determined by stress relaxation experiments and, on the other hand obtained from dilatometry measurement at small stress, vanishes if adequate measuring conditions are applied. In other words, when performing elongational creep experiments at small stresses the detection of the topology freezing transition is more of qualitative nature, since the values for the onset of plastic flow may differ strongly from the  $T_v$  values derived from stress relaxation data (see Table S1).

#### *Influence of catalyst type and quantity on the onset of plastic flow in epoxy-acid vitrimers*

We further investigated the effect of the amount and type of catalyst on the vitrification transition in elongational creep measurements. To validate our test method, we prepared a DGEBA-Pripol 1040 network containing 10 mol% (related to the COOH groups) of TBD. To demonstrate the dependency of the onset temperature of plastic flow on the external force, measurements were conducted at various stresses starting from 10 kPa. A similar

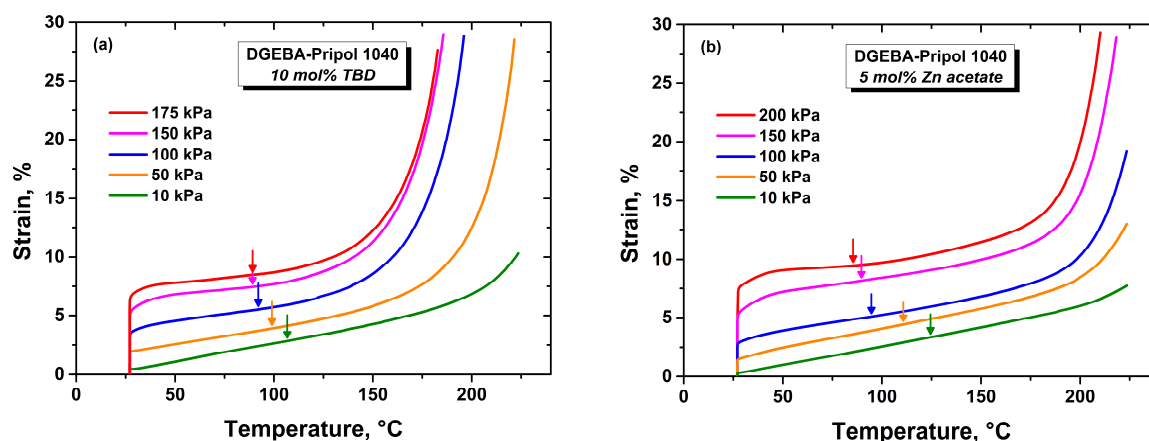


**Figure 4** – Elongational creep curves for a series of stresses at a heating rate of 3 K/min of the DGEBA-Pripol 1040 vitrimer containing (a) 10 mol% of TBD and (b) 5 mol% of zinc acetate (related to the COOH groups in each case) as transesterification catalyst. The arrows indicate the respective onset of plastic flow.

trend as for the network containing 5 mol% of TBD is found, involving a shift in the onset to lower temperature with increasing stress (Figure 4a). Also for this material, entropic rubber-elastic contraction upon heating is more pronounced for higher stress levels, resulting in a decrease of the rate in steady-state creep. The DGEBA-Pripol 1040 vitrimer with 10 mol% TBD shows a shift of the onset of plastic flow from 106 °C for 10 kPa to 89 °C when measuring with 175 kPa. It should be noted that the specimens were not able to withstand stresses higher than 175 kPa. The shift occurs gradually and the extent decreases with the stress, approaching a limit temperature from stresses of 150 kPa. The  $T_v$  of this network is about 89 °C, measured at 175 kPa. Moreover, derived from shear stress relaxation experiments, Leibler et al. reported a decrease in  $T_v$  from about 97 to 83 °C for the DGEBA-Pripol 1040 network when using 5 mol% of zinc acetate instead of 5 mol% TBD as transesterification catalyst.<sup>9</sup> Accordingly, we also performed elongational creep measurements on DGEBA-Pripol 1040 with 5 mol% of zinc acetate at various stresses (Figure 4b). The results clearly show that the onset temperature of the vitrification transition is shifted gradually to lower temperature with increasing stress and reaches a limit temperature of 85 °C when applying 200 kPa (samples were not able to withstand stresses higher than 200 kPa). This temperature is considered as the  $T_v$  of the material.

Both of these variations in the network composition confirm that the method is applicable for determining the onset temperature of the plastic flow regime ( $T_v$ ) in a direct way. We would like to point out that measurements applying 10 kPa result in completely different and obviously wrong values for  $T_v$  – for 10 mol% TBD: 106 vs. 89 °C; for 5 mol% Zn acetate: 124 vs. 85 °C. Ji et al. stated that the  $T_v$  is an intrinsic property of a network and thus independent of the catalyst loading.<sup>12</sup> Nevertheless, it should be considered that curing with either zinc acetate or TBD as well as varying catalyst quantities most likely affects the network structure and thus, the topology freezing transition.

#### *Applicability of the method to other epoxy-acid vitrimers*

To demonstrate the general applicability of the method we investigated two additional epoxy-acid vitrimers. The networks were synthesised from DGEBA and adipic acid as well as from DGEBA and dodecanedioic acid as previously reported in literature<sup>5,12</sup>, again with 5 mol% (related to the COOH groups) of TBD as transesterification catalyst.

Figure 5 displays the elongational creep measurements of these two materials, conducted at various stresses and a heating rate of 3 K/min. The samples were not able to withstand stresses exceeding 150 kPa and 70 kPa, respectively. Starting from 10 kPa, the DGEBA-adipic acid network (Figure 5a) shows the familiar distinctive shift of the onset temperature of plastic flow to lower temperature with increasing stress. Since the load is applied well below  $T_g$  the typical curve characteristic emerges when approaching  $T_g$ . At stresses higher than 100 kPa no further shift is observed and a limit temperature is reached. This temperature amounts to about 85 °C and corresponds to the  $T_v$  of the material according to our definition. For this network, the creep curves reveal a distinctive entropic rubber-elastic contraction with increasing stress and upon heating, resulting in a negative steady-state creep region. Due to this effect, the onset of plastic flow slightly shifts to higher temperatures for stresses exceeding 100 kPa. Thus, the minimum onset

temperature (i.e.  $T_v$ ) is not obtained at the maximum applicable external force but already before.

Going from DGEBA-adipic acid to DGEBA-dodecanedioic acid (Figure 5b) a similar picture is obtained. Again, the typical large shift of the onset of plastic flow to lower temperatures with increasing stress is found, when comparing the creep curves from 10 to 50 kPa. Similarly as for the network cured with adipic acid, the minimum onset temperature is not observed at the highest stress but undergoes a minimum at 60 kPa and shifts to a slightly higher temperature for 70 kPa. This can be attributed to the strong entropic rubber-elastic contraction of the material causing negative creep, superimposing the stress-induced shifting effect of the onset of plastic flow at this particular stress level. However, the shift is very small and according to our interpretation the  $T_v$  of this vitrimer is about 72 °C, measured at 60 kPa.

Using AIE luminogens, Ji et al. detected topology freezing transition temperatures of 102 and 82 °C for the networks with adipic acid and dodecanedioic acid, respectively.<sup>12</sup> It should be noted, that Ji's method allows to detect a  $T_v$  value and a  $T_v$  range. The values mentioned above correspond to the  $T_v$  values, while the onsets of the respective  $T_v$  ranges were reported to amount to 85 and 65 °C. For both investigated materials the found values of  $T_v$  correlate well with the data reported by Ji et al.<sup>12</sup> We would like to emphasise that also for these two networks elongational creep measurements applying 10 kPa result in wrong values for  $T_v$  – for DGEBA-adipic acid: 132 vs. 85 °C; for DGEBA-dodecanedioic acid: 95 vs. 72 °C.

It is reasonable to assume that the minimum onset temperature of plastic flow in our creep measurements corresponds to the onset of associative bond exchange reactions in the network. At least to the point at which the topology rearrangements become macroscopically apparent under external force, which is crucial for the possible practical application of vitrimers. Thus, the minimum onset temperatures of the different measurement series are designated as the respective topology freezing transition temperatures,  $T_v$ . At lower temperatures, the macroscopic network architecture is

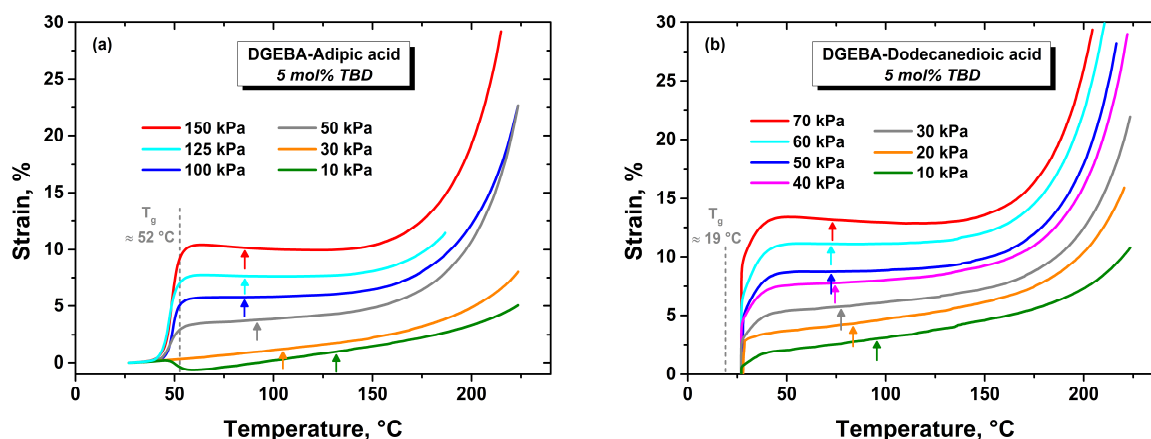


**Figure 5** – Elongational creep curves for a series of stresses at a heating rate of 3 K/min of the (a) DGEBA-adipic acid and (b) DGEBA-dodecanedioic acid vitrimer with 5 mol% (related to the COOH groups) of TBD as transesterification catalyst. The arrows indicate the respective onset of plastic flow.

essentially fixed, although transesterifications are likely to occur already, albeit at a very small rate.

Figure 6 summarises the onset temperatures of plastic flow as a function of the applied stress for the different vitrimers under investigation. Networks from DGEBA and Pripol 1040 with TBD or zinc acetate as catalyst approach a limit temperature ( $T_v$ ) with increasing stress. The networks cured with adipic acid or dodecanedioic acid in the presence of TBD, however, exhibit a minimum onset temperature ( $T_v$ ) of plastic flow at 100 and 60 kPa due to entropic elasticity effects. The high- $T_g$  vitrimer from DGEBA and glutaric anhydride also follows this typical behaviour with increasing stress, but to a lower extent, and a good estimation of  $T_v$  is already possible at a stress of 10 kPa.

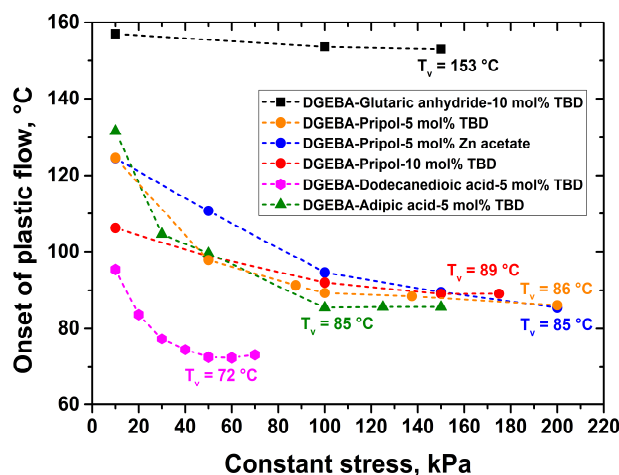


**Figure 6** – Stress dependency of the onset temperature of plastic flow for the investigated vitrimers determined from elongational creep measurements at various constant stresses and increasing temperature (3 K/min).

#### *Investigation of the coefficient of thermal expansion in vitrimers by thermal strain analysis relying on DIC*

In literature it is stated that the topology freezing transition in vitrimers causes an increase in the coefficient of thermal expansion (CTE) because a reorganising network is supposed to have a higher CTE than the respective static network.<sup>2,3,9</sup> This is indicated by a rise of the measurement curve when monitoring the length change of a sample in tensile mode as a function of temperature and time at constant stress. This measurement method is commonly referred to as dilatometry.<sup>2,3,9,17–19,24</sup> Apparently, this statement regarding the CTE was based on dilatometry applying small stresses (e.g. 10 kPa), since – to the best of our knowledge – no contact force-free dilatometry measurement in static state in the context of vitrimers has been reported yet.

Ideally, dilatometry measurements should be performed with a sample that can move freely without any mechanical constraints for the exact characterisation of dimensional changes of the sample as a function of temperature. The grey creep curve of the DGEBA-Pripol network with 5 mol% of TBD displayed in Figure 7a was carried out under the classical dilatometry conditions (10 kPa, 5 K/min) found in literature. Other groups applied a heating rate of 3 K/min with a load of 10 kPa.<sup>17,19</sup> These measurement conditions

are reflected by the orange curve in Figure 7a. A key observation of the herein performed elongational creep measurements is that at small stresses no conclusions can be drawn regarding the precise  $T_v$  of the material, as discussed above. Thus, measuring at small stresses only allows for a qualitative demonstration of the existence of the vitrification transition of a certain vitrimer. Going to very low stresses, the creep measurements approach static state dilatometry. For this reason, we were interested in creep measurements applying a stress smaller than 10 kPa. The green and blue creep curves in Figure 7a were measured at 1 kPa and a heating rate of 3 and 1 K/min, respectively. Under these conditions a linearly increasing expansion is observed up to a temperature of at least 150 °C, and it hardly changes afterwards.

Derived from this data we assumed that the topology freezing transition might not show any signature in a contact force-free dilatometry measurement. Consequently, we conducted optical thermal strain measurements using digital image correlation (DIC) to determine strains without the interference of external force. Figure 7b shows the optical thermal strain data for the different vitrimers that were previously investigated in this work by elongational creep measurements. The curves were recorded using a heating rate of 1 K/min and represent the average value of the strains in  $x$  and  $y$  direction, which is possible because all materials exhibit an isotropic expansion behaviour.

The curves of the networks with a  $T_g$  well above room temperature show a clear signature in the region of the classical glass transition, and a linearly increasing expansion thereafter is detected for the entire measured temperature range for all networks. Interestingly, for none of the vitrimers an increase in strain, i.e. of the CTE, is observed in the proximity of  $T_v$ . The marked  $T_v$  values were derived from the elongational creep measurements conducted in this paper and the  $T_g$  values from DMA experiments. We conclude that the observed plastic flow of a vitrimer from  $T_v$  is strictly a response to external force. The small stresses usually applied in dilatometry measurements are already high enough to cause an increase in strain of specimens at the topology freezing transition. Without applying any

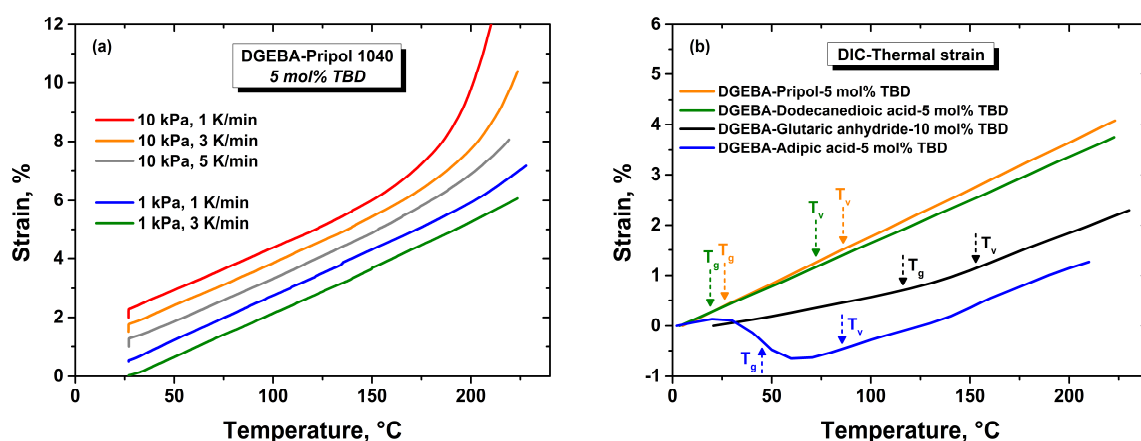


**Figure 7** – (a) Elongational creep curves for the DGEBA-Prisol 1040 network with 5 mol% of TBD at stresses of 1 and 10 kPa under variation of the heating rate. (b) Digital image correlation (DIC) thermal strain data of the different vitrimers investigated in the framework of this paper. Measurements were carried out with a heating rate of 1 K/min and the data represent the average value of the expansions in  $x$  and  $y$  direction.

external force, dynamic network characteristics of a sample could remain undetected. This illustrates the importance of applying an external force in elongational creep measurements of vitrimers to obtain a signature from thermo-activated bond exchange reactions. Furthermore, only the application of the proper stress allows for an accurate estimation of the  $T_v$ , which solely in this case makes elongational creep experiments an equivalent alternative to stress relaxation measurements or the usage of AIE luminogens.

## 6.5 Experimental

### *Materials and chemicals*

Diglycidyl ether of bisphenol A (abcr, Karlsruhe, Germany), Pripol 1040 (Croda, Snaith, UK), dodecanedioic acid (Sigma-Aldrich, St. Louis, USA), adipic acid (BASF, Ludwigshafen, Germany), glutaric anhydride (Sigma-Aldrich), 1,5,7-triazabicyclo[4.4.0]dec-5-ene (Sigma-Aldrich), and zinc acetate dihydrate (Sigma-Aldrich) were used as received without further purification.

### *Preparation of epoxy vitrimers*

Vitrimer networks from diglycidyl ether of bisphenol A (DGEBA) and Pripol 1040 or glutaric anhydride using either zinc acetate dihydrate or triazabicyclodecene as catalyst were synthesised according to the procedures previously reported by Leibler et al.<sup>2,9</sup> Networks from DGEBA and dodecanedioic acid or adipic acid were synthesised as previously reported by Ji et al.<sup>12</sup> The indicated quantities of catalyst refer to  $x$  mol% relative to the carboxylic acid functions or acyl groups.

### *Elongational creep measurements*

The elongational creep behaviour was measured using an Anton Paar (Graz, Austria) modular compact rheometer MCR 702 MultiDrive in uniaxial tensile mode. The measurements were performed on rectangular samples with a width of 10 mm and a thickness of 1.5–2.5 mm at a clamping length of 30 mm. During temperature equilibration at 27 °C the specimens were held unloaded before the desired stress was applied instantaneously and kept constant for the duration of the experiment. Depending on the particular vitrimer network, the various constant tensile stresses ranged from 10 to 200 kPa. The measurements were conducted from 27 to 230 °C at heating rates of 1 and/or 3 K/min and the corresponding strain profiles were recorded as a function of temperature.

Regarding the analysis of the onset temperature of the plastic flow regime of the creep curves, the following mathematical approach was defined and applied to all elongational creep measurements conducted in this paper. Figure 8 displays the procedure on the example of the DGEBA-Pripol 1040 vitrimer with 5 mol% of TBD (see also Figure 3). ① Fitting of an exponential function to the relevant portion (load application has been omitted) of data points (about 600 per measurement curve) of the creep curve using a 5th-order Gaussian approximation. This Gaussian model is a linear combination of exponential functions with three independent and freely adjustable variables. Afterwards, a curve analysis based on the first, second, and third derivative of the exponential function follows. In each step a certain tolerance criterion is applied for the progressive reduction

of the primary data set. The specific values of the derivatives 1, 2, and 3 are displayed in Figure S1 in ESI, and the data points marked in pink in Figure 8 correspond to the creep data whose derivative(s) have fulfilled the respective tolerance criteria. ② Formation of the first derivative and determination of data points with similar slope that obey the tolerance (Data set 1). ③ Formation of the second derivative and determination of data points within tolerance (Data set 2). ④ Formation of the third derivative and determination of data points within tolerance (Data set 3). ⑤ Calculation

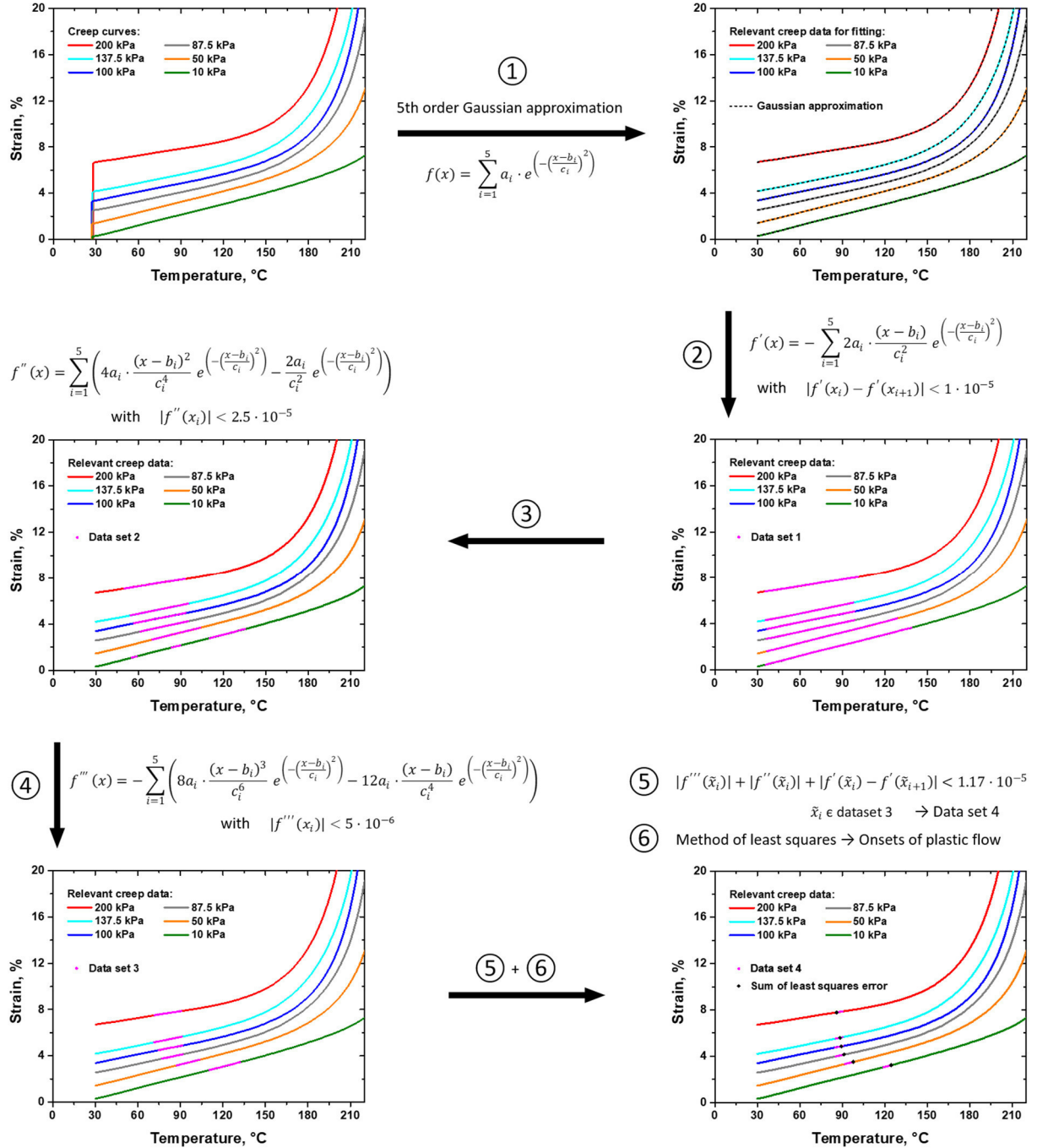


**Figure 8** – Illustration of the defined mathematical analysis procedure applied in the determination of the onset temperature of the plastic flow regime in elongational creep measurements of epoxy-vitrimers on the example of the DGEBA-Pripol 1040 network with 5 mol% of TBD (see also Figure 3).



of the least squares error from steps ②-④ for data points of Data set 3 and determination of data points that obey the tolerance (Data set 4). The error estimation was based on the L2 norm, which is a standard method in error analysis.<sup>26</sup> ⑥ Determination of the data point from Data set 4 for which the least squares error of steps ②-④ is minimal. This data point then corresponds to the onset temperature of plastic flow of the respective creep curve according to our definition, and the minimum onset temperature within a series of stresses for a particular vitrimer network is considered as its  $T_v$ . It should be noted that Data set 2 is included in Data set 1, Data set 3 in Data set 2, and Data set 4 in Data set 3. Moreover, the specified tolerances were chosen such that for each load level of the respective material a data set was found satisfying an error accuracy that was as small as possible. The defined tolerances vary slightly for the different materials under investigation.

### *Optical thermal strain measurements*

The optical thermal strain measurements were conducted on a Dantec Q400 (Dantec Dynamics A/S, Skovlunde, Denmark). This device relies on the principle of digital image correlation (DIC) to detect thermally induced strains on the specimen.<sup>27,28</sup> The samples (length: 20 mm, width: 20 mm, thickness: 1.5–2.5 mm) were coated with a random speckle pattern, which enables displacement tracking *via* a stereoscopic camera system. First, all samples were treated with a white primer to establish a non-reflective surface, and subsequently the speckle pattern was applied using a black graphite aerosol lacquer. The measurements were performed from 5 to 220 °C with a heating rate of 1 K/min and an image acquisition frequency of 1 Hz. The detected strains were evaluated over the entire measurement area providing an averaged strain in  $x$  and  $y$  direction for each sample. The gathered data was post-processed using a cubic smoothing spline to reduce noise within the full-field strain measurement. As the strains in the  $x$  and  $y$  directions clearly indicated an isotropic expansion behaviour for all investigated materials the two directions were averaged.

### *Dynamic mechanical analysis*

The indicated glass transition temperatures ( $T_g$ ) of the different vitrimer networks under investigation were derived from DMA measurements that were performed on a Mettler Toledo (Columbus, USA) SDTA61 dynamic mechanical analyser in tensile mode. Rectangular samples with a width of 3.0 mm and a thickness of 1.5–2.5 mm at a clamping length of 9.0 mm were tested in displacement controlled oscillation of 2.5  $\mu\text{m}$  amplitude at 1 Hz. Heating ramps were applied at 2 K/min from -50 to 230 °C.

## **6.6 Conclusions**

The analysis of the (intrinsic) topology freezing transition temperature ( $T_v$ ), which is the key characteristic of vitrimers, is not readily accessible by a simple and accurate method yet, as it is the case for the glass transition temperature ( $T_g$ ) with differential scanning calorimetry (DSC) or dynamic mechanical analysis (DMA). Moreover, the classical dynamic analytical methods commonly employed, stress relaxation and dilatometry,

mostly yield quite different results. This becomes apparent when comparing corresponding  $T_v$  values reported in literature. Led by these discrepancies, we aimed to gain new insights into the direct analysis of precise  $T_v$  values of vitrimers using elongational creep measurements at increasing temperature.

We systematically investigated the creep behaviour of several epoxy-acid vitrimers and worked out the importance of external force when it comes to the estimation of an accurate value for the  $T_v$ . Applying a series of stresses, the data clearly show a stress-dependent onset temperature of plastic flow in the creep curves. The onset either levels at a certain lower limit temperature or undergoes a minimum temperature. These temperatures then correspond to the  $T_v$  of the respective material. Comparison of our data with reported values for  $T_v$  derived from stress relaxation measurements (and the respective Arrhenian plots) or from the application of AIE luminogens confirm the validity of our findings. We would like to point out that only for the selection of suitable measurement conditions, which is an appropriate external force, elongational creep experiments allow the direct and precise detection of  $T_v$  values in accordance with the theoretical data derived from stress relaxation experiments. In any other case, elongational creep curves serve only for a qualitative representation of occurring topology rearrangements, displayed at temperatures well above  $T_v$ . We attribute this to the prerequisite of a certain degree of pre-stretching of a sample to reveal macroscopically the onset of thermo-activated associative bond exchange reactions. Hence, in practice, a screening of stresses is necessary for the correct estimation of the minimum onset temperature of plastic flow ( $T_v$ ), similar to the approach using stress relaxation. It should be noted that the present strategy does not describe the intrinsic properties of the vitrimer networks under investigation, but that the  $T_v$  values identified are rather influenced by the test parameters (external force, heat rate).

At this stage, the present study covers isotropic and amorphous (epoxy-acid) vitrimers. Further research work could include semi-crystalline vitrimers and vitrimeric composites to validate the applicability of the present method towards the analysis of  $T_v$  in these materials. And whether certain discrepancies and limitations exist for such more complex networks similar, for instance, to the case of glass transition temperature and heat distortion method (HDT).<sup>10</sup>

The crucial role of external force in the context of the properties of vitrimers was also highlighted in the determination of the coefficient of thermal expansion (CTE). By going to contact force-free measurement conditions applying digital image correlation (DIC) thermal strain analysis, our data showed no signature in the region of the  $T_v$ . In static state, for none of the vitrimers under investigation the CTE increased at or beyond  $T_v$ . Thus, the increase in strain observed in elongational creep measurements (i.e. dilatometry in literature) can solely be attributed to the applied external force, even if it is very small.

We hope that our results could increase the understanding of dilatometry and elongational creep experiments as a function of temperature in the context of vitrimers, and demonstrate the potential of these analysis methods in terms of networks comprising dynamic covalent bonds.

## 6.7 Acknowledgements

The research work was performed within the COMET-Module “Chemitecture” (project-no.: 21647048) at the Polymer Competence Center Leoben GmbH (PCCL, Austria) within the framework of the COMET-program of the Federal Ministry for Transport, Innovation and Technology and the Federal Ministry for Digital and Economic Affairs with contributions by the Institute of Materials Science and Testing of Polymers (Montanuniversitaet Leoben, Austria). The PCCL is funded by the Austrian Government and the State Governments of Styria, Upper and Lower Austria. In addition, the authors thank Anton Paar (Graz, Austria) for providing the modular compact rheometer MCR 702 MultiDrive for elongational creep measurements.

## 6.8 References

- 1 Kloxin C.J., Bowman C.N., *Chem. Soc. Rev.* 42 (17) (2013) 7161–7173.
- 2 Montarnal D., Capelot M., Tournilhac F., Leibler L., *Science* 334 (6058) (2011) 965–968.
- 3 Denissen W., Winne J.M., Du Prez F.E., *Chem. Sci.* 7 (1) (2016) 30–38.
- 4 Capelot M., Montarnal D., Tournilhac F., Leibler L., *J. Am. Chem. Soc.* 134 (18) (2012) 7664–7667.
- 5 Yang Y., Pei Z., Zhang X., Tao L., Wei Y., Ji Y., *Chem. Sci.* 5 (9) (2014) 3486–3492.
- 6 Denissen W., Rivero G., Nicolaÿ R., Leibler L., Winne J.M., Du Prez F.E., *Adv. Funct. Mater.* 25 (16) (2015) 2451–2457.
- 7 Liu T., Hao C., Zhang S., Yang X., Wang L., Han J., et al., *Macromolecules* 51 (15) (2018) 5577–5585.
- 8 Kaiser S., Wurzer S., Pilz G., Kern W., Schögl S., *Soft Matter* 15 (30) (2019) 6062–6072.
- 9 Capelot M., Unterlass M.M., Tournilhac F., Leibler L., *ACS Macro Lett.* 1 (7) (2012) 789–792.
- 10 Takemori M.T., *Polym. Eng. Sci.* 19 (15) (1979) 1104–1109.
- 11 Van Zee N.J., Nicolaÿ R., *Prog. Polym. Sci.* 104 (2020) 101233.
- 12 Yang Y., Zhang S., Zhang X., Gao L., Wei Y., Ji Y., *Nat. Commun.* 10 (1) (2019) 3165.
- 13 Yang Y., Terentjev E.M., Wei Y., Ji Y., *Nat. Commun.* 9 (1) (2018) 1906.
- 14 Yu K., Taynton P., Zhang W., Dunn M.L., Qi H.J., *RSC Adv.* 4 (89) (2014) 48682–48690.
- 15 Dyre J.C., *Rev. Mod. Phys.* 78 (3) (2006) 953–972.
- 16 Angell C.A., *Science* 267 (5206) (1995) 1924–1935.
- 17 Liu Y., Tang Z., Chen Y., Zhang C., Guo B., *ACS Appl. Mater. Interfaces* 10 (3) (2018) 2992–3001.
- 18 Wu S., Yang Z., Fang S., Tang Z., Liu F., Guo B., *J. Mater. Chem.* 7 (4) (2019) 1459–1467.
- 19 Xu C., Cui R., Fu L., Lin B., *Compos. Sci. Technol.* 167 (2018) 421–430.
- 20 Yang Z., Wang Q., Wang T., *ACS Appl. Mater. Interfaces* 8 (33) (2016) 21691–21699.
- 21 Pritchard R.H., Redmann A.-L., Pei Z., Ji Y., Terentjev E.M., *Polymer* 95 (2016) 45–51.

- 22 Niu X., Wang F., Li X., Zhang R., Wu Q., Sun P., *Ind. Eng. Chem. Res.* 58 (14) (2019) 5698–5706.
- 23 Tang Z., Liu Y., Guo B., Zhang L., *Macromolecules* 50 (19) (2017) 7584–7592.
- 24 Feng Z., Hu J., Zuo H., Ning N., Zhang L., Yu B., et al., *ACS Appl. Mater. Interfaces* 11 (1) (2019) 1469–1479.
- 25 Rösler J., Bäker M., Harders H., *Mechanical Behaviour of Engineering Materials: Metals, Ceramics, Polymers, and Composites*, Springer-Verlag Berlin Heidelberg, Berlin, Heidelberg, 2007.
- 26 Farebrother R.W., *Visualizing Statistical Models and Concepts*, Dekker, New York, 2002.
- 27 Chu T.C., Ranson W.F., Sutton M.A., *Exp. Mech.* 25 (3) (1985) 232–244.
- 28 Pan B., Qian K., Xie H., Asundi A., *Meas. Sci. Technol.* 20 (6) (2009) 62001.

## 6.9 Supporting information

# CRUCIAL ROLE OF EXTERNAL FORCE IN THE ESTIMATION OF THE TOPOLOGY FREEZING TRANSITION TEMPERATURE OF VITRIMERS BY ELONGATIONAL CREEP MEASUREMENTS

Simon Kaiser<sup>a</sup>, Patrick Novak<sup>a</sup>, Michael Giebler<sup>a</sup>, Mario Gschwandl<sup>a</sup>, Philipp Novak<sup>a</sup>, Gerald Pilz<sup>b</sup>, Matthias Morak<sup>a</sup> and Sandra Schlögl<sup>a†</sup>

<sup>a</sup> Polymer Competence Center Leoben GmbH, Roseggerstrasse 12, A-8700 Leoben, Austria.

<sup>†</sup>E-mail: sandra.schloegl@pccl.at

<sup>b</sup> Institute of Materials Science and Testing of Polymers, Montanuniversitaet Leoben, Otto Glöckel-Strasse 2, A-8700 Leoben, Austria.

## Overview of $T_v$ data obtained from literature for various vitrimers

**Table S1** – Comparison of  $T_v$  values reported in literature for the selected vitrimers obtained from stress relaxation data and dilatometry experiments.

Reference	Network type/ Exchange reaction chemistry	Catalyst type/ Catalyst content	Topology freezing transition temperature ( $T_v$ ), ° C	
			obtained from	
			Stress relaxation data or Arrhenius plot	Dilatometry (measurement parameters)
1	Epoxy (DGEBA <sup>a</sup> )- acid (Pripol 1040)/ Transesterification	TBD/5 mol% to COOH Zn(ac) <sub>2</sub> /1 mol% to COOH Zn(ac) <sub>2</sub> /5 mol% to COOH Zn(ac) <sub>2</sub> /10 mol% to COOH	97 113 83 75	- 235 (5 K min <sup>-1</sup> , 10 kPa) 214 (5 K min <sup>-1</sup> , 10 kPa) 192 (5 K min <sup>-1</sup> , 10 kPa)
2	Epoxy (Esilica <sup>b</sup> )-acid (CSBR <sup>c</sup> )/ Transesterification	TBD/20 mol% to COOH	80 < $T_v$ < 120	168 (3 K min <sup>-1</sup> , 10 kPa)
3	Epoxy (ENR <sup>d</sup> )-acid (CABT <sup>e</sup> )/ Transesterification	Catalyst-free	<< 150	198 (3 K min <sup>-1</sup> , 10 kPa)
4	Epoxy (DGEBA)- acid (sebacic acid)/ Transesterification	Zn <sup>2+</sup> ionomer/0.75 mol% to COOH Zn(ac) <sub>2</sub> /0.75 mol% to COOH TBD/0.75 mol% to COOH	<< 170 << 170 << 170	171 (5 K min <sup>-1</sup> , 10 kPa) 172 (5 K min <sup>-1</sup> , 10 kPa) 177 (5 K min <sup>-1</sup> , 10 kPa)
5	Epoxy (ENR)-silica/ Silyl ether exchange (trans- oxyalkylation)	Lewis acids (e.g. AlCl <sub>3</sub> )	<< 150	153 (3 K min <sup>-1</sup> , - kPa)
6	Epoxy (ENR)-acid (DDDA <sup>f</sup> )/ Transesterification	Zn(ac) <sub>2</sub> /20 mol% to COOH	<< 160	187 (3 K min <sup>-1</sup> , 4 kPa)
7	Epoxy (DGEBA)- acid (adipic acid)/ Transesterification	TBD/5 mol% to COOH	80 < $T_v$ < 100	> 160 (3 K min <sup>-1</sup> , 24 kPa)

8	Epoxy (ENR)-acid (CD <sup>§</sup> )/ Transesterification	Zn(ac) <sub>2</sub> /10 mol% to COOH	<< 160	≈ 210 (3 K min <sup>-1</sup> , 10 kPa)
---	--	--------------------------------------	--------	--

<sup>a</sup>DGEBA = bisphenol A diglycidyl ether

<sup>b</sup>Esilica = epoxy group-functionalised silica

<sup>c</sup>CSBR = carboxyl group-grafted styrene-butadiene rubber

<sup>d</sup>ENR = epoxidised natural rubber

<sup>e</sup>CABt = citric acid-modified bentonite

<sup>f</sup>DDDA = dodecanedioic acid

<sup>g</sup>CD = carbon nanodot

- 1 Capelot M, Unterlass MM, Tournilhac F, Leibler L. *ACS Macro Lett.* 2012; 1 (7): 789–92.
- 2 Liu Y, Tang Z, Chen Y, Zhang C, Guo B. *ACS applied materials & interfaces* 2018; 10 (3): 2992–3001.
- 3 Xu C, Cui R, Fu L, Lin B. *Composites Science and Technology* 2018; 167: 421–30.
- 4 Niu X, Wang F, Li X, Zhang R, Wu Q, Sun P. *Ind. Eng. Chem. Res.* 2019; 58 (14): 5698–706.
- 5 Wu S, Yang Z, Fang S, Tang Z, Liu F, Guo B. *J. Mater. Chem. A* 2019; 7 (4): 1459–67.
- 6 Feng Z, Hu J, Zuo H, Ning N, Zhang L, Yu B et al. *ACS applied materials & interfaces* 2019; 11 (1): 1469–79.
- 7 Yang Y, Pei Z, Zhang X, Tao L, Wei Y, Ji Y. *Chemical science* 2014; 5 (9): 3486–92.
- 8 Tang Z, Liu Y, Guo B, Zhang L. *Macromolecules* 2017; 50(19): 7584–92.

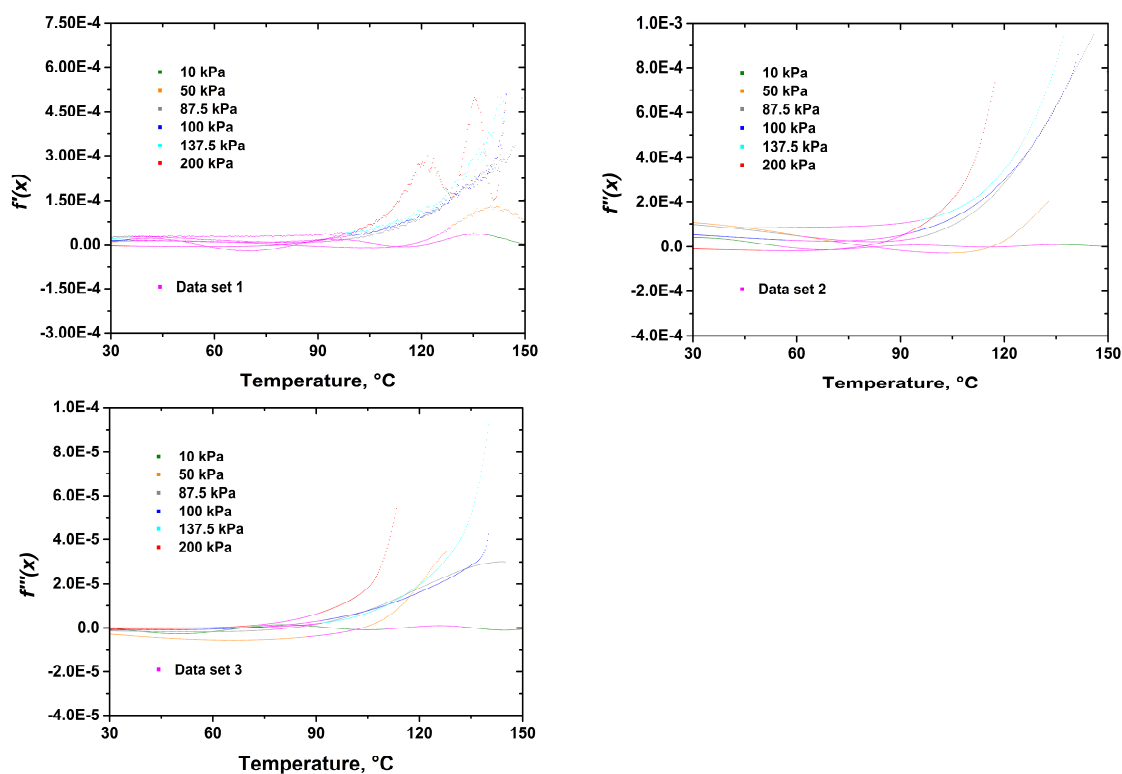


**Figure S1** – Data plots showing the values of the first ( $f'(x)$ ), second ( $f''(x)$ ), and third ( $f'''(x)$ ) derivative, which were formed from the exponential function that was fitted to the relevant portion of the creep data of the network DGEBA-Prisol 1040 with 5 mol% of TBD. Application of the particular defined tolerance criterion in each step resulted in data sets 1, 2, and 3.

# Chapter 7

## FINAL CONCLUSIONS AND PERSPECTIVES

### 7.1 Objectives of the work

The present thesis aimed at the preparation and comprehensive characterisation of stimuli-responsive elastomers from a high molecular weight linear polymer. In particular, three synthetic strategies relying on two fundamentally different bond exchange chemistries were explored for the incorporation of dynamic covalent bonds (DCB) into elastomeric polymer networks based on a hydrogenated carboxylated nitrile butadiene rubber (HXNBR). The different bond exchange mechanisms employed, being dissociative and associative in nature, constitute the two strategies that are currently available in the design of covalent adaptable networks (CANs). CANs are promising candidates for bridging the gap between thermosets and thermoplastics, which are recognised as the two classical categories of polymer networks considering a division based on the type of intermolecular interactions. After curing, the networks display properties reminiscent of thermosets, since the linkages between the macromolecular chains are of covalent nature. Nevertheless, the application of a certain stimulus allows altering the connectivity of the cross-links in a controlled way. Vitrimers, which constitute a rather new type of polymer networks, have dramatically extended the realm of associative CANs. Since their introduction in 2011, the terms associative CAN and vitrimer chemistry are virtually used synonymously. Herein, the approach applied towards associative dynamic HXNBR elastomers followed vitrimer chemistry, exploiting catalysed transesterification as the exchange chemistry. Regarding the stimuli employed, in the framework of this thesis reversible networks taking advantage of heat and light as the stimulus have been explored. Furthermore, a strategy towards particle-reinforced yet adaptable HXNBR composites was pursued. Besides the network design and the detailed analysis of the chemical and physical properties of the different materials prepared, particular focus was placed on demonstrating structure-property relationships. The observed macroscopic features are a direct result of the chemical reactions that occur on the molecular level, highlighting a possible applicability of these adaptable materials in structural applications.

Moreover, in the course of this thesis a new methodology for assessing the topology freezing transition temperature ( $T_v$ ) of vitrimers has been developed. This temperature is a unique characteristic of vitrimeric polymer networks, and its determination is ultimately not only crucial in terms of the service temperature of these materials. However, the estimation of the  $T_v$  of vitrimers lacks a direct and facile analysis method by now.

## 7.2 Overview of the results

In the first part of this research (**Chapter 3**), a chemistry relying on dynamic covalent bonds that were dissociative in nature has been pursued. In previous work of our group, Manhart et al. synthesised an anthracene-functionalised HXNBR rubber (anth-HXNBR), which was used for the preparation of photo-reversible elastomeric networks relying on the reversible  $[4\pi_s+4\pi_s]$  cycloaddition reaction of the pending anthracene moieties. Besides the detailed characterisation of the light-induced changes in the network structure, the preparation of reversible photoresists was successfully demonstrated. Building on these studies, the present work aimed at the preparation of dry adhesives from anth-HXNBR that exhibit switchable and controllable bonding properties. In addition to the photo-induced cleavage route ( $\lambda=254$  nm), the thermal dissociation of the previously formed anthracene photodimers was explored. The results showed that thermolysis is feasible at a moderate temperature of 70 °C, reaching a maximum dissociation yield in less than 5 min. In thin spin-cast films with a thickness of a few micrometers, it was found that photolysis is more efficient than thermal cleavage. However, going to a macroscopic sample size of about 100  $\mu\text{m}$ , the data revealed that thermolysis is superior to the photo-induced dissociation of the anthracene dimers. This observation was attributed to the limited penetration depth of the deep UV-light into the HXNBR matrix. In general, for both cleavage pathways a repeatable switching between the cross-linked and decrosslinked state was shown by UV-Vis experiments, highlighting the dual-responsiveness of the new elastomers. Moreover, derived from DMA measurements, the reversible cross-linking allowed for a modulation of the dissipation factor ( $\tan\delta$ ) and the  $T_g$  of the material. Thus, a reversible alteration of the surface tack of anth-HXNBR samples was envisaged. Indeed, photo-cross-linking led to a significant decrease (44%) in adhesion force towards aluminium. On the other hand, a successful recovery of the surface tack was accomplished by treatment of the sample with either UV-light ( $\lambda=254$  nm) or heat (70 °C), amounting to 75 and 80% of the initial adhesion force. Importantly, the switchable adhesion properties were shown over two cycles of cross-linking and subsequent cleavage of the photodimers. The effect is due to the changes in the viscoelastic properties of anth-HXNBR, with the viscoelasticity being lower in the decrosslinked state and thus, facilitating energy dissipation that induces a higher surface tack. To complement the tack measurements, adhesion force mapping was conducted on photo-patterned samples. The results confirmed a spatial control of the adhesion properties, further highlighting the versatility of the prepared anth-HXNBR networks, which is already enabled at a low modification yield of only 1.3 mol%.

In the second part of this thesis (**Chapter 4**), an approach following vitrimer chemistry was investigated to impart adaptable properties into HXNBR. In stark contrast to the dissociative anthracene-dimer linkages introduced into the rubber in the previous study, the network dynamics relied on an associative bond exchange mechanism. This chemistry yielded dynamic elastomeric networks that displayed a fundamentally different material response upon the application of the stimulus, which was exclusively heat. First, HXNBR was covalently cross-linked *via* its pending carboxylic acid moieties using a di-functional epoxide and in presence of a suitable transesterification catalyst, which was triazabicyclodecene (TBD). The successful cross-linking reaction resulted in  $\beta$ -hydroxyl ester bonds, which was confirmed by IR spectroscopy, rheology, and equilibrium swelling



experiments. At moderate temperatures ( $<80\text{ }^{\circ}\text{C}$ ), the elastomers performed like permanent networks. However, they were susceptible to TBD-catalysed transesterifications at elevated temperatures. The network dynamics was studied by stress relaxation measurements, revealing substantial relaxation capabilities (74% at  $180\text{ }^{\circ}\text{C}$  with 20 mol% of TBD) and that the rate and extent of relaxation increases with both temperature and catalyst concentration. A key focus of the work was to correlate the bond exchanges that occur on the molecular level with the macroscopic properties of the samples. Accordingly, the thermal adaptability of the networks was studied by reshaping experiments, confirming the plasticity of the covalently cross-linked samples under external force. Furthermore, a controlled enhancement of the self-adhesion properties was proven by means of lap shear tests indicating a certain weldability. Moreover, stress-rupture tests demonstrated improved repair properties in fractured samples, probably due to both an increased polymer chain mobility and interfacial transesterifications at high temperatures. A comparative study with the respective catalyst-free samples clearly confirmed that the thermally triggered adaptability of the elastomers originates from catalysed transesterifications. For the first time, dynamic associative covalent bonds were successfully incorporated into HXNBR, thus enlarging the scope of skeletons in the vitrimer(-like) chemistry of rubbers, which was previously limited to natural rubber (NR) and styrene-butadiene rubber (SBR).

The third part of this thesis (**Chapter 5**) explored the preparation of elastomeric composites that exhibit vitrimer-like properties. Since the application of fillers (at high contents) is of fundamental importance in the field of rubbers, the synthesis of filled yet dynamic networks from HXNBR was of great interest. For this purpose, a modified filler comprising reactive surface groups was selected, presumably acting as cross-linker and reinforcing filler at the same time. In particular, HXNBR was cured in presence of epoxy group-functionalised calcium silicate (Esilicate) and the transesterification catalyst TBD. The successful formation of covalent linkages between the carboxylic acid moieties of the rubber chains and the filler particles was proven by IR spectroscopy, rheology, and equilibrium swelling measurements. Due to the selected network design, all existing (exchangeable) covalent cross-links were naturally located at the HXNBR-Esilicate interface. These chemical bonds were expected to consist of  $\beta$ -hydroxyl esters that can undergo thermo-activated and TBD-catalysed interfacial transesterifications. Indeed, covalently cross-linked but dynamic HXNBR networks were obtained, showing distinct stress relaxation at high temperature. The bond exchange kinetics increased with temperature, and interestingly with the Esilicate loading (15 vs. 30 phr). This unusual behaviour was attributed to a certain amount of filler necessary to address a maximum of carboxylic acid moieties in the cross-linking process, highlighting the role of the dynamic bond density as well as the availability of free hydroxyl groups on the transesterification kinetics. Also here, comparison with a catalyst-free reference material clearly confirmed that the thermal adaptability of the composites could be solely associated with topology rearrangements on the molecular level. Besides the network dynamic, the Esilicate provided a distinct reinforcement effect, considerably improving the mechanical properties, such as the tensile strength and Young's modulus. The physical properties benefited from the good dispersion of the filler particles within the rubber matrix, consequently leading to a strong interfacial adhesion. In addition to the characterisation of the mechanical properties, a detailed investigation of the nature of the interactions

between HXNBR and Esilicate was carried out. Cyclic stress-strain experiments gave insights into the contribution of physical and chemical interactions to the interfacial adhesion in the present composites. Synthesising filled HXNBR compounds following vitrimer chemistry for the first time, this research constitutes a promising approach towards the preparation of HXNBR composites that combine the highly desired properties of permanent composites with the dynamics of vitrimer-like materials. The composites relied on readily available commercial materials and a solvent-free, straightforward and scalable synthesis route using classical rubber compounding techniques.

Simultaneous with the research on covalently adaptable HXNBR networks, in the framework of the present thesis a new analysis procedure to estimate the  $T_v$  of vitrimers has been established (**Chapter 6**). Vitrimers and vitrimer-like polymeric networks exhibit an exceptional viscoelastic behaviour due to the associative nature of the underlying bond exchange mechanism. Upon heating, these networks display a gradual, Arrhenius-like decrease in viscosity because of the acceleration of the (catalysed) exchange kinetics with temperature. Besides a glass transition temperature ( $T_g$ ), vitrimers exhibit a topology freezing transition temperature ( $T_v$ ). The  $T_v$  reflects the temperature below which the viscosity increases above  $10^{12}$  Pa·s. In other words, it describes the temperature where chemical exchanges become significant for the observed time scale in a particular experiment. The quantification of  $T_v$  is of great importance regarding the possible application of vitrimers as structural parts, since it governs the upper service temperature of the materials. The most common analysis method to quantify the bond exchanges in vitrimers is stress relaxation. However, these measurements are typically conducted at temperatures significantly higher than  $T_v$ . Thus, only hypothetical values for  $T_v$  are obtained by extrapolation of the viscosity trends measured at high temperature, and no direct estimation of the  $T_v$  is feasible. In literature, so-called dilatometry measurements are regularly conducted on vitrimers to monitor the vitrification transition as a function of temperature and to derive a value for  $T_v$ . However,  $T_v$  data obtained from dilatometry consistently shows higher  $T_v$  compared to values from stress relaxation measurements. Consequently, a systematic study was conducted on different epoxy-vitrimers (epoxy-acid and epoxy-anhydride) that undergo thermo-activated transesterifications by means of elongational creep measurements as a function of temperature and external force. Applying a series of tensile stresses, the data revealed a pronounced decrease in the onset temperature of the plastic flow regime with increasing external force. The shift occurred gradually and was shown to reach a limit temperature at a particular stress level. It was rationalised that this temperature corresponds to the  $T_v$  of the material, and that a certain degree of pre-stretching (i.e. external force) of the specimens is a crucial prerequisite for its precise identification. This behaviour was confirmed for all networks investigated. The consistent analysis of the creep data by a defined mathematical procedure allowed the reliable identification of trends. Importantly, at low stresses only a qualitative signature of the topology freezing transition is obtained and thus, the values for  $T_v$  stated in literature that were derived from dilatometry measurements may be subject to certain inaccuracies. In general, the method presents a new approach towards the direct analysis of  $T_v$  values of vitrimers. It should be noted that this procedure detects a macroscopic phenomenon (and not intrinsic), which is stress-induced creep as a result of topology rearrangements on the molecular level. Therefore, it is indeed unclear at which extent bond exchange reactions already occur before the onset of macroscopic flow can be

identified from the creep curves. Another new insight into the thermal behaviour of vitrimers was given regarding the material's coefficient of thermal expansion (CTE). Contact force-free thermal strain analysis based on digital image correlation (DIC) has been applied on vitrimers for the first time. No increase in CTE in the temperature range of  $T_v$  was detected for any of the compositions under investigation. This finding is in striking contrast to the literature, stating an increase in CTE at the onset of the topology freezing transition, which was concluded from dilatometry applying small yet too large stresses. This study contributes valuably to the understanding of dilatometry/elongational creep measurements in the context of vitrimers and covalent adaptable networks in general.

### 7.3 Perspectives

Regarding the photo-responsive anth-HXNBR networks, the major drawback of these systems are significant side reactions. The latter are more pronounced for thermolysis than photolysis in the cleavage step of the photodimers, which is due to the involvement of radical intermediates. A consequence of the side reactions is the limited repeatability of the switching of the cross-link state, which directly affects the endurance of the reversible changes in adhesion properties. Thus, the dynamic lifetime of these networks has to be considered as comparatively short. Importantly, the susceptibility to side reactions can be assumed to be inherently higher for reversible networks relying on a dissociative bond exchange mechanism compared to associative chemistries. In addition, the preparation of the materials is solvent-based, preventing a simple and straightforward processing using common rubber compounding procedures.

Several disadvantages of the anth-HXNBR networks could be circumvented by the incorporation of vitrimer chemistry into the rubber. Owing to the associative nature of the bond exchanges, these networks are less prone to side reactions due to the temporary formation of a higher cross-linked intermediate. Moreover, the networks exhibit a higher solvent resistance, remaining insoluble in a good solvent even at high temperatures. On the downside, the vitrimer-like materials are not sensitive to light as stimulus, wherefore no spatial control of the network dynamics is feasible. The introduction of photo-responsive properties, for instance through photosensitive catalysts, could constitute part of further research.

In general, the dynamic lifetime of the vitrimer-like networks, both without and with filler, was not examined in detail. The repeatability of consecutive stress relaxation, reshaping, and repairing cycles should be studied in more depth. Another intriguing feature of vitrimers that has not been investigated in the framework of this thesis are their reprocessing and recycling capabilities. It should also be noted that the lifetime of the organic catalyst TBD must be considered more limited than for example of inorganic zinc acetate. Additional research on the ageing of the catalyst, and the materials in general, will be essential. Knowledge about the limitations is crucial towards improved strategies for dynamic elastomers from rubbers.

Particularly promising is the approach involving modified fillers for the preparation of vitrimer-like HXNBR networks. In rubber industry, the usage of fillers is indispensable to improve the mechanical properties of elastomers. More insights into these composites

should be gained, for instance regarding the possible applicability of even higher filler contents and the combination of modified and pristine fillers to tailor the mechanical properties by finding an ideal balance between physical and chemical contributions to the interfacial adhesion.

Regarding the newly established measurement routine for the estimation of the  $T_v$  of vitrimers, at this stage, the study covered isotropic and amorphous (epoxy-acid) vitrimers. Further research work could include semi-crystalline vitrimers and vitrimeric composites to validate the applicability of the present method towards the analysis of  $T_v$  in these more complex materials. Furthermore, the performed investigations focused on epoxy-vitrimers relying on transesterifications as the dynamic bond exchanges. It would be valuable to explore the method regarding other vitrimer chemistries to verify its possible universality in the determination of  $T_v$  values.

# Appendix

## 1. Curriculum vitae

### Personal data

Name Simon Johannes Kaiser (M. Sc.)  
Date of birth 12 October 1989  
Place of birth Munich, Germany



### Education

Since 10/2016 DOCTORAL PROGRAM AT THE MONTANUNIVERSITÄT LEOBEN  
Research on dynamic covalent polymer networks/vitrimers.

10/2013 – 12/2015 MASTER'S PROGRAM CHEMISTRY AT THE TECHNICAL UNIVERSITY OF MUNICH (TUM)  
Focus on organic, construction, and macromolecular chemistry.  
Topic of the master's thesis: Hydrosilylation kinetics and surface coverage in the functionalisation of silicon nanocrystals using radical initiators.

10/2010 – 09/2013 BACHELOR'S PROGRAM CHEMISTRY AT THE TECHNICAL UNIVERSITY OF MUNICH (TUM)  
Topic of the bachelor's thesis: Acid-base properties of Cs promoted WS<sub>2</sub>/Al<sub>2</sub>O<sub>3</sub> catalysts.

2000 – 2009 ANNE-FRANK-GYMNASIUM ERDING  
General qualification for university entrance (Abitur).

### Experience

Since 05/2016 POLYMER COMPETENCE CENTER LEOBEN GMBH  
Working on a research project in cooperation with Semperit Technische Produkte GmbH (Wimpassing, Austria).

03 and 11/2019 LATEXX PARTNERS BERHAD  
Research visit in the R&D department (Kamunting, Malaysia).

---

## 2. List of publications

## PAPERS

- (1) **Kaiser, Simon**; Jandl, Julius; Novak, Patrick; Schlögl, Sandra (2020): Design and characterisation of vitrimer-like elastomeric composites from HXNBR rubber. In: *Soft Matter* 15 (30), 6062–6072. DOI: 10.1039/d0sm00362j.
- (2) **Kaiser, Simon**; Novak, Patrick; Giebler, Michael; Gschwandl, Mario; Novak, Philipp; Pilz, Gerald; Morak, Matthias; Schlögl, Sandra (2020): The crucial role of external force in the estimation of the topology freezing transition temperature of vitrimers by elongational creep measurements. In: *Polymer* (204): 122804. DOI: 10.1016/j.polymer.2020.122804.
- (3) Giebler, Michael; Sperling, Clemens; **Kaiser, Simon**; Duretek, Ivica; Schlögl, Sandra (2020): Epoxy-anhydride vitrimers from aminoglycidyl resins with high glass transition temperature and efficient stress relaxation. In: *Polymers* 12 (5), 1148. DOI: 10.3390/polym12051148.
- (4) **Kaiser, Simon**; Wurzer, Stefan; Pilz, Gerald; Kern, Wolfgang; Schlögl, Sandra (2019): Stress relaxation and thermally adaptable properties in vitrimer-like elastomers from HXNBR rubber with covalent bonds. In: *Soft Matter* 15 (30), 6062–6072. DOI: 10.1039/c9sm00856j.
- (5) **Kaiser, Simon**; Radl, Simone Viola; Manhart, Jakob; Ayalur-Karunakaran, Santhosh; Griesser, Thomas; Moser, Andreas; Ganser, Christian; Teichert, Christian; Kern, Wolfgang; Schlögl, Sandra (2018): Switching "on" and "off" the adhesion in stimuli-responsive elastomers. In: *Soft Matter* 14 (13), 2547–2559. DOI: 10.1039/c8sm00284c.
- (6) Giebler, Michael; Radl, Simone Viola; Ast, Markus; **Kaiser, Simon**; Griesser, Thomas; Kern, Wolfgang; Schlögl, Sandra (2018): Dual-responsive polydimethylsiloxane networks. In: *J. Polym. Sci. Part A: Polym. Chem.* 56 (20), 2319–2329. DOI: 10.1002/pola.29206.
- (7) Kehrle, Julian; Purkait, Tapas K.; **Kaiser, Simon**; Raftopoulos, Konstantinos N.; Winnacker, Malte; Ludwig, Theresa; Aghajamali, Maryam; Hanzlik, Marianne; Rodewald, Katia; Helbich, Tobias; Papadakis, Christine M.; Veinot, Jonathan G. C.; Rieger, Bernhard (2018): Superhydrophobic silicon nanocrystal-silica aerogel hybrid materials: synthesis, properties, and sensing application. In: *Langmuir: the ACS journal of surfaces and colloids* 34 (16), 4888–4896. DOI: 10.1021/acs.langmuir.7b03746.
- (8) Kehrle, Julian; **Kaiser, Simon**; Purkait, Tapas K.; Winnacker, Malte; Helbich, Tobias; Vagin, Sergei; Veinot, Jonathan G. C.; Rieger, Bernhard (2017): In situ IR-spectroscopy as a tool for monitoring the radical hydrosilylation process on silicon nanocrystal surfaces. In: *Nanoscale* 9 (24), 8489–8495. DOI: 10.1039/C7NR02265D.

- 
- (9) Radl, Simone V.; Schipfer, Christian; **Kaiser, Simon**; Moser, Andreas; Kaynak, Baris; Kern, Wolfgang; Schlögl, Sandra (2017): Photo-responsive thiol-ene networks for the design of switchable polymer patterns. In: *Polym. Chem.* 8, 1562-1572. DOI: 10.1039/C7PY00055C.
- (10) Sahin, Melahat; Schlögl, Sandra; **Kaiser, Simon**; Kern, Wolfgang; Wang, Jieping; Grützmacher, Hansjörg (2016): Efficient initiation of radical-mediated thiol-ene chemistry with photoactive silica particles. In: *J. Polym. Sci. Part A: Polym. Chem.* 55 (5), 894-902. DOI: 10.1002/pola.28442.

POSTER PRESENTATIONS

- (1) **Kaiser, Simon**; Wurzer, Stefan; Pilz, Gerald; Kern, Wolfgang; Schlögl, Sandra: Vitrimeric elastomers from HXNBR rubber with fast stress relaxation and thermally adaptable properties. In: *9th European Polymer Federation (EPF) summer school 2019 on dynamic and reversible polymer networks*. Bertinoro, Italy.
- (2) **Kaiser, Simon**; Radl, Simone Viola; Kern, Wolfgang; Schlögl, Sandra: Switching “on” and “off” the adhesion in stimuli-responsive elastomers. In: *Deutsche Kautschuk-Tagung (DKT) 2018*. Nuernberg, Germany.
- (3) **Kaiser, Simon**; Radl, Simone Viola; Manhart, Jakob; Ayalur-Karunakaran, Santhosh; Griesser, Thomas; Oesterreicher, Andreas; Moser, Andreas; Pinter, Gerald; Kern, Wolfgang; Schlögl, Sandra: Design of thermal and photo-reversible adhesives by exploiting the [4π<sub>s</sub>+4π<sub>s</sub>] cycloaddition reactions of pendant anthracene groups. In: *Danube Vltava Sava Polymer Meeting (DVSPM) 2017*. Vienna, Austria.
- (4) **Kaiser, Simon**; Manhart, Jakob; Ayalur-Karunakaran, Santhosh; Moser, Andreas; Ganser, Christian; Oesterreicher, Andreas; Pinter, Gerald; Teichert, Christian; Kern, Wolfgang; Griesser, Thomas; Schlögl, Sandra: Photo-reversible cross-linking of elastomeric materials comprising spatially resolved switchable characteristics. In: *4th European Symposium of Photopolymer Science (ESPS) 2016*. Leipzig, Germany.